



Analyse fonctionnelle de protéines métal- ou redox-dépendantes chez les plantes

Flavien Zannini

► To cite this version:

Flavien Zannini. Analyse fonctionnelle de protéines métal- ou redox- dépendantes chez les plantes. Biologie végétale. Université de Lorraine, 2019. Français. NNT : 2019LORR0276 . tel-02558987

HAL Id: tel-02558987

<https://hal.univ-lorraine.fr/tel-02558987>

Submitted on 3 Sep 2020

HAL is a multi-disciplinary open access archive for the deposit and dissemination of scientific research documents, whether they are published or not. The documents may come from teaching and research institutions in France or abroad, or from public or private research centers.

L'archive ouverte pluridisciplinaire **HAL**, est destinée au dépôt et à la diffusion de documents scientifiques de niveau recherche, publiés ou non, émanant des établissements d'enseignement et de recherche français ou étrangers, des laboratoires publics ou privés.



AVERTISSEMENT

Ce document est le fruit d'un long travail approuvé par le jury de soutenance et mis à disposition de l'ensemble de la communauté universitaire élargie.

Il est soumis à la propriété intellectuelle de l'auteur. Ceci implique une obligation de citation et de référencement lors de l'utilisation de ce document.

D'autre part, toute contrefaçon, plagiat, reproduction illicite encourt une poursuite pénale.

Contact : ddoc-theses-contact@univ-lorraine.fr

LIENS

Code de la Propriété Intellectuelle. articles L 122. 4

Code de la Propriété Intellectuelle. articles L 335.2- L 335.10

http://www.cfcopies.com/V2/leg/leg_droi.php

<http://www.culture.gouv.fr/culture/infos-pratiques/droits/protection.htm>

Thèse

Présentée et soutenue publiquement pour l'obtention du titre de

DOCTEUR DE L'UNIVERSITE DE LORRAINE

Mention « Biologie et écologie des forêts et des agrosystèmes »

par **Flavien ZANNINI**

Analyse fonctionnelle de protéines métal- ou redox-dépendantes chez les plantes

Soutenance le 04 décembre 2019

Membres du jury :

Rapporteurs : Mme Claire REMACLE
M. Stéphane LEMAIRE

PR, Université de Liège
DR CNRS, IBPC, Paris

Examinateurs : Mme Sophie RAHUEL-CLERMONT
M. Pascal REY

DR CNRS, Université de Lorraine
Ingénieur CEA, Cadarache

M. Nicolas ROUHIER

PR, Université de Lorraine
directeur de thèse
MCF, Université de Lorraine
co-directeur de thèse

M. Jérémy COUTURIER

UMR INRA/UL 1136, Interactions Arbres/Micro-organismes
Faculté des sciences, Boulevard des aiguillettes
54500 Vandoeuvre-lès-Nancy

Remerciements

Voici la dernière partie de ce manuscrit que j'écris, elle est la plus courte mais n'est pas pour autant la plus facile.

Cette thèse est pour moi un aboutissement aussi bien personnel que professionnel, et c'est pourquoi je me dois de remercier beaucoup de personnes.

Je remercie tout d'abord les membres du jury, Claire Remacle, Stéphane Lemaire, Sophie Rahuel-Clermont et Pascal Rey d'avoir accepté de lire ainsi que juger les travaux réalisés durant ces trois années de thèse.

Comment remercier mes deux encadrants de thèse. Tâche compliquée car les mots restent difficiles à trouver ... Jé, tu m'accompagnes depuis si longtemps qu'il est compliqué de nommer tout ce que tu m'as apporté. Je te dois une grande partie de ma culture scientifique ainsi que ma manière d'appréhender la science. Même dans des situations complexes et stressantes, tu fais preuve de patience et d'optimisme. Nico, j'ai été extrêmement touché par ton sens du partage et ta générosité. Tu considères le labo comme une famille qui se traduit par l'attention que tu porte à chacun de nous. Merci pour ce que tu m'as apporté personnellement et professionnellement, de m'avoir amené à Kaiserslautern et de m'avoir permis de travailler à tes côtés. Ta rigueur scientifique m'a permis d'évoluer. Je suis extrêmement reconnaissant pour ce que vous m'avez apporté au cours de ces différentes années. Vous avez grandement contribué à mon épanouissement.

Une thèse c'est aussi une bonne partie de son temps au labo. Il était important de trouver une ambiance agréable qui contribuait à ne pas voir le temps passer. Je vais donc commencer par mes anciens et présent collègues de bureau. Johny, ton surnom en dis long, fan de moto dont il est difficile d'enlever les différents poster qui trônent dans le bureau et permettent d'identifier facilement ta passion. Néanmoins, tu es d'une gentillesse indéniable et d'une générosité incontestable. Toto, merci pour les purifs IMAC nécessitant 8000 L de tampon ainsi que les feux d'artifices lors des transfos de Rosetta. Tu es une personne agréable et dans l'empathie, et sans toi ma thèse n'aurais sûrement pas été la même. NicoV, sincèrement pour quelqu'un qui vient de Vesoul tu es une révélation. Mon compagnon de munster, et de courses au Super U. Elodie, la force tranquille des GSTs et du rhum qui plus est adorable. Anna, the german girl not liking the beer and favoring the wine... It debated about your real country origin regarding this preference... Ich danke dir für deine freundlichkeit. Mélanie, merci pour ton optimisme à toute épreuve, nos discussions à propos de nos sujets respectifs et de notre soutien mutuel lors de la dernière ligne droite. Eric, toujours relax, tu es un DU toujours disponible et je pense que c'est très rare. Tiphaine, notre maman de paillasse, pour tes nombreux conseils avisés, ta grande disponibilité et ta gentillesse. Mumu, derrière une grande timidité ce cache une grande bienveillance. Alexis, ton amour des produits locaux et ton sens de la sécurité. Raph, ta bonne humeur quelque soit le temps et les circonstances. Rod, pour être resté souvent tard le soir afin que l'on ne soit pas seuls. Ben le Ouf pour nos discussions diverses et variées.

Benji, pour ton coté fun, ton apport scientifique et ton imagination débordante dans l'innovation de nouvelles crasses à expérimenter. Arnaud, pour tes conseils et ton regard objectif. Mél, pour ton immense générosité, ta gentillesse et les différentes tartes aux quetches, mirabelles, pommes (bientôt les bretzels) que tu confectionnes pour le labo. J2P, un vosgien est forcément quelqu'un de bien. Merci d'avoir relu ce manuscrit mais surtout merci pour ta sagesse et l'apport de connaissances.. Jean-Michel, le pro du lait de chamelle, pour tes blagues que l'on ne relève jamais. Wuong, thank's for the funny moments, especially regarding delphonse traching. Et les nouveaux, Kevin, Delphine, Loïck et Damien la relève. Essayés au moins de faire aussi bien que nous.

A mes amis, difficile de tous les citer, les poulets en grande partie vosgiens: Ben (Benjamin), Juju, Cyey, Yoyo, Yenyen, C.Mama, Ben (Benoit), Chlo, Coco, Remi, Préz, Geugeu, Tonfis, Moumout, Elsa. Merci pour ces grands moments, ces nombreuses et folles soirées (en espérant qu'aucune n'a fuité sinon je retire ces remerciements).

Merci Mecton, j'aurais aimé que l'on face cette thèse dans des labos proches mais je sais que tu seras toujours là...

Merci à ma famille... Mes parents sans vous je ne serais certainement pas la personne que je suis aujourd'hui, merci infiniment pour votre amour et votre confiance, de m'avoir permis de faire mes propres choix,. Merci pour tout ce que vous représentez. Ma sœur, mon modèle et tu le seras toujours, tu es la personne la plus adorable que je puisse connaître... Marian, mon petit Butternut et Vianney pour tous ces moments inoubliables passés en famille. En parlant de moments inoubliables, certaines personnes le resteront, à Flora, Malo et Gianni merci pour les moments passés.

Bien sûr, ces remerciements seraient incomplets sans la gratitude que je te dois Savannah... Tu le sais mais ça fait toujours plaisir à entendre. Merci pour tout, ton écoute, les moments passés à échanger sur diverses théories jusqu'à des heures tardives, de m'avoir supporté durant ces années (tâche qui n'est pas évidente), pour les nombreux moments difficiles, tu étais là et je ne sais pas si j'aurais pu réussir sans toi.... Maëlio cette thèse elle est aussi pour toi... A l'heure où j'écris tu as 2 dents et tu es une petite loutre !

Je n'ai pas de talent particulier. Je suis simplement curieux.
Albert Einstein

Table des Matières

Remerciement	
Sommaire	
Abbréviation	
Introduction	1
I. Origine de la réactivité des cystéines	5
II. Modifications post-traductionnelles des cystéines par les espèces réactives de l'oxygène (ROS) et de l'azote (RNS)	7
1. Production des ROS et RNS	7
2. Les systèmes de protection contre les espèces réactives	13
2.1. Les systèmes non enzymatiques	13
2.2 Les systèmes enzymatiques	17
3. Modifications post-traductionnelles (MPT) des cystéines par les ROS et les RNS	21
4. Les systèmes de réduction contrôlant ces MPTs	23
III. Le repliement oxydatif des protéines	29
1. Les protéines Dsb du système périplasmique bactérien	31
2. Repliement oxydatif des protéines résidant ou transitant par le réticulum endoplasmique et l'appareil de Golgi	35
2.1. La réponse cellulaire aux protéines non structurées (UPR) : mécanismes et conséquences	37
2.2. Les systèmes de repliement oxydatif	39
3. L'import des protéines au sein de l'espace intermembranaire mitochondriale (IMS), séquestration par repliement oxydatif, la voie MIA40/ERV1	51
3.1. La mitochondrie, un organite pas comme les autres...	51
3.2. L'import des protéines dans l'IMS, prédominance de la voie par repliement oxydatif	53
3.3. Détails sur les mécanismes moléculaires et structuraux de la voie MIA40/ERV1	59
4. Les systèmes de repliement oxydatif au sein du lumen des thylakoïdes	63
IV. Les systèmes de réduction intervenant dans la maturation des cytochromes de type c dans l'IMS et le lumen des thylakoïdes	67
1. Le système I de maturation des cytochromes c au sein de l'IMS des organismes photosynthétiques	69
2. Le système de réduction et de maturation de type II des cytochromes c au sein du lumen des thylakoïdes	71
Présentation et objectifs du sujet de thèse	75
Résultats	79
In Vitro Alkylation Methods for Assessing the Protein Redox State	81
The thioredoxin-mediated recycling of <i>Arabidopsis thaliana</i> GRXS16 relies on a conserved C-terminal cysteine	97
Mitochondrial <i>Arabidopsis thaliana</i> TRXo isoforms bind an iron–sulfur cluster and reduce NFU proteins in vitro	119

<i>Atypical protein disulfide isomerase (PDI): Comparison of the molecular and catalytic properties of poplar PDI-A and PDI-M with PDI-L1A</i>	147
<i>Erv1 of Arabidopsis thaliana can directly oxidize mitochondrial intermembrane space proteins in the absence of redox-active Mia40</i>	171
<i>Oxidation of Arabidopsis thaliana MIA40 substrates by the combined action of ERV1 and glutathione</i>	187
<i>Conclusion générale</i>	209
<i>I. Rôle(s) de la GRXS16 d'A. thaliana : maturation des protéines Fe-S et réduction par le système TRX chloroplastique</i>	211
<i>II. Y'a-t-il un lien entre les TRX o1 et o2 et la maturation des centres Fe-S mitochondriaux chez A. thaliana ?</i>	215
<i>III. La singularité de la voie MIA40 chez A. thaliana : le rôle central d'ERV1</i>	219
<i>Références bibliographies</i>	225

Abbréviation

- •NO/NO : oxyde nitrique
- $^1\text{O}_2$: oxygène singulet
- *A. thaliana*: *Arabidopsis thaliana*
- ABA: acide absissique
- ADN: acide désoxyribonucléique
- ALR: augmenter of liver regeneration
- AOX: alternative oxydase
- APX: ascorbate peroxydase
- ASC: ascorbate
- ATF6/4: facteur de transcription 6/4
- ATP: adénosine triphosphate
- BIP: Binding protein
- BRI1: récepteur à brassinostéroïdes
- CAT: catalase
- CCHL: cytochrome hème lyase
- CCM: cytochrome *c* maturation
- CCS: chaperonne a superoxyde dismutase
- CHCHD4: coiled-coil-helix-coiled-coil-helix domain 4
- CO₂: dioxyde de carbone
- COX: cytochrome *c* oxidase
- CRM: chaine respiratoire mitochondriale
- CSD: copper superoxyde dismutase
- Cyt *b*₆*f*: cytochrome b(6)f
- Cyt b6f: cytochrome b6/f
- Da: Dalton
- DHA: déhydroascorbate
- DHAR: déhydroascorbate réductase
- Dsb : disulfide bond
- *E. coli*: *Escherichia coli*
- eh: potentiel redox
- ERAD: ER associated degradation
- ERO1 : ER oxydase 1
- ERV1: essential for respiration and vegetative growth 1
- ETR1: récepteur à éthylène
- FAD: flavine adénine dinucléotide
- FBPase: fructose-1,6-biphosphate
- FDX/FTR/TRX: voie ferrédoxine/ferrédoxine-thiorédoxine-réductase/thiorédoxine
- FDX: Ferrédoxine
- Fe-S: centre fer-soufre
- FTR: ferrédoxine thiorédoxine reductase
- GAPDH: glyceraldéhyde-3-phosphate déshydrogénase
- GFP: green fluorescente protein
- GOX: glycolate oxidase
- GPX: glutathion peroxydase

- GPXL: glutathion peroxydase like
- GR: glutathion réductase NADPH dépendante
- GRX: Glutarédoxines
- GS[•]: glutathion radicalaire
- GSH: Glutathion
- GSH1: γ -EC synthase
- GSH2: glutathion synthase
- GSNO: S-nitrosoglutathion
- GSSG: Glutathion disulfure
- GST: glutathion-S-transférase
- H₂O: molécule d'eau
- H₂O₂: peroxyde d'hydrogène
- HCF164: high chlorophyll fluorescence 164
- HSP: heat shock protein
- IgG: Immunoglobuline G
- IM: inner membrane
- IMS: intermembrane space
- IRE1: inositol-requiring kinase 1
- ITS: intermembrane space targeting signal
- JTT: méthode Jones, Taylor et Thornton
- kDa: kilo Dalton
- LECA: last eukaryotic commun acestor
- LHC: light harvesting complex
- LTO1: lumen thiol oxydoréductase 1
- MDHA: monodéhydroascorbate
- MDHAR: NADPH-monodéhydroascorbate réductase
- MIA40: mitochondrial intermembrane space assembly 40
- MIC: MICOS complex subunit
- MISS: mitochondrial IMS-sorting signal
- MPT: modifications post-traductionnelles
- MTS: mitochondrial targeting sequence
- mV: millivolt
- N₂O₃: trioxyde d'azote
- NADP : nicotinamide adénine dinucléotide phosphate oxydé
- NADPH : nicotinamide adénine dinucléotide phosphate réduit
- NO₂ : dioxyde d'azote
- NO₂: dioxyde d'azote
- NR : nitrate réductase
- NTR: NADPH-thiorédoxine reductase
- O₂: dioxygène
- O₂^{•-}: radical superoxyde
- OH[•]: radical hydroxyle
- OM: outer membrane
- ONOO⁻ : peroxynitrite
- OSM1: fumarate reductase
- PC: phytochélatine
- PCS: phytochélatine synthase

- PDI: protéine disulfure isomérase
- PERK: protein endoplasmic reticulum kinase
- pH: potentiel d'hydrogène
- pKa: constante d'acidité
- PQ: plastoquinone
- PRK: phosphoribulokinase
- PRX: peroxyrédoxine
- PRX: peroxyrédoxine
- PSI: photosystème I
- PSII: photosystème II
- QSOX: quiescine sulfhydrile oxydase
- RALF1: rapid-alkalinization factor
- RBOH : NADPH oxydases
- RE: réticulum endoplasmique
- RNS: reactive nitrogen species
- ROS: reactive oxygen species
- RS⁺-OO⁻: peroxyde zwitterionique
- RubisCO: ribulose-1,5-bisphosphate carboxylase/oxygénase
- *S. cerevisiae*: *Saccharomyces cerevisiae*
- S[•]: radical thiyl
- SBPase: sédoheptulose-1,7-bisphosphatase
- SH: thiol
- S-O₂H: acide sulfinique
- S-O₃H: acide sulfénique
- SOD: superoxyde dismutase
- S-OH: acide sulfénique
- SRX: sulfirédoxines
- TCP: trichlorophénol
- TIM: translocase of inner membrane
- TIM: translocase of inner membrane
- TM: domaine transmembranaire
- TMX: thioredoxin-related transmembrane protein
- TOM: translocase of outer membrane
- TPX: thiol peroxydase
- TRX: thiorédoxine réductase
- TRX: Thiorédoxines: TRX
- UPR: unfolded protein response
- VKOR: vitamine K époxyde réductase

Introduction

Les cystéines sont l'un des acides aminés dont la teneur est la plus faible dans les protéines (en moyenne entre 1 et 3%). Nonobstant, leur présence gouverne fréquemment l'activité, la stabilité, la localisation ou la fonction de nombreuses protéines et il est paradoxalement relativement rare de rencontrer des protéines dépourvues de cystéines. . La singularité de cet acide aminé est conférée par la présence d'un groupement thiol (SH) au niveau de la chaîne latérale qui va permettre la formation de ponts disulfure après oxydation. Ces ponts disulfure peuvent être structuraux mais ils peuvent avoir aussi des fonctions régulatrices via des échanges dithiol-disulfure. De plus, de nombreuses autres modifications post-traductionnelles qui sont formées par modification oxydative des cystéines jouent également des rôles régulateurs.

Pour illustrer le premier aspect, il est important de mentionner qu'environ 30% des protéines de la cellule vont transiter par les voies de sécrétion et que de nombreuses protéines secrétées possèdent des cystéines formant des ponts disulfure dits structuraux dont la fonction est de permettre un repliement correct des protéines mais aussi de les rendre plus compactes et de limiter leur dégradation dans un environnement extracellulaire plus hostile que les compartiments intracellulaires. Ce repliement oxydatif est également important pour les protéines présentes dans l'espace intermembranaire de la mitochondrie et dans le lumen des thylakoïdes chez les eucaryotes et dans le périplasme chez certaines bactéries. Les acteurs et les mécanismes permettant la formation de ces ponts disulfure seront détaillés dans le chapitre IV.

La meilleure illustration concernant les mécanismes de régulation redox concerne certainement la régulation par la lumière et le système ferrédoxine-thiorédoxine (FDX-TRX) des enzymes du cycle de Calvin-Benson et d'autres enzymes associées à ce métabolisme carboné. Plusieurs enzymes sont régulées par réduction/oxydation d'un ou de plusieurs ponts disulfure par les thiorédoxines, dont l'état redox est contrôlé par la lumière, via la chaîne de transfert d'électrons linéaire chloroplastique, les ferrédoxines et la ferrédoxine-thiorédoxine réductase. Il est intéressant de noter un rôle potentiel du système glutathion (GSH)/Glutarédoxine (GRX), molécules qui contrôlent la (dé)nitrosylation et la (dé)glutathionylation des protéines. En effet, des études de protéomique redox suggèrent que plusieurs enzymes du cycle de Calvin-Benson sont également modifiées/régulées par la formation d'adduits glutathion et de groupements S-nitrosothiols (Bedhomme et al., 2009; Michelet et al., 2008, 2013; Morisse et al., 2014;

Zaffagnini et al., 2007, 2016a) Les acteurs et les mécanismes permettant la formation/réduction de ces ponts disulfures seront détaillés dans le chapitre II.

Il est à noter pour finir ce paragraphe introductif que les cystéines sont aussi fréquemment impliquées dans la fixation d'ions métalliques ou de cofacteurs métalliques, comme les motifs à doigt de zinc ou les centres fer-soufre (Fe-S) (Couturier et al., 2015; Giles et al., 2003; Peralta and Huidobro-Toro, 2016; Rouhier, 2010) Ces aspects ne seront pas ou peu traités dans cette introduction mais l'intérêt que j'ai porté aux protéines possédant des motifs Cx₂C conservés (C représentant les cystéines et x indiquant la présence d'acides aminés variables) afin de caractériser la fonction de nouvelles oxydoréductases m'a amené à purifier certaines protéines contenant des centres Fe-S.

I. Origine de la réactivité des cystéines

Outre leur exposition au solvant, la réactivité des cystéines est gouvernée notamment par leur capacité à exister sous forme déprotonée ou thiolate, beaucoup plus réactive que la forme thiol (protonée), et donc à effectuer des attaques nucléophiles sur un certain nombre de molécules. Cette caractéristique est directement reliée à la constante d'acidité (pKa) du groupement thiol qui est contrôlée par le microenvironnement dans lequel les cystéines se trouvent (Trost et al., 2017). Les acides aminés situés à proximité de la cystéine considérée, notamment ceux chargés positivement (His, Arg et Lys), auront un rôle prépondérant en formant des paires ioniques. D'autres facteurs influençant la valeur du pKa sont les réseaux de liaisons hydrogène formées entre le thiolate et les groupes polaires non chargés de chaînes principales ou latérales d'acides aminés, le moment dipolaire électrique généré lorsque le résidu cystéinyl est situé à l'extrémité N-terminale d'une hélice α et enfin la désolvatation, qui se produit souvent dans les sites catalytiques, et qui peut influencer le pKa du thiol en diminuant la constante diélectrique par rapport à l'eau, augmentant ainsi toutes les interactions électrostatiques (Ferrer-Sueta et al. 2011). La contribution individuelle relative de chacun des facteurs structuraux à la valeur globale du pKa d'une cystéine reste difficile à appréhender.

Le pKa reflète donc l'équilibre entre les formes thiol et thiolate et gouverne ainsi la réactivité intrinsèque de la cystéine à une valeur de pH physiologique. Par exemple, une cystéine libre possède un pKa d'environ 8,3, celle contenue dans le glutathion (GSH) de 8,8 (Paulsen and

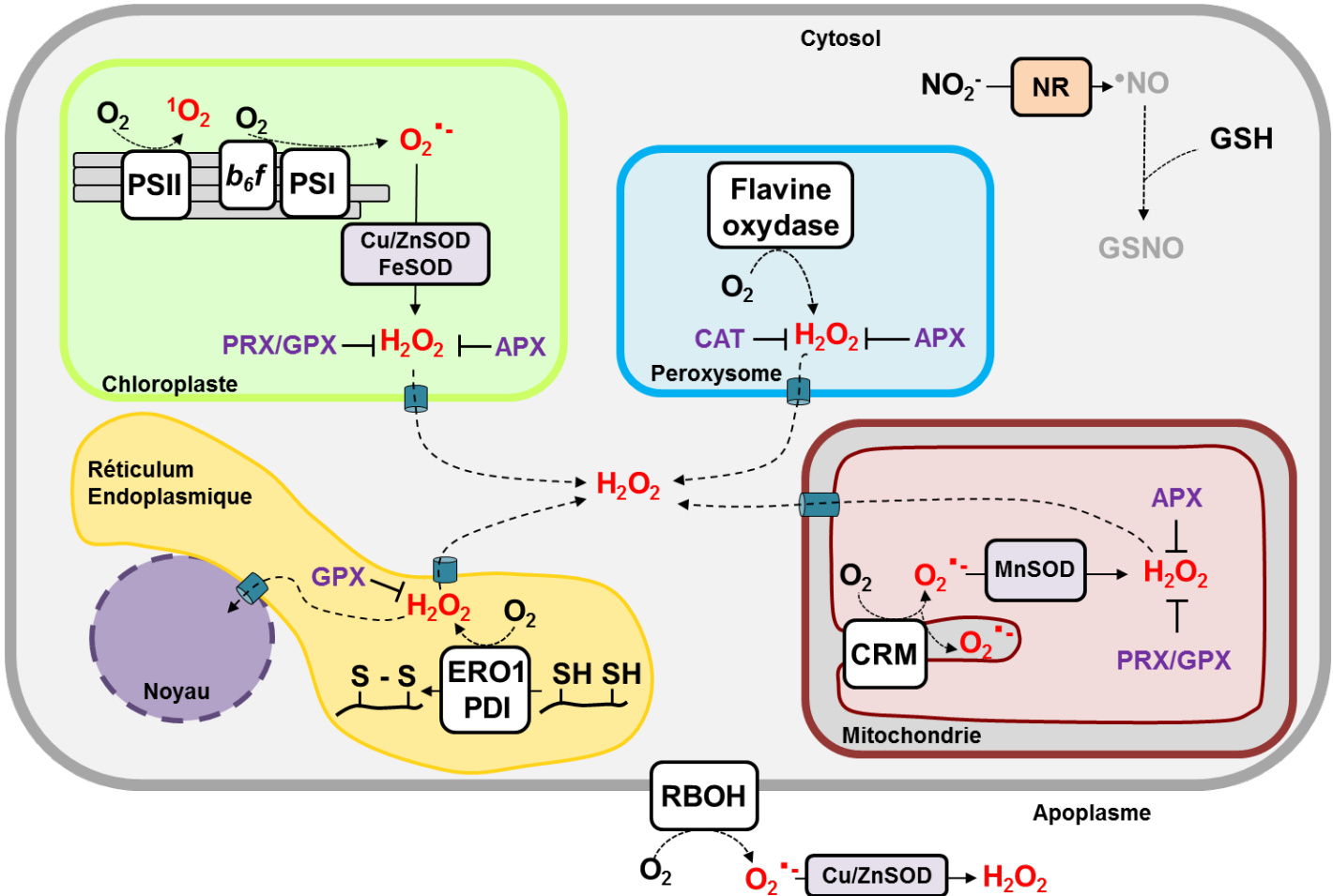


Figure 1 : Représentation schématique des principaux sites de production d'espèces réactives de l'oxygène et de l'azote et des enzymes intervenant dans leur détoxication chez les organismes photosynthétiques. Au sein du chloroplaste, les photosystèmes I et II (PSI et PSII) et le cytochrome *b6f*, sont les principaux sites de production de ROS (¹O₂: oxygène singulet, O₂^{•-}: radical superoxyde). Sous l'action de superoxyde dismutases à Cu/Zn ou à Fe (Cu/ZnSOD et FeSOD), l'O₂^{•-} est réduit en H₂O₂. Au niveau des mitochondries, la chaîne respiratoire mitochondriale (CRM) est responsable la production d'O₂^{•-} qui sera réduite en H₂O₂ par l'action des MnSODs. Le peroxysome représente un site important de production d'H₂O₂ via la photorespiration (glycolate oxydase, GOX) et l'activité d'autres flavine oxydases. Il est réduit en H₂O par des catalases (CAT) et ascorbate peroxydases (APX). Ces dernières sont également présentes au sein du chloroplaste et de la mitochondrie avec les thiol peroxydases (PRX et GPXL) pour réduire H₂O₂. Le réticulum endoplasmique est également un site de production d'H₂O₂ au travers du repliement oxydatif des protéines sécrétées catalysé par le système PDI/ERO1. De récentes études ont également mis en évidence la présence de GPXL dans ce compartiment subcellulaire. Le dernier site de production d'H₂O₂ est l'apoplaste, sous l'action conjointe d'une NADPH oxydase (RBOH) et d'une SOD.

La production de •NO par la nitrate réductase (NR) à partir de nitrites se déroule dans le cytosol. En présence de glutathion réduit (GSH), du glutathion nitrosylé (GSNO) sera formé. Adapté de Zaffagnini et al., 2019, Smirnoff et Arnaud., 2019

Carroll, 2013). Cela signifie qu'à une valeur de pH physiologique (généralement inférieure à 8), ces cystéines seront présentes majoritairement sous forme protonées, pas ou peu réactives. Les cystéines catalytiques retrouvées dans certaines familles de protéines, notamment les oxydoréductases à thiol, possèdent en revanche un pKa acide. Celui-ci se situe autour de 5-6 pour les TRXs et les peroxydases à thiol de la classe des peroxyrédoxines (PRX) et autour de 3 à 5 pour les GRXs (Couturier et al., 2013a; Winterbourn and Hampton, 2008; Zaffagnini et al., 2008, 2012). Bien que les GRXs présentent un pKa plus faible et donc une réactivité théorique plus importante, il s'avère que la réactivité de la cystéine catalytique des GRXs vis-à-vis du peroxyde d'hydrogène (H_2O_2) par exemple est 10^5 à 10^6 fois plus faible que celle présente dans les PRXs, indiquant que le pKa n'est pas le seul déterminant de la réactivité des cystéines et que d'autres facteurs sont importants (Winterbourn and Hampton, 2008). A l'inverse, les GRXs sont plus réactives vis-à-vis des formes du glutathion (GSSG et GSNO), sans doute du fait de la présence d'un site de fixation spécifique pour ces produits.

II. Modifications post-traductionnelles des cystéines par les espèces réactives de l'oxygène (ROS) et de l'azote (RNS)

1. Production des ROS et RNS

Le paradoxe de la vie dans des conditions aérobies est la production d'espèces réactives de l'oxygène (Reactive Oxygen Species en anglais : ROS) et dans une moindre mesure de l'azote (Reactive Nitrogen Species en anglais : RNS). La formation de ces espèces moléculaires prend principalement place au sein des chaînes de transport d'électrons mitochondriale et chloroplastique mais également au sein du peroxysome via des flavine oxydases et notamment la glycolate oxydase (GOX) qui participe à la photorespiration chez les plantes (Figure 1). Cette enzyme génère des quantités stœchiométriques d' H_2O_2 liées à l'activité oxygénase de la ribulose-1,5-bisphosphate carboxylase/oxygénase (RubisCO). Cette voie, au cœur des cellules photosynthétiques et des plantes à métabolisme C3, est une des voies importantes de production d' H_2O_2 indépendamment des stress biotique et abiotique (Noctor, 2002; Noctor et al., 2018). Même si ces espèces sont produites de façon basale au sein des cellules dans des conditions normales de croissance et sont même éventuellement requises pour des processus

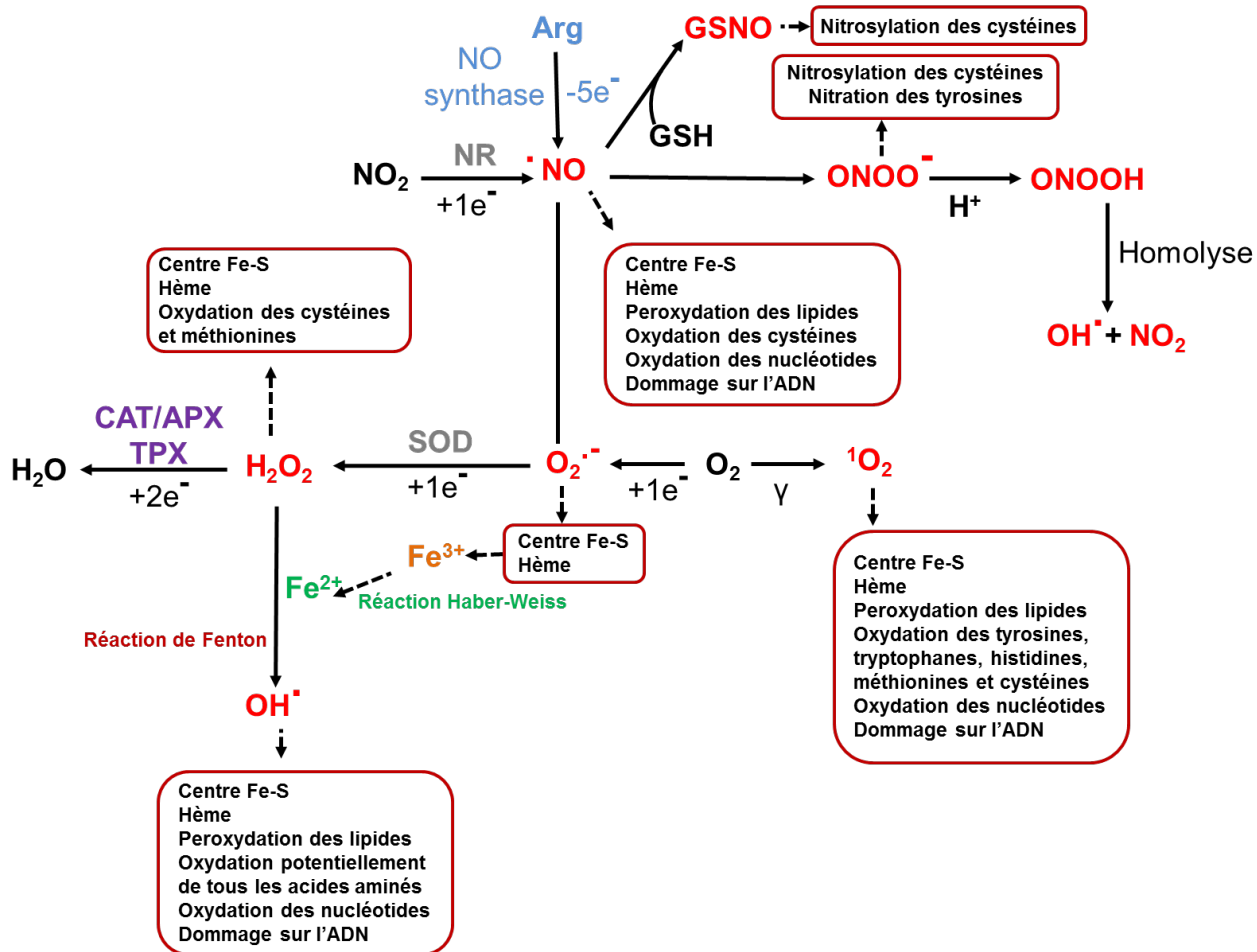


Figure 2: Principales voies de production de ROS et de RNS et dommages induits sur les biomolécules.

L' O_2 peut passer sous un état d'excitation singulet (${}^1\text{O}_2$) ou être partiellement réduit en anion superoxyde ($\text{O}_2^{\bullet-}$). Ce dernier est généralement réduit par une superoxyde dismutase (SOD) en peroxyde d'hydrogène (H_2O_2) qui est réduit en H_2O par des thiol peroxydases (TPXs), catalases (CAT) ou ascorbate peroxydases (APX). En présence de Fe^{2+} , H_2O_2 peut produire des radicaux hydroxyles (OH^\bullet) via la réaction de Fenton. L'oxyde nitrique ($\cdot\text{NO}$) peut être produit au travers de la réduction des NO_2 par les nitrate réductases (NR) ou par une activité de type NO synthase via l'oxydation de l'arginine (Arg). Le $\cdot\text{NO}$ est globalement peu réactif mais forme du peroxynitrite (ONOO^-) par réaction avec $\text{O}_2^{\bullet-}$. Il peut également réagir avec du glutathion (GSH) pour former du nitrosoglutathion (GSNO). Une fois protonée, ONOO^- forme de l'acide peroxynitrique (ONOOH) qui se décompose par homolyse et des radicaux hydroxyles et du dioxyde d'azote (NO_2).

développementaux (Rouhier et al., 2015), leur production est souvent exacerbée dans des conditions de stress biotique et abiotique (Couturier et al., 2013b; Danon, 2012).

Chez les plantes comme au sein des cellules animales (Huang et al., 2016), la chaîne respiratoire mitochondriale est le théâtre de la production de ROS, notamment au niveau des complexes I et III qui produisent un radical superoxyde ($O_2^{\bullet-}$) par réaction d'un électron avec une molécule d'oxygène. Ce radical superoxyde est normalement rapidement dismuté en H_2O_2 par l'action de superoxyde dismutases à manganèse (MnSOD). Du fait de sa moindre réactivité et de sa spécificité, l' H_2O_2 possède la durée de vie la plus importante parmi les ROS. De plus, n'étant pas chargée et avec une structure proche de l' H_2O , cette molécule possède la particularité de diffuser assez facilement au travers des membranes biologiques et d'être transportée par certaines aquaporines, ce qui lui permet en principe de passer d'un compartiment subcellulaire à un autre. La formation des radicaux hydroxyles (OH^{\bullet}) est possible par la réaction de Fenton par réaction d' H_2O_2 avec des ions métalliques (Fe^{2+} et Cu^{2+}) ou par la réaction d'Haber Weiss par réaction avec $O_2^{\bullet-}$ (Hurd and Murphy, 2009). Etant l'un des plus puissants oxydants, ce radical possède la capacité de réagir avec toutes les molécules biologiques comprenant en particulier les acides nucléiques, les protéines et les lipides (Figure 2). Cependant son temps de demi-vie étant relativement court (~ 1 ns), son action délétère se produira principalement aux sites de production (Halliwell and Gutteridge, 1992, 1995). Chez les organismes photosynthétiques, l'expression d'une alternative oxydase (AOX) permet de limiter la production de ROS dans la mitochondrie en dissipant le pouvoir réducteur excédentaire par réaction avec les quinones de la chaîne respiratoire, formant des molécules d' H_2O (Zaffagnini et al., 2019). Ainsi, le complexe III ne produira pas de ROS. Toutefois, en contournant 2 sites d'expulsion de protons, cette oxydase terminale alternative limite la production d'ATP.

Au sein des organismes photosynthétiques, un autre organite singulier est également responsable d'une production conséquente d'espèces moléculaires réactives, le chloroplaste au niveau du photosystème II (PSII), du photosystème I (PSI) mais aussi lors des transferts d'électrons entre les plastoquinones et le cytochrome b6/f. Concernant le PSII, lorsque les antennes chlorophylliennes (Light Harvesting Complex (LHC)) recueillent l'énergie lumineuse et que l'état d'excitation triplet de la chlorophylle n'est pas dissipé rapidement, cela peut induire la production d'oxygène singulet (1O_2) par interaction avec une molécule d' O_2 (Fischer et al., 2007). La fermeture des stomates en réponse à un stress hydrique a pour conséquence la

diminution des concentrations en CO₂ dans les cellules photosynthétiques. Ceci peut générer une sur-réduction de la chaîne de transport des électrons chloroplastique et augmente la probabilité de production d'¹O₂ au sein du PSII (Fischer et al., 2013; Noctor et al., 2014). D'un point de vue quantitatif, la majorité des ROS serait produite par le PSI via la réaction de Mehler qui consiste en un transfert d'électron de la ferrédoxine vers l'oxygène, produisant ainsi des radicaux superoxydes (Asada, 2006) qui seront ensuite réduits en H₂O₂ via des SOD à cuivre/zinc (Cu/Zn). La présence de ces deux ROS peut via les réactions d'Haber-Weiss et de Fenton induire la production de OH[•] (Ivanov and Khorobrykh, 2003). De la même manière qu'au niveau du complexe III de la chaîne respiratoire mitochondriale, il a été mis en évidence une implication importante du cytochrome b6f et plus précisément du pool de plastoquinone dans la production d'O₂^{•-} qui peut également aboutir à la production d'une quantité non négligeable d'H₂O₂ via les Cu/Zn SODs (Baniulis et al., 2013; Ivanov and Khorobrykh, 2003).

Concernant les ROS, il est intéressant de mentionner deux autres sources importantes. En effet, le repliement oxydatif des protéines via le couple PDI/ERO1 dans le réticulum endoplasmique (voir chapitre IV.2) génère des quantités importantes d'H₂O₂ dans ce compartiment. Les NADPH oxydases (RBOH) présentes au niveau de l'apoplasme forment de l'O₂^{•-}, qui conduit à la production d'H₂O₂ par l'intermédiaire de SODs. L'apoplasme étant un compartiment cellulaire relativement pauvre en systèmes antioxydants, l'H₂O₂ peut y être accumulé plus facilement que dans les autres compartiments cellulaires (Foyer and Noctor, 2011). Cet H₂O₂ servira de fait dans un très grand nombre de voies de signalisation en réponse à des contraintes biotique et abiotique mais aussi lors de processus développementaux tels que la croissance de la racine primaire ou l'émergence des racines latérales (Lüthje et al., 2013; Orman-Ligeza et al., 2016; Tsukagoshi et al., 2010).

Les voies de production des RNS et notamment d'oxyde nitrique ([•]NO ou NO) au sein des organismes photosynthétiques restent encore assez peu connues. Outre des processus non enzymatiques se produisant à partir de nitrite dans des compartiments à pH acide tel que l'apoplasme il existerait une voie enzymatique dans le cytosol où les nitrate réductases (NR) peuvent réduire des nitrites en NO notamment dans des conditions de stress (Astier et al., 2018; Pucciariello and Perata, 2017). La mitochondrie est également le siège de production de NO par réduction de dioxyde d'azote (NO₂) via les complexes III et IV. Dans tous ces compartiments, le

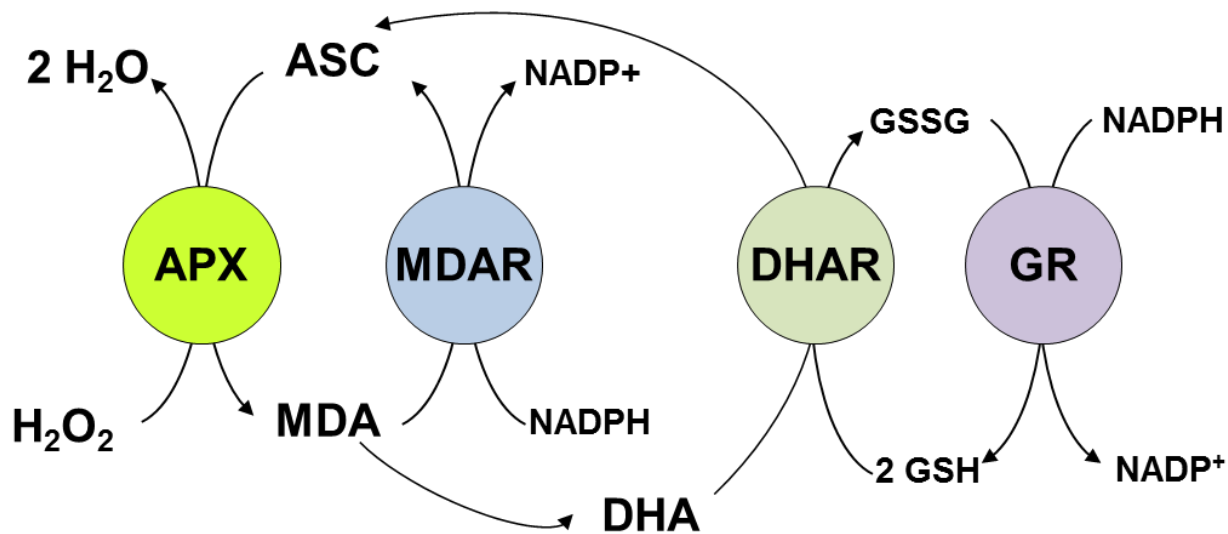


Figure 3 : Représentation schématique du cycle Ascorbate/Glutathion (ASC/GSH) chez les organismes photosynthétiques.

APX: Ascorbate peroxydase; ASC: Ascorbate; MDA: Monodéshydroascorbate, MDAR: Monodéshydroascorbate réductase; NADP^{+/H}: Nucléotide adénosine phosphate oxydé/réduit; DHA: Déshydroascorbate; DHAR: Déshydroascorbate réductase; GSH/GSSG: Glutathion réduit/oxydé; GR: Glutathion réductase.

NO pourra former du peroxynitrite (ONOO⁻) par réaction avec O₂^{•-}) (Gupta et al., 2011) ou du S-nitrosoglutathion (GSNO) lorsqu'il est combiné avec du glutathion réduit (GSH/GS[•]). Ces deux molécules peuvent réagir avec les résidus cystéinyls des protéines provoquant leur S-nitrosylation (voir partie 3) mais aussi dans le cas d'ONOO⁻ provoquer la nitration de tyrosines, ce qui peut avoir des conséquences importantes notamment pour la phosphorylation des protéines (Figure 2).

2. Les systèmes de protection contre les espèces réactives

2.1. Les systèmes non enzymatiques

Les molécules anti-oxydantes les plus importantes sont l'ascorbate (ASC), le glutathion (GSH), les caroténoïdes et l' α -tocophérol. Ce dernier est présent au niveau des membranes et il est notamment important pour contenir la peroxydation lipidique en donnant un atome d'hydrogène aux lipides radicalaires. La régénération du radical α -tocophéryl formé suite à cette réaction sera assurée par l'ascorbate. Les caroténoïdes présents dans le chloroplaste sont importants pour neutraliser la production d'¹O₂ produit en cas de stress photooxydant. Les deux caroténoïdes présents au niveau du centre réactionnel du PSII peuvent réagir directement avec l'¹O₂. Les produits de d'oxydation/dégradation de ces molécules constituent des molécules de signalisation pour la mise en place d'une réponse physiologique adaptée (Havaux, 2014). Par ailleurs, les xanthophylles participent au quenching non-photochimique (Pinnola and Bassi, 2018; Ruban, 2016). Suite à un changement de structure (passage de formes violaxanthine à anthérazanthine puis zéaxanthine), ces pigments associés à l'antenne du PSII permettent une dissipation sous forme de chaleur de l'excès d'énergie lumineuse reçue en réagissant avec la chlorophylle excitée. Une des enzymes impliquées, la violaxanthine dé-époxydase, utilise le pouvoir réducteur de l'ascorbate. En plus des rôles déjà évoqués, l'ASC est également crucial en tant que cofacteur des ascorbate peroxydases qui réduisent H₂O₂ en H₂O (voir section suivante). Toutes ces réactions conduisent à la formation de déhydroascorbate (DHA) et monodéhydroascorbate (MDHA), ces formes oxydées étant recyclées en ASC par le cycle ASC/GSH (Figure 3). Celui-ci comprend trois enzymes présentes dans différents compartiments subcellulaires sous forme d'isoenzymes. Les déhydroascorbate réductases (DHAR) qui réduisent le DHA en ASC au dépend du GSH formant ainsi du glutathion disulfure (GSSG) ; les NADPH-glutathion réductases (GR) qui régénèrent le GSH et les NADPH-monodéhydroascorbate réductases (MDHAR) qui réduisent le

MDHA en ASC. Le GSH et l'ASC sont présents à des concentrations relativement élevées de l'ordre du mM dans la plupart des compartiments subcellulaires (Calabrese et al., 2017; Foyer and Noctor, 2011; Kojer et al., 2012; Meyer et al., 2019a; Mittler et al., 2004; Noctor et al., 2012; Queval et al., 2011; Schafer and Buettner, 2001). En plus de contribuer au recyclage de l'ASC, le GSH intervient dans une multitude de processus, étant le plus abondant des composés thiol à faible poids moléculaire. Il est important pour la détoxication des ROS, directement en réagissant avec certaines molécules, notamment H_2O_2 , ou comme réducteur de PRX dépendantes du GSH ou des GRXs. Il est le précurseur via la phytochélatine synthase (PCS1) de la synthèse de phytochélatines (PCs), molécules qui contribuent à la détoxication des métaux lourds tels que le cadmium, le nickel, le mercure, ou l'arsenic (Cazalé and Clemens, 2001; Freeman et al., 2004; Howden and Cobbett, 1992). Le complexe PC-métal est normalement séquestré au sein de la vacuole et des γ -glutamyl transpeptidases permettent le recyclage du GSH (Grzam et al., 2007). La conjugaison de GSH à des molécules toxiques est également utilisée pour la détoxication de composés électrophiles tel que les xénobiotiques. Cette réaction, dite de conjugaison est catalysée par des glutathion S-transférases (GSTs) et plus précisément par les classes phi ϕ (phi) et τ (tau) (Dixon and Edwards, 2010; Dixon et al., 2002; Sylvestre-Gonon et al., 2019). Après conjugaison, le complexe GSH-xénobiotique est ensuite dirigé vers la vacuole via un transporteur ATP dépendant et enfin dégradé (Foyer and Noctor, 2011; Rouhier et al., 2008). Le GSH intervient également dans divers processus biologiques comme la transition du cycle cellulaire des stades G1/S durant le développement post-embryonnaire racinaire (Vernoux et al., 2000), la différenciation des trachéides au sein du xylème (Henmi et al., 2005), la signalisation hormonale lors de l'interaction plante-pathogène (Ball et al., 2004; Maughan et al., 2010; May et al., 1996) ou encore l'accumulation d'anthocyanes au niveau de la vacuole (Xiang et al., 2001).

Le GSH est synthétisé par deux enzymes dépendantes de l'ATP, la γ -EC synthase (GSH1) et la glutathion synthase (GSH2). Chez les organismes photosynthétiques, la première de ces enzymes est uniquement située au sein du chloroplaste alors que la seconde est également présente au niveau du cytosol. Sa biosynthèse est finement régulée par un rétrocontrôle assuré par le GSH, qui réduit un pont disulfure au niveau d'un homodimère de GSH1 pour l'inactiver (Hothorn et al., 2006). Des glutathion réductases (GR) sont retrouvées après double adressage au sein des chloroplastes, des mitochondries, des peroxysomes et du cytosol et assurent la réduction du GSSG, forme généralement très minoritaire, retrouvée à faible concentration. Dans un milieu

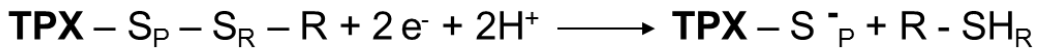
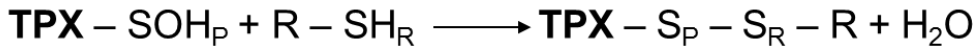
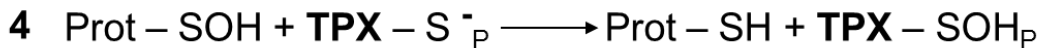
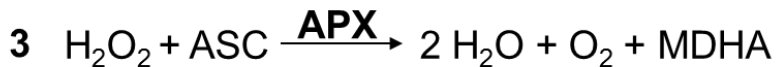
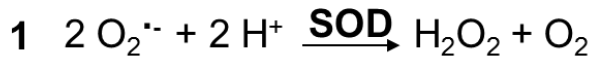


Figure 4: Réactions enzymatiques permettant la réduction d' H_2O_2 en H_2O . Les réactions peuvent être dépendantes de la présence d'un ion métallique comme dans le cas des superoxydes dismutases (SOD) (1), catalases (CAT) (2) ou ascorbate peroxydases (APX) (3). Elles peuvent également être dépendantes d'une ou plusieurs cystéines dans le cas des protéines de la famille des thiol-peroxydases: TPX (4).

aqueux le GSH est donc quand même en permanence accompagné de sa forme oxydée formant le couple GSH/GSSG. Ces deux formes redox permettent de maintenir un environnement plus ou moins réducteur au sein des différents compartiments subcellulaires. Il est estimé aux alentours de -300 mV dans le cytosol, -225 mV dans le RE et -360 mV dans le peroxysome (Schwarzländer et al., 2008). Dans le chloroplaste, il varie de -350 mV et -306 mV en fonction du cycle jour/nuit (Schnaubelt et al., 2015; Smirnoff and Arnaud, 2019). Au sein de la mitochondrie peu d'études ont été réalisées chez les organismes photosynthétiques et la majorité des données obtenues concernent la levure *S. cerevisiae*.

2.2 Les systèmes enzymatiques

Outre les enzymes participant au cycle ASC-GSH plusieurs familles d'enzymes, dont certaines déjà mentionnées, interviennent activement dans le contrôle des niveaux d' H_2O_2 et d' $O_2^{\bullet-}$. Concernant les SODs, trois classes peuvent être distinguées chez les plantes en fonction des ions métalliques associés mais toutes ces enzymes réduisent deux molécules d' $O_2^{\bullet-}$ en H_2O_2 et O_2 (Figure 4) (Gill et al., 2015). Les Mn-SODs sont retrouvées dans les mitochondries, les Fe-SODs dans les plastes, les Cu/Zn-SODs au niveau du cytosol, des plastes, du peroxysome et de l'espace extracellulaire. Si chez la levure la présence d'une Cu/ZnSOD a été clairement établie au sein de l'IMS, ce n'est peut-être pas le cas chez *A. thaliana* (Huang et al., 2012; Riemer et al., 2015). Chez *A. thaliana*, il existe 7 SODs au total, 1 Mn-SOD, 3 Fe-SOD et 3 Cu/Zn-SOD (Kliebenstein et al., 1998).

Une diversité plus importante existe au niveau des peroxydases qui interviennent dans la réduction d' H_2O_2 mais aussi de peroxydes plus complexes formés notamment au niveau des membranes par peroxydation lipidique et de peroxynitrite. En effet, les catalases (CATs), ascorbate peroxydases (APXs), peroxyrédoxines (PRXs), glutathion peroxydases-like (GPXs-like) et certaines glutathion transférases (GSTs) possèdent une activité peroxydase et font partie de familles multigéniques. Les CAT sont localisées dans les peroxysomes et sont les peroxydases majeures de ce compartiment (Mhamdi et al., 2010), même si les GST théta et au moins une APX sont présentes dans ce compartiment (Dixon et al., 2009). Ce sont des hémoprotéines, l'hème permettant la réduction d' H_2O_2 en H_2O et O_2 (Figure_4) (Gill et al., 2015). Chez *A. thaliana*, il

Propriétés	Oxygène singulet (${}^1\text{O}_2$)	Anion superoxyde ($\text{O}_2^{\cdot-}$)	Peroxyde d'hydrogène (H_2O_2)	Radical hydroxyle (OH^{\cdot})
Temps de demi-vie	1 µs	1 µs	1 ms	1 ns
Distance parcourue	30 nm	30 nm	1 µm	1 nm
Concentration cellulaire	?	?	µM-mM ²	?

Tableau 1: Persistance des principaux ROS dans les cellules. Le temps de demi-vie, la distance parcourue et la concentration cellulaire (connus ou présumés) sont indiqués pour ${}^1\text{O}_2$, $\text{O}_2^{\cdot-}$, H_2O_2 et OH^{\cdot} . D'après Möller et al., 2007.

existe 3 catalases. Les APXs sont également des hémoprotéines, elles catalysent la réduction d' H_2O_2 en H_2O (Figure 4) aux dépens de l'ascorbat libérant du MDHA qui sera par la suite recyclé par le cycle ASC-GSH. Il existe 7 APXs chez *A. thaliana* présentes au niveau du cytosol, de la mitochondrie, du chloroplaste et du peroxysome (Jespersen et al., 1997; Lisenbee et al., 2003; Mullen et al., 1999; Pandey et al., 2017; Shigeoka et al., 2002). Les PRXs et GPXs-like sont des peroxydases thiol-dépendante (TPX) c'est-à-dire que leur mécanisme réactionnel dépend d'au moins une cystéine catalytique et non plus d'un hème. Cette cystéine catalytique conservée (appelée aussi cystéine peroxydatique) est située dans la partie N-terminale et permet la réduction d' H_2O_2 en H_2O (Figure 4) mais aussi de peroxydes plus complexes en alcool voire de peroxynitrite pour certaines (Rouhier and Jacquot, 2005). Cette réaction résulte en la formation d'un acide sulfénique qui réagira le plus souvent avec une seconde cystéine dite cystéine de recyclage pour former un pont disulfure. Il existe 9 PRXs chez *A. thaliana* regroupée en 4 classes (2Cys-PRX, 1Cys-PRX, PRX de type II et PRXQ) qui diffèrent par le nombre et la position des cystéines impliquées dans le mécanisme catalytique et la formation d'un pont disulfure intra- (PRXQ) ou intermoléculaire (2Cys-PRX), y compris avec le GSH par exemple dans le cas des PRX de type II ou des 1Cys-PRX (Rouhier and Jacquot, 2005; Rouhier et al., 2001). Les adduits glutathion seront préférentiellement réduits par les GRXs et les ponts disulfure par les TRXs. Contrairement à leur appellation, les GPXs-like possèdent un mécanisme catalytique comparable à celui des PRX Q avec formation d'un pont disulfure intramoléculaire régénéré par les TRXs (Herbette et al., 2002; Lee et al., 2002; Navrot et al., 2006). Cette classification provient du fait qu'elles ont une identité de séquence forte avec les GPX animales qui contiennent pour la plupart une sélénocystéine à la place de la cystéine peroxydatique qui les rendent effectivement dépendantes du GSH.

Pour finir, il est important de noter que des GSTs appartenant à plusieurs classes (Zeta, Phi, Theta, Tau), en tout plusieurs dizaines d'isoformes, possèdent une activité peroxydase GSH-dépendante avec des peroxydes complexes mais en général pas avec H_2O_2 (Dixon et al., 2009; Sylvestre-Gonon et al., 2019). Bien que leur efficacité catalytique soit la plupart du temps inférieure à celles des autres peroxydases à hème ou à thiol, cela pourrait être compensé par une forte expression des protéines, notamment en conditions de stress. De plus, elles ont cette spécificité de dépendance au GSH qui n'est partagée que par certaines PRX de type II chez les plantes, la plupart nécessitant également une GRX (Rouhier and Jacquot, 2005).

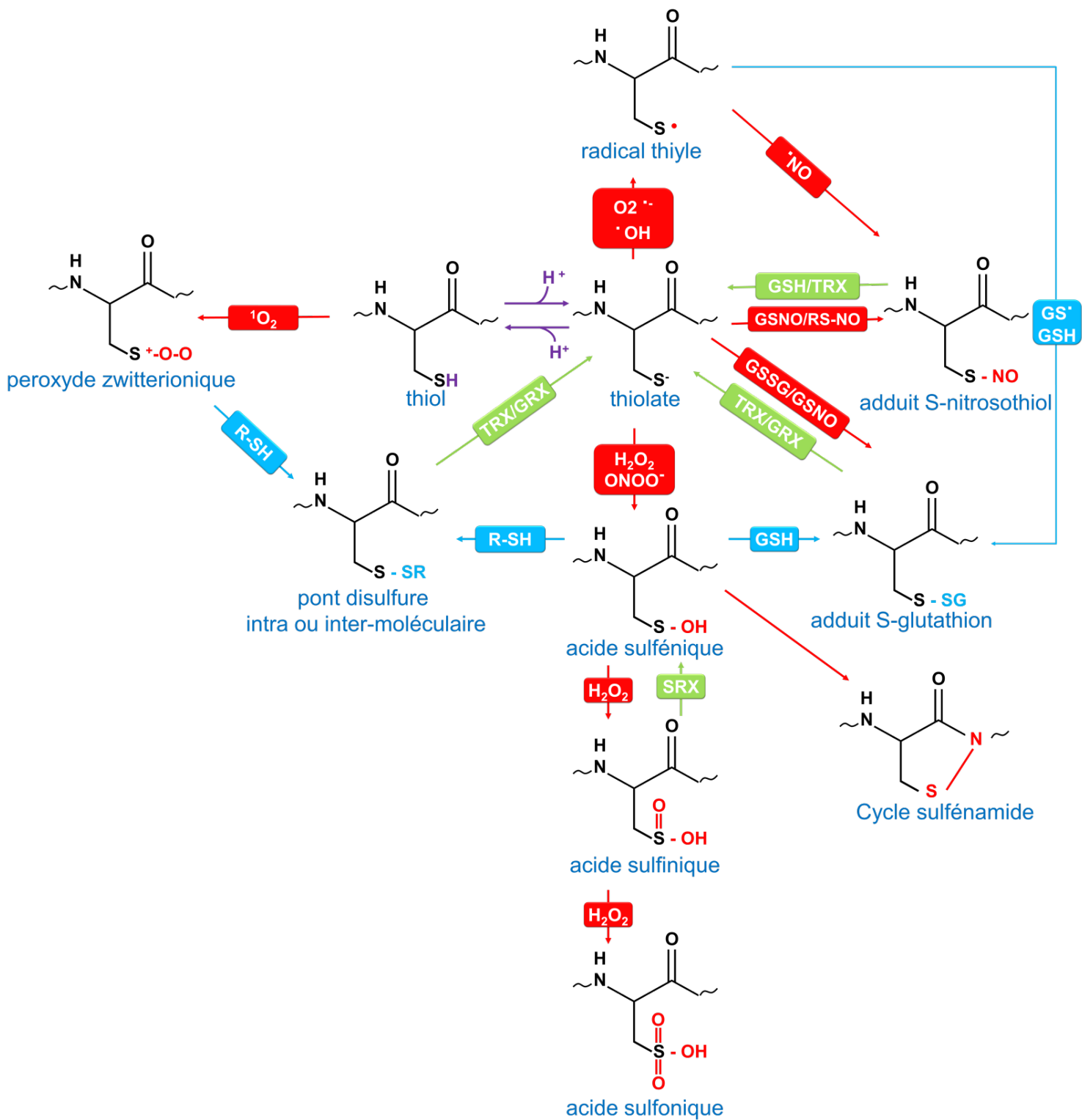


Figure 5: Représentation schématique des principales modifications post-traductionnelles subies par les fonctions thiol et thiolate des cystéines. Les molécules oxydantes ainsi que les modifications post-traductionnelles associées sont représentées en rouge. Les molécules intervenant dans l'inter-conversion des PTMs sont indiquées en bleu et les systèmes de réduction qui permettent la régénération des cystéines oxydées sont représentés en vert. Adapté de Zaffagnini et al., 2019.

3. Modifications post-traductionnelles (MPT) des cystéines par les ROS et les RNS

La plupart des espèces radicalaires (notamment $\cdot\text{OH}$) et l'oxygène singulet présentent une durée de demi-vie très courte et une diffusion limitée du fait de leur réactivité. Elles vont interagir et oxyder la plupart des macromolécules présentes à proximité, en particulier les lipides, les acides nucléiques ou les protéines (Figure 2 et Tableau 1). Les autres molécules sont globalement moins réactives et plus sélectives. L'anion superoxyde réagit préférentiellement avec les hèmes et les centre Fe-S, $\text{L'}\text{H}_2\text{O}_2$ oxyde préférentiellement les protéines et plus particulièrement les acides aminés soufrés, méthionines et cystéines. L'oxydation des méthionines par H_2O_2 produit des méthionine sulfoxydes qui peuvent être réduites par des méthionine sulfoxyde réductases (MSR), des enzymes thiol-dépendantes qui utilisent la chimie des acides sulféniques et des mécanismes réactionnels comparables à ceux utilisés par les PRXs et GPXs-like (Rey and Tarrago, 2018). Dans ce chapitre, je vais uniquement me focaliser sur les modifications oxydatives des cystéines par les ROS et RNS (Figure 5) (Couturier et al., 2013b). Les cystéines peuvent ainsi être modifiées par réactions peu ou pas spécifiques avec des espèces radicalaires ($\text{O}_2^{\bullet-}$ et OH^{\bullet}) formant un radical thiyl, qui deviendra lui-même capable de réagir avec le NO formant un groupement S-nitrosothiol ou éventuellement un glutathion radicalaire (GS^{\bullet}) par exemple formant un adduit S-glutathion (Zaffagnini et al., 2016b). $\text{L}'\text{O}_2$ peut en principe réagir avec les groupements thiols des cystéines générant un peroxyde zwitterionique (RS^+-OO^-) qui sera rapidement décomposé en cystines, thiosulfinates voire modifié en acide sulfonique en absence de cystéine capable de réagir avec cet intermédiaire (Pattison et al., 2012).

Toutefois, étant relativement stable et modérément réactif avec les autres molécules et acides aminés, le peroxyde d'hydrogène (et d'autres peroxydes sans doute) est la molécule qui doit oxyder préférentiellement et spécifiquement les cystéines. Dans un premier temps, la réaction entre un groupement thiolate des cystéines et H_2O_2 (et le peroxynitrite également) forme un acide sulfénique (S-OH) qui sera à l'origine de plusieurs autres modifications post-traductionnelles. S'il réagit séquentiellement avec d'autres molécules d' H_2O_2 des acides sulfinique ($\text{S-O}_2\text{H}$) puis sulfonique ($\text{S-O}_3\text{H}$) seront formés. Si l'on excepte le cas des PRXs où un acide sulfinique formé au niveau de la cystéine peroxydatique peut être réduit en acide sulfénique par les sulfirédoxines (SRX) (Biteau et al., 2003), ces formes d'oxydation sont *a priori* irréversibles. Par réaction avec un thiol, l'acide sulfénique sera converti en pont disulfure intramoléculaire si la cystéine est

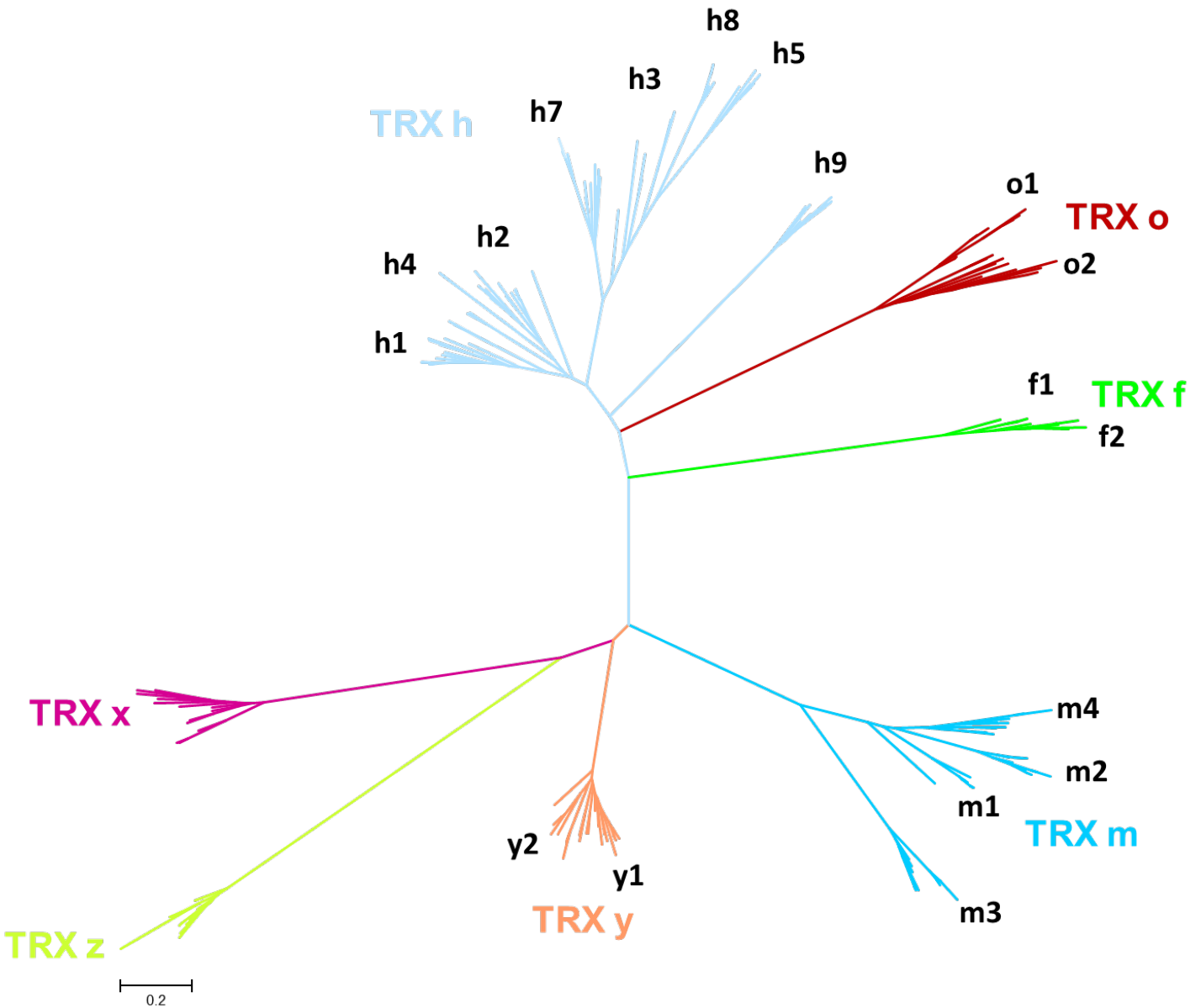


Figure 6: Arbre phylogénétique des différentes isoformes de TRXs comportant un motif WC[G/P]GC chez les plantes terrestres. Cette analyse phylogénétique a été réalisée en utilisant le logiciel MEGA7. L'histoire évolutive a été déterminée en utilisant la méthode Neighbor-Joining et les distances évolutives sont basées sur l'analyse des matrices selon la méthode de Jones, Taylor & Thornton (JTT).

située au sein de la même protéine, ou intermoléculaire si la cystéine est présente au niveau d'une autre protéine. S'il s'agit d'une cystéine libre ou de la cystéine d'un glutathion, on parlera de S-thiolation ou S-glutathionylation. C'est probablement la voie majeure permettant la S-glutathionylation des protéines mais il est utile de mentionner que le GSNO ou le GSSG, seul ou par l'intermédiaire des GRXs, pourraient constituer au moins dans certaines circonstances des voies non-négligeables. En absence de thiol à proximité, l'acide sulfénique pourra par exemple réagir avec un groupement amide de la chaîne principale adjacente par attaque électrophile sur l'atome azote formant un cycle sulfénamide à cinq membres (aussi appelé sulfénylamide) comme démontré initialement pour la phosphatase PTP1B (Salmeen et al., 2003). Outre des fonctions régulatrices et de signalisation, ces modifications permettent de protéger des cystéines réactives, catalytiques ou exposées, d'une oxydation irréversible qui pourrait intervenir lors d'épisodes de stress oxydatif.

Alors que les études protéomiques indiquent que plusieurs cystéines sont nitrosylées au sein de nombreuses protéines, les molécules à l'origine de cette modification post-traductionnelle ne sont pas toujours précisément définies (Hu et al., 2015; Morisse et al., 2014). Le $\bullet\text{NO}$ étant un radical relativement peu réactif, la S-nitrosylation des protéines se produit via des espèces moléculaires dérivées plus réactives formées dans la cellule telles que des oxydes d'azote (NO_2 et N_2O_3), mais aussi par l'intermédiaire du GSNO ou de protéines déjà nitrosylées par des réactions de trans-nitrosylation (Zaffagnini et al., 2016b). De la même manière les études protéomiques récentes indiquent que plusieurs centaines de protéines sont persulfurées/persulfidées, y compris chez les plantes (Aroca et al., 2017). Cependant, il n'est pas non plus clair de savoir quelles espèces réactives du soufre sont impliquées (Mishanina et al., 2015). Cet aspect de persulfidation n'est pas détaillé dans la figure 5 ni le texte. Néanmoins, ces modifications sont à considérer dans cet ensemble de MPTs redox car elles peuvent d'une part interférer avec les autres modifications en ciblant les mêmes cystéines ou se produire séquentiellement après les autres MPTs en fonction du type de molécules produites/signal émis.

4. Les systèmes de réduction contrôlant ces MPTs

La durée de vie (formation et réduction) de ces MPTs redox est contrôlée majoritairement et directement par deux familles d'oxydoréductases, les thiorédoxines et les glutarédoxines (figure 5). Ce sont généralement des petites protéines (aux alentours de 10-15 kDa) qui adoptent un

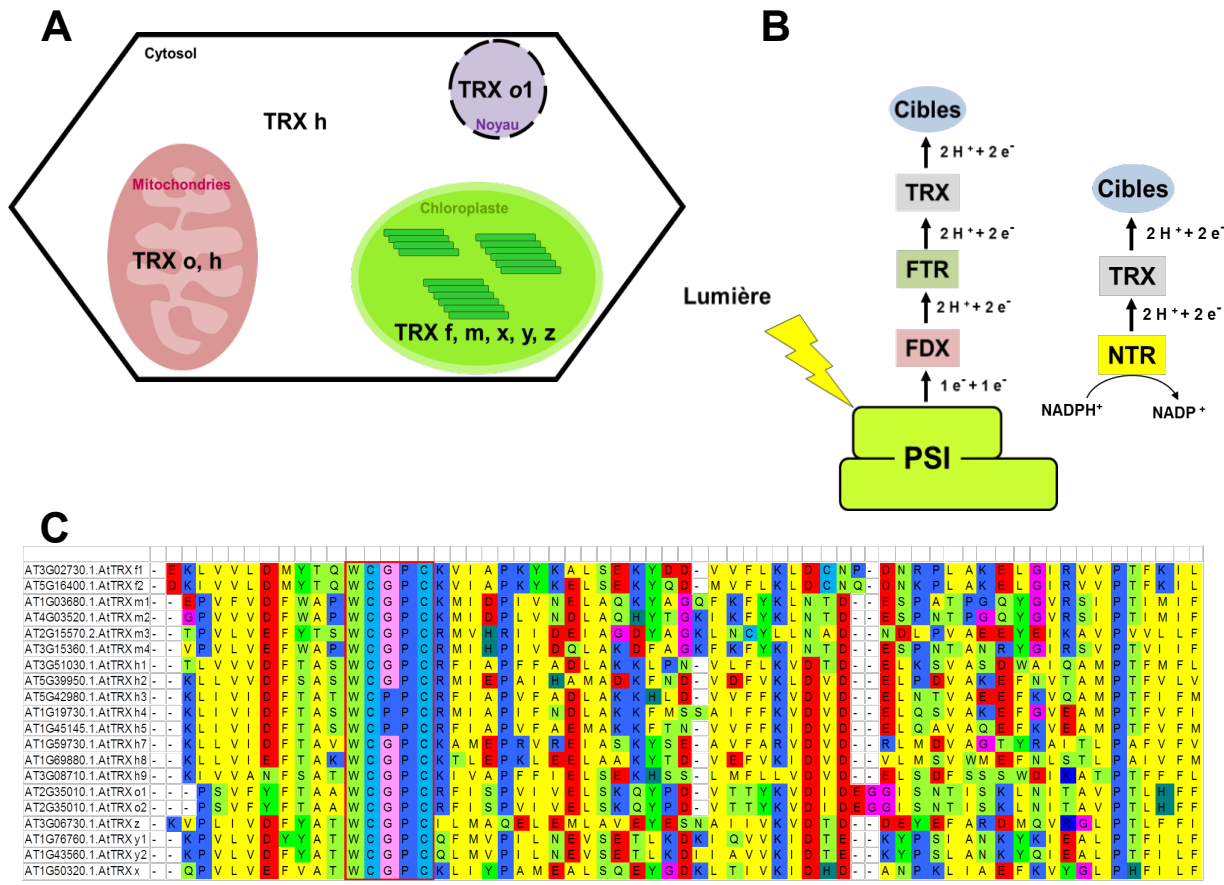


Figure 7 : Caractéristiques majeures des TRXs typiques présentes chez les plantes terrestres.

(A) Répartition subcellulaire des TRXs h, m, f, x, y, z et o chez les plantes terrestres. (B) Représentation schématique des deux principales voies de réduction des TRXs chez les organismes photosynthétiques. Dans le cas de la voie Ferrédoxine/Ferrédoxine-Thiorédoxine Réductase/Thiorédoxine (FDX/FTR/TRX), le pouvoir réducteur provient directement de l'énergie lumineuse via le photosystème I (PSI) alors que pour la voie NADPH Thiorédoxine Réductase/thiorédoxine (NTR/TRX), le pouvoir réducteur provient du NADPH.

(C) Conservation des résidus entourant le signature WC[G/P]GC des différentes isoformes de TRXs chez *A. thaliana*. L'alignement a été généré par l'algorithme MUSCLE du logiciel MEGA7.

repliement typique comportant un feuillet β central composé de quatre brins β entourés de trois à cinq hélices α . Elles sont retrouvées au sein de tous les règnes du vivant mais ces systèmes sont particulièrement développés chez les organismes photosynthétiques.

Concernant les TRXs, pas moins de 37 isoformes ont été dénombrées chez *A. thaliana* (Chibani et al., 2009). On distingue les TRXs typiques avec des signatures catalytiques de type WC[G/P]PC, des TRXs atypiques dans lesquelles cette signature varie, WCR[V/K]C dans les TRXs-like et W/G/S]C[A/G][G/]C dans les TRXs-lilium (Chibani et al., 2009). Les analyses phylogénétiques ont permis de mettre en évidence 7 classes différentes de TRXs typiques (Figure 6), TRX f, m, z, x, y, h et o, qui présentent des localisations subcellulaires variées (Figure 7A) (Gelhaye et al., 2005). Il faut ajouter la NTRC chloroplastique qui est une protéine chimère formée d'un domaine NADPH-thiorédoxine-réductase (NTR) couplé à un domaine TRX typique. Dans le paragraphe à venir, je ne me focaliserai que sur les TRXs typiques possédant donc un site actif WC[G/P]PC que l'on peut regrouper dans un même clade (Figure 7C) (Gelhaye et al., 2004). Alors que l'activité de la NTRC est dépendante du NADPH et indépendante (au moins directement) de la présence de lumière, les autres TRXs présentes au sein du chloroplaste, sont maintenues réduites par la voie ferrédoxine/ferrédoxine-thiorédoxine réductase (FDX/FTR), la réduction des FDXs étant directement dépendante du PSI et donc du flux d'électrons linéaire chloroplastique. Ce système est donc à la base de la régulation diurnale d'un grand nombre d'enzymes du métabolisme carboné notamment celles du cycle de Calvin-Benson. Il a été démontré, il y a de cela plusieurs décennies, que l'activité de la phosphoribulokinase (PRK), glyceraldéhyde-3-phosphate déshydrogénase (GAPDH), fructose-1,6-bisphosphatase (FBPase) et sédoheptulose-1,7-bisphosphatase (SBPase) est contrôlée par les TRXs (Buchanan and Luan, 2005; Gütle et al., 2016, 2017; Lemaire et al., 2007; Schürmann and Buchanan, 2008). La réduction des TRXs cytosolique et mitochondriale s'opère via deux NTRs chez *A. thaliana* appelées NTRA et NTRB (Figure 7C).

Concernant les GRXs, 30 à 40 isoformes sont généralement recensées chez les plantes, avec des sites actifs très variables par rapport au motif YCPYC retrouvé initialement dans les isoformes d'*E. coli* par exemple et qui a été longtemps pris comme référence (Alves et al., 2009; Couturier et al., 2009). En réalité, une séquence consensus de type Cxx[C/S]x₃₅₋₄₀TVPx₈₋₁₀GG, qui comprend le site actif lui-même (Cxx[C/S]) et les résidus impliqués dans la fixation du GSH (TVPx₈₋₁₀GG), permet plutôt de définir ce qu'est un domaine GRX (Couturier 2009). Cela a

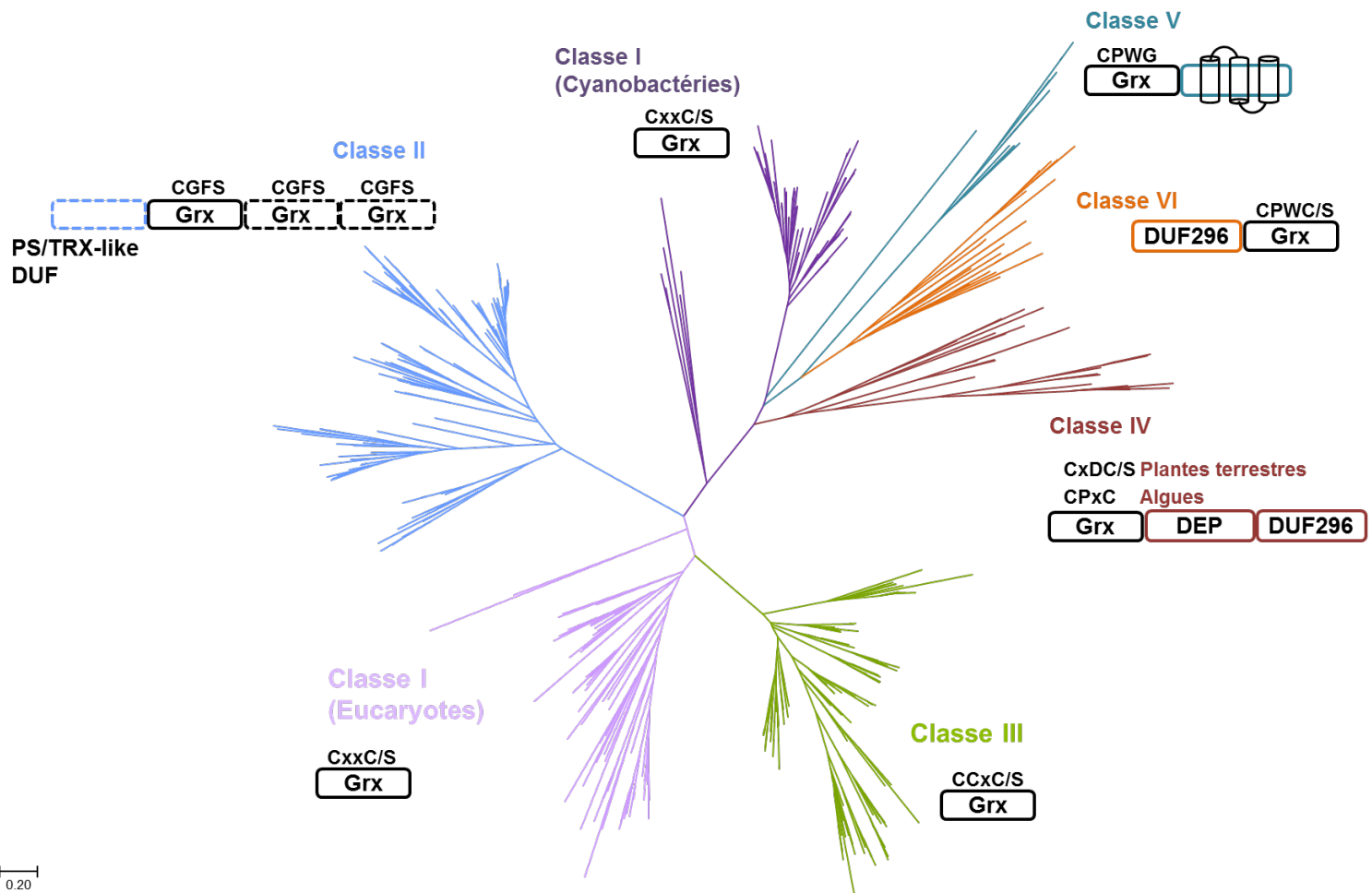


Figure 8: Analyse phylogénétique et organisation structurale des GRXs présentes chez les organismes photosynthétiques. La signature catalytique conservée de chaque classe est indiquée au-dessus des domaines GRX. Les classes I et II sont présentes chez tous les organismes photosynthétiques. Les GRXs de classe I possèdent un seul domaine, alors que l'architecture des GRXs de classe II est très variable, certaines isoformes ayant plusieurs domaines de fonctions distinctes. Les classes III et IV sont respectivement spécifiques aux plantes supérieures et aux organismes eucaryotes. Les GRXs de classe IV comportent deux domaines additionnels (DEP et DUF547) dont la fonction est inconnue. Les GRXs des classes V et VI sont spécifiques aux cyanobactéries et contiennent deux modules. Le motif catalytique de leur domaine GRX (CPWC/S et CPWG respectivement) est spécifique à ces classes. Les GRXs de classe VI comportent également un domaine dont la fonction est inconnue (DUF296). L'analyse phylogénétique a été réalisée en utilisant le logiciel MEGA7. L'histoire évolutive a été déterminée en utilisant la méthode Neighbor-Joining et les distances évolutives sont basées sur l'analyse des matrices selon la méthode de Jones, Taylor & Thornton (JTT).

permis d'établir une classification des GRXs chez les organismes photosynthétiques eucaryotes et procaryotes en 6 classes (Figure 8) (Couturier et al., 2009). Les classes I et II sont communes à la majorité des organismes vivants, procaryotes et eucaryotes. La classe I regroupe principalement des GRXs "dithiol" avec un site actif CP[Y/F]C et la classe II comprend des GRXs dites "monothiol" ayant un site actif conservé de type CGFS (Alves et al., 2009). Les GRXs de classe III sont spécifiques aux plantes terrestres et possèdent un site actif particulier CCxx. La classe IV, présente chez les eucaryotes photosynthétiques regroupe quant à elles des protéines présentant un module GRX fusionné à deux autres modules aux fonctions inconnues. Enfin, les classes V et VI sont uniquement présentes chez les cyanobactéries et regroupent également des protéines multi-modulaires donc la fonction est encore inconnue (Couturier et al., 2009). La majorité des GRXs de classe I sont dépendantes du glutathion bien qu'il ait été démontré que certaines peuvent être réduites par des TRX réductases (Fernandes et al., 2005; Johansson et al., 2004; Zaffagnini et al., 2008). Ainsi, lorsque les GRXs sont réduites par le GSH, il y a formation concomitante de GSSG. Ce dernier sera alors recyclé par les GRs. On parle du système de réduction GSH/GRX. Les GRXs de classe II sont requises pour la maturation des protéines Fe-S à travers leur capacité à lier et transférer des centres Fe-S (Couturier et al., 2015; Rouhier et al., 2007). Il est généralement considéré qu'elles n'ont pas ou peu d'activité oxydoréductase. Les GRXs de classe III sont capables de lier des centres Fe-S et possèdent une activité oxydoréductase *in vitro*, mais plus faible que celle des GRXs de classe I (Couturier et al., 2010). Il n'est pas clair si ces propriétés sont requises pour la régulation des facteurs de transcription TGA qui ont des fonctions importantes dans le développement des plantes mais aussi pour certaines dans la réponse aux stress (Gutsche et al., 2015). Au niveau biochimique, il n'est pas toujours aisés de distinguer des TRXs et des GRXs sans doute à cause de leur origine commune et de variations importantes dans les propriétés qui sont apparues au cours du temps. Néanmoins, on peut considérer que les TRXs sont plutôt impliquées dans la réduction des ponts disulfure, les GRXs réduisent préférentiellement les protéines glutathionylées et le GSH les protéines nitrosylées. Il est néanmoins surprenant par exemple, et cela complique le tableau, que les TRXs réduisent aussi un certain nombre de protéines nitrosylées. Les deux systèmes TRX et GSH/GRX semblent également participer au contrôle de la persulfidation (Dóka et al., 2016).

Les TRXs permettent la réduction des ponts disulfures selon un mécanisme dithiol (Figure 9A). La première cystéine du motif WC[G/P]PC réalise une attaque nucléophile sur le pont disulfure

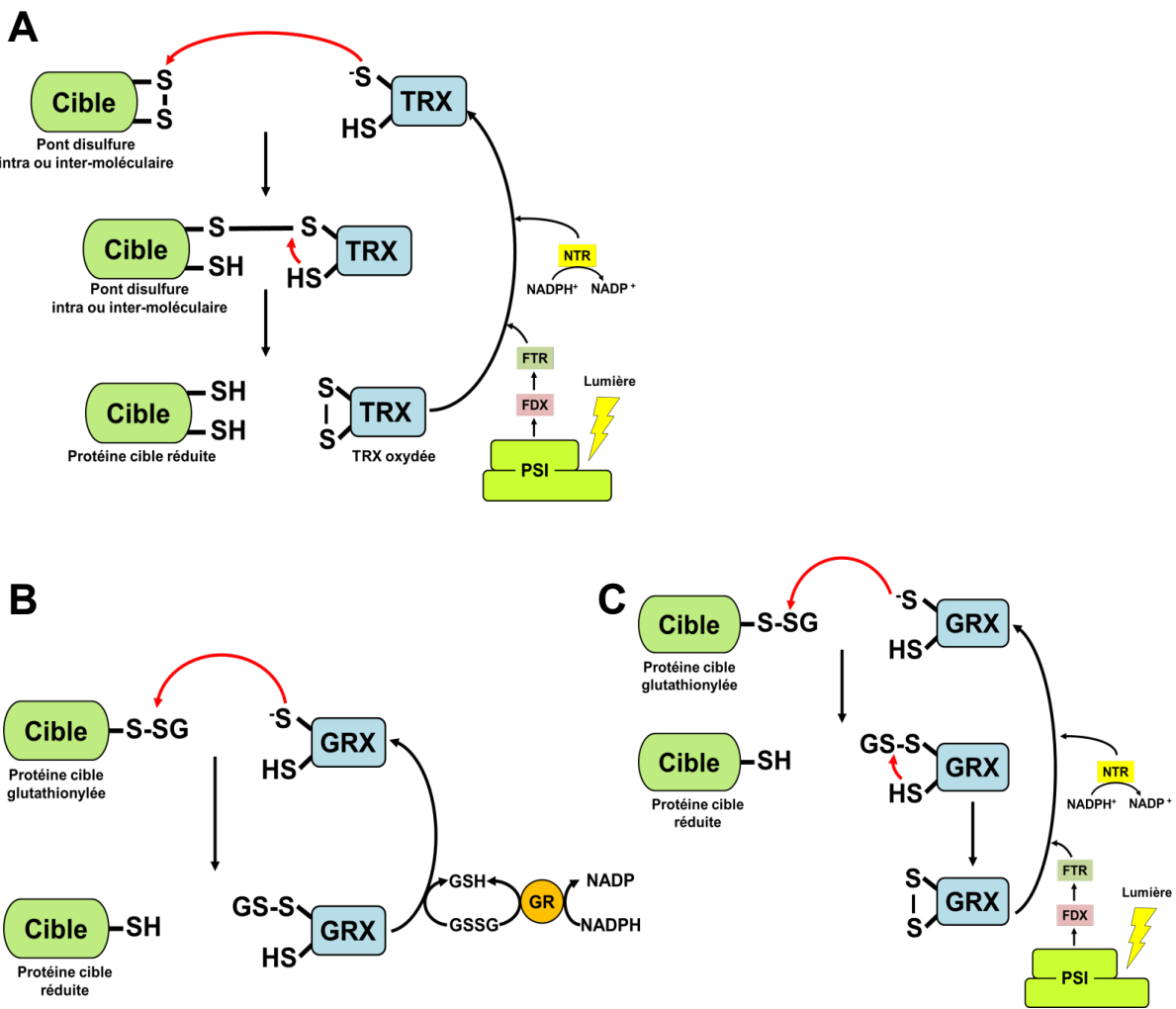


Figure 9 : Représentation schématique du mécanisme catalytique dithiol des TRXs (A) et des mécanismes de réduction de type monothiol (B) et dithiol (C) des GRXs. Pour les TRXs, la cystéine catalytique du site actif ($\text{TRX}-\text{S}^-$) réalise une attaque nucléophile sur le pont disulfure inter ou intra-moléculaire de la protéine cible. Un hétérodimère covalent est alors formé entre la TRX et la protéine cible ($\text{TRX}-\text{S}-\text{S}-\text{Cible}$). Ce dernier est résolu via la cystéine de recyclage (en C-terminal du motif CxxC). La TRX oxydée (pont disulfure intramoléculaire) est recyclée par les systèmes FDX/FTR ou NTR dont le pouvoir réducteur provient respectivement du PSI ou du NADPH. Pour les GRXs, dans les deux mécanismes, dits monothiol ou dithiol, la cystéine catalytique du site actif de la GRX ($\text{GRX}-\text{S}^-$) réalise une attaque nucléophile sur l'adduit glutathion de la protéine glutathionylée (cible-S-SG), conduisant à la libération de la protéine réduite (cible-SH) et de la GRX sous forme oxydée ($\text{GRX}-\text{S}-\text{SG}$). Pour le mécanisme monothiol, la GRX est ensuite régénérée par l'action d'une molécule de GSH qui donnera une molécule de GSSG, elle-même réduite par la Glutathion Réductase (GR) NADPH-dépendante. Pour le mécanisme dithiol, l'adduit GSH présent sur la $\text{GRX}-\text{S}-\text{SG}$ est éliminé par l'action d'une seconde cystéine dit de recyclage, menant à la formation d'un pont disulfure. Ce dernier est ensuite réduit par les systèmes FDX/FTR ou NTR.

de la protéine cible. Cela conduira à la formation d'un complexe covalent entre la TRX et sa protéine cible via la présence d'un pont disulfure intermoléculaire. Ce dernier est très rapidement réduit par la seconde cystéine dite cystéine de recyclage et va aboutir à la formation d'un pont disulfure intramoléculaire sur les TRXs, réduit par les thiorédoxine réductases (Collin et al., 2003; Gelhaye et al., 2004, 2005; Jacquot et al., 2002a, 2002b; Marri et al., 2009; Rouhier et al., 2002; Sparla et al., 2005).

Les GRXs catalysent les réactions de déglutathionylation selon deux mécanismes, monothiol ou dithiol, la première étape étant commune aux deux mécanismes. Ainsi, la cystéine catalytique de la GRX réalise une attaque nucléophile du pont disulfure de la protéine cible glutathionylée, il en résulte la libération de glutathion ainsi que la réduction du substrat (protéine-SH) et la formation d'un intermédiaire GRX glutathionylée. Ensuite, dans le cas du mécanisme monothiol (Figure 9A), une seconde molécule de GSH permet de réduire l'intermédiaire réactionnel (GRX-SSG), libérant du GSSG et la GRX sous forme réduite. Dans le cas du mécanisme dithiol (Figure 9B), une seconde cystéine de la GRX va réagir avec la cystéine catalytique oxydée et conduire à la formation d'un pont disulfure intramoléculaire et la libération de GSH. La GRX est par la suite réduite soit, par l'action d'une thiorédoxine réductase soit par l'action successive de deux molécules de GSH. Il est important de mentionner que les GRXs avec un site actif dithiol (C_x_2C) peuvent potentiellement utiliser les deux mécanismes catalytiques (Couturier et al., 2013a).

IV. Le repliement oxydatif des protéines

Bien que les modifications oxydatives des protéines soient généralement perçues comme étant un phénomène délétère, leur oxydation et notamment la formation de ponts disulfure intra- ou intermoléculaires est parfois essentielle pour leur repliement structural et donc leur stabilité. Cela concerne par exemple les anticorps des cellules animales, des récepteurs membranaires, des hormones ou des protéines de réserve. Cette oxydation est catalysée et accompagnée par différents systèmes enzymatiques qui diffèrent selon leur localisation subcellulaire et leur origine évolutive. Néanmoins, ces systèmes présentent comme caractéristiques communes de recourir à (i) une oxydoréductase intervenant dans l'interaction et l'oxydation du substrat, (ii) une thiol oxydase permettant la régénération de l'oxydoréductase et enfin (iii) un accepteur final d'électrons.

1. Les protéines Dsb du système périplasmique bactérien

Le cytoplasme des bactéries possède un environnement réducteur. Les bactéries Gram positives ne présentant pas de périplasme à proprement parler, le repliement oxydatif concerne les protéines sécrétées. Ainsi, chez les actinobactéries, il est contrôlé par une oxydoréductase membranaire MdbA qui est maintenue oxydée par l'intermédiaire d'une vitamine K époxyde réductase (VKOR) (Luong et al., 2017; Reardon-Robinson and Ton-That, 2016). Chez les bactéries Gram négatives, la formation des ponts disulfures ainsi que leur isomérisation sont contrôlées au sein de l'espace périplasmique par les protéines Dsb (pour Disulfide bond), le couple DsbA/DsbB participant à l'oxydation des protéines périplasmiques ou secrétées et le couple DsbC/DsbD permettant l'isomérisation des ponts disulfure aberrants.

L'oxydoréductase DsbA est l'acteur principal permettant l'introduction de ponts disulfure au sein des protéines exportées par la machinerie Sec. Elle possède un repliement de type TRX ainsi qu'un site actif Cx₂C (C₃₀PHC₃₃ dans DsbA d'*E. coli*) présentant un potentiel redox relativement élevé de -122 mV à pH 7.0 favorable pour catalyser ces réactions d'oxydation (Ito and Inaba, 2008). Bien que les mécanismes moléculaires sous-jacents à la reconnaissance et à l'oxydation ne soient pas complètement élucidés, il semble clair qu'un patch de résidus hydrophobes situés à proximité du site actif joue un rôle prépondérant dans la reconnaissance et l'interaction avec les substrats mais aussi avec la thiol oxydase, DsbB, qui maintient DsbA oxydée (Grauschoff et al., 1995). La protéine DsbB est ancrée à la membrane interne via quatre hélices α avec deux boucles (P1 et P2) faisant face au périplasme (Inaba et al., 2006a). L'oxydation de DsbA est médiée par un pont disulfure impliquant deux cystéines présentes au niveau de la boucle P2 (Cys104-Cys130). La ré-oxydation de ce pont disulfure s'opère par transfert d'électrons vers un pont disulfure impliquant deux cystéines présentes au niveau de la boucle P1 (Cys41-Cys44) puis vers les ubiquinones et la cytochrome oxydase en condition aérobie (Inaba et al., 2006b). Ceci s'accompagne donc de la réduction d'une molécule d'oxygène en eau. En condition anaérobie, les électrons sont transférés à une molécule de ménquinone qui va permettre la réduction de fumarate en succinate (Bader et al., 1999). Pour des substrats possédant plusieurs cystéines et ne formant pas des ponts disulfures entre cystéines consécutives ou lors de conditions de stress qui perturbent l'homéostasie redox du périplasme, des ponts disulfure aberrants peuvent être intégrés dans la protéine cible.

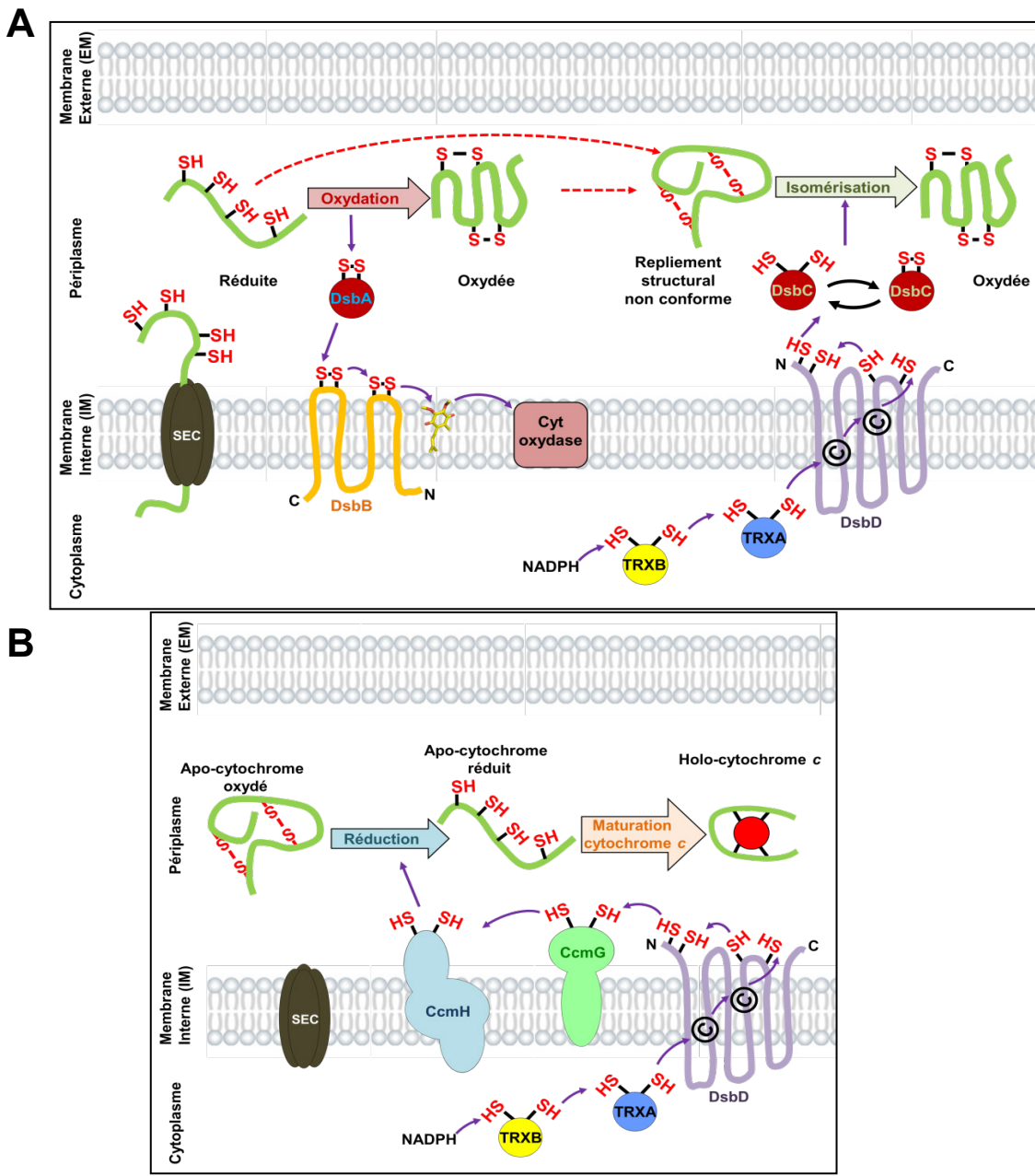


Figure 10: Représentation schématique du système de repliement oxydatif catalysé par les protéines Dsb et du système de réduction permettant la réduction de l'apo-cytochrome *c* au niveau du périclasse des bactéries Gram négatives. (A) Systèmes d'oxydation (DsbA/DsbB) et d'isomérisation (DsbC/DsbD). La protéine cible pénètre au sein du périclasse au travers du canal transmembranaire SEC, puis est prise en charge par l'oxydoréductase DsbA qui permet son oxydation. Cette dernière est par la suite régénérée afin de réaliser un nouveau cycle oxydatif par l'oxydase quinone-dépendante DsbB. Ancrée dans la membrane, elle sera réoxydée en transférant les électrons à la cytochrome bo ou bd oxydase. Dans le cas où des ponts disulfure aberrants sont introduits, l'oxydoréductase DsbC permet l'isomérisation des ponts disulfure. Elle est maintenue réduite par l'action de la réductase membranaire DsbD qui tire son pouvoir réducteur du cytosol via la thioredoxine A (TRXA) et la NADPH thioredoxine réductase (TRXB). (B) Système de réduction présent au sein du périclasse permettant la réduction des apo-cytochromes *c*. La réductase DsbD est également capable de réduire la protéine CcmG, qui elle-même pourra réduire son partenaire physiologique CcmH (système I)

L'introduction de ponts disulfure corrects nécessite donc une protéine à activité disulfure isomérase. D'un point de vue structural, l'isomérase DsbC est un homodimère, chaque monomère possédant un domaine TRX comprenant un motif Cx₂C (CGYC dans DsbC d'*E. coli*) conservé dans la région N-terminale associé à un domaine de dimérisation dans la partie C-terminale. Pour être active, il est nécessaire que DsbC soit maintenue sous forme réduite afin de réduire les protéines anormalement repliées qui pourront ensuite être de nouveau oxydées via DsbA. La réduction de DsbC est effectuée par la protéine transmembranaire DsbD. Cette dernière comporte trois domaines, deux font face au périplasme, DsbD α qui comporte un repliement TRX et DsbD γ présentant un repliement de type IgG, le dernier domaine, DsbD β , est encastré dans la membrane. Chaque domaine possède une paire de cystéines conservées indispensables à l'activité de la protéine (Stewart, 1999). Le motif catalytique Cx₇C (Cys103-Cys109) qui permet la réduction de DsbC est situé au niveau du domaine TRX DsbD α (Depuydt et al., 2011; Stewart, 1999). Les électrons permettant la réduction de ce motif catalytique proviennent du système NTR/TRX cytoplasmique (TrxB et TrxA chez *E. coli*) et sont relayés successivement par les paires de cystéines présentes au niveau du domaine transmembranaire DsbD β , puis du motif Cx₂C du domaine DsbD γ (Figure 10 A) (Goulding et al., 2002; Haebel, 2002; Joly and Swartz, 1997; Katzen and Beckwith, 2000; Kim et al., 2003; Krupp et al., 2001)..

En plus d'intervenir dans l'isomérisation de ponts disulfure, il a été démontré que DsbC régule l'état redox de la protéine de liaison à la L-arabinose, AraF. Cette protéine contient une seule cystéine, qui intervient dans la formation d'un homodimère après formation d'un intermédiaire acide sulfénique, ce qui empêche la liaison du L-arabinose (Denoncin et al., 2014). En réduisant le pont disulfure intermoléculaire d'AraF, DsbC (mais pas son homologue proche DsbG) restaure ses propriétés de liaison de l'arabinose, ce qui constitue un mécanisme de défense contre les effets du stress oxydatif. Alors que toutes ces protéines co-existent dans un même compartiment, il est intéressant de noter que DsbD est incapable de réduire DsbA et que DsbD est incapable d'oxyder DsbC. Il a été montré qu'une simple mutation de la glycine en position 49 de DsbC, transformant ce dimère en monomère était suffisante pour que DsbC puisse agir comme une oxydase et être régénérée par DsbB (Bader et al., 2001; Segatori et al., 2006).

D'autres protéines à activité oxydoréductase coexistent dans le périplasme. La protéine DsbG est une réductase des acides sulféniques (Depuydt et al., 2009). Cette activité est particulièrement

importante pour les nombreuses protéines périplasmiques qui ne contiennent qu'un résidu cystéinyl. Cela empêche donc la formation de modifications irréversibles de ces cystéines (acides sulfinique et sulfonique). Là encore, il est intéressant de noter que la mutation de quelques résidus clés dans DsbG permet à cette protéine d'agir comme une disulfure isomérase de type DsbC (Chatelle et al., 2015). Les protéines CcmG (aussi appelé DsbE) et CcmH font partie du système de maturation du cytochrome c participant à la réduction d'un motif Cx₂C de l'apocytochrome c qui est nécessaire à la coordination covalente d'un hème de type c apporté par CcmF. Il a été avancé que ces deux partenaires pourraient potentiellement réduire certaines protéines comportant des ponts disulfure aberrants (Figure 10B) (Fabianek et al., 1998, 2000). Toutes ces protéines (DsbG, CcmG et CcmH) dépendent *a priori* de DsbD pour leur réduction.

2. Repliement oxydatif des protéines résidant ou transitant par le réticulum endoplasmique et l'appareil de Golgi

Le réticulum endoplasmique (RE) présent chez toutes les cellules eucaryotes forme un important réseau membranaire à travers toute la cellule. Chez les mammifères, près d'1/3 des protéines (secrétées et membranaires) sont structurées au travers du RE. Cette proportion peut même être plus importante au sein de cellules spécialisées dans la sécrétion de protéines telles que les cellules pancréatiques et les hépatocytes par exemple (Shimizu and Hendershot, 2007). Afin de catalyser le repliement structural des protéines, le lumen du RE possède un environnement unique, oxydant et comprenant de fortes concentrations en protéines chaperons, en enzymes impliquées dans le repliement structural et en ATP (Gething and Sambrook, 1992). Il existe plusieurs voies d'adressage des protéines dans le RE mais la plus commune est un adressage cotraductionnel au travers du complexe de translocation SEC. Dès lors que le polypeptide émerge dans la lumière du RE et afin d'éviter toute agrégation ou de prévenir un repliement structural

prématué, ce dernier est pris en charge par des protéines chaperons, des facteurs de repliements structuraux et des enzymes spécialisées (Strasser, 2018). La protéine BIP (Binding Protein), appartenant à la grande famille des HSP70 (heat shock protein 70), est la protéine chaperon prédominante au sein du RE. Contrairement aux levures et mammifères, les spermatophytes possèdent 3 isoformes BIPs (BIP1, BIP2 et BIP3) qui sont dépendantes de l'ATP et se fixent aux

polypeptides nouvellement synthétisés (Fujimori et al., 2017; Meunier et al., 2002). Ces protéines chaperons peuvent agir en synergie avec des facteurs de repliement structural, c'est par exemple le cas d'ERdj3 de la famille des protéines DNAJ. Cette protéine a été initialement mise en évidence chez les mammifères, permettant avec la protéine BIP le repliement structural de la chaîne lourde de l'immunoglobuline G1 (Jin et al., 2009). Parmi les chaperons se trouvent des thiol oxydases et disulfure isomérasées qui vont permettre à un grand nombre de protéines résidant ou transitant par le RE d'acquérir des ponts disulfure et ainsi d'adopter leur repliement structural définitif.

Chez les eucaryotes photosynthétiques, les protéines nécessitant d'être oxydées sont par exemple des protéines de stockage, des récepteurs membranaires comme le récepteur à brassinostéroïdes (BRI1) et à éthylène (ETR1) (Hong et al., 2008; Hothorn et al., 2011; Meyer et al., 2019a; Noguchi et al., 1999) ou des petits peptides riches en cystéines qui peuvent être excrétées au sein de l'apoplaste. Par exemple, l'insertion de ponts disulfure dans le peptide RALF1 (rapid-alkalinization factor en anglais) permet son interaction avec le récepteur FERONIA intervenant dans la modulation du développement racinaire (Haruta et al., 2014).

2.1. La réponse cellulaire aux protéines non structurées (UPR) : mécanismes et conséquences

En principe, l'action des facteurs de maturation précédemment cités empêche l'accumulation de protéines non structurées. Malgré tout, des protéines dont le repliement structural est aberrant et qui vont s'agréger peuvent s'accumuler, notamment dans des conditions de stress biotique et abiotique (Malhotra and Kaufman, 2007). Ceci initie l'activation d'une cascade de signalisation aboutissant à une réponse appelée UPR (unfolded protein response). Une activation de la réponse UPR aboutit au déclenchement des processus d'autophagie et d'apoptose (mort cellulaire programmée) (Kaufman, 2002; Wu and Kaufman, 2006). Chez les métazoaires, l'UPR

est activée via trois grandes voies faisant intervenir des protéine kinases, une voie IRE1 (inositol-requiring kinase 1) une voie PERK (protein ER kinase) et une voie dépendante de l'activation du facteur de transcription 6 (ATF6) (Figure 11) (Harding et al., 2000; Sidrauski and Walter, 1997; Yoshida et al., 2001).

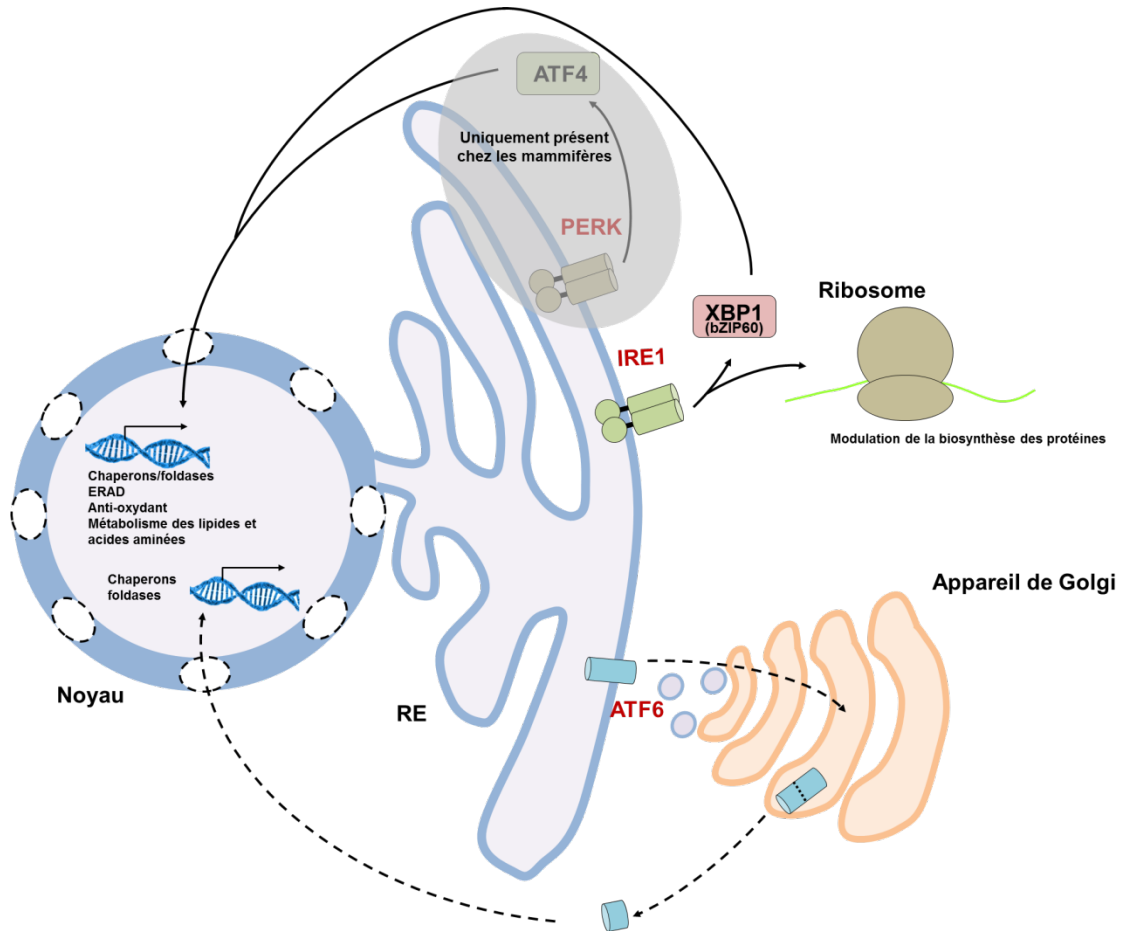


Figure 11: Représentation schématique des trois principales voies de signalisation conduisant à la réponse UPR (Unfolded protein response). L'activation de la phosphatase PERK via sa dimérisation permet l'activation du facteur de transcription 4 (ATF4). Cette voie non présente chez les organismes photosynthétiques permet l'expression de gènes impliqués dans la détoxication des ROS et de protéines chaperons notamment. Les deux autres voies sont présentes chez les organismes photosynthétiques. La phosphatase IRE1 module l'épissage de l'ARNm bZIP6 permettant de diminuer la synthèse ribosomale mais aussi l'expression de protéines impliquées dans la dégradation des protéines (ERAD) et de protéines chaperons entre autres. La dernière voie implique la protéine ATF6 (activating transcription factor 6) qui va induire l'expression de protéines chaperons et foldases.

Dans le cadre de cette réponse UPR, la voie PERK est la première à se mettre en place pour limiter l'entrée de nouveaux polypeptides au sein du RE. Elle nécessite une étape de dimérisation et d'autophosphorylation de PERK (Kaufman, 2004). Cette voie va également permettre l'activation d'ATF4 (activating transcription factor 4) qui induit l'expression de gènes codant des protéines impliquées dans la lutte contre les ROS, des protéines chaperons et des protéines impliquées dans le métabolisme des acides aminés (Harding et al., 1999, 2003; Ma et al., 2002). De la même manière, la protéine kinase IRE1, inactive sous forme monomérique, dimérisé et s'auto-phosphoryle lors de la mise en place de l'UPR. Ce changement permet de moduler l'épissage de l'ARNm XBP1 aboutissant à la diminution de la traduction ribosomale, à l'expression de protéines chaperons, à l'augmentation de la biosynthèse lipidique ainsi qu'à l'activation de la voie de dégradation des protéines ERAD (ER Associated Degradation) (Cox et al., 1997; Travers et al., 2000). Enfin, ATF6, qui réside normalement dans la membrane du RE (Zanetti et al., 2012), est exportée vers l'appareil de Golgi dans des conditions de stress conduisant à l'UPR. Après avoir été clivé, il est transféré dans le noyau conduisant à l'expression de protéines chaperons, notamment des foldases. Chez les plantes supérieures, seules les voies de réponse UPR dépendantes d'IRE1 et d'ATF6 (AtbZIP17 et 28 sont les 2 orthologues d'*A. thaliana*) ont été identifiées jusqu'à présent (Liu et al., 2007a, 2007b; Wan and Jiang, 2016). D'une manière générale, si l'activation de l'UPR faillit à contrebalancer les défauts de repliement structural des protéines, chacune des voies précédemment citées peut déclencher l'activation d'une mort cellulaire programmée par différents mécanismes que je ne décrirai pas ici.

2.2. Les systèmes de repliement oxydatif

Le repliement oxydatif des protéines qui résident dans le RE ou qui seront excrétées, implique essentiellement deux familles de protéines qui agissent de concert, les protéine disulfure isomérasées (PDI) appartenant à la superfamille des TRXs (Freedman et al., 1994) et les protéines ERO1 (ER oxydase 1) (Ellgaard et al., 2018). Les couples PDI/ERO1 catalysent la formation des ponts disulfures (activité oxydase) ou leur isomérisation en cas de combinaisons aberrantes (activité isomérase) qui peuvent se produire notamment pour les protéines possédant 3 cystéines ou plus (Buchner, 1996; Hartl and Hayer-Hartl, 2002). Dans ce système, les PDIs sont les oxydoréductases intervenant dans l'oxydation/isomérisation des substrats tandis qu'ERO1 est la

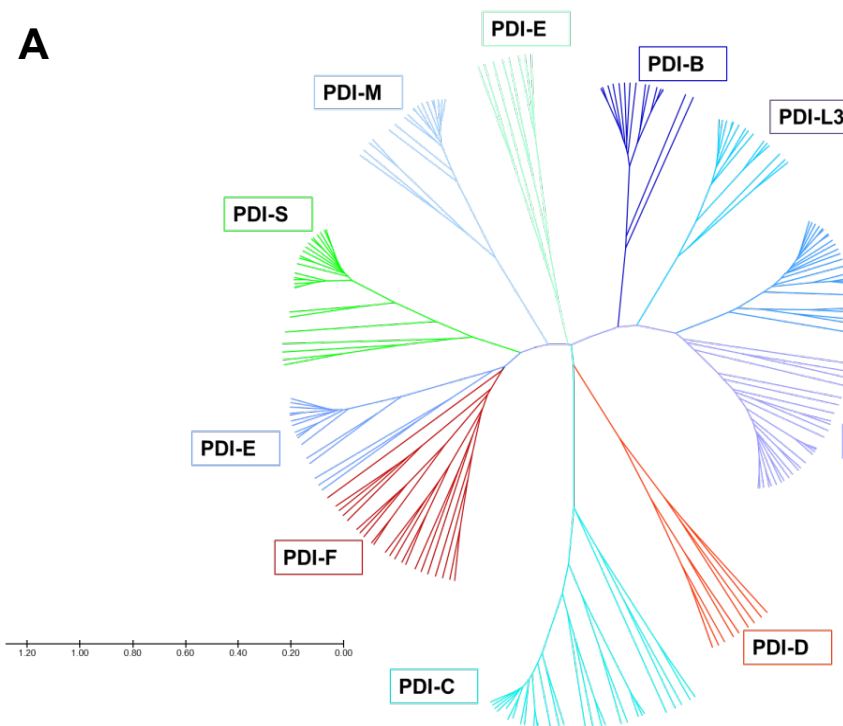
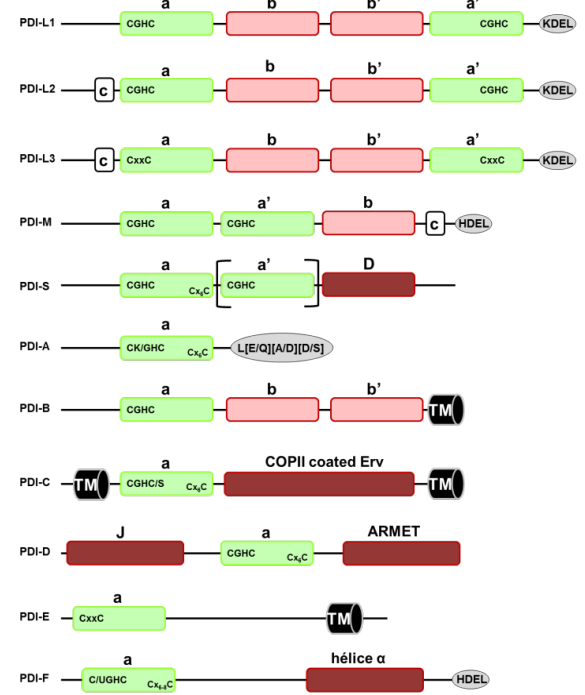
A**B**

Figure 12: Analyse phylogénétique des différentes classes de PDIs présentes chez les organismes photosynthétiques.

(A) Arbre phylogénétique des PDIs présentes chez les organismes photosynthétiques. L'analyse a été réalisée en utilisant le logiciel MEGA7. L'histoire évolutive a été déterminée en utilisant la méthode Neighbor-Joining et les distances évolutives sont basées sur l'analyse des matrices selon la méthode de Jones, Taylor & Thornton (JTT).

(B) Représentation schématique de l'organisation structurale des différentes isoformes de PDIs chez les organismes photosynthétiques. Adapté de Selles et al., 2011.

thiol oxydase permettant la régénération des oxydoréductases et l’oxygène l’accepteur final d’électrons, conduisant à la formation d’H₂O₂.

Les PDIs constituent une famille multigénique composée de 5 isoformes chez la levure *Saccharomyces cerevisiae*, 19 chez l’Homme (Appenzeller-Herzog and Ellgaard, 2008; Kozlov et al., 2010) et 13 chez *A. thaliana*. En revanche, le nombre de copies de gènes *ERO1* est de 1 chez *Saccharomyces cerevisiae*, *Drosophila melanogaster* ou *Oryza sativa* ou 2 chez la souris (*Mus musculus*, ERO α /ERO β) ou bien *A. thaliana* (ERO1/ERO2) (Aller and Meyer, 2013; Dixon et al., 2003; Sevier et al., 2007; Zito et al., 2010).

Les analyses phylogénétiques ont mis en évidence que les organismes photosynthétiques eucaryotes possèdent 9 classes de PDIs, qui diffèrent par leur organisation structurale et la présence de domaines spécifiques. Les classes PDI-L, M, B, S et C sont retrouvées chez tous les organismes, la classe PDI-A est spécifique des plantes terrestres alors que les classes PDI-D, E et F sont présentes uniquement chez les algues vertes (Selles et al., 2011) (Figure 12A). L’architecture conventionnelle des PDIs, retrouvée dans les PDI-L chez les plantes, comporte 4 domaines qui possèdent tous un repliement TRX avec un arrangement *a-b-b'-a'* (Figure 12B). Toutefois, les domaines *a* et *a'* sont les seuls à posséder un site actif typique de la superfamille des TRXs avec une signature catalytique souvent de type WCGHC (Edman et al., 1985) alors que les domaines *b* et *b'* ne possèdent pas de signature Cx₂C et seraient importants pour la reconnaissance du substrat (Yagi-Utsumi et al., 2015). Trois sous-classes (PDI-L1, PDI-L2 et PDI-L3) ont été définies entre autres en fonction de la présence ou absence d’un domaine supplémentaire du côté C-terminal et de la conservation des acides aminés au sein des signatures catalytiques présentes dans les domaines *a* et *a'*. Enfin, les PDI-L possèdent un motif [K/H/N]DEL à l’extrémité C-terminale qui permet leur rétention dans le RE. Le groupe PDI-M possède deux domaines catalytiques *a* et *a'* suivis par un seul domaine *b*, ainsi qu’un domaine additionnel (appelé *c*) en partie C-terminale. La classe PDI-S comprend des isoformes qui possèdent deux domaines catalytiques *a* et *a'* et un domaine D de fonction inconnue. Tous les autres groupes ne possèdent qu’un seul domaine TRX catalytique, unique dans le cas des PDI-A ou fusionné à d’autres domaines, éventuellement des ancrès transmembranaires (TM). L’absence de signal de rétention au RE dans les PDI-A pose d’ailleurs la question de sa localisation, de même que l’observation que ces protéines lient un centre Fe-S (Remelli et al., 2017; Selles et al., 2017). Les PDI-B possèdent, en plus du domaine *a*, deux domaines *b* et *b'* et un domaine TM en

C-terminal pour un ancrage à la membrane du RE. Les PDI-C comportent deux domaines TM présents aux extrémités N- et C-terminales ainsi qu'un domaine COPII coated Erv, retrouvé dans les protéines ERGIC-32 et Erv46 respectivement présentes chez l'homme et la levure (Appenzeller-Herzog, 2006; Breuza et al., 2004). Les PDI-C pourraient donc par analogie aux protéines ERGIC-32 et Erv46 participer au contrôle du trafic protéique entre le RE et l'appareil de Golgi des protéines sécrétées. Les PDI-D possèdent deux domaines additionnels, un domaine J en N-terminal généralement présent au sein des protéines chaperons de type DNAJ/Hsp40 et un domaine ARMET en C-terminal typiquement retrouvé dans des protéines résidant dans le RE et intervenant dans la réponse UPR (Apostolou et al., 2008; Qiu et al., 2006). Les PDI-E sont les homologues des protéines TMX (thioredoxin-related transmembrane protein) des mammifères et contiennent uniquement un domaine TM en position C-terminale. Enfin, chez les chlorophytes, la grande majorité des PDI-F possèdent une extension du côté C-terminal qui correspondrait à une longue hélice α n'étant pas prédictée comme étant transmembranaire. Cependant l'absence de ce domaine transmembranaire serait compensée par l'existence d'un signal de rétention au RE ([K/N][D/T]EL) (Selles et al., 2011).

D'un point de vue structural, les protéines ERO1 des différents organismes modèles ont globalement la même structure qui permet notamment la fixation d'un cofacteur FAD. Toutefois, les isoformes ERO1/2 présentes chez les plantes supérieures contiennent un domaine transmembranaire du côté N-terminal permettant leur ancrage à la membrane du réticulum. La régulation de l'activité de cette protéine est complexe car il y aurait au moins 3 ponts disulfure requis pour la catalyse et la régulation de l'activité. L'oxydation des PDIs serait permise par un pont disulfure externe présent dans une région flexible de la protéine. Les électrons sont ensuite relayés par un pont disulfure interne, vers le cofacteur FAD puis vers l'oxygène (Cuozzo and Kaiser, 1999; Gross et al., 2004, 2006; Sevier et al., 2007). Les cystéines impliquées sont conservées dans les isoformes de tous les organismes. En plus de ces cystéines catalytiques, les protéines ERO1 contiennent des cystéines additionnelles qui sont souvent conservées et qui pourraient avoir un rôle régulateur. De plus, des ponts disulfure se forment entre des cystéines catalytiques et non catalytiques dans les isoformes de levure et humaine, régulant ainsi leur activité en inactivant transitoirement les protéines (Appenzeller-Herzog and Ellgaard, 2008; Baker et al., 2008; Zhang et al., 2014).

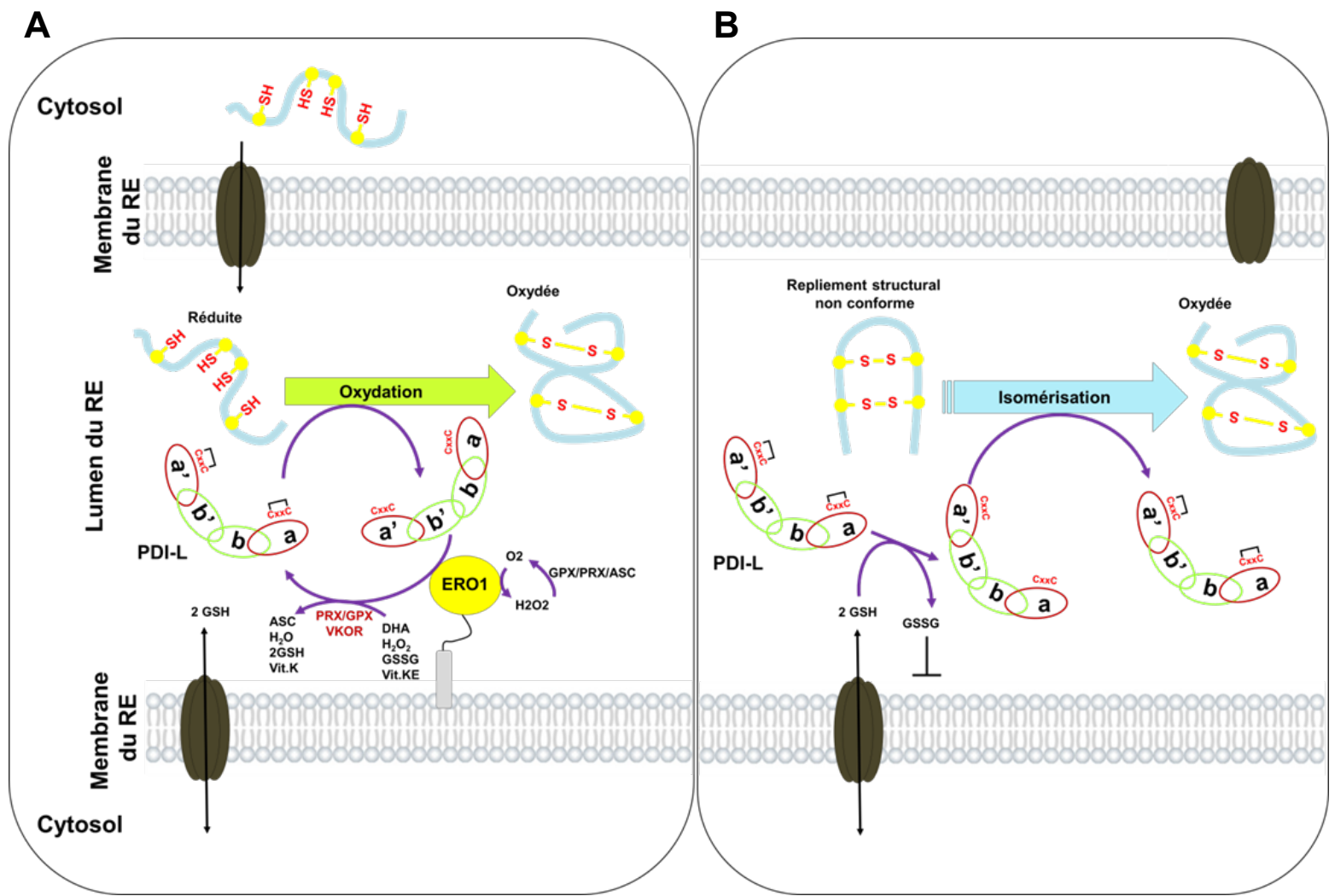


Figure 13: Représentation schématique du système de repliement oxydatif catalysé par le couple PDI/ERO1 au sein du Réticulum Endoplasmique (RE). (A) Sous forme oxydée, les PDIs (ici PDI-L comportant une organisation structurale *a-b-b'-a'*), vont interagir avec leur substrat réduit afin de l'oxyder pour qu'il acquière un repliement structural correct (activité oxydase). Une fois réduites, les PDIs sont régénérées plus ou moins directement par l'action de l'oxydase FAD-dépendante, ERO1. Cette dernière va transférer les électrons directement à une molécule d'oxygène formant de l' H_2O_2 . Cette production d' H_2O_2 est contrebalancée notamment par l'action de thiol peroxydases (PRX/GPX). Les PDIs peuvent également être régénérées par l'action d'enzymes comme les PRX/GPX ainsi que le couple vitamine K époxide/vitamine K époxyde réductase (VKOR) mais également par l'intermédiaire de différentes molécules comme le déshydroascorbat (DHA), H_2O_2 et le GSSG.

(B) Les PDIs possèdent également une activité isomérase pour les protéines présentant un repliement structural non conforme. Pour cette fonction, les PDIs doivent être sous forme réduite. Leur réduction peut être catalysée par le GSH, cette réaction formant du GSSG. Il est important de noter que le GSSG ne peut être exporté au travers de la membrane du RE, ce qui conduit à l'existence d'un potentiel redox GSH/GSSG significativement oxydant comparé au cytosol.

Pour les PDIs possédant plusieurs domaines catalytiques, leurs rôles respectifs et leur propension à être oxydées par les protéines ERO1 ne sont pas toujours clairs. Le modèle classique d'oxydation d'un substrat par les PDIs puis sa régénération par son partenaire physiologique ERO1, est présenté en Figure 13A. Cependant, il n'existerait pas qu'une seule voie permettant l'oxydation des PDIs. En effet, alors qu'un mutant *ero1* chez la levure est létal (Frand and Kaiser, 1998; Pollard et al., 1998), la mutation de l'unique copie d'Ero1 chez la Drosophile n'est pas létale (Tien et al., 2008) de même que la mutation des deux isoformes chez la souris (Zito et al., 2010). Des études ont ainsi suggéré une ré-oxydation des PDIs par des voies non enzymatiques (H_2O_2 , GSSG ou DHA) (Ellgaard et al., 2018; Hudson et al., 2015) ou enzymatiques faisant intervenir la vitamine K et la vitamine K époxyde réductase (Cao et al., 2016; Schulman et al., 2010), ou des thiol peroxydases oxydées par des peroxydes, H_2O_2 en particulier (Kakihana et al., 2012; Zito, 2013). Cette dernière hypothèse repose sur la présence de plusieurs thiol peroxydases (GPx7, GPx8 et PrxIV) dans le RE chez l'homme (Ramming et al., 2014, p. 20; Ramming and Appenzeller-Herzog, 2013; Tavender et al., 2008, Tavender et al., 2008). Il est à noter que ces TPXs pourraient ainsi permettre la réduction d' H_2O_2 en H_2O et donc d'éviter que le RE ne devienne trop oxydant. Chez les plantes, la GPx-like 3 se trouve liée à la membrane du RE et pourrait donc avoir un rôle similaire (Attacha et al., 2017). Néanmoins, un double mutant *ero1 ero2* est *a priori* létal chez *A. thaliana*, suggérant que ces protéines sont essentielles au moins au stade gamétophytique (Fan et al., 2019). Cela n'exclut pas néanmoins que d'autres voies puissent co-exister pour certaines PDIs ou à certains stades de développement.

La question de la redondance entre PDIs doit également être posée compte-tenu de l'existence de nombreuses isoformes de PDIs au sein du règne végétal. La réponse n'est pas connue à l'heure actuelle mais les différences d'architectures et de propriétés catalytiques laissent penser que ce n'est pas le cas entre PDIs de classes différentes. Pour les PDIs de même classe, la question est toute autre car l'identité de séquence peut être forte. Dans ce cas, la réponse est peut-être à chercher du côté des territoires d'expression.

Un autre élément à prendre en compte concerne les différences de propriétés redox et notamment de potentiel redox entre PDIs qui vont influer sur l'état d'oxydoréduction de la protéine dans le RE. En effet, pour les réactions d'isomérisation de ponts disulfure aberrants, les PDIs doivent être réduites (Figure 13B). La proportion de formes réduites *vs* oxydées pour une même PDI pourrait

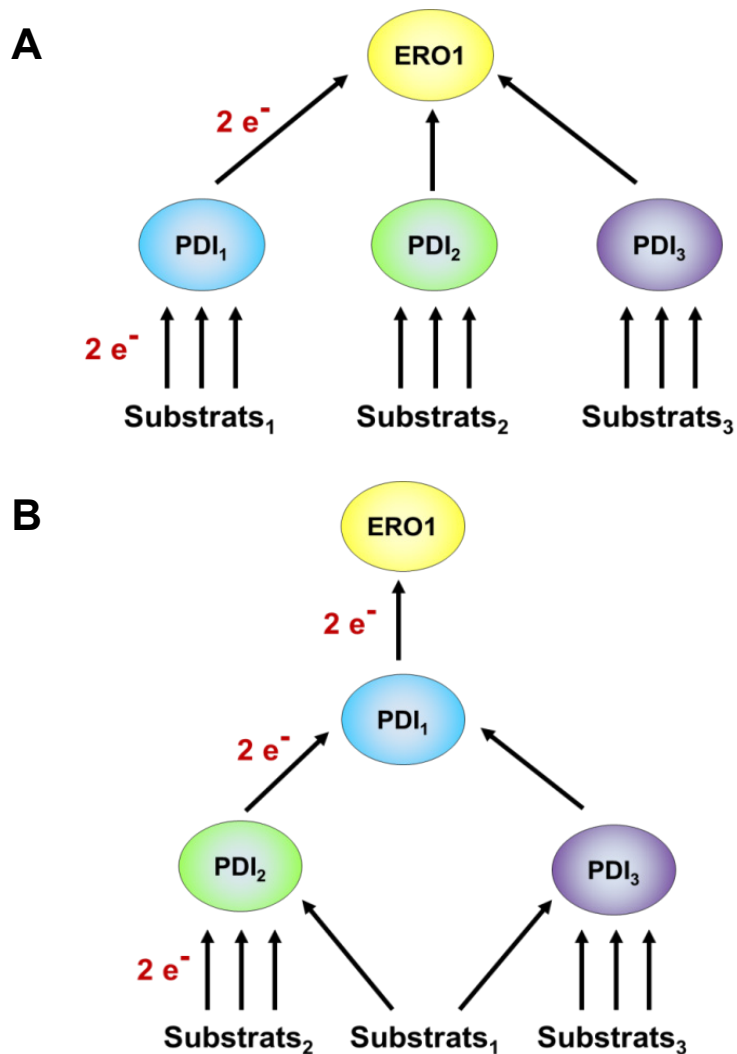


Figure 14: Représentation schématique des deux modèles de régénération des PDIs par ERO1.
 (A) Régénération directe de toutes les PDIs par ERO1. (B) Régénération directe d'une ou de quelques PDIs par ERO1, la régénération des autres PDIs étant catalysée par celles qui interagissent avec ERO1. D'après Meyer et al., 2019.

donc déterminer son type d'activité réductase/isomérase vs oxydase. Une protéine qui ne réagirait pas avec ERO1 aurait donc plus de chance de rester réduite. Il a été suggéré que certaines PDIs pourraient être en équilibre avec le pool de glutathion réduit/oxydé (GSH/GSSG) (Delaunay-Moisan et al., 2017; Ellgaard et al., 2018). Globalement, il n'est pas certain qu'ERO1/2 (ou d'autres oxydants) puissent oxyder les membres de toutes les classes de PDIs. Ainsi, deux modèles existent actuellement, un modèle linéaire où les protéines ERO1 possèdent la capacité d'oxyder toutes les PDIs et un modèle, dit de coopération, qui propose que les protéines ERO1 présentent une spécificité envers certaines PDIs qui vont relayer cette oxydation vers d'autres isoformes (Figure 14). Ce second modèle est notamment appuyé par une étude montrant la capacité d'une PDI-L2 de *Glycine max* à oxyder une PDI-M qui n'était pas oxydée par ERO1a (Matsusaki et al., 2016; Urade, 2019).

Différentes études ont mis en évidence l'importance des PDIs au sein de différents processus biologiques, comme dans la maturation du pollen et des graines (Onda et al., 2011; Wadahama et al., 2007). Il a été récemment rapporté chez le blé tendre (*Triticum aestivum*) une forte augmentation des transcrits et des protéines PDI-L et S ainsi que d'ERO1 juste après la fécondation de l'ovocyte (Kimura et al., 2015). Ces dernières sont également plus abondantes et apparaissent intervenir lors de la synthèse des protéines de stockage telle que les gliadines et les gluténines (d'Aloisio et al., 2010; Kimura et al., 2015). Chez le soja (*Glycine max*), toujours lors du processus de formation des graines, il a été mis en évidence qu'un grand nombre de PDIs tels que les PDI-L, S et M ainsi qu'ERO1 étaient plus fortement exprimées. Elles sont fortement représentées lors de la maturation des cotylédons et de surcroît leur expression est corrélée avec la biosynthèse de β -conglycinine, de β -glycine (Iwasaki et al., 2009; Okuda et al., 2014). De plus, il a été démontré que les PDI-D et S avaient une activité oxydoréductase *in vitro* et que l'absence de cette isoforme chez *A. thaliana* entraînait des défauts de croissance et d'orientation du tube pollinique lors de l'application d'un stress réducteur (Fan et al., 2018; Wang et al., 2008). En réponse à différents stress abiotiques et notamment osmotique, plusieurs études mettent en avant qu'un certain nombre de PDIs permettent la production de proline et l'accumulation de saccharose (Kayum et al., 2017; Kumar et al., 2015; Xia et al., 2018). Chez *Solanum tuberosum*, le mutant *pdl1* présente une sensibilité accrue à la sécheresse et au stress salin, corrélée avec une diminution d'ASC et une augmentation des concentrations en H₂O₂ dans les parties aériennes de la

plante (Eggert et al., 2016). Les PDIs apparaissent également intervenir dans la détoxication des xénobiotiques tels que le trichlorophénol (TCP) (Peng et al., 2017).

Curieusement, il a été démontré que les PDIs pouvaient avoir une fonction autre que le repliement structural des protéines. En effet, chez l’algue verte *Chlamydomonas reinhardtii*, PDI2, avec l’aide d’une 2-Cys PRX, interviendrait dans la régulation du rythme circadien (Filonova et al., 2013).

In planta l’absence de redondance peut, lorsque l’expression de l’unique isoforme est fortement diminuée, induire une modification du protéome des graines mais n’a aucun effet sur la croissance des parties végétatives (Onda et al., 2009). Cela suggère que, comme chez les animaux, nous pouvons retrouver un système annexe chez les organismes photosynthétiques.

En plus du système ERO1/PDI, un autre acteur du repliement oxydatif existe chez les protistes, les animaux et les plantes mais pas la levure. La protéine appelée QSOX (quiescin sulfhydryl oxidase en anglais) agirait toutefois plus tardivement dans la voie de sécrétion des protéines (Kodali and Thorpe, 2010). La localisation des deux isoformes présentes chez *A. thaliana* a été déterminée via leur fusion traductionnelle à la GFP ou déduite d’études protéomiques. QSOX1 serait localisée au niveau de l’apoplaste et QSOX2 au niveau de l’appareil de Golgi (Alejandro et al., 2007; Nikolovski et al., 2012). Au niveau de leur organisation structurale, ces protéines sont en réalité des chimères possédant un ou deux domaines TRX du côté N-terminal, intervenant dans l’interaction et l’oxydation des substrats, suivi par un domaine thiol oxydase, assez proche de la protéine ERV1 mitochondriale. De la même manière, celui-ci lie un cofacteur FAD indispensable à l’activité qui permet de transférer les électrons à une molécule d’oxygène. Un domaine transmembranaire est en général présent à l’extrémité C-terminale pour un ancrage aux membranes. Les électrons issus d’un substrat réduit, sont donc transférés séquentiellement vers le site actif Cx₂C présent au niveau du domaine TRX puis vers deux motifs Cx₂C présents au sein du domaine ERV qui réduira une molécule d’O₂ en H₂O₂ grâce à son cofacteur FAD (Chakravarthi et al., 2007; Coppock and Thorpe, 2006; Okuda et al., 2014). Malgré le manque de données chez les organismes photosynthétiques, une étude génétique basée sur la résistance à la norspermidine a permis de mettre en évidence qu’une surexpression de la protéine QSOX2 chez *A. thaliana* améliore la croissance des plantules en présence de cations toxiques (Li⁺ et Na⁺) alors qu’un mutant perte de fonction *qsx2* présente un phénotype inverse confirmant le rôle de QSOX2 dans la détoxication des cations toxiques (Alejandro et al., 2007)..

Protéines	Motifs cystéiniques	Fonctions
PAM16/17/18		Insertion des protéines dans la membrane interne
Cytochrome b2		Respiration mitochondriale
ATP4/7/6/14/17/18/19/20		Facteur de maturation de l'ATP synthase
ATP23	Cx ₁₁ C-Cx ₁₆ C-Cx ₉ C-Cx ₄ C-Cx ₁₉ C-Cx ₁₅ C	Facteur de maturation de l'ATP synthase
SOD1		Dismutation d'O ₂ ⁻
CCS1	Cx ₄₀ C	Facteur de maturation de la SOD1
Famille TIM (TIM8, 9, 10, 12, 13)	Cx ₃ C-Cx ₃ C	Protéines chaperons et Import des protéines membranaires
Famille COX (COX11, 12, 17, 19, 23)	Cx ₉ C-Cx ₉ C	Facteurs d'assemblage de la cytochrome c oxydase (Complexe IV)
MDM35	Cx ₉ C	Morphologie des mitochondries
MIC17 et MIC14	Cx ₉ C	Respiration mitochondriale
MICU	CxC	Contrôle du flux de Ca ²⁺ dans l'IMS
SLP2	Cx ₁₂ C	Phosphatase impliquée dans la régulation de la germination

Tableau 2: Fonctions des principales protéines localisées au sein de l'espace intermembranaire mitochondrial chez *A. thaliana*. L'import des protéines contenant un motif Cx_nC repose sur le système MIA40/ERV1. Cette liste a été constituée principalement à partir d'études menées chez *S. cerevisiae*.

3. L'import des protéines au sein de l'espace intermembranaire mitochondriale (IMS), séquestration par repliement oxydatif, la voie MIA40/ERV1

3.1. La mitochondrie, un organite pas comme les autres...

La mitochondrie est un organite dont l'apparition est consécutive au phénomène d'intégration endosymbiotique d'une α -protéobactérie au sein d'une cellule proto eucaryote (plus précisément l'ancêtre commun à toutes les cellules eucaryotes LECA (Last eukaryotic common ancestor)). Au cours de l'évolution, le génome ainsi que le protéome de cette α -protéobactérie ont constamment évolué conduisant notamment à des gains, des pertes ou des relocalisations de fonction et donnant finalement naissance aux mitochondries que l'on connaît aujourd'hui (Huynen et al., 2013). Cette endosymbiose a également conduit à une architecture particulière. Les mitochondries contiennent deux compartiments aqueux (la matrice et l'espace intermembranaire : IMS) séparés par deux membranes biologiques : la membrane externe (Outer Membrane : OM) et la membrane interne (Inner membrane : IM). Les données protéomiques actuelles révèlent la présence de 1000 à 2000 protéines dans des mitochondries de levure et d'homme respectivement, une valeur comparable à celle pour des mitochondries de plantes (Morgenstern et al., 2017; Mueller et al., 2017). De manière intéressante, l'ADN mitochondrial code 1% ou moins de ces protéines ce qui signifie que la majorité des protéines mitochondrielles sont synthétisées dans le cytosol. Elles sont importées dans les différents sous-compartiments selon un assez grand nombre de voies/mécanismes qui ne seront pas détaillés ici (Fischer and Riemer, 2013; Neupert and Herrmann, 2007; Peleh et al., 2016; Riemer et al., 2009). En ce qui concerne l'IMS, les études suggèrent la présence d'une cinquantaine de protéines au sein de ce compartiment subcellulaire chez la levure mais trois fois plus (cent cinquante) chez l'homme, mais ce chiffre paraît un peu important (Itzhak et al., 2016; Vögtle et al., 2012). Ces protéines font partie d'un grand nombre de complexes protéiques indispensables au bon fonctionnement des mitochondries (Morgenstern et al., 2017).

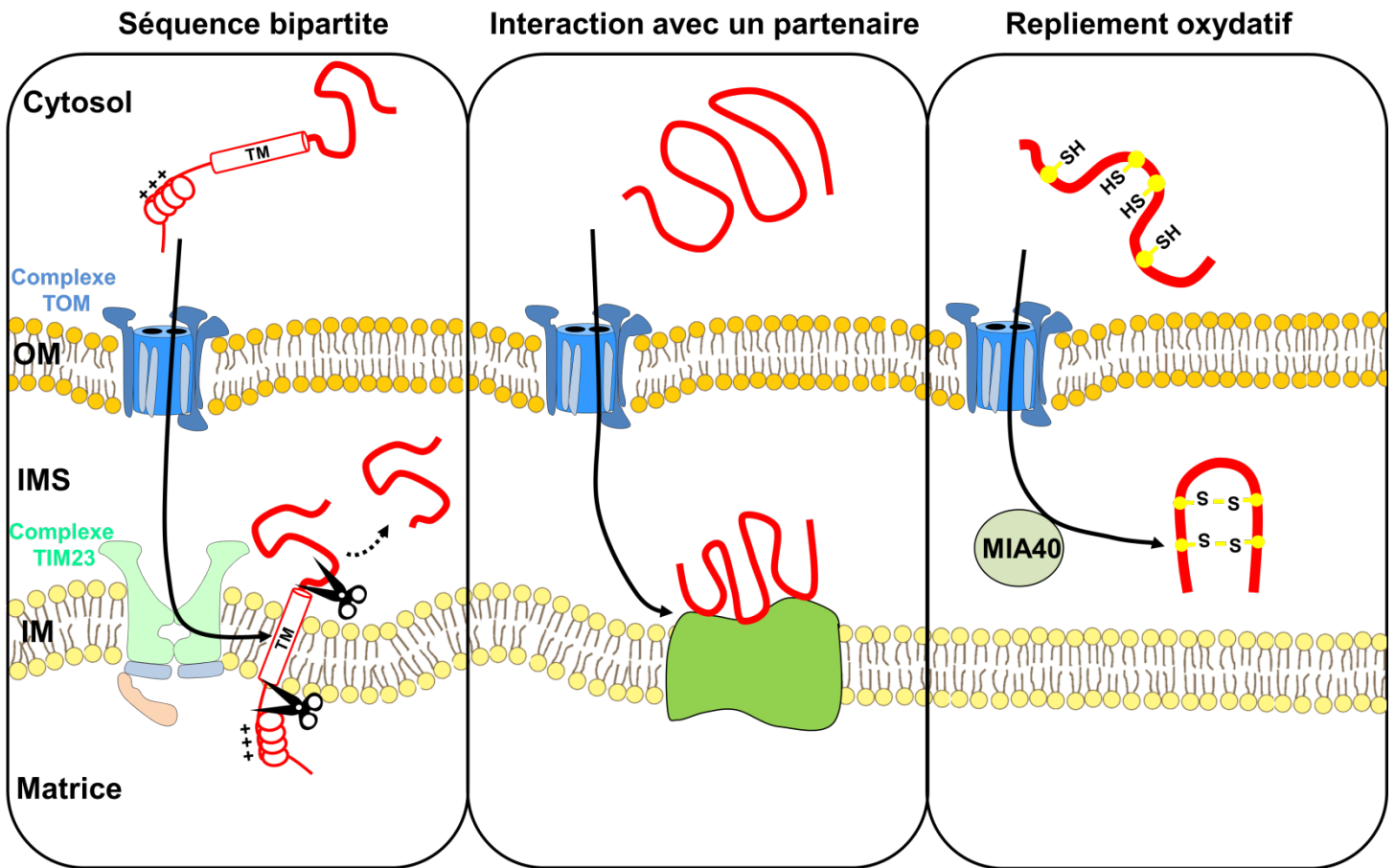


Figure 15: Représentation schématique des trois grandes voies d'import des protéines dans l'IMS des mitochondries. La première voie repose sur la présence d'une séquence bipartite. Celle-ci est composée d'une hélice amphipathique permettant l'adressage de la protéine au sein de la matrice mitochondriale (MTS) suivie d'un domaine transmembranaire (TM). L'import de la protéine est stoppé par ce dernier domaine au niveau du complexe TIM23 puis cette séquence bipartite est clivée induisant la libération de la partie soluble dans l'IMS. La deuxième voie est dite d'affinité car elle repose sur l'interaction de la protéine importée avec un partenaire physiologique, permettant sa séquestration au sein de l'IMS. Pour la troisième voie, le repliement oxydatif des substrats importés par MIA40 permet le repliement structural de la protéine de manière concomitante à son import

3.2. L'import des protéines dans l'IMS, prédominance de la voie par repliement oxydatif

La totalité des protéines résidant dans l'IMS (Tableau 2) sont synthétisées dans le cytosol à partir de gènes nucléaires et trois voies sont actuellement proposées pour leur import (Figure 15). Ces voies d'import ont comme point commun le passage des protéines au travers du complexe TOM (Translocase of Outer Membrane) et leur rétention au sein de l'IMS. La première voie fait intervenir une séquence N-terminale dite bipartite constituée d'une séquence permettant l'adressage à la matrice mitochondriale (MTS pour mitochondrial targeting sequence en anglais) formant souvent une hélice amphipathique, suivie d'un domaine TM. Ce dernier va empêcher le passage de la protéine au niveau du complexe TIM22 (Translocase of Inner Membrane 22) qui sert normalement à l'entrée des protéines matricielles. La partie soluble de ces protéines est libérée dans l'IMS après clivage de ces deux extensions (Neupert and Herrmann, 2007; Nicholson et al., 1987). L'exemple le mieux documenté pour cette voie est peut-être celui de l'import du cytochrome b2 chez la levure. La seconde voie d'import des protéines résidant dans l'IMS est réalisée par interaction avec un partenaire physiologique présent dans l'IMS, aboutissant donc à leur rétention dans ce compartiment. C'est la voie empruntée par la cytochrome hème lyase ou la créatine kinase. Enfin, la troisième et principale voie d'import implique le repliement oxydatif des protéines, catalysé par une oxydoréductase appelée MIA40 (Mitochondrial Intermembrane space Assembly 40) ou CHCHD4 (coiled-coil-helix-coiled-coil-helix domain 4) chez l'homme associée à la thiol oxydase ERV1 (Essential for Respiration and Vegetative growth 1) ou ALR (Augmenter of Liver Regeneration) (Mesecke et al., 2005). L'oxydoréductase MIA40 étant capable de coordonner un ion zinc et/ou cuivre *in vivo* (Terziyska et al., 2005), un troisième acteur, Hot13 chez la levure et RCHY chez l'homme, pourrait servir indirectement à l'oxydation de MIA40 en catalysant sa démétallisation, mais aucun orthologue n'est connu chez les plantes (Mesecke et al., 2008). Dans les 3 cas, l'adoption de la structure tridimensionnelle des protéines empêche leur sortie de l'IMS (Neupert and Herrmann, 2007). Les protéines cibles/substrats de MIA40 sont caractérisées par la présence d'une séquence d'adressage interne typique appelée ITS (Intermembrane space Targeting Signal en anglais) ou MISS (Mitochondrial IMS-Sorting Signal en anglais). Ces séquences comportent une hélice amphiphile la plupart du temps à proximité d'un motif cystéinique spécifique, deux répétitions Cx₃C dans le cas par exemple des protéines chaperons TIM (TIM8, TIM9, TIM10 et TIM13) ou

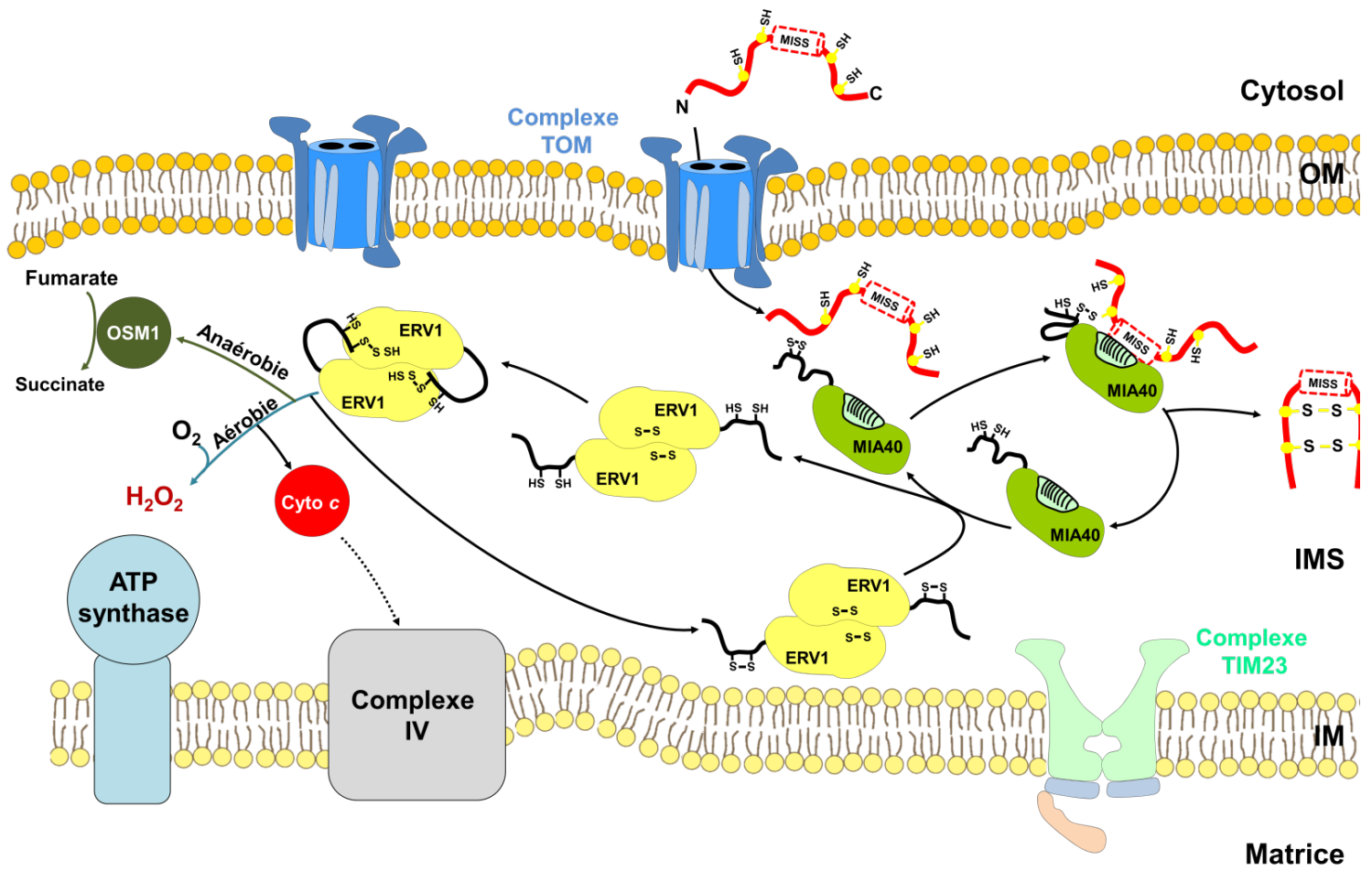


Figure 16: Import et repliement oxydatif des protéines au sein de l'espace intermembranaire des mitochondries par le couple MIA40/ERV1.

La protéine sous forme réduite est importée dans l'IMS via le complexe TOM. Elle interagit avec l'oxydoréductase MIA40 via la présence d'une séquence interne d'adressage à l'IMS (MISS) présente à proximité des motifs Cx_nC-Cx_nC. Cette interaction conduit à l'oxydation, au repliement structural et à la rétention de la protéine nouvellement importée. La régénération de MIA40 est effectuée par ERV1 qui se retrouve ainsi sous forme réduite. ERV1 est ensuite ré-oxydée, dans des conditions aérobies via la réduction d'une molécule d'oxygène, soit au travers du cytochrome c et de la cytochrome c oxydase (complexe IV) permettant la production d'une molécule d'eau (H₂O) ou directement aboutissant à la production d'H₂O₂. Dans des conditions anaérobies, la fumarate réductase permet de transférer les électrons à une molécule de fumarate et de libérer du succinate. Ce modèle a été réalisé à partir de différentes études élaborées chez la levure et l'humain.

deux répétitions Cx₉C dans le cas des facteurs de maturation de la cytochrome c oxydase (COX11, COX12, COX17, COX19, COX23) (Longen et al., 2009; Milenkovic et al., 2009; Peleh et al., 2016; Sideris et al., 2009). Chez les organismes possédant les deux protéines, ce système fonctionne de la manière suivante (Figure 16). MIA40 reconnaît ses substrats grâce à une zone hydrophobe puis catalyse l'introduction de(s) ponts disulfure au sein de la protéine cible par l'intermédiaire de son motif catalytique CPC. MIA40 se trouve alors réduite et le motif CPC de MIA40 est ré-oxydé par l'oxydase ERV1 qui transfère les électrons à l'accepteur final (cytochrome c ou O₂) grâce à la présence de son cofacteur FAD.

L'interaction de MIA40 avec ses substrats est donc médiée par l'intermédiaire d'une zone hydrophobe (appelée également clé hydrophobe) qui reconnaît la séquence d'adressage ITS ou MISS en aval des cystéines du substrat à oxyder (Riemer et al., 2011). Une récente étude a mis en avant que cette clé hydrophobe présente au sein de MIA40 est essentielle pour son activité et permet même de compenser dans une certaine mesure la perte de l'activité oxydase. En effet, une version redox-inactive de la protéine (mutée pour les 2 cystéines du motif CPC) est suffisante et permet d'assurer les fonctions respiratoires chez *S. cerevisiae* (Peleh et al., 2016). Les auteurs suggèrent que cette forme non active d'un point de vue redox permettrait de piéger les substrats qui seraient oxydés directement par ERV1 même si cette activité est faible.

Néanmoins, *in vivo*, après avoir oxydé son substrat, MIA40 doit être régénérée par l'oxydase FAD dépendante ERV1 afin d'accomplir un nouveau cycle oxydatif. Cette oxydase possède deux motifs Cx₂C qui participent au transfert d'électrons. Celui qui régénère le motif CPC de MIA40 est situé à l'extrémité C-terminale ou N-terminale selon les organismes considérés (voir plus bas). Le second motif Cx₂C, situé au centre de la protéine, transfère les électrons vers le cofacteur FAD adjacent. Dans des conditions aérobies, l'accepteur final d'électrons est vraisemblablement le cytochrome c puis la cytochrome c oxydase (complexe IV de la chaîne respiratoire) qui réduira donc O₂ en H₂O. Si les électrons sont transférés directement à l'O₂, il y aura formation d'H₂O₂. Dans des conditions anaérobies, il a été mis en évidence récemment que l'accepteur final d'électrons chez la levure était le fumarate. Via l'action de la fumarate réductase (OSM1) il permettrait la régénération de la protéine ERV1 de façon concomitante à la production de succinate (Neal et al., 2017). De manière intéressante, des études *in vivo* ont montré que le GSH présent à des concentrations de l'ordre du mM améliorerait significativement l'oxydation des protéines en favorisant l'activité catalytique de MIA40 (Bien et al., 2010). Mais également, en

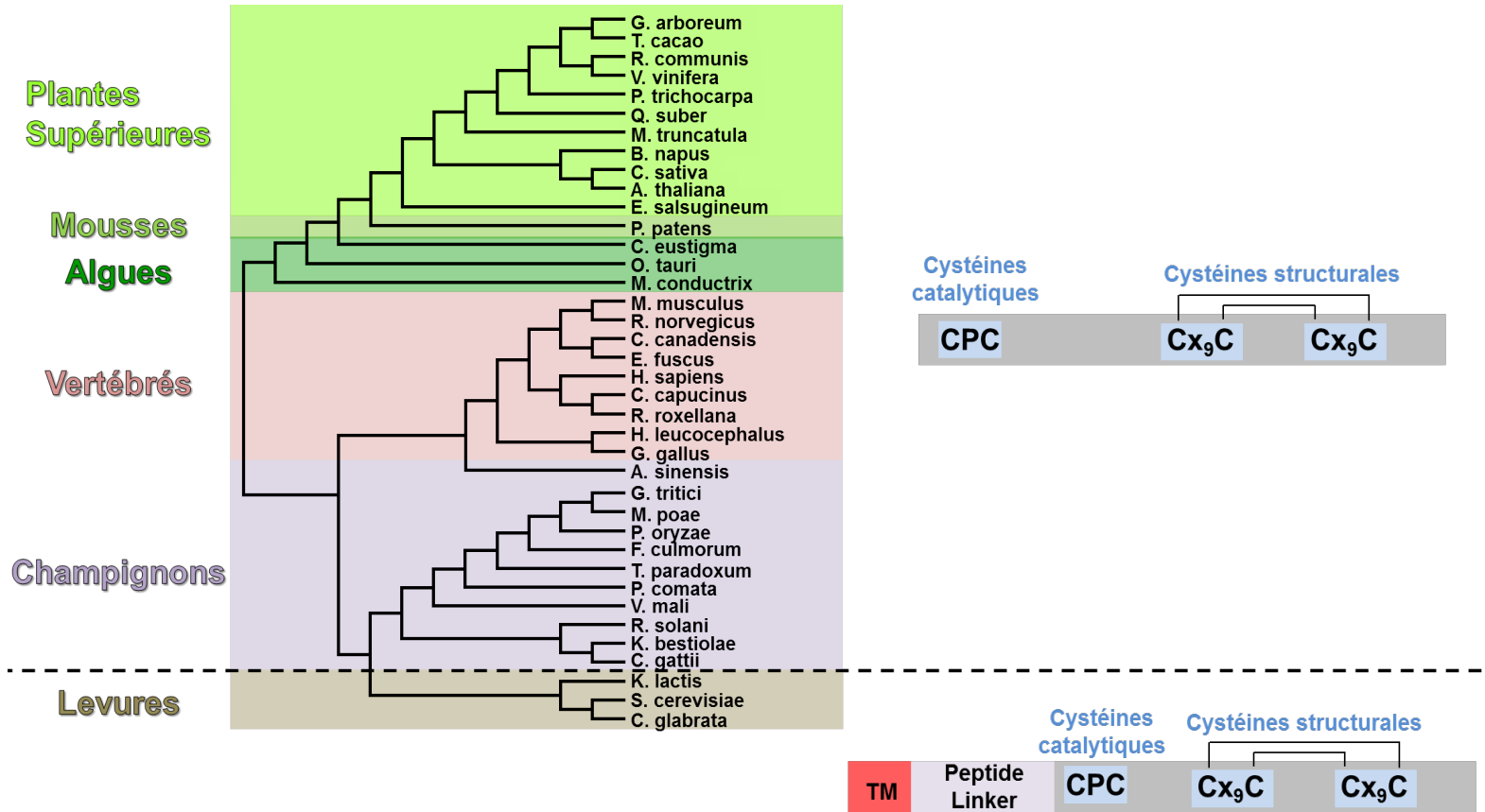


Figure 17: Analyse phylogénétique des protéines MIA40 présentes chez différents organismes eucaryotes et organisation structurale. L'analyse phylogénétique a été réalisée en utilisant le logiciel MEGA7. L'histoire évolutive a été déterminée en utilisant la méthode Neighbor-Joining et les distances évolutives sont basées sur l'analyse des matrices selon la méthode de Jones, Taylor & Thornton (JTT).

réduisant les protéines présentant un repliement structural non conforme (Bien et al., 2010; Riemer et al., 2011). Diverses études mettent en avant un ratio GSH/GSSG très proche ou identique à celui du cytosol (entre -250 et -300 mV) mais beaucoup plus réducteur au sein de la matrice (entre -300 et 330 mV) (Calabrese et al., 2017; Hu et al., 2008; Kojer and Riemer, 2014; Kojer et al., 2012, 2015; Østergaard et al., 2004). Chez la levure *S. cerevisiae*, les mutations des gènes *erv1* et *mia40* sont létales mais l'étude de mutants conditionnels indique notamment des défauts d'import des protéines clés de la chaîne respiratoire mitochondriale et une hypersensibilité aux agents réducteurs (Chacinska et al., 2004; Mesecke et al., 2005; Peleh et al., 2016). Les défauts de maturation des protéines Fe-S cytosoliques initialement observés dans le mutant *erv1* sont *a priori* liés à une mutation présente dans un des 2 gènes de biosynthèse du glutathion, confirmant au passage l'importance du GSH pour ce processus (Lange et al., 2001; Ozer et al., 2015). Dans ce contexte, il est également surprenant que Mia40 de levure soit capable de fixer un centre Fe-S lorsque la protéine recombinante est exprimée dans *E. coli* (Spiller et al., 2013). La signification physiologique de cette observation n'a pas été démontrée. Des travaux réalisés chez *A. thaliana* indiquent que la mutation du gène codant pour ERV1 est létale au stade embryonnaire alors que le mutant *mia40* est viable et ne présente pas de phénotype macroscopique lorsqu'il est cultivé en conditions standards (Carrie et al., 2010; Levitan et al., 2004). De plus, MIA40 serait localisée au sein des peroxysomes du fait d'une séquence d'adressage SKL présente à l'extrémité C-terminale (Carrie et al., 2010). Il a été suggéré que cela pourrait être lié à la présence d'une SOD dans ce compartiment (CSD3) qui nécessite la formation d'un pont disulfure et dont l'expression est fortement diminuée dans le mutant *mia40* (Carrie et al., 2010).

Dans ce contexte, il est également intéressant de noter que les eucaryotes inférieurs appartenant notamment à la classe des Kinéoplastides, comprenant notamment les ordres Leishmania et Trypanosomes, ne contiennent pas la protéine MIA40 mais possèdent une protéine ERV1 avec une architecture atypique similaire aux protéines de plantes et d'ERV2 chez les levures. Il avait été suggéré que la protéine ERV1 était capable d'oxyder directement les substrats de MIA40. Cependant, la protéine ERV1 de Leishmania n'est pas capable de complémenter le mutant *mia40* de levure, bien qu'une protéine chimérique mimant la protéine de levure soit capable de complémenter le mutant *erv1* (Specht et al., 2018). Ces résultats suggéraient donc la nécessité d'un autre acteur dans ce processus d'oxydation. Une des protéines qui pourrait pallier à

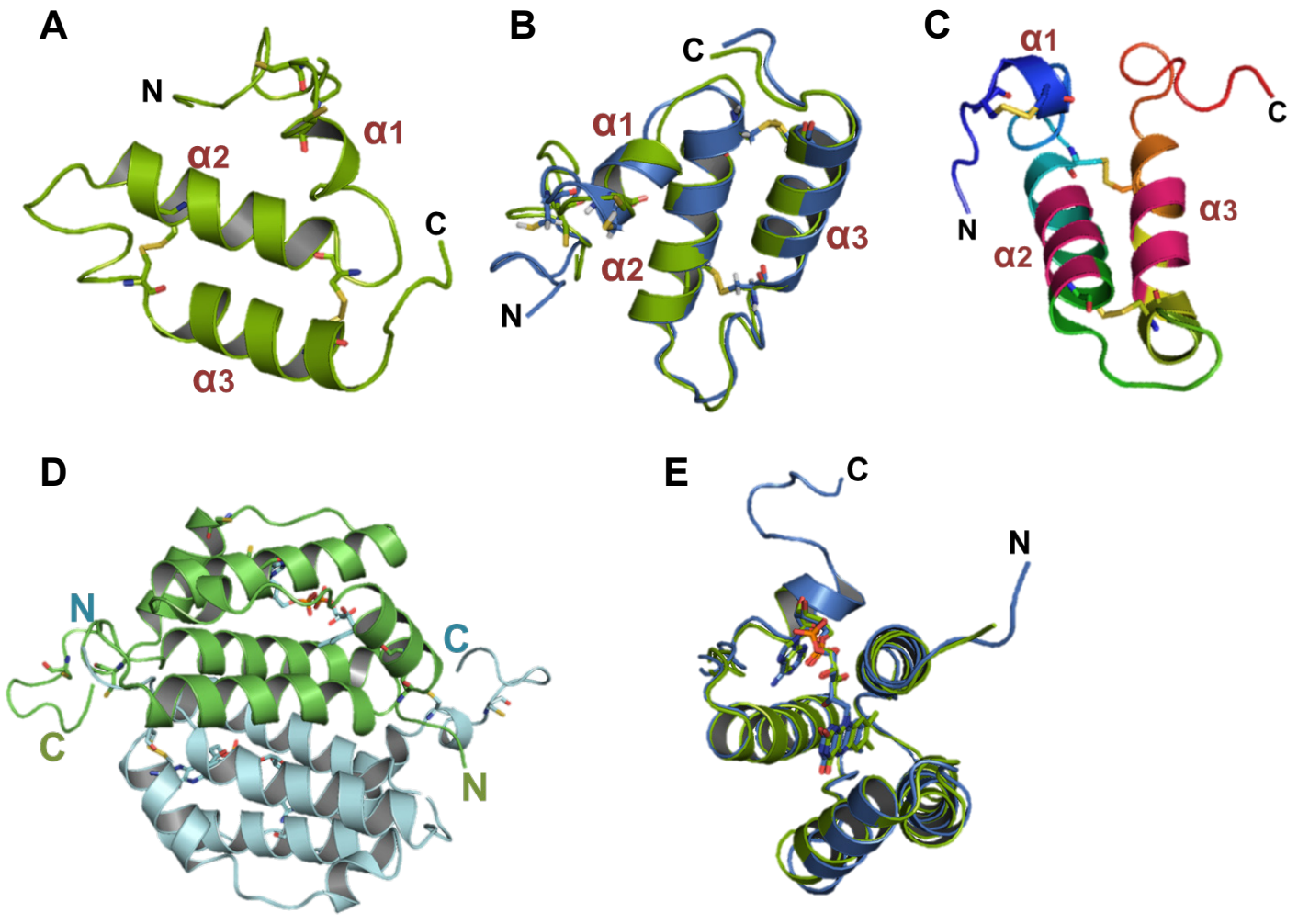


Figure 18: Analyse des structures tridimensionnelles des protéines MIA40 et ERV1 d'*A. thaliana*.

(A) Modèle structural de la protéine MIA40 d'*A. thaliana* (AtMIA40) à partir de la structure résolue par RMN de la protéine CHCHD4 humaine (code PDB, 2K3J). (B) Alignement structural des protéines MIA40 humaine (bleu) et d'*A. thaliana* (vert). (C) Localisation du patch hydrophobe (en rose) présent sur les hélices α_2 et α_3 d'AtMIA40. (D) Structure tridimensionnelle de la protéine ERV1 d'*A. thaliana* (AtERV1, code PDB 2HJ3). La protéine est présente sous la forme d'un homo-dimère avec les monomères (en bleu ou vert) orientés tête-bêche. L'extrémité C-terminale contenant le site actif, trop flexible, a été modélisée en utilisant la protéine ERV2 de *S. cerevisiae* (code PDB, 1JRA). (E) Alignement structural des domaines centraux FAD d'AtERV1 (vert) et de ScERV1 (bleu). Les différentes structures représentées ici ont été obtenues à l'aide des logiciels SWISS-MODEL, PyMOL et WinCoot.

l'absence de la protéine MIA40 est la protéine MIC20 qui comporte un repliement de type TRX et intervient dans le complexe de formation des jonctions cristallines au sein de la membrane interne (Kaurov et al., 2018).

3.3. Détails sur les mécanismes moléculaires et structuraux de la voie MIA40/ERV1

Les mécanismes moléculaires et structuraux décrits pour cette voie proviennent principalement d'études menées chez la levure et l'humain. Il existe assez peu d'éléments en ce qui concerne cette voie chez les organismes photosynthétiques. Les analyses phylogénétique et structurale des protéines MIA40 (Figure 17) laissent penser qu'il y a peu de différence entre isoformes d'organismes différents. En effet, l'ossature de la protéine est relativement bien conservée quel que soit l'organisme. La protéine adopte un repliement hélice-tour-hélice, les 2 hélices étant reliées par deux ponts disulfure impliquant les deux motifs Cx₉C alors que la région N-terminale à proximité des deux cystéines catalytiques présentes au sein du motif CPC forme une courte hélice α formant une sorte de crochet. Les différences existantes concernent la présence d'extensions N-terminales de longueur et de nature très variables. Chez la levure, cette extension est formée par un domaine transmembranaire permettant son ancrage à la membrane interne et donc sa rétention dans l'IMS (Peleh et al., 2016) ainsi que par une longue séquence peptidique qui n'est pas essentielle à la fonction de la protéine *in vitro* ni *in vivo* (Peleh et al., 2016, 2017). Bien que nous n'ayons aucune donnée structurale concernant la protéine MIA40 d'*A. thaliana*, la forte conservation de séquence a permis l'obtention d'un modèle relativement robuste en utilisant le logiciel SWISS-MODEL (<https://swissmodel.expasy.org/>) (Figure 18A). La superposition (Figure 18B) de ce modèle avec la protéine humaine (40.5% d'identité) indique que les principales caractéristiques structurales sont conservées. En effet, du côté N-terminal, nous pouvons observer une partie non structurée et très flexible comportant le site actif CPC (Cys68-Cys70 numérotation chez *A. thaliana*), qui devrait *a priori* être relativement bien exposée au solvant. Les hélices α 2 et α 3, orientées tête bêche sont reliées via deux ponts disulfure impliquant les deux motifs Cx₉C (Cys79-Cys88x₁₂Cys102-Cys111, numérotation chez *A. thaliana*). Ce corps hélice α forme un patch hydrophobe (ou clé hydrophobe) et est impliqué dans l'interaction avec les motifs MISS présents au sein des différents substrats (Banci et al., 2009, 2012; Milenkovic et

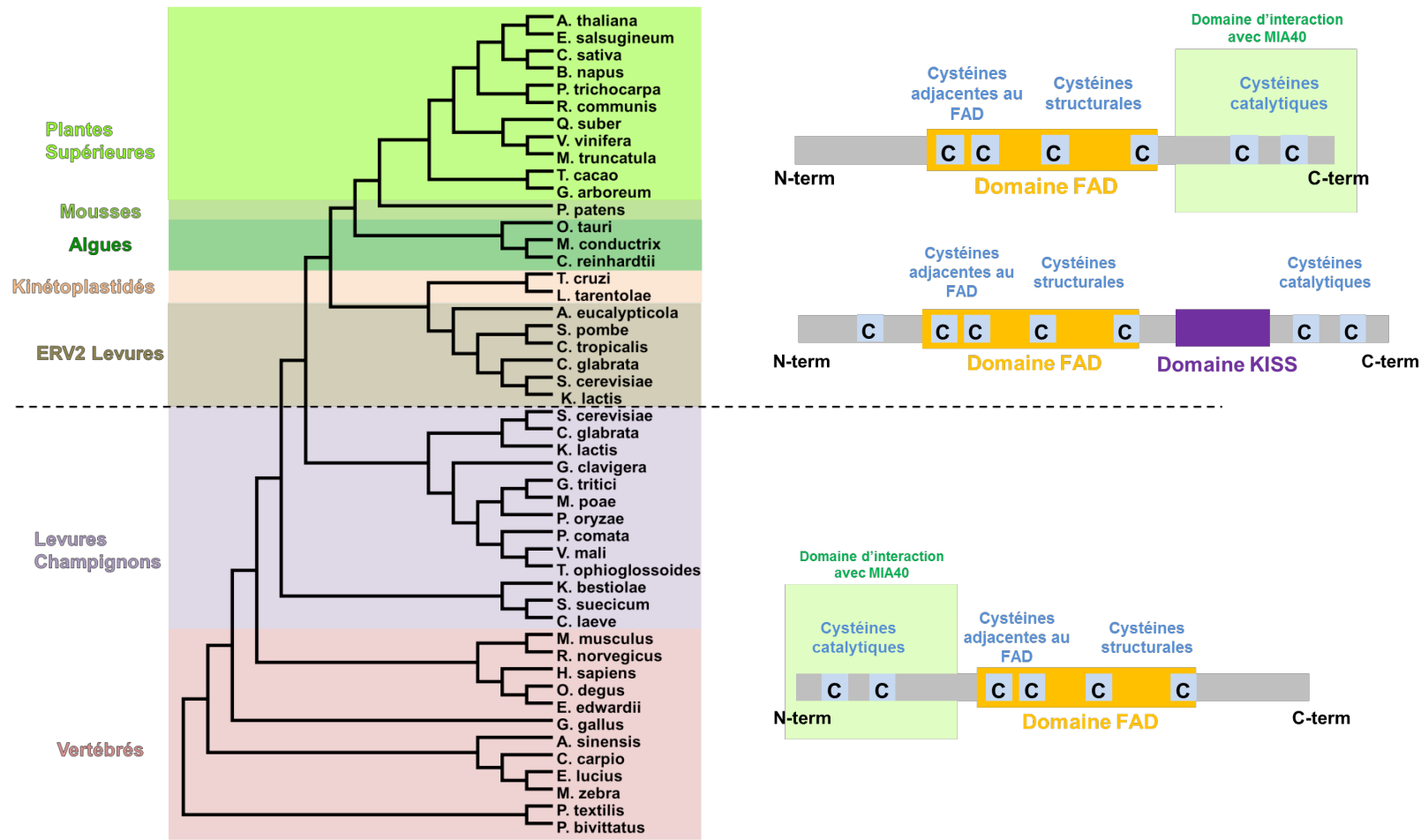


Figure 19: Analyse phylogénétique des protéines ERV1 présentes chez différents organismes eucaryotes « supérieurs » et « inférieurs » et organisation structurale. Cette analyse phylogénétique a été réalisée en utilisant le logiciel MEGA7. L'histoire évolutive a été déterminée en utilisant la méthode Neighbor-Joining et les distances évolutives sont basées sur l'analyse des matrices selon la méthode de Jones, Taylor & Thornton (JTT).

al., 2009; Sideris et al., 2009). L'hélice α 1 interagit avec cette clé hydrophobe conduisant à l'interaction du site actif CPC avec le substrat puis son oxydation (Meyer et al., 2019a).

Concernant la protéine *AtERV1*, il a été montré qu'elle adoptait en solution une structure en homodimère (Vitu et al., 2006), chaque monomère étant en orientation tête-bêche. Les analyses phylogénétique et structurale (Figure 19) mettent en avant que le domaine central de la protéine semble être relativement bien conservé. Il est constitué de cinq hélices α et possède quatre cystéines (Cys119, Cys122, Cys148 et Cys165 chez l'isoforme d'*A. thaliana*) (Vitu et al., 2006). Les Cys148-Cys165 permettent la formation d'un pont disulfure intramoléculaire structural et n'interviennent donc pas dans le mécanisme catalytique. En revanche, les Cys119-Cys122 forment le motif thiol-disulfure proche du domaine FAD. Ce dernier va transférer les électrons jusqu'à une molécule d'oxygène, soit directement en la réduisant partiellement en H_2O_2 , ou indirectement via le cytochrome c permettant sa réduction complète en H_2O au travers du complexe IV de la chaîne respiratoire mitochondriale (Bihlmaier et al., 2007; Vitu et al., 2006). L'inversion des cystéines catalytiques permettant la régénération de la protéine MIA40 représente la différence majeure entre l'isoforme ERV1 des mammifères, champignons et levures (embranchement des Opistochontes) et l'isoforme ERV1 présente chez les organismes photosynthétiques. En effet, le motif catalytique Cx_2C est localisé à l'extrémité N-terminale chez les opistochontes tandis qu'il est présent au niveau de la partie C-terminale de la protéine des organismes photosynthétiques. Il est également intéressant de noter que chez les opistochontes, ce domaine N-terminal est important pour la reconnaissance de la protéine MIA40. Contrairement aux opistochontes, le site catalytique des protéines ERV1 présente une grande diversité chez les organismes photosynthétiques. En effet, les isoformes des plantes terrestres possèdent un motif $Cx_{3-5}C$, alors que les isoformes des algues vertes ont un motif $Cx_{8-18}C$ ou présentant un site dégénéré où l'une des deux cystéines est quelquefois absente suggérant un mécanisme d'action différent. Il peut être intéressant de noter que la protéine ERV1 présente chez les kinétoplastides comporte une architecture similaire à celle des organismes photosynthétiques. Les cystéines catalytiques forment également un site actif Cx_3C localisé dans la partie C-terminale de la protéine. Toutefois, dans cet embranchement nous observons un domaine additionnel KISS présent entre le domaine FAD et le site actif Cx_3C . Cette différence structurale peut expliquer pourquoi la protéine ERV1 de *Leishmania* est incapable de complémenter fonctionnellement le mutant *erv1* de levure (Eckers et al., 2013; Specht et al., 2018).

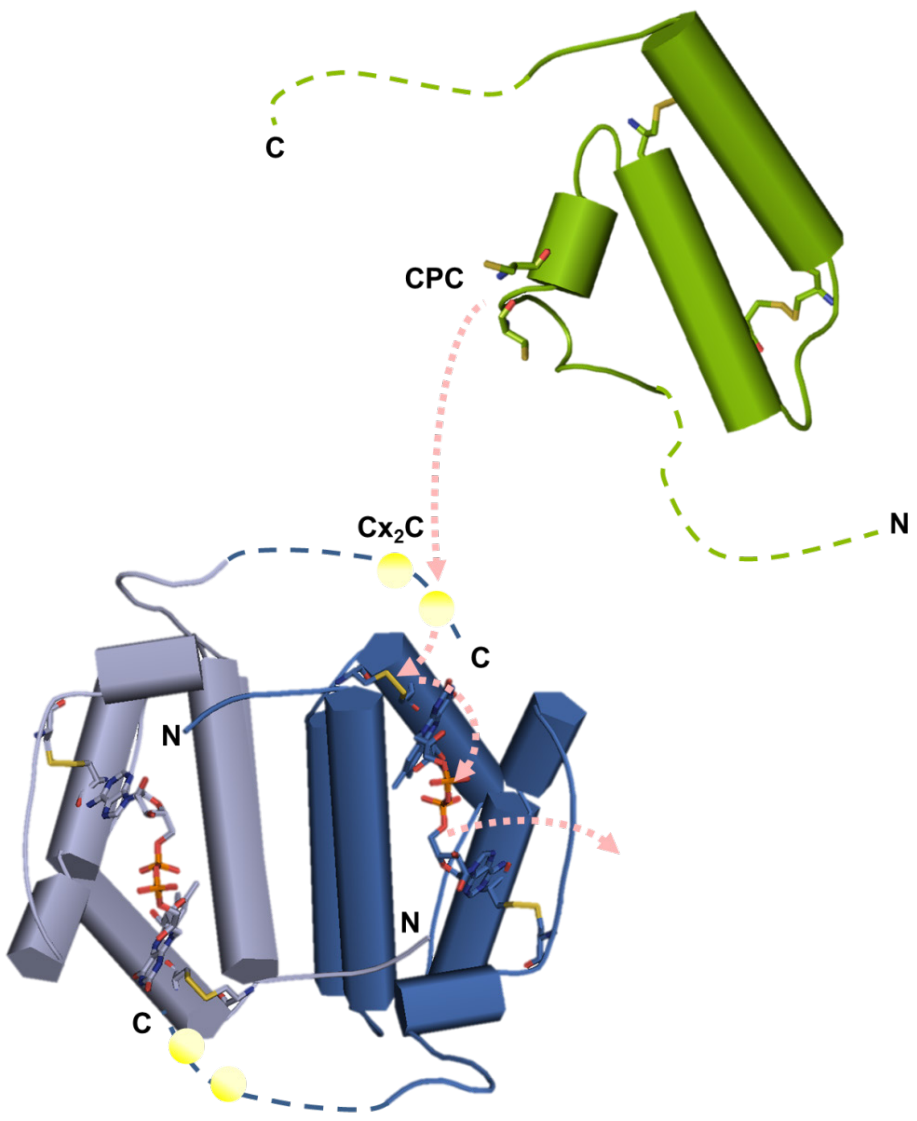


Figure 20: Echanges électroniques impliqués dans la régénération de MIA40 (vert) par ERV1 (bleu) chez *A. thaliana*. Le motif CPC de MIA40 transfère les électrons aux cystéines du site actif Cx₂C présent en C-terminal d'un des monomères ERV1, ces électrons sont ensuite transférés aux cystéines adjacentes au cofacteur FAD présentes au sein du motif Cx₂C de l'autre monomère puis enfin au cofacteur FAD de ce même monomère.

Les études réalisées chez les kinétoplastidés de même que les analyses phylogénétique et structurale pourraient expliquer l'incapacité des protéines ERV1 et MIA40 d'*A. thaliana* à complémer les mutants correspondants de levure ainsi que l'absence de phénotype chez le mutant *mia40* d'*A. thaliana* (Carrie et al., 2010; Levitan et al., 2004). En se basant sur le modèle de l'eucaryote inférieur *Leishmania*, ces différences structurales pourraient empêcher la protéine *AtERV1* de régénérer la protéine Mia40 de levure et l'absence de phénotype chez le mutant *mia40* de plante pourrait s'expliquer par un rôle non-essentiel de MIA40 ou la présence d'une protéine MIA40-like accomplissant la même fonction.

Néanmoins, le mécanisme catalytique permettant le transfert des électrons du substrat jusqu'à une molécule d' O_2 semble être conservé quel que soit l'organisme (Figure 20). Les électrons provenant du substrat sont transférés séquentiellement du site actif CPC de MIA40 jusqu'au site catalytique Cx_nC du monomère 1 de ERV1. Ce dernier qu'il soit présent en N- ou C-terminal est régénéré par le site actif Cx_2C du domaine central du monomère 2 qui, présent à proximité du cofacteur FAD va permettre sa réduction puis celle d'une molécule d'oxygène.

4. Les systèmes de repliement oxydatif au sein du lumen des thylakoïdes

Comme au sein du RE et de l'IMS des mitochondries, le lumen des thylakoïdes possède un système de formation des ponts disulfure permettant le repliement structural de certaines protéines.

Le système de repliement oxydatif des protéines présent au niveau du lumen des thylakoïdes comporte lui aussi les trois grands composants nécessaires à l'oxydation : (i) une oxydoréductase, (ii) une thiol oxydase et (iii) un accepteur final d'électrons. Les deux premières fonctions sont assurées par une seule protéine, appelée Lumen Thiol Oxydoréductase 1 (LTO1), qui est une protéine fusion entre un domaine C-terminal TRX/DsbA-like et un domaine VKOR permettant la régénération de l'oxydoréductase (Figure 21) (Karamoko et al., 2011). Le domaine VKOR comporterait entre quatre et cinq domaines transmembranaires insérés dans la membrane des thylakoïdes. Il compte également deux paires de cystéines conservées présentes au sein de motifs $Cx_{4-6}C$ et Cx_2C . Le premier est responsable de l'oxydation des motifs cystéiniques présents au sein du domaine DsbA-like et le deuxième transfère les électrons vers l'accepteur final qui pourrait être une phylloquinone (PQ) ou une naphtoquinone, ce qui permettrait de connecter ce

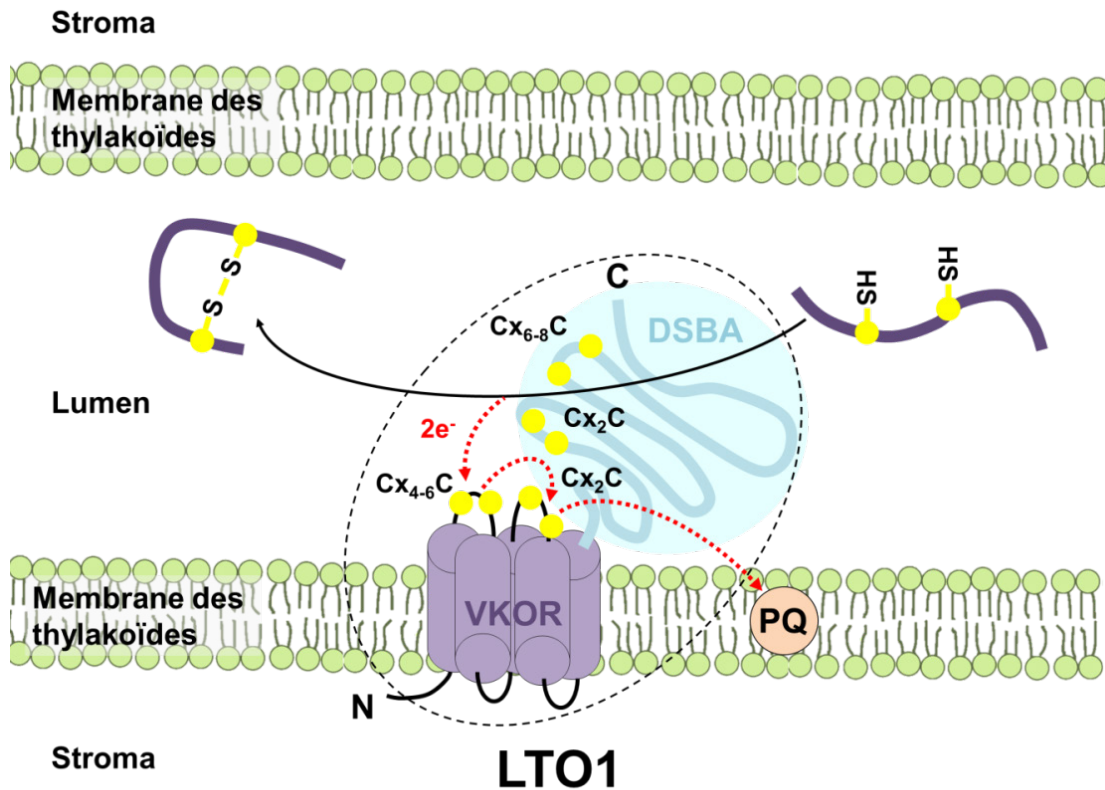


Figure 21: Représentation schématique du système d’oxydation des protéines présent au niveau du lumen des thylakoïdes.

La protéine LTO1 est une fusion entre un domaine N-terminal VKOR (thiol oxydase) permettant l’oxydation d’une ou deux paires de cystéine présentes dans le domaine DSBA en position C-terminale et qui permettent l’oxydation des protéines cibles. Bien que le mécanisme moléculaire ne soit pas totalement élucidé, le motif $Cx_{4-6}C$ assurerait l’oxydation de l’un des deux ou des deux motifs (Cx_2C et $Cx_{6-8}C$) du domaine DSBA puis de transférer les électrons résultant de cette oxydation à la plastoquinone (PQ), présente au niveau de la membrane des thylakoïdes par l’intermédiaire du motif Cx_2C .

système au PSII et à la biosynthèse de NADPH (Furt et al., 2010). Le domaine DsbA contient également deux paires de cystéines conservées au sein des motifs Cx₂C et Cx₆₋₈C, permettant le transfert d'électrons du substrat vers le domaine VKOR (Figure 21). Les paires de cystéines composant les deux motifs Cx₆₋₈C et Cx₂C au sein du domaine DsbA de LTO1 et impliquées dans l'oxydation des substrats n'ont pas été précisément identifiées à l'heure actuelle.

Au niveau fonctionnel, LTO1 est capable de compléter partiellement les simples mutants *dsbA*, *dsbB* et un double mutant *dsbA/dsbB* d'*E. coli*, confirmant ainsi la fonctionnalité des 2 domaines et l'existence d'activités oxydoréductase et thiol oxydase au sein de la même protéine (Feng et al., 2011; Karamoko et al., 2011). De plus, ces études ont montré que les huit cystéines conservées de la protéine LTO1 étaient indispensables à la complémentation fonctionnelle des mutants bactériens (Feng et al., 2011). L'importance des 4 cystéines du domaine VKOR a également été confirmée *in planta* par complémentation fonctionnelle du mutant *lto1* d'*A. thaliana* avec des mutants monocystéiniques de LTO1 (Du et al., 2015). Ce mutant *lto1* d'*A. thaliana* présente un déficit d'efficacité du photosystème II (PSII) associé à une réduction sévère de l'abondance des sous-unités structurales du PSII et notamment de la protéine D1 alors que l'abondance des protéines formant le cytochrome b(6)f ou le photosystème I reste inchangée (Karamoko et al., 2011; Lu et al., 2013). De ce fait, la croissance végétative de ce mutant est fortement affectée dans des conditions standard et des phénomènes de photo-inhibition sont observés en réponse à de fortes intensités lumineuses (Yu et al., 2014). Ce dernier phénotype serait lié à un défaut de dissipation d'énergie dû à l'inefficacité du cycle des xanthophylles. De plus, ce mutant accumule des ROS en situation de stress osmotique et LTO1 pourrait dans ce cadre affecter la biosynthèse d'ABA (Lu et al., 2015). Cette sensibilité aux ROS semble liée à une diminution de l'abondance de certaines enzymes antioxydantes telles que l'APX1, la CAT2 et la DHAR1 (Lu et al., 2013).

La plupart de ces phénotypes sont *a priori* expliqués par des défauts de repliement oxydatif de certaines protéines. Ainsi, il a été montré par double hybride en levure que le domaine TRX/DsbA de LTO1 interagit avec PsbO, une sous-unité du PSII qui nécessite la formation d'un pont disulfure (Karamoko et al., 2011). La protéine recombinante catalyse l'oxydation *in vitro* de PsbO mais aussi de FKBP13 (FK-506 binding protein 13), une peptidyl-prolyl cis-trans isomérase qui est inactive lorsque ses 2 paires de cystéines sont réduites (Gopalan et al., 2004; Karamoko et al., 2011; Lu et al., 2013). Ce dernier résultat est plus surprenant car AtFKBP13 est

essentielle pour la formation du complexe Cyt b₆f (Gupta et al., 2002), mais celui-ci ne semble pas affecté dans un mutant *lto1*. D'autres cibles potentielles de LTO1 ont été isolées par double hybride binaire en levure en utilisant le domaine TRX/DsbA comme appât. Il s'agit d'HCF164 (High Chlorophyll Fluorescence 164), du cytochrome c6A, de la violaxanthine dé-époxidase, de la protéine d'arrêt du développement du sac embryonnaire (EDA3), de deux protéines PPR (TL17 et TL20.3) et d'une autre protéine de liaison à FK-506, FKBP20-2 (Lu et al., 2015). L'interaction avec la violaxanthine dé-époxidase, dont l'activité est inhibée par réduction (Hall et al., 2011), explique sans doute le défaut de dissipation thermique observé dans le mutant *lto1*. L'interaction avec HCF164 peut paraître surprenante car celle-ci possède une activité réductase (Motohashi and Hisabori, 2006). En réalité, au moins 30 protéines sur les 80-100 protéines identifiées à l'heure actuelle dans le lumen des thylakoïdes possèdent un pont disulfure, ce qui suggère que le nombre de partenaires de LTO1 est plus important et/ou qu'une autre protéine possède une activité oxydase (Hall et al., 2011; Kang and Wang, 2016).

V. Les systèmes de réduction intervenant dans la maturation des cytochromes de type c dans l'IMS et le lumen des thylakoïdes

Un certain nombre de protéines présentes dans les compartiments où se déroule le repliement oxydatif nécessitent *a contrario* d'être sous forme réduite. C'est le cas des cytochromes de type c. En effet, à la différence des hèmes a et b, les hèmes c sont attachés de manière covalente aux apocytochromes c par l'intermédiaire de deux résidus cystéines présents au sein d'un motif caractéristique Cx₂CH. Ces dernières forment une liaison thioéther entre leur groupement thiol et la fonction vinyle du groupement prosthétique de l'hème. La maturation des cytochromes de type c (cyto-c) est réalisée de manière post-traductionnelle. Leur présence au sein de compartiments ayant une nature plutôt oxydante (périplasme, IMS, lumen des thylakoïdes) implique l'existence de machineries particulières et/ou d'un système de réduction spécifique afin que les cystéines présentes soient maintenues sous forme réduite. Jusqu'à présent trois grands systèmes d'assemblage des cyto-c ont été distingués. Le système I est présent chez les α - et γ -protéobactéries et certaines β - et δ -protéobactéries, mais également au sein des mitochondries des organismes photosynthétiques et de certains protozoaires. Le système II est trouvé au sein des chloroplastes, des bactéries Gram positive, des cyanobactéries et la plupart des β - et δ -protéobactéries. Enfin, le système III est essentiellement retrouvé au niveau des mitochondries

des Opistochontes (champignons et vertébrés), d'invertébrés et de quelques protozoaires (Kranz et al., 2009). Ce dernier semble relativement rudimentaire mais efficace (Dumont et al., 1987). En effet, après import de l'apo-cytochrome et de l'hème au sein de l'espace intermembranaire, une cytochrome hème lyase (CCHL) associée à la membrane interne permet la liaison de l'hème afin de produire un holo-cytochrome c. Ce système ne nécessite aucune autre enzyme (Bernard et al., 2003; Travaglini-Allocatelli, 2013).

1. Le système I de maturation des cytochromes c au sein de l'IMS des organismes photosynthétiques

Le système I paraît le plus complexe des trois types d'assemblage utilisant jusqu'à 8 ou 9 protéines associées à la membrane interne appelées protéines CCM (Cytochrome C Maturation) chez les bactéries (Verissimo et al., 2017). D'une façon simpliste, il peut être divisé en deux grandes étapes, l'import de l'hème au niveau du site d'assemblage par les protéines CcmABCDE et la fixation covalente de l'hème à l'apo-cytochrome par les protéines CcmFGHI. Chez *E. coli*, il a été mis en évidence que la protéine CcmF était capable de fixer un hème et permettrait également sa réduction par l'intermédiaire d'une quinone (Richard-Fogal et al., 2009). Bien qu'il soit maintenant certain que les protéines CcmG et H interviennent dans la réduction de l'apo-cytochrome, leurs fonctions exactes restent incertaines (Meyer et al., 2019b; Verissimo et al., 2017). L'assemblage des cytochromes c au sein de mitochondries des organismes photosynthétiques diffère de celui retrouvé chez les bactéries. En effet, *A. thaliana* possède des gènes codant pour les protéines CCMA, CCME et CCMH dans le génome nucléaire et pour les protéines CCMB, CCMC et CCMF dans le génome mitochondrial mais pas pour CCMG et la réductase transmembranaire DsbD (Meyer et al., 2005; Rayapuram et al., 2008), soulevant ainsi la question de la réduction de l'apo-cytochrome c au sein de l'IMS des plantes terrestres. En accord avec l'idée qu'il n'y a pas de redondance fonctionnelle avec CCMG comme suggéré chez les bactéries ou de voie alternative, la mutation du gène *CCMH* chez *A. thaliana* est létale au stade embryonnaire (Meyer et al., 2005). CCMH diffère de son homologue bactérien par la perte de son domaine CcmI-like dans sa partie C-terminale (Ahuja et al., 2008). La protéine CCMH retrouvée chez les plantes est constituée de 3 domaines, le domaine N-terminal comportant le site actif Cx₂CH et exposé vers l'IMS, un domaine transmembranaire et un domaine C-terminal exposé vers la matrice (Meyer et al., 2005). Cette dernière étude a mis en évidence que la

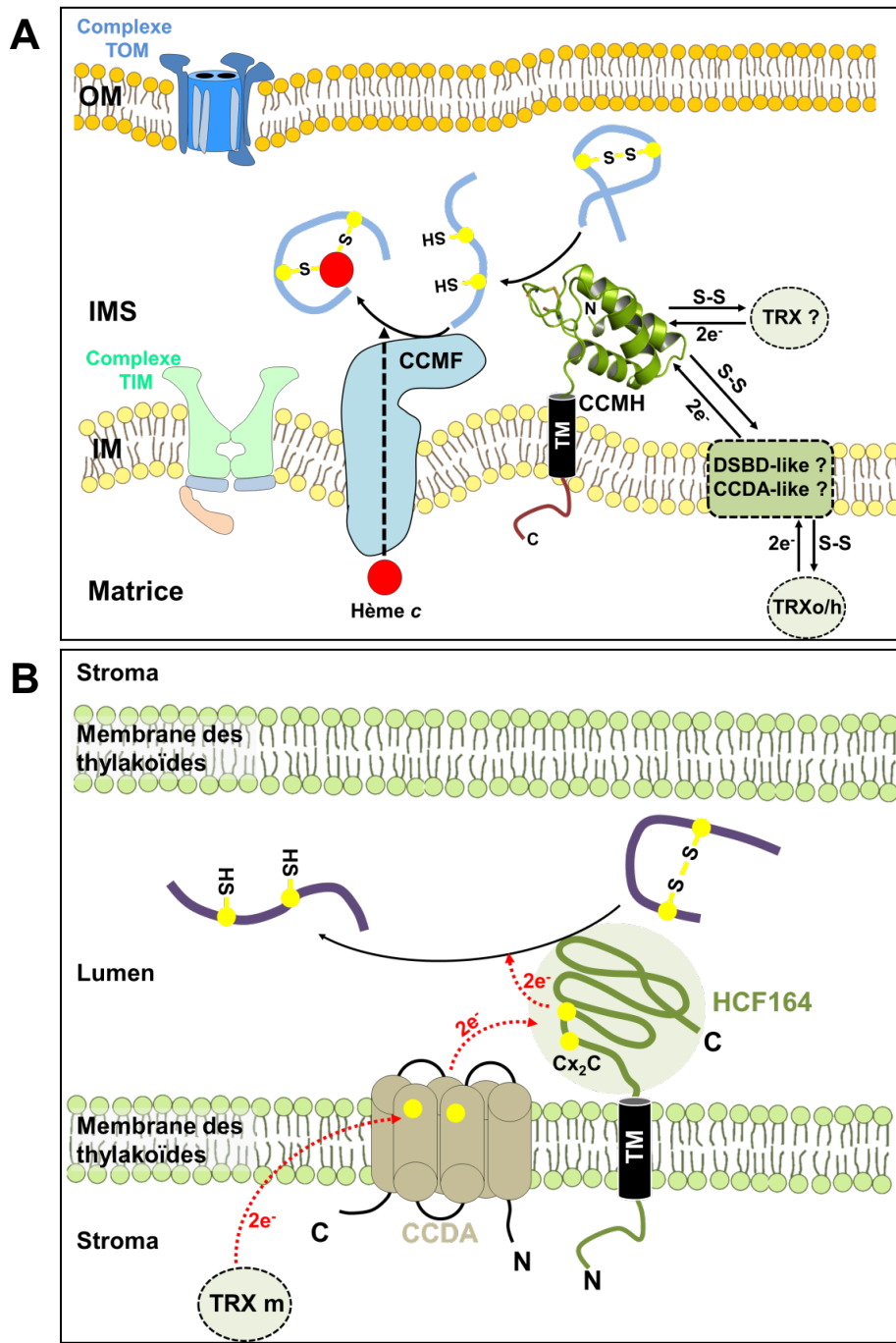


Figure 22: Systèmes de réduction présents au sein de l'IMS des mitochondries (A) et du lumen des thylakoïdes (B) et intervenant dans la maturation des cytochromes c.

(A) Le système de réduction au sein de l'IMS est un système de maturation du cytochrome c de type I. La réductase CCMH est composée d'un domaine C-terminal exposé vers la matrice, d'un domaine central membranaire (TM) et d'un domaine N-terminal exposé face à l'IMS, permettant la réduction de l'apo-cytochrome c (le domaine réductase d'*A. thaliana* a été modélisé à partir de la protéine de *Pseudomonas aeruginosa* (2HL7)). Une fois réduit, l'apo-cytochrome interagit avec la protéine CCMF permettant l'import et l'incorporation de l'hème afin de former l'holo-cytochrome c.

(B) Le système de réduction situé au niveau du lumen des thylakoïdes est un système de maturation type II. Ce système fait intervenir deux protéines dénommées CCDA et HCF164. HCF164 est une réductase (TRX-like) permettant l'interaction et la réduction des protéines cibles (apo-cytochrome entre autres) via son site actif Cx₂C. Elle est ancrée à la membrane via un domaine transmembranaire (TM). Cette protéine est maintenue sous une forme réduite grâce à l'action de la protéine CCDA qui permettrait de transférer le pouvoir réducteur provenant d'une TRX m localisée au sein du stroma.

protéine recombinante correspondant au domaine N-terminal est capable de réduire des peptides contenant le motif Cx₂CR retrouvé au sein de l'apo-cytochrome c. Cependant il n'a toujours pas été démontré comment la protéine CCMH était elle-même réduite et ainsi, si et comment des électrons transitaient à travers la membrane interne. Une des hypothèses émise par (Meyer et al., 2019b) est la présence d'une protéine inconnue ayant une fonction analogue à la protéine DsbD bactérienne voire que CCDA, le paralogue chloroplastique, soit aussi adressé à la mitochondrie. Le pouvoir réducteur proviendrait de TRXs mitochondriales présentes dans la matrice telle que les TRXo1, o2 ou h2 (Figure 22A). D'autres hypothèses reposent sur la présence d'un système TR-TRX au sein de l'IMS comme chez la levure ou la participation du pool de GSH.

2. Le système de réduction et de maturation de type II des cytochromes c au sein du lumen des thylakoïdes

Le système de type II a été mis en évidence dans les années 1990 par l'intermédiaire d'études génomiques chez *Chlamydomonas* (Dreyfuss et al., 2003). Comme dans l'IMS de la mitochondrie, ce système doit permettre (i) la réduction de l'apo-cytochrome et (ii) la fixation de l'hème à ce dernier. Ce système repose sur la présence de quatre protéines chez les bactéries. La protéine membranaire CcsA comporte un domaine WWD avec trois histidines conservées et permet de transporter l'hème vers l'espace intermembranaire. Elle forme un complexe avec la protéine CcsB qui aide à maintenir l'apo-cytochrome à proximité de l'hème et de deux derniers acteurs, DsbD et CcsX qui interviennent dans la réduction des cystéines du motif Cx₂CH de l'apo-cytochrome. La protéine CcsX participe directement à la réduction, alors que DsbD (comme pour le système Dsb périplasmique section IV 1) transfère le pouvoir réducteur provenant d'une TRX à travers la membrane interne jusqu'à la réductase (Kranz et al., 2009). Au sein du lumen des thylakoïdes, huit protéines seraient impliquées(Gabilly and Hamel, 2017). Les protéines CCDA et HCF164 permettraient la réduction ou le maintien sous forme réduite de l'apo-cytochrome. L'absence de l'un de ces deux acteurs chez *A. thaliana* conduit à un défaut d'assemblage du cytochrome b6f au sein des thylakoïdes (Page et al., 2004).

Du point de vue structural, CCDA est similaire à la protéine DsbB bactérienne. Elle possède six hélices α transmembranaires lui permettant de s'insérer au sein de la membrane des thylakoïdes

mais également de recevoir des électrons des TRXs-m présentes au niveau du stroma des chloroplastes (Figure 22B). Les TRXs-m réduiraient un pont disulfure formé entre deux cystéines conservées au niveau des hélices α transmembranaires 1 et 4, ces cystéines assureraient ensuite la réduction du pont disulfure catalytique formé par les cystéines présentes au sein du motif Cx₂C d'HCF164 (Motohashi and Hisabori, 2006, 2010). En effet, cette TRX-like possède un domaine transmembranaire en position N-terminale permettant un ancrage au niveau de la membrane et un domaine TRX en position C-terminale contenant un motif Cx₂C. Une protéine recombinante correspondant au domaine TRX présente une activité réductase *in vitro* (Lennartz et al., 2001; Motohashi and Hisabori, 2006). Les cibles connues de cette réductase sont la sous-unité N du PSI (psaN) ainsi que l'holo-cytochrome f faisant partie du complexe cytochrome *b6f* (Hisabori et al., 2005; Motohashi et al., 2009). La capacité d'interagir avec l'oxydase LTO1 suggère qu'HCF164 pourrait assurer l'isomérisation de ponts disulfure de protéines dont le repliement structural est non conforme au niveau du lumen des thylakoïdes (Lu et al., 2015).

Présentation et objectifs du sujet de thèse

Cette thèse a été effectuée au sein de l'équipe Réponse aux stress et régulation redox de l'UMR 1136 « Interactions Arbres Micro-organismes » Université de Lorraine-INRA. Un des objectifs de ce laboratoire est de comprendre dans un contexte de changement climatique global les interactions des plantes avec leur environnement, et notamment les mécanismes de défense des organismes végétaux en réponse à des stress abiotiques ou biotiques. Ma thèse s'inscrit plus particulièrement dans le projet MetOx (Identification de nouvelles fonctions régulées par des métaux ou par des processus redox chez les plantes) financé par le Labex ARBRE (Advanced Research on the Biology of Tree and Forest Ecosystems). L'objectif de ce projet est de caractériser des protéines possédant un ou plusieurs motifs Cx₂C conservés et dont la fonction est inconnue ou peu caractérisée chez deux plantes modèles *Arabidopsis thaliana* et *Populus trichocarpa*. En effet les protéines comportant un ou plusieurs motifs Cx₂C ont la capacité d'intervenir dans différents processus d'échanges dits dithiol/disulfure mais également dans la coordination d'ions métalliques seuls ou présents au sein de cofacteurs tels que les hèmes de type c et les centres Fe-S. Le travail mené lors de ce doctorat a porté sur trois grands axes de recherche: (i) un axe rédoxines qui a eu pour but de caractériser d'un point de vue biochimique la glutarédoxine chloroplastique de classe II d'*A. thaliana* (AtGRXS16); (ii) un axe orienté sur la coordination des centres Fe-S qui a permis de mettre en évidence de manière surprenante la capacité des TRX o1 et o2 d'*A. thaliana* à coordonner un centre 4Fe-4S; et enfin, (iii) un axe oxydase qui par l'intermédiaire d'approches fonctionnelle et biochimique nous a permis de mettre en lumière la spécificité du système MIA40/ERV1 chez *A. thaliana*.

Résultats

In Vitro Alkylation Methods for Assessing the Protein Redox State

Flavien Zannini¹, Jérémie Couturier¹, Olivier Keech², and Nicolas Rouhier¹

¹ Université de Lorraine, Inra, IAM, F-54000 Nancy, France.

² Department of Plant Physiology, Umeå Plant Science Centre, Umeå University, Umeå, Sweden.

Article publié dans Methods in molecular biology, Photorespiration.

Dans ce chapitre de méthodes, nous avons fourni des protocoles détaillés pour la caractérisation des propriétés redox (pka des cystéines, potentiel redox d'un pont disulfure et analyse de la sensibilité d'oxydoréductases à la réduction/oxydation par alkylation) de protéines comportant des cystéines réactives, telles que celles étudiées au cours de cette thèse.

Chapter 4

In Vitro Alkylation Methods for Assessing the Protein Redox State

Flavien Zannini, Jérémie Couturier, Olivier Keech, and Nicolas Rouhier

Abstract

Cysteines are important residues for protein structure, function, and regulation. Owing to their modified reactivity, some cysteines can undergo very diverse redox posttranslational modifications, including the reversible formation of disulfide bonds, a widespread protein regulatory process as well exemplified in plant chloroplasts for Calvin-Benson cycle enzymes. Both core- and peripheral-photorespiratory enzymes possess conserved cysteines, some of which have been identified as being subject to oxidative modifications. This is not surprising considering their presence in subcellular compartments where the production of reactive species can be important. However, in most cases, the types of modifications and their biochemical effect on protein activity have not been validated, meaning that the possible impact of these modifications in a complex physiological context, such as photorespiration, remains obscure.

We here describe a detailed set of protocols for alkylation methods that have been used so far to (1) study the protein cysteine redox state either *in vitro* by submitting purified recombinant proteins to reducing/oxidation treatments or *in vivo* by western blots on protein extracts from plants subject to environmental constraints, and its dependency on the two major reducing systems in the cell, i.e., the thioredoxin and glutathione/glutaredoxin systems, and (2) determine two key redox parameters, i.e., the cysteine pK_a and the redox midpoint potential.

Key words Alkylation, Cysteine, Oxidative modification, pK_a , Redox potential

1 Introduction

Cysteine (Cys) is one of the least abundant amino acids in proteins; however, it is very important for protein structure and function being for instance found in protein active sites and/or subject to co- or posttranslational modifications including lipidation (prenylation or palmitoylation) but also disulfide bond formation, glutathionylation or nitrosylation to only cite the major ones. In specific protein environments, e.g., in active sites, the pK_a of some cysteine residues is decreased towards acidic values compared to the $pK_a \sim 8.3$ of free cysteines [1]. Thus, under certain physiological conditions, e.g., around neutral pH, the more reactive thiolate (S^-) form will predominate as compared to the thiol

(SH) form. On the other hand, such a chemical property implies that these residues are usually more sensitive to oxidative modifications. Hence, in subcellular compartments or under specific conditions, the cysteine residues will be oxidized by various types of molecules/agents leading notably to the formation of sulfenic acids (SOH), disulfide bonds (S–S), and glutathionylated (S–SG) or nitrosylated (S–NO) forms [2]. All these aforementioned post-translational modifications are reversible, mostly through the action of the thioredoxin (TRX) and/or glutathione (GSH)/glutaredoxin (GRX) reducing systems. If not condensed with another cysteine, e.g., in the absence of a vicinal thiol group or a reductant, sulfenic acids may eventually be irreversibly oxidized to sulfinic (SO_2H) and sulfonic (SO_3H) acids. The only documented case of sulfinic acid reduction concerns the ATP- and Mg^{2+} -dependent reduction of sulfinylated peroxiredoxins catalyzed by sulfiredoxins [3]. Depending on the physiological context, the oxidative modification of cysteine residues may have diverse impacts on protein function, for which many examples of protein activation or inactivation have been reported. A well-documented example of redox regulation concerns the Calvin-Benson cycle enzymes that are activated by light and incidentally by the ferredoxin/ferredoxin-thioredoxin reductase/TRX system, through dithiol-disulfide exchanges [4]. Besides these regulatory mechanisms, a transient and reversible inactivation by oxidation can also be seen as a protective mechanism preventing irreversible protein over-oxidation.

A targeted *in vitro* approach to study cysteine sensitivity to oxidation within a given protein is to perform cysteine alkylation using maleimide-containing reagents, which specifically bind thiol groups. The cysteine derivatization will result in a mobility shift on nonreducing SDS-PAGE that is dependent on the number of cysteines oxidized. One of the first compounds used was the 4-acetamido-4'-maleimidylstilbene-2,2'-disulfonic acid (AMS), which induced an electrophoretic migration shift of ~0.5 kDa per free thiol group [5–7]. However, as this was sometimes insufficient for separating a mixture of different species, especially for proteins with a high molecular weight, it has sometimes been replaced by maleimides linked to polymers, such as polyethylene glycol (PEG) of different sizes ranging generally from 1 to 30 kDa [8, 9]. The drawback of these PEG-maleimide compounds is that PEG polymerization likely generates a heterogeneous mixture that often results in broad bands on SDS-PAGE. Moreover, the fact that these polymers are not charged prevents linear mobility shifts on SDS-PAGE. Therefore, researchers in both academic and industrial settings have developed chemically synthesized maleimide probes coupled to peptides [10] or nucleic acids [11].

Such an alkylation method can be used with both recombinant proteins and protein extracts, under the condition that a specific

antibody is available for the western blot detection. Besides evaluating the sensitivity of a given protein to a specific oxidative condition, this method also has the ability to determine which of the TRX or GSH/GRX systems can reduce a given oxidized form [9, 12]. Using protein extracts made from plants grown under specific controlled conditions, this method enables the assessment of changes in the levels of oxidation over time-course experiments, and is partially quantitative. That being said, without using chemicals specific to a given modification in tandem with mass spectrometry analyses, this method will neither indicate the type(s) of modification, nor the identity of which cysteine(s) is/are modified. The method described here has been successfully and elegantly tested for detecting the activation of Calvin-Benson cycle enzymes in response to various light intensities and/or in specific genetic backgrounds as *trx* knockout plants [13].

By analyzing the lists of potential redox-regulated proteins identified by large-scale redox proteomic analyses, we recently pointed to the fact that nearly all photorespiratory enzymes from the canonical pathway, as well as most of the known photorespiration-associated enzymes, may be subject to redox regulation, even though the type of modifications and the effect on activity have in fact almost never been investigated [14]. Hence, we describe here three complementary methods that aim at assessing the cysteine redox properties and redox states into a protein of interest. The first method describes the analysis of a protein redox state, which can be applied both *in vitro* and *in vivo* by anyone interested in the regulation of the activity of photorespiratory enzymes and of course of any other protein susceptible to redox regulation. The two other *in vitro* methods also rely on cysteine alkylation and allow determining cysteine pK_a and the redox midpoint potential of protein disulfides.

2 Materials

2.1 Required Instrumentation

Bench size shaker, benchtop centrifuge, dialysis membrane tubing and/or desalting columns, fluorometer, gel electrophoresis system, power supplier, UV-visible spectrophotometer.

2.2 Buffers and Solutions

2.2.1 Compound Solubility for Stock Solutions

Stock solutions of hydrogen peroxide (H_2O_2), iodoacetamide (IAM), reduced glutathione (GSH), oxidized glutathione (GSSG), nitrosoglutathione (GSNO), 1,4-dithiothreitol (DTT_{red}), trans-4,5-dihydroxy-1,2-dithiane (DTT_{ox}), tris(2-carboxyethyl) phosphine hydrochloride (TCEP), and trichloroacetic acid (TCA) are prepared in distilled or Milli-Q water. For GSH, GSSG, and GSNO solutions, the pH has to be readjusted to pH 7.0 or 8.0 using sodium hydroxide. Stock solutions of

5-iodoacetamidofluorescein (fluo-IAM), of monobromobimane (mBrB) and of 5,5'-dithiobis-(2-nitrobenzoic Acid) (DTNB) are prepared, respectively, at 9.7 mM in dimethylsulfoxide (DMSO), at 73 mM in acetonitrile and at 10 to 20 mM in ethanol.

2.2.2 Preparation of pH 2.0–10.0 Buffers for the Determination of Cysteine pK_a

1. 100 mM Citrate buffers between pH 2.0 and 6.0 are prepared by mixing 100 mM citric acid and sodium citrate solutions.
2. 100 mM Phosphate buffers between pH 6.5 and 8.0 are prepared by mixing 100 mM potassium phosphate monobasic and dibasic solutions.
3. 100 mM Borate buffers between pH 8.5 and 10.0 are prepared by mixing 100 mM boric acid and potassium chloride solutions and by adjusting pH with sodium or potassium hydroxide 100 mM.

2.2.3 Other Solutions

1. Alkylation solution: 100 mM Tris–HCl pH 8.0, 1% SDS, 2 mM alkylating agent (maleimide polyethylene glycol of 2 kDa (2 kDa mPEG-maleimide) or 4-acetamido-4'-maleimidylstilbene-2,2'-disulfonic acid (AMS)).
2. 2× Non-reducing Laemmli buffer: 120 mM Tris–HCl pH 6.8, 4% sodium dodecyl sulfate (SDS), 20% glycerol, and 0.02% (w/v) bromophenol blue.

3 Methods

All procedures can be carried out at room temperature unless otherwise stated.

3.1 Examination of the Cysteine Redox State and Susceptibility to Oxidative Treatments

The Ellman's reagent (DTNB) is often used to examine the number of free thiol groups of a purified recombinant protein subject to oxidative treatments. However, this titration is often hampered or imprecise when there is a high number of cysteines. Moreover, the interpretation can be made difficult when disulfide-linked oligomers are formed because the results are expressed as moles of SH per moles of monomer. The alkylation method described here associated to SDS-PAGE separation constitutes a good complement, giving access in particular to the oligomerization state of the protein. Moreover such an approach can also be employed to evaluate the capacity of known oxidoreductases to reduce or oxidize the protein of interest. Before studying the sensitivity of a protein towards different oxidative compounds, a prerequisite is to obtain a completely reduced protein. Procedures for reduction, oxidation, and alkylation of the target proteins are described below together with a case example.

3.1.1 Reducing Treatment

1. Add a tenfold molar excess of reductant (DTT_{red} or TCEP) to the purified recombinant protein (*see Note 1*).

2. Incubate for 30 min (*see Note 2*).
 3. Dialyze the protein against the desired buffer using membrane tubing or small desalting columns, preferentially at 4 °C (*see Note 3*).
- 3.1.2 Oxidizing Treatment**
1. Add a fivefold molar excess of oxidizing reagents (GSSG, GSNO, H₂O₂, DTT_{ox}) to the pre-reduced sample (*see Note 4*).
 2. Incubate for 2 h (*see Note 5*).
 3. Dialyze the protein against the desired buffer using membrane tubing or small desalting columns, preferentially at 4 °C (optional, *see Note 6*).
- 3.1.3 Protein Alkylation for SDS-PAGE Analysis**
1. Add 50 µL of 20% TCA to 50 µL of sample containing 5–10 µg of protein (either untreated, oxidized, or reduced) (*see Notes 7 and 8*).
 2. Gently mix by inverting the tube several times and place on ice for 15 min.
 3. Centrifuge for 10 min at 12,100 × *g* in a benchtop centrifuge.
 4. Remove carefully and discard the supernatant (*see Note 9*).
 5. Wash the pellet with 100% acetone kept at –20 °C without resuspending it and centrifuge for 10 min at 12,100 × *g*.
 6. Remove carefully and discard the supernatant (*see Note 9*).
 7. Dry the pellet at ambient air for 5 min (*see Note 10*).
 8. Add 10 µL of alkylation solution (*see Note 11*).
 9. Gently shake for 15 min at room temperature (*see Note 12*).
 10. Add 10 µL of 2× non-reducing Laemmli buffer (*see Note 13*).
 11. At this step, samples can be stored at –25 °C or subject to a non-reducing SDS-PAGE (*see Notes 14–16*).

3.1.4 Possible Result Obtained Upon Oxidative Treatment of a Protein of 12 kDa with a Single Cysteine

Firstly, it is important to verify that the oxidation/reduction of a protein does not impact per se its mobility on non-reducing SDS-PAGE, which might be the case when it induces conformational rearrangements as observed for glutathione peroxidase-like proteins [15]. Secondly, it is strongly advised to include controls for fully reduced and fully oxidized (if possible) proteins, which will give both extremities of the scale, as long as there is no disulfide-linked oligomer. In addition to delimiting the extremities of the scale, having alkylated and non-alkylated reduced proteins on the same gel allows in principle to control that there is no atypical shift relatively to the expected number of cysteines. For instance, we observed previously that treating a recombinant poplar TRX z possessing two cysteines with the 2 kDa mPEG maleimide generated a shift of 15 kDa instead of 4 kDa [8].

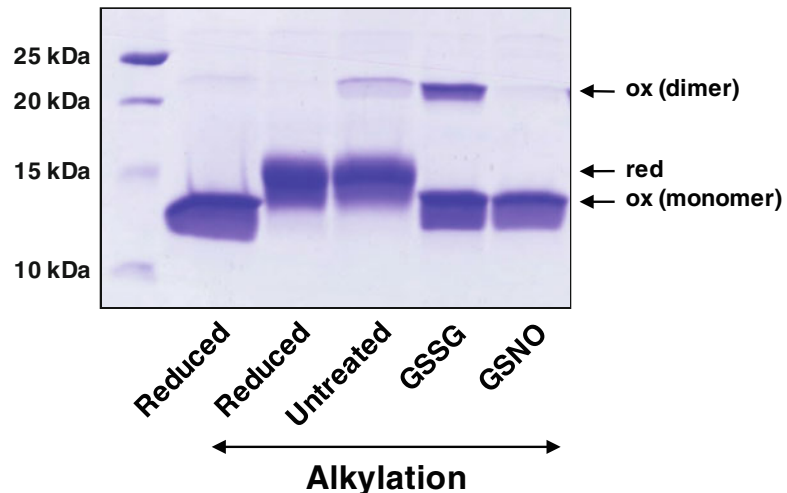


Fig. 1 Protein sensitivity to oxidative treatments. Around 5 µg of pre-reduced, untreated, or oxidized proteins obtained after 2-h oxidative treatments with GSSG or GSNO were alkylated with 2 kDa mPEG maleimide prior to separation on non-reducing SDS-PAGE [9]

Afterwards, one can indeed compare reduced, untreated, and oxidized proteins. In the example shown in Fig. 1, the absence of shift at the level of the monomer upon GSSG or GSNO treatments is interpreted here as GSSG or GSNO oxidizing the cysteine, with GSSG also promoting the formation of a dimer linked by an intermolecular disulfide. The untreated protein is mostly present as a reduced monomer with a small proportion of disulfide-linked dimer. The fact that this band is also seen in the non-alkylated reduced protein but not in the alkylated reduced protein suggests that some oxidation of the untreated protein occurred during sample preparation/migration, as explained in Note 14.

3.2 Estimation of Cysteine pK_a

The pK_a of cysteines into proteins is influenced by several factors, in particular their amino acid environment. Considering that thiolates are more reactive than thiols, measuring this parameter will give clue about their capacity to act or not as a nucleophile in a thiol-disulfide exchange reaction or to be susceptible to oxidation. Determining the pK_a value of cysteine residues using this method can be done only with proteins possessing a single cysteine or eventually two cysteines with sufficiently different pK_a .

3.2.1 Protein Alkylation for SDS-PAGE Analysis

1. Incubate around 10 µM of pre-reduced protein (*see Subheading 3.1.1*) with a 100-fold excess IAM for 15 min under gentle stirring in buffers ranging from pH 2.0 to 10.0 (every 0.5 unit for precision) in a final volume of 50 µL (*see Notes 17 and 18*).

2. Add 50 μ L of 20% TCA to 50 μ L of reaction mixture.
3. The following steps are similar to **steps 2–11** of Subheading **3.1.3**.

3.2.2 Protein Alkylation for Fluorescence Detection

1. Incubate around 10 μ M of pre-reduced protein (*see* Subheading **3.1.1**) with a 20-fold excess of fluo-IAM for 15 min in the dark under gentle stirring in buffers of different pHs (every 0.5 unit for precision) in a final volume of 200 μ L (*see* Notes **17** and **18**).
2. Add 200 μ L of 20% TCA to 200 μ L of reaction mixture.
3. Place on ice for 15 min in the dark (*see* Note **19**).
4. Centrifuge for 10 min at 12,100 $\times g$ in a benchtop centrifuge.
5. Remove carefully and discard the supernatant (*see* Note **9**).
6. Wash the pellet with 100% acetone kept at –20 °C and centrifuge for 10 min at 12,100 $\times g$.
7. Remove carefully and discard the supernatant (*see* Note **9**).
8. Dry the pellet at ambient air for 5 min in the dark (*see* Note **19**).
9. Add 400 μ L of 100 mM Tris–HCl pH 8.0 and 1% SDS.
10. Gently shake for 15 min at room temperature (*see* Note **12**).
11. Measure the fluorescence emission of the resulting solution at 515 nm after excitation at 492 nm (*see* Note **20**).

3.2.3 Possible Result Obtained for a Protein of 12 kDa with a Single Cysteine and Interpretation

The IAM specifically binds to deprotonated (i.e., thiolate forms) but not to protonated (i.e., thiol forms) cysteines. Hence, subsequent alkylation will only happen on thiol forms. This can be visualized on non-reducing SDS-PAGE by a retarded migration when the cysteine is in a thiol form (Fig. **2a**). By performing alkylation at different pHs, the cysteine pK_a can be approximately determined (in this example around 7.5) as the pH value where

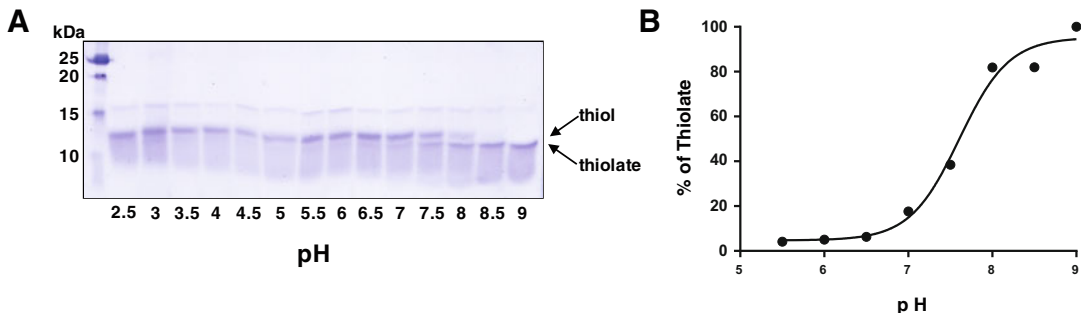


Fig. 2 pK_a determination of cysteine sulfhydryl group. This was done either by coupling reaction with a nonfluorescent alkylating reagent and protein separation on SDS-PAGE (**a**) or by measuring fluorescence after reaction with a fluorescent alkylating reagent (**b**)

50% of each form is encountered. Performing similar experiment by using fluo-IAM enables a more precise determination of the pK_a value (Fig. 2b). The fluorescence intensity is proportional to the quantity of cysteine under thiolate form. In this example, fitting the data to the following nonlinear regression $Y = \text{Bottom} + (\text{Top} - \text{Bottom}) / (1 + 10^{((\text{LogIC50} - X) \times \text{HillSlope})})$ gives a pK_a value of 7.6 which is comparable to the value deduced with nonfluorescent IAM.

3.3 Determination of the Redox Midpoint Potential of a Reversible Oxidative Modification

Measuring the redox midpoint potential will give clue about the capacity of a species to accept or donate electrons which in the case of a dithiol-disulfide couple translates into the capacity to be oxidized or reduced. Since a single protein can undergo several redox modifications involving the same or different cysteines and unless the redox potentials of two modifications found in a given protein are enough different to be distinguished, it is important to start with a homogenous oxidized protein sample, i.e., with a large majority having the same oxidative modification. In the absence of indication about the midpoint potential of the redox modification, it is worth trying either glutathione or DTT to generate reference redox potentials because they cover a different range from -100 mV to -250 mV and from -220 mV to -400 mV, respectively.

3.3.1 Protein Alkylation for SDS-PAGE Analysis

1. Incubate around 10 μM of oxidized protein in 100 mM HEPES pH 7.0 for 2 h in 50 μL reaction mixtures adjusted to different redox potentials by varying ratios between oxidized and reduced DTT or glutathione at a final concentration of 2 mM (see Tables 1 and 2) (see Notes 21 and 22).
2. The following steps are similar to steps 2–11 of Subheading 3.1.3.

3.3.2 Protein Alkylation for Fluorescence Detection

1. Incubate around 10 μM of oxidized protein in 100 mM HEPES pH 7.0 for 2 h in 200 μL reaction mixtures adjusted to different redox potentials by varying ratios between oxidized and reduced DTT or glutathione (see Tables 1 and 2) (see Notes 22 and 23).
2. Add mBBr to a final concentration of 2.5 mM and incubate for a further 20 min in the dark (see Notes 19 and 24).
3. The following steps are similar to steps 2–10 of Subheading 3.2.2.
4. Measure the fluorescence emission of the resulting solution at 472 nm after an excitation at 380 nm (see Note 25).

Table 1
Redox potentials obtained by mixing DTT_{ox}/DTT_{red} solutions

DTT _{ox} 2 mM (μ L)	DTT _{red} 2 mM (μ L)	Final volume (μ L)	Final [DTT _{ox}] (mM)	Final [DTT _{red}] (mM)	Ratio [DTT _{ox}]/[DTT _{red}]	Redox potential E_h (mV)
499.88	0.12	500	1.99952	0.00048	4166	-220
499.74	0.26	500	1.99896	0.00104	1922	-230
499.43	0.57	500	1.99772	0.00228	876	-240
498.76	1.24	500	1.99504	0.00496	402	-250
497.3	2.7	500	1.98920	0.00108	184	-260
494.16	5.84	500	1.97664	0.02336	85	-270
487.45	12.55	500	1.94980	0.05020	39	-280
473.45	26.55	500	1.89380	0.10620	18	-290
445.57	54.43	500	1.78228	0.21772	8	-300
394.9	105.1	500	1.57960	0.42040	4	-310
316.5	183.5	500	1.26600	0.73400	2	-320
220.93	279.07	500	0.88372	1.11628	0.8	-330
113.27	386.73	500	0.45308	1.54692	0.29	-343
71.48	428.52	500	0.28592	1.71408	0.16	-350
35.57	464.43	500	0.14228	1.85772	0.077	-360
16.97	483.03	500	0.06788	1.93212	0.035	-370
7.94	492.06	500	0.03176	1.96824	0.016	-380
3.67	496.33	500	0.01468	1.98532	0.007	-390
1.69	498.31	500	0.00676	1.99324	0.003	-400

The 2 mM oxidized and reduced DTT solutions are prepared in 100 mM HEPES pH 7.0

Calculations were made accordingly to the Nernst equation by taking an E_m value for the DTT_{ox}/DTT_{red} couple of -327 mV at pH 7.0

3.3.3 Possible Result Obtained for a Protein of ~20 kDa with Two Cysteines Forming an Intramolecular Disulfide Bridge and Interpretation

Using the SDS-PAGE analysis, the redox midpoint potential of the intramolecular disulfide, i.e., the value where there is 50% of reduced forms and 50% of oxidized forms, can be roughly estimated to be between -290 mV and -300 mV (Fig. 3A). For the same protein, the use of mBBr allows to calculate a redox midpoint potential of -298 ± 1 mV at pH 7.0 (Fig. 3B) after fitting fluorescence variations as a function of E_h values using the following nonlinear regression: $Y = \text{Bottom} + (\text{Top} - \text{Bottom})/(1 + 10^{((\text{LogIC50} - X) \times \text{HillSlope})})$.

Table 2
Redox potentials obtained by mixing GSH and GSSG solutions

GSSG 2 mM (μ L)	GSH 2 mM (μ L)	Final volume (μ L)	Final [GSSG] (mM)	Final [GSH] (mM)	Ratio [GSSG]/[GSH] ²	Redox potential E_h (mV)
454.8	45.2	500	1.8192	0.1808	55,652	-100
434.7	65.3	500	1.7388	0.2612	25,486	-110
406.7	93.3	500	1.6268	0.3732	11,680	-120
368.8	131.2	500	1.4752	0.5248	5356	-130
319.6	180.4	500	1.2784	0.7216	2455	-140
259.7	240.3	500	1.0388	0.9612	1124	-150
193.5	306.5	500	0.7740	1.2260	515	-160
129.5	370.5	500	0.5180	1.4820	236	-170
77.3	422.7	500	0.3092	1.6908	108	-180
41.6	458.4	500	0.1664	1.8336	49.5	-190
20.8	479.2	500	0.0832	1.9168	22.6	-200
9.98	490.02	500	0.0399	1.9601	10.4	-210
4.7	495.3	500	0.0188	1.9812	4.8	-220
2.2	497.8	500	0.0088	1.9912	2.2	-230
0.996	499.004	500	0.0040	1.9960	1	-240
0.457	499.543	500	0.0018	1.9982	0.46	-250

The 2 mM GSH and GSSG solutions are prepared in 100 mM HEPES pH 7.0

Calculations were made accordingly to the Nernst equation by taking an E_m value for the GSSG/GSH couple of -240 mV at pH 7.0

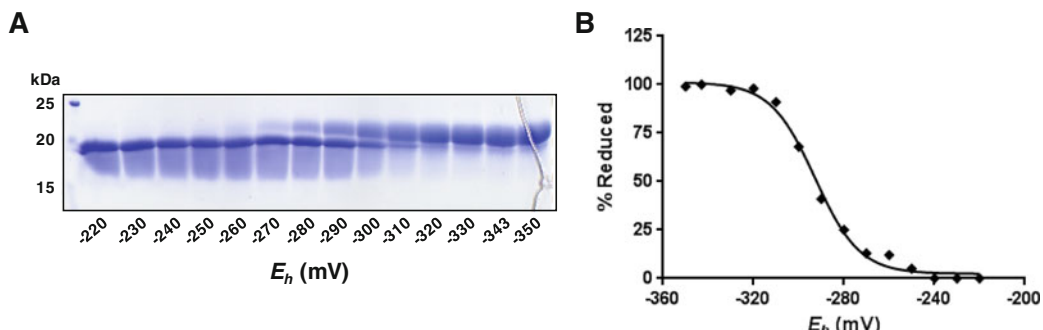


Fig. 3 Determination of the redox midpoint potential of a disulfide bond. This was done by alkylation with 2 kDa MPEG-maleimide and separation on SDS-PAGE (A) or by alkylation with mBBr (B). The 0% and 100% reduced indicate the proportion of reduced proteins and correspond to the minimum and maximum values of fluorescence, respectively

4 Notes

1. The procedures for producing and purifying recombinant proteins are out of the scope and will not be detailed here.
2. This time can be increased for proteins, the disulfides of which are more recalcitrant to reduction by DTT or TCEP.
3. While desalting columns are all more or less equivalent, the membrane tubing exists in different diameters and more importantly pore sizes that you have to adapt depending on the molecular weight of the protein of interest. Desalting columns are preferable because it is more rapid which thus could avoid reoxidation that might occur upon removal of the reductant.
4. Performing experiments by varying the ratio between concentrations of protein and oxidizing agents allows evaluating and comparing protein sensitivity to these agents.
5. Performing time-course experiments by varying the incubation time allows evaluating and comparing protein sensitivity to oxidizing agents.
6. The chemical treatment of the proteins (oxidation or reduction) before alkylation can be performed without subsequent dialysis as TCA specifically precipitates proteins but not chemical reagents that remain in the supernatant after centrifugation. In the case where proteins are initially reduced for the subsequent examination of their sensitivity to oxidizing reagents, they have to be dialyzed.
7. Any sample/TCA combination which leads to a final 10% TCA solution should be fine.
8. It is worth noting that a similar alkylation procedure can be applied to a cellular protein extract by starting at this step. The preparation of this extract will not be detailed here but it has to be done in the presence of the alkylating agent to avoid modifications of the redox state of the proteins occurring during sample preparation. If the samples do not have to be concentrated, TCA precipitation can eventually be replaced by a denaturation step with buffers containing 8 M urea or 6 M guanidine-HCl. By this approach, you can then directly proceed to **step 9**.
9. When removing the supernatant, do not touch the pellet.
10. It is important to remove all acetone traces before resuspending pellets of precipitated proteins to avoid subsequent perturbation of protein migration.
11. The molecular weight and the number of cysteine residues present in the protein of interest can influence the choice of

the alkylating reagent. Companies usually offer a large panel of mPEG maleimide compounds with variable molecular weight (1–30 kDa) which might be very convenient. That said, the fact that it generates broad bands on SDS-PAGE may prevent the separation between reduced and oxidized forms particularly for proteins with high molecular weights. In this case, DNA-maleimide forms are certainly more adapted since it gives more focused bands on SDS-PAGE and one currently commercialized version generates shift around 15 kDa per cysteine. Finally, despite generating a smaller migration shift (0.5 kDa), AMS may still be preferred for small-molecular-weight proteins because bands remain focused and in the same gel area.

12. Alternatively, after adding the alkylation solution, vortex for several seconds and wait for 15 min.
13. Any sample/Laemmli buffer combination which leads to a 1× final concentration is fine.
14. Oxidation of non-alkylated samples can take place during migration since it is performed in non-reducing conditions.
15. Prior to efficient protein separation, you have to adapt the type and the percentage of acrylamide of your gel to maximize separation in the molecular weight range of interest. Hence, for proteins smaller than 25 kDa, a Tricine gel may be required, whereas for bigger proteins, standard 15% acrylamide glycine SDS-PAGE may be sufficient to separate protein bands.
16. Depending on whether the experiment has been done with recombinant protein or protein extract, protein bands can be detected by Coomassie blue staining or by Western blotting with specific antibody, respectively.
17. For recombinant proteins, the concentration used has to be adapted according to its size to avoid using more than 10 µg of protein. Indeed, using a too important protein amount may prevent an efficient separation on SDS-PAGE.
18. For protein with multiple cysteines, it is usually necessary to perform site-directed mutagenesis to generate protein variants with a single cysteine.
19. As fluorescent alkylating reagents such as fluo-IAM and mBBr are photolabile, it is important to protect the reaction mixture from light.
20. Fluorescence emission of alkylating reagents depends on pH. In order to make accurate pK_a determinations, it is absolutely necessary to precipitate and resuspend protein samples in the same buffer to make sure that differences in fluorescence values are related to the thiol/thiolate state of cysteine residue and not to the pH value of initial solutions used for incubation.

21. A 2-h incubation time is often sufficient to reach equilibration but you can increase this time up to 4 h. In some cases, owing to the fact that the formation of a disulfide bond can sometimes induce a large conformational rearrangement, the two oxidation states can be visualized on a non-reducing SDS-PAGE without alkylation step. In contrast with the determination of pK_a value of cysteine residues, the presence of additional cysteines should not interfere if their redox state does not change along the incubation period.
22. Higher concentrations (for example 5 mM) of both oxidizing and reducing reagents can be used. It is necessary to recalculate the corresponding redox potential of each reaction mixture accordingly.
23. Redox potentials depend on pH value. Similar experiments can be performed at different pH but it will be necessary to employ different buffers and to recalculate the corresponding redox potentials of each reaction mixture accordingly. By doing measurements at different pHs, you can determine from the slope (either ~30 or ~60 mV pH/unit) whether the two-electron reduction process is accompanied by the uptake of one or of two protons over a given pH range.
24. mBBr reacts with all thiol groups, both from the protein cysteine residues and from the reducing agent. Hence, the final mBBr concentration has to be adapted to be slightly higher than to the total concentration of thiol groups present in the reaction mixture.
25. Measure first the fluorescence emission of the most reduced sample (i.e., incubated in the solution with the lowest redox potential) to determine whether the excitation intensity used is adequate and does not lead to signal saturation.

Acknowledgments

The UMR1136 is supported by a grant overseen by the French National Research Agency (ANR) as part of the “Investissements d’Avenir” program (ANR-11-LABX-0002-01, Lab of Excellence ARBRE). The Swedish Research Council “VetenskapsRådet” (grant: 621-2014-4688) as well as the Kempe Foundations are acknowledged for their financial support to O.K.

References

1. Poole LB (2015) The basics of thiols and cysteines in redox biology and chemistry. *Free Radic Biol Med* 80:148–157
2. Couturier J, Chibani K, Jacquot JP, Rouhier N (2013) Cysteine-based redox regulation and signaling in plants. *Front Plant Sci* 4:105

3. Biteau B, Labarre J, Toledano MB (2003) ATP-dependent reduction of cysteine-sulphinic acid by *S. cerevisiae* sulphiredoxin. *Nature* 425:980–984
4. Michelet L, Zaffagnini M, Morisse S, Sparla F, Perez-Perez ME, Francia F et al (2013) Redox regulation of the Calvin-Benson cycle: something old, something new. *Front Plant Sci* 4:470
5. Appenzeller-Herzog C, Ellgaard L (2008) *In vivo* reduction-oxidation state of protein disulfide isomerase: the two active sites independently occur in the reduced and oxidized forms. *Antioxid Redox Signal* 10:55–64
6. Cho SH, Porat A, Ye J, Beckwith J (2007) Redox-active cysteines of a membrane electron transporter DsbD show dual compartment accessibility. *EMBO J* 26:3509–3520
7. Lu H, Allen S, Wardleworth L, Savory P, Tokatlidis K (2004) Functional TIM10 chaperone assembly is redox-regulated *in vivo*. *J Biol Chem* 279:18952–18958
8. Chibani K, Tarrago L, Schürmann P, Jacquot JP, Rouhier N (2011) Biochemical properties of poplar thioredoxin z. *FEBS Lett* 585:1077–1081
9. Couturier J, HC W, Dhalleine T, Pégeot H, Sudre D, Gualberto JM et al (2014) Mono-thiol glutaredoxin-BolA interactions: redox control of *Arabidopsis thaliana* BolA2 and SufE1. *Mol Plant* 7:187–205
10. Parent A, Elduque X, Cornu D, Belot L, Le Caer JP, Grandas A et al (2015) Mammalian frataxin directly enhances sulfur transfer of NFS1 persulfide to both ISCU and free thiols. *Nat Commun* 6:5686
11. Hara S, Nojima T, Seio K, Yoshida M, Hisabori T (2013) DNA-maleimide: an improved maleimide compound for electrophoresis-based titration of reactive thiols in a specific protein. *Biochim Biophys Acta* 1830:3077–3081
12. Shaikhali J, Davoine C, Brännström K, Rouhier N, Bygdell J, Björklund S, Wingsle G (2015) Biochemical and redox characterization of the mediator complex and its associated transcription factor GeBPL, a GLABROUS1 enhancer binding protein. *Biochem J* 468:385–400
13. Yoshida K, Hara S, Hisabori T (2015) Thioredoxin selectivity for thiol-based redox regulation of target proteins in chloroplasts. *J Biol Chem* 290:14278–14288
14. Keech O, Gardeström P, Kleczkowski LA, Rouhier N (2017) The redox control of photorespiration: from biochemical and physiological aspects to biotechnological considerations. *Plant Cell Environ.* 40:553–569
15. Navrot N, Collin V, Gualberto J, Gelhaye E, Hirasawa M, Rey P et al (2006) Plant glutathione peroxidases are functional peroxiredoxins distributed in several subcellular compartments and regulated during biotic and abiotic stresses. *Plant Physiol* 142:1364–1379

The thioredoxin-mediated recycling of *Arabidopsis thaliana* GRXS16 relies on a conserved C-terminal cysteine

Flavien Zannini^a, Anna Moseler^{a,b}, Raphaël Bchini^a, Tiphaine Dhalleine^a, Andreas J. Meyer^b,

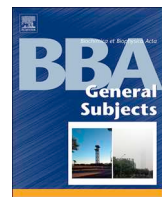
Nicolas Rouhier^a, Jérémie Couturier^{a,*}

^a Université de Lorraine, Inra, IAM, F-54000 Nancy, France.

^b INRES-Chemical Signalling, University of Bonn, Friedrich-Ebert-Allee 144, 53113, Bonn, Germany.

Article publié dans BBA General Subjects

L'étude de protéines possédant un repliement TRX représente un des thèmes de recherche principaux de notre laboratoire. Si les caractéristiques biochimiques des GRXs de classe I sont relativement bien documentées, celles des GRXs de classe II et plus particulièrement leur activité oxydoréductase le sont beaucoup moins. Cette étude avait pour objectif de caractériser biochimiquement l'isoforme chloroplastique de classe II, AtGRXS16 chez *A. thaliana*. Cette isoforme présente la particularité de posséder un domaine endonucléase en position N-terminale et un domaine GRX en position C-terminale. La protéine recombinante correspondante ainsi que des variants pour les différentes cystéines (simple et double mutants cystéiniques) ont été purifiés afin de caractériser les propriétés redox de cette isoforme. Les résultats obtenus démontrent la formation d'un pont disulfure entre les deux cystéines du domaine GRX après traitement avec des formes oxydées du glutathion, GSSG et GSNO. Le potentiel redox de ce pont disulfure (*ca* - 300 mV à pH 7.0) est cohérent avec un mode de réduction impliquant le système TRX et non le système GSH. Cette étude suggère donc que l'état redox de cette protéine pourrait être contrôlé par la lumière via la chaîne d'électrons photosynthétique et le système FTR/TRX.



The thioredoxin-mediated recycling of *Arabidopsis thaliana* GRXS16 relies on a conserved C-terminal cysteine

Flavien Zannini^a, Anna Moseler^{a,b}, Raphaël Bchini^a, Tiphaine Dhalleine^a, Andreas J. Meyer^b, Nicolas Rouhier^a, Jérémie Couturier^{a,*}

^a Université de Lorraine, Inra, IAM, F-54000 Nancy, France.

^b INRES-Chemical Signalling, University of Bonn, Friedrich-Ebert-Allee 144, 53113, Bonn, Germany.



ARTICLE INFO

Keywords:

Chloroplast
Disulfide bond
Glutaredoxin
Redox regulation
Thioredoxin

ABSTRACT

Background: Glutaredoxins (GRXs) are oxidoreductases involved in diverse cellular processes through their capacity to reduce glutathionylated proteins and/or to coordinate iron-sulfur (Fe-S) clusters. Among class II GRXs, the plant-specific GRXS16 is a bimodular protein formed by an N-terminal endonuclease domain fused to a GRX domain containing a ¹⁵⁸CGFS signature.

Methods: The biochemical properties (redox activity, sensitivity to oxidation, pK_a of cysteine residues, midpoint redox potential) of *Arabidopsis thaliana* GRXS16 were investigated by coupling oxidative treatments to alkylation shift assays, activity measurements and mass spectrometry analyses.

Results: Activity measurements using redox-sensitive GFP2 (roGFP2) as target protein did not reveal any significant glutathione-dependent reductase activity of *A. thaliana* GRXS16 whereas it was able to catalyze the oxidation of roGFP2 in the presence of glutathione disulfide. Accordingly, *Arabidopsis* GRXS16 reacted efficiently with oxidized forms of glutathione, leading to the formation of an intramolecular disulfide between Cys¹⁵⁸ and the semi-conserved Cys²¹⁵, which has a midpoint redox potential of -298 mV at pH 7.0 and is reduced by plastidial thioredoxins (TRXs) but not GSH. By promoting the formation of this disulfide, Cys²¹⁵ modulates GRXS16 oxidoreductase activity.

Conclusion: The reduction of AtGRXS16, which is mandatory for its oxidoreductase activity and the binding of Fe-S clusters, depends on light through the plastidial FTR/TRX system. Hence, disulfide formation may constitute a redox switch mechanism controlling GRXS16 function in response to day/night transition or oxidizing conditions.

General significance: From the *in vitro* data obtained with roGFP2, one can postulate that GRXS16 would mediate protein glutathionylation/oxidation in plastids but not their deglutathionylation.

1. Introduction

The formation and reduction of disulfide bonds constitute a major post-translational modification modulating the activity of numerous proteins. This modification is specifically referred to as glutathionylation when the disulfide is formed between the cysteines of a glutathione (GSH) molecule and of a protein. Thioredoxins (TRXs) and glutaredoxins (GRXs) represent the two main reductase families controlling these redox modifications [1]. Although sharing a similar structural fold, they display different biochemical properties. First, numerous

GRXs have the ability to coordinate iron-sulfur (Fe-S) clusters whereas TRXs usually do not [2,3]. Second, GRXs are rather specific to the reduction of glutathionylated proteins whereas TRXs are rather specialized in the reduction of intra/intermolecular disulfide bonds or nitrosylated proteins. Third, they usually differ by their reduction system. GRXs are mostly dependent on glutathione and the associated NADPH-dependent glutathione-disulfide reductase (GR) whereas TRXs are reduced by NADPH- or ferredoxin (FDX)-thioredoxin reductases (NTRs or FTRs) [4,5]. Nevertheless, crosstalk between both pathways is possible since some GRXs can be recycled by TRX reductases [6–8] and some

Abbreviation list: DHA, dehydroascorbate; DTT, dithiothreitol; FTR, ferredoxin-thioredoxin reductase; GAPDH, glyceraldehyde 3-phosphate dehydrogenase; GR, glutathione-disulfide reductase; GRX, glutaredoxin; GSH, glutathione; GSNO, nitrosoglutathione; GSSG, glutathione disulfide; H₂O₂, hydrogen peroxide; HED, 2-hydroxyethyl disulfide; IAM, iodoacetamide; mBBR, monobromobimane; NTR, NADPH-thioredoxin reductase; TRX, thioredoxin

* Correspondence author at: Université de Lorraine, Interactions Arbres/Microorganismes, UMR1136, F-54500 Vandœuvre-lès-Nancy, France.

E-mail address: jeremy.couturier@univ-lorraine.fr (J. Couturier).

<https://doi.org/10.1016/j.bbagen.2018.11.014>

Received 20 June 2018; Received in revised form 16 November 2018; Accepted 22 November 2018

Available online 28 November 2018

0304-4165/© 2018 Elsevier B.V. All rights reserved.

TRXs by GSH and/or GRX [9–11].

Among GRXs, there are also important variations, notably in the domain organization and active site signatures which contain one (CxxS), two (CCxx or CxxC) or three cysteine residues (CCxC) [1,12]. This situation is exacerbated in higher plants, where the GRX family comprises 25 to 40 genes that group into four classes. Except members of the class II GRX, which have an extremely conserved CGFS signature, isoforms found in the other three classes possess a variable number of cysteines in their signature [1]. The active site motifs and the number of cysteines therein generate important differences in the activity profile and regeneration mechanisms of these proteins. Indeed, GRXs having at least two cysteines could employ a so-called dithiol mechanism for the reduction of disulfide bridges, as catalyzed by TRXs [13]. The catalytic cysteine forms a mixed disulfide with the target protein and the second resolving cysteine releases the fully reduced target protein. On the contrary, GRXs having a single cysteine or using only one of their cysteinyl residue to catalyze protein deglutathionylation use a so-called monothiol mechanism [13]. In this case, the subsequent reduction of the glutathionylated GRX intermediate formed after the first step necessitates a free GSH molecule. The complexity of possible thiol-disulfide exchange reactions is increased further by the presence of an additional cysteine in the C-terminal region of some class I and II GRXs, very often in a GGCD sequence, and which is situated in close proximity to the active site in the mature protein (Fig. 1A) [14]. Thus, any GRX possessing at least two of these cysteines may in principle exhibit a reductase activity using a monothiol or a dithiol mechanism (Fig. 1B). For instance, the class II (CGFS) isoform GRX3 of *Chlamydomonas reinhardtii* catalyzes the reduction of disulfide bonds on target proteins

using a dithiol mechanism employing the C-terminal cysteine as a resolving cysteine [8]. This unusual disulfide is reduced by a light activation system comprising thylakoids, ferredoxin, and FTR. On the other hand, numerous studies using class I GRXs possessing a CxxC signature have shown that the second active site cysteine is dispensable for the GSH-dependent reduction of glutathionylated substrates although it does influence the reaction rate. This cysteine would determine the glutathione specificity of the glutathionylated GRX reduction step [15] or would slow down the reaction rate by forming an intramolecular intermediate disulfide with the catalytic cysteine, adding thus two steps in the catalytic mechanism [16]. Besides its requirement for the dithiol mechanism, having a resolving cysteine may avoid a possible overoxidation in specific situations serving as a transient and reversible protection mechanism [17].

In plants, biochemical characterization of class III and IV GRXs has been precluded by the inability to purify intact soluble recombinant proteins [18]. In contrast, class I and II GRXs have been extensively studied. Depending on the organisms, the class I comprises 4 to 6 members. In *Arabidopsis*, members of this subfamily are named GRXC1 to GRXC5 (CxxC active site signature) and GRXS12 (CxxS active site signature) [1]. Only GRXC1 and GRXC5 have the capacity to incorporate a [2Fe-2S] cluster [19,20]. However, all these isoforms have quite comparable *in vitro* enzymatic capacity being notably able to regenerate thiol peroxidases and methionine sulfoxide reductases [5,14,17,19,21]. Hence, the reason why such a number of isoforms has been maintained during evolution after duplication is likely related to their expression pattern or subcellular localization rather than to their activity [5].

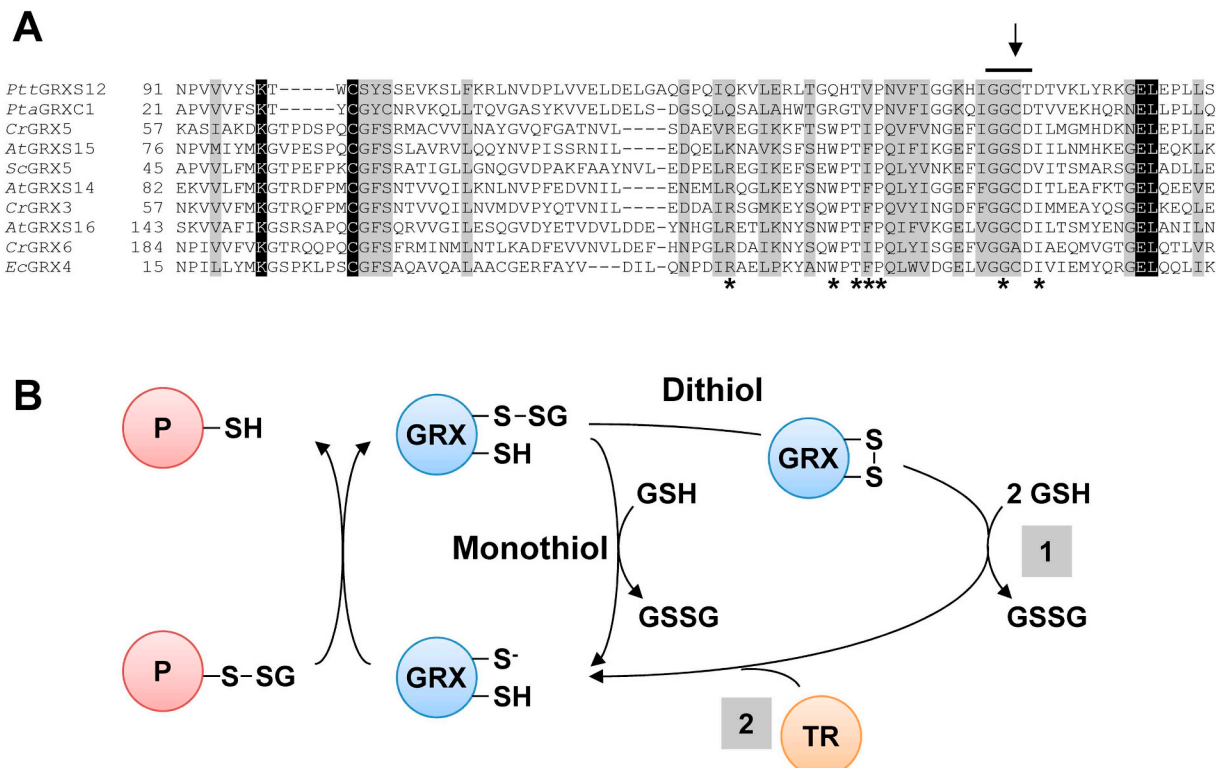


Fig. 1. Amino acid sequence comparison and catalytic mechanisms for the deglutathionylation activity of GRXs. A. Multiple sequence alignment of AtGRXS16 with orthologs from several model organisms (At, *Arabidopsis thaliana*; Cr, *Chlamydomonas reinhardtii*; Ec, *Escherichia coli*; Pta, *Populus tremula x alba*; Ptt, *Populus tremula x tremuloides*; Sc, *Saccharomyces cerevisiae*) using ClustalW. Strictly conserved residues are highlighted in black and other conservative residue changes are shown in grey. The conserved C-terminal GGC motif and its cysteine are indicated by a continuous line and an arrow, respectively. The residues constituting the glutathione scaffold site identified previously [38] are highlighted by stars. B. Monothiol and dithiol catalytic mechanisms. After reduction of the protein-glutathione adduct, GRX becomes glutathionylated in all cases. In the monothiol mechanism, only the catalytic cysteine is needed as GRX is regenerated by another glutathione molecule. In the dithiol mechanism, a resolving cysteine, which could be either the second active site cysteine or an extra active site cysteine, is responsible for the reduction of the GRX glutathione adduct leading to the formation of an intramolecular disulfide bond. This disulfide can possibly be reduced by two molecules of GSH (1) or by a TRX reductase (2).

The class II GRX subgroup contains at least four members named GRXS14 to GRXS17 in *Arabidopsis*. In most non-plant species, these GRXs are involved in Fe-S cluster assembly but our knowledge about the role of the respective plant isoforms remains scarce [2]. Indeed, although all four plant proteins have the ability to incorporate an Fe-S cluster [22–24], *in vivo* evidence for their involvement in the maturation of Fe-S proteins has been only obtained for the mitochondrial GRXS15 but not for the cytosolic GRXS17 and the plastidial GRXS14 and GRXS16 [23–27]. For all four GRXs it is possible that their physiological function relies on a yet unknown oxidoreductase activity and/or on their Fe-S cluster binding properties. The measurement of an oxidoreductase activity may have been hampered by the fact that classical activity assays are performed using a glutathione regeneration system and small molecules such as 2-hydroxyethyl disulfide (HED) or dehydroascorbate (DHA) but not or rarely with protein substrates. Among *in vitro* evidence obtained so far, it was shown that *Arabidopsis* GRXS17 and *Chlamydomonas* GRX3 are able to reduce oxidized forms of BOLA2 and of a glutathionylated glyceraldehyde 3-phosphate dehydrogenase (GAPDH) respectively whereas *Arabidopsis* GRXS14 and GRXS16 are able to reduce a glutathionylated SUFE1 although only with low efficiency [8,28].

The natural fusion protein GRXS16 is unique to plants. It possesses three cysteines, Cys⁶² in an N-terminal endonuclease domain, Cys¹⁵⁸ as part of the characteristic CGFS motif and Cys²¹⁵ in the C-terminal GGCD motif. A previous study suggested that formation of an intramolecular Cys⁶²-Cys¹⁵⁸ disulfide bridge controlled the endonuclease activity of the protein [29]. Here, we have investigated the biochemical properties of *A. thaliana* GRXS16 demonstrating that it is efficiently oxidized by GSSG and GSNO but not by H₂O₂. The oxidation leads to formation of an intramolecular Cys¹⁵⁸-Cys²¹⁵ disulfide, which enables the protein to catalyze oxidation reaction. The low redox potential measured is consistent with the observed reduction by plastidial TRXs but not by GSH. Therefore, the activity and Fe-S cluster binding capacity of GRXS16 may be controlled by light *via* the FTR-TRX system.

2. Experimental

2.1. Cloning and site-directed mutagenesis

The cloning of *A. thaliana* GRXS16 in the pET3d expression plasmid was described previously [22]. All cysteines were individually substituted into serines by site-directed mutagenesis by primer extension using two complementary mutagenic primers. In a first round of PCR, two fragments with overlapping ends are generated by using GRXS16 forward and mutagenic reverse primers and GRXS16 reverse and mutagenic forward primers, respectively. For the second round of PCR, these fragments were mixed with GRXS16 forward and reverse primers added after 10 PCR cycles to obtain the final product with the desired mutation. The corresponding variants were named GRXS16 C62S, C158S and C215S and used to mutate a second cysteine in order to generate C62S/C158S, C62S/C215S and C158S/C215S variants. All primers used in this study are listed in Supplementary Table 1.

2.2. Heterologous expression in *E. coli* and purification of recombinant proteins

For protein production, the *E. coli* BL21 (DE3) strain, containing the PSBET plasmid, was co-transformed with recombinant pET3d plasmids. Cultures were progressively amplified up to 2.4 l in LB medium at 37 °C supplemented with 50 µg/ml of ampicillin and kanamycin. Protein expression was induced at exponential phase by adding 100 µM isopropyl β-D-thiogalactopyranoside either for 4 h at 37 °C for expressing GRXS16 or for 16 h at 20 °C for expressing GRXS16 variants. After centrifugation (20 min at 6238g), the cell pellets were resuspended in about 20 ml of TE NaCl (30 mM Tris-HCl pH 8.0, 1 mM EDTA, 200 mM NaCl) and conserved at –20 °C. Cell lysis was performed by sonication (3 × 1 min

with intervals of 1 min) and the soluble and insoluble fractions were separated by centrifugation for 30 min at 27,216g and at 4 °C.

The soluble fraction was first precipitated by ammonium sulfate from 0 to 40% and then to 80% of the saturation. The 40–80% ammonium sulfate-precipitated fraction was subjected to gel filtration chromatography (AC34) equilibrated with TE NaCl buffer. After dialysis against TE (30 mM Tris-HCl, 1 mM EDTA) buffer and concentration, the interesting fractions were loaded to a DEAE (diethylaminoethyl) sepharose column equilibrated in TE buffer. All proteins were retained and eluted using a linear 0–0.4 M NaCl gradient. The purest fractions, as judged by SDS-PAGE gel analysis, were pooled and dialyzed against TE buffer by ultrafiltration in Amicon cells equipped with a YM10 membrane. Finally, the fractions were concentrated and stored at –20 °C until further use. Protein concentrations were determined spectrophotometrically using a molar extinction coefficient at 280 nm of 25,565 M^{−1} cm^{−1} for GRXS16 and its monocysteine variants and of 25,440 M^{−1} cm^{−1} for double cysteine variants, respectively.

Other recombinant proteins used in this work *e.g.* GRXS12, TRXh1 and TRXz from poplar, NTRB and GRXC1 from *A. thaliana*, TRXF from *Pisum sativum*, ferredoxin-NADP reductase (FNR) and TRXm from *Chlamydomonas reinhardtii*, FDX and FTR from *Synechocystis*, and roGFP2 have been purified as described previously [14,20,30–36].

2.3. Alkylation shift assay for determination of the redox state of GRXS16

Around 3 mg of GRXS16 and of the respective cysteine mutated variants were reduced using 30 mM DTT in 200 µl of 30 mM Tris-HCl pH 8.0 buffer for 1 h at 25 °C. The reduced proteins were then desalted on a G25 column pre-equilibrated with 30 mM Tris-HCl pH 8.0 buffer. Unless otherwise stated in the figure or table legends, 5 µM protein were incubated with a 5-fold excess of either GSSG, GSNO or H₂O₂ in a final volume of 50 µl of 30 mM Tris-HCl pH 8.0 buffer for 1 h at 25 °C, protein free thiol groups have been alkylated with methoxyl-PEG (mPEG)-maleimide of 2 kDa as described previously before separating the protein mixture on non-reducing 12% SDS-PAGE [37].

For monobromobimane (mBBr) labelling, reduced GRXS16 (5 µM) was incubated for 1 h at 25 °C in a final volume of 200 µl of 30 mM Tris-HCl pH 8.0 buffer in the presence of 0 to 1 mM GSSG, GSNO or H₂O₂ at 25 °C. Alkylation of protein free thiol groups was carried out in the dark for 20 min using 100 µM mBBr. The reaction was stopped by adding 200 µl of 20% TCA and the mixture was incubated on ice for 30 min. After centrifugation (10 min at 14,000 g) and washing with 100% acetone, the pellet was resuspended into 400 µl of 100 mM Tris-HCl pH 8.0, 1% SDS. Fluorescence emission was measured at 472 nm after excitation at 380 nm using a Varian Cary Eclipse fluorimeter (Agilent). Gain settings for detection of mBBr-labeled thiol groups were always adjusted before each experiment, and the absolute values thus obtained might differ between the experiments. Therefore, these values were transformed into % of fluorescence decrease to the respective initial value of pre-reduced protein and fitted to the following equation: % fluorescence decrease = (% fluorescence decrease)_{max} × [Oxidant]/(S_{0.5} + [Oxidant]) where S_{0.5} corresponds to the oxidant concentration necessary to reach half-maximal oxidation.

2.4. Determination of pK_a of cysteine residues

The measurement of pK_a of each cysteine residue has been performed with variants possessing a single cysteine by incubating 10 µM of protein with 200 µM 5-iodoacetamido fluorescein (fluorescein IAM) in 200 µl of 100 mM sodium citrate, phosphate or borate buffers ranging from pH 2.0 to 11 at 25 °C as described previously [37]. Values were transformed into percentage of thiolate and fitted to the following nonlinear regression: % thiolate = Bottom + (Top-Bottom)/(1 + 10^(LogpK_a – pH x HillSlope)).

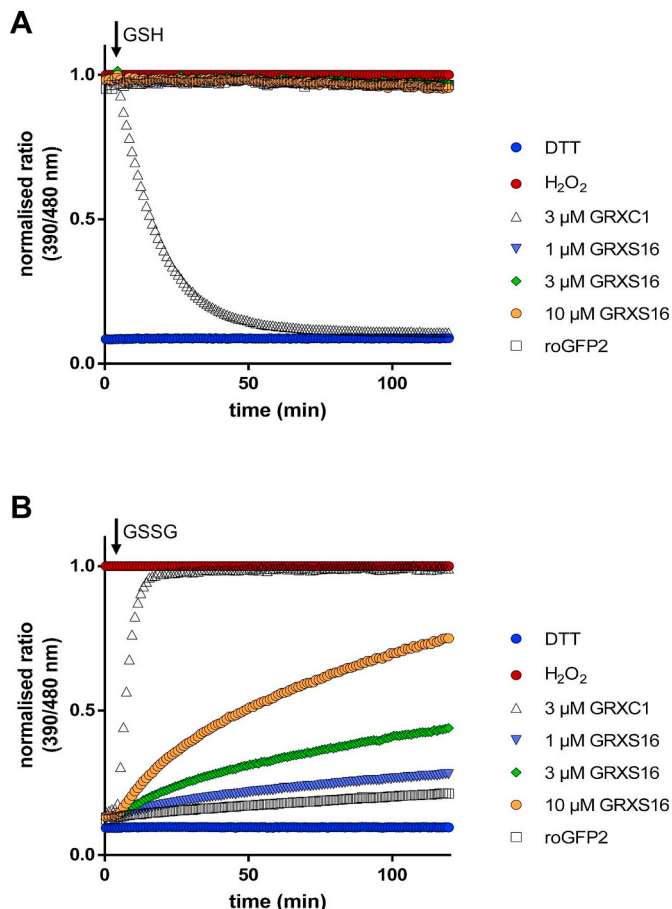


Fig. 2. GRXS16 catalyzes oxidation but not reduction of roGFP2. GSH-dependent reduction kinetics of 1 μM oxidized roGFP2 (A) and GSSG-dependent oxidation kinetics of 1 μM reduced roGFP2 (B) in presence of three different concentrations of AtGRXS16. Samples with DTT or H₂O₂ were used as fully reduced or oxidized roGFP2. AtGRXC1 served as positive control. Gain settings for the detection of the roGFP2 fluorescence after excitation at 390 and 480 nm were always adjusted before each experiment resulting in different absolute ratio values calculated for each experiment.

2.5. Determination of midpoint redox potential (E_m)

An oxidized GRXS16 was prepared by incubating a reduced protein with a 5-fold excess GSSG for 1 h at 25 °C before desalting on G25 column. The presence of the intramolecular disulfide bond was then verified by electrospray ionization mass spectrometry analysis as described previously [19] and the oxidation-reduction titrations using mixtures of oxidized and reduced DTT were carried out as described previously [17].

2.6. GRX- and TRX-mediated reduction of GRXS16

Three different systems were used. The GSH/GRX system was composed of 200 μM NADPH, 0.1 units GR, 1 mM GSH, and 2.5 μM plastidial GRXS12. Two TRX systems have been reconstituted *in vitro*. The first one comprised 200 μM NADPH, 500 nM NTRB and 2.5 μM cytosolic TRXh1. The second one mimics a plastidial TRX system and included 200 μM NADPH, 5 μM TRXm, f or z, 25 nM FNR, 0.5 μM FDX and 0.5 μM FTR. Each reducing system was incubated at 25 °C for 15 min prior addition of around 2.5 μM of oxidized GRXS16 in 50 μl of 30 mM Tris-HCl pH 8.0 buffer. The reaction was stopped after 15 min by the addition of one volume of 20% TCA. Alkylation of protein free thiol groups with mPEG-maleimide of 2 kDa was performed as described above.

2.7. roGFP2 oxidation/reduction experiments

The capacity of GRX to oxidize and reduce roGFP2 was analyzed *in vitro* by ratiometric time-course measurements on a fluorescence plate reader (POLARstar Omega; BMG) with filter-based excitation at 390 ± 10 and 480 ± 10 nm and detection of emitted light at 520 nm with a bandwidth of 10 nm. The reactions (100 μl) contained 1 μM roGFP2 and 1, 3 or 10 μM of the respective GRXs in 0.1 M KP_i buffer pH 7.8. When working with oxidized roGFP2, the sensor was used as purified showing already maximal oxidation. Pre-reduced roGFP2 was obtained by incubation with 10 mM DTT for 30 min and subsequent desalting to remove excess DTT (ZebaTM Spin Desalting Columns, Thermo Scientific). Oxidation of the pre-reduced sensor was performed with 40 μM GSSG. For the reduction assay using oxidized roGFP2, reduced glutathione (in 0.1 M KP_i buffer pH 7.8) was automatically injected to a final concentration of 2 mM using the built-in injectors. A highly negative redox state of the glutathione buffer was maintained by addition of 1 U GR and 0.1 mM NADPH. In the case of an additional TRX/TR system, 0.2 mM NADPH was added as well as 1 μM TRXh1 and 1 μM NTR. Furthermore, H₂O₂ and DTT were used at a final concentration of 10 mM to define maximum oxidation and reduction of roGFP2. A basal background fluorescence of buffer or buffer containing 0.1 mM NADPH was subtracted from the fluorescence measured in analyzed samples. Gain settings for detection of roGFP2 fluorescence after excitation with 390 and 480 nm were always adjusted before each experiment, and thus the absolute ratio values calculated might differ between the experiments. Therefore, the ratio was normalized to the respective value of maximal oxidation by H₂O₂.

2.8. Endonuclease activity

In vitro digestion of 150 ng lambda DNA (Promega) was carried out for 30 min at 37 °C in 20 μl of 50 mM Tris-HCl pH 7.5 containing 50 mM NaCl and 1 mM MgCl₂ using 10 μM of reduced or oxidized protein. The reaction was stopped by the addition of a DNA loading buffer containing EDTA and the reaction products were loaded on 1% agarose gels in the presence of ethidium bromide.

3. Results

3.1. GRXS16 can oxidize but not reduce roGFP2 in the presence of glutathione

Like for many other class II GRXs, good evidence for an oxidoreductase activity of AtGRXS16 is lacking because the protein is inactive in classical activity assays using small non-protein compounds such as HED or DHA and a glutathione recycling system. The only *in vitro* evidence obtained so far is a weak deglutathionylation activity using a glutathionylated SUFE1 protein and a glutathione recycling system [28]. The redox-sensitive GFP2 (roGFP2) was recently shown to enable the evaluation of both the reductase and oxidase activity of the mitochondrial AtGRXS15 [24,38]. Hence, in the absence of an identified target protein, roGFP2 was used to characterize the biochemical properties of AtGRXS16. The activities as an oxidase and a reductase were compared to GRXC1, a class I GRX having both types of activities. In the presence of GSH, GRXS16, used at different concentrations, was unable to catalyze the reduction of oxidized roGFP2 that possesses an intramolecular disulfide (Fig. 2A). On the other hand, GRXS16 catalyzed the oxidation of a pre-reduced roGFP2 in the presence of GSSG although less efficiently compared to GRXC1 (Fig. 2B). The reaction was dependent on the concentration of GRXS16 used. Given that GSSG in the absence of GRX is not or only poorly able to oxidize roGFP2, this result indicated that GRXS16 most likely got glutathionylated upon reaction with GSSG and subsequently transferred the glutathione moiety to reduced roGFP2 in a thiol-disulfide exchange reaction followed by formation of the intramolecular disulfide on roGFP2.

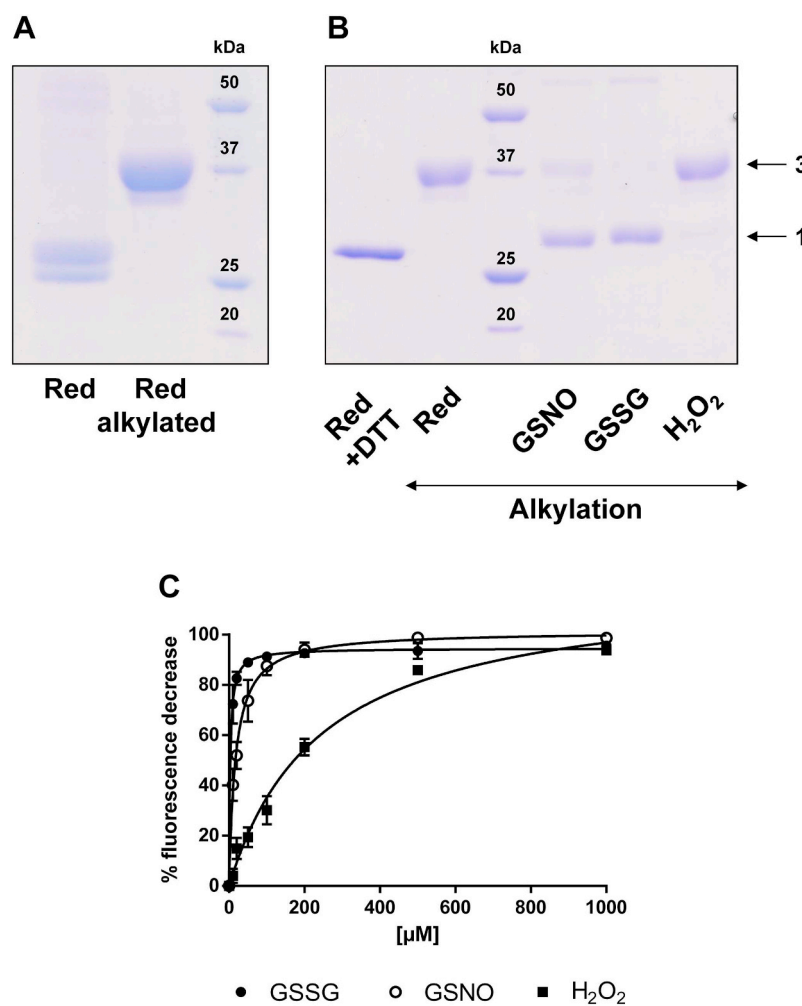


Fig. 3. GRXS16 is efficiently oxidized by disulfide glutathione. A. Non-reducing SDS-PAGE of 5 μM reduced GRXS16 before and after alkylation with 2 kDa mPEG maleimide. For the non-alkylated sample the reductant DTT was washed out before loading the sample on the gel. B. Non-reducing SDS-PAGE of 5 μM reduced GRXS16 subjected to oxidation by 5-fold excess of GSSG, GSNO or H₂O₂ for 1 h. After oxidation remaining free thiols were alkylated with 2 kDa mPEG maleimide. Non-alkylated GRXS16 incubated with DTT to avoid re-oxidation during electrophoresis is shown as a control. The numbers on the right correspond to the number of thiols that remained reduced upon treatment and thus were alkylated with mPEG maleimide. C. Relative oxidation of 5 μM GRXS16 by increasing concentrations of GSSG, GSNO or H₂O₂ for 1 h. The remaining free thiols were alkylated with mBBr and quantified through measurement of the resulting fluorescence. The decrease of fluorescence was plotted against the oxidant concentration for determination of S_{0.5}. The data represent the mean ± SD of three separate experiments.

3.2. GRXS16 is highly sensitive to oxidized glutathione forms

The oxidase/glutathionylation activity prompted us to analyze the sensitivity of reduced GRXS16 to oxidation by treating the protein with a 5-fold excess GSNO, GSSG or H₂O₂. The resulting redox state was first analyzed by non-reducing SDS-PAGE after alkylation of the remaining free thiol groups with 2 kDa mPEG maleimide, which enables to distinguish reduced and oxidized forms of the protein. First of all, it is important to note that a redox shift was visible for the non-alkylated protein on non-reducing SDS-PAGE (Fig. 3A). Indeed, two bands were observed in the monomeric size range even though the protein had been reduced before electrophoresis. As these bands condensed as a single band after adding DTT just before electrophoresis (Fig. 3B) and only one band is visible in alkylated samples migrated in non-reducing SDS-PAGE, we concluded that re-oxidation of GRXS16 occurred during electrophoresis. From this observation, we decided to add DTT in each reduced non-alkylated protein to avoid protein re-oxidation during electrophoresis. Concerning the oxidative treatments, no condition led to the loss of 3 thiols which would correspond to the formation of a completely oxidized protein (Fig. 3B). After incubation with a 5-fold excess H₂O₂ for 1 h only a faint band corresponding to 1 free thiol group was visible. This result indicates that H₂O₂ caused the formation of only very few intramolecular disulfide bonds and that the vast majority of GRXS16 remained reduced. Upon treatment of GRXS16 with GSSG or GSNO the band indicating one remaining free thiol was predominant. GSNO, however, seemed less efficient as an oxidant than GSSG, as a small fraction of fully reduced protein remained.

To better quantify the oxidation sensitivity of GRXS16, similar

experiments were performed in the presence of increasing concentrations of the oxidants and subsequent thiol alkylation with mBBr. The results were expressed as % of fluorescence decrease relatively to the initial fluorescence value of pre-reduced proteins (Fig. 3C). From these results, we determined the concentration of oxidant necessary to reach half-maximal oxidation (S_{0.5}) which reflects the sensitivity of GRXS16 to the respective oxidant. With this approach, we obtained S_{0.5} values of 3 ± 1 μM for GSSG, 17 ± 1 μM for GSNO and 247 ± 29 μM for H₂O₂. Altogether, these results indicated that AtGRXS16 was more sensitive to GSSG, then to GSNO and much less sensitive to H₂O₂.

3.3. The pK_a of Cys¹⁵⁸ is consistent with its sensitivity to oxidation

The reactivity of each cysteine of GRXS16 towards these agents was assessed by generating C158S/C215S, C62S/C215S and C62S/C158S mutated variants, which possess only Cys⁶², Cys¹⁵⁸ or Cys²¹⁵, respectively. After reduction, treatment with a 80-fold excess GSNO, GSSG or H₂O₂ and alkylation by 2 kDa mPEG maleimide, the redox state of the protein variants was analyzed on non-reducing SDS-PAGE. Under these conditions, Cys⁶² and Cys²¹⁵ did neither react with GSSG nor with H₂O₂ and only poorly with GSNO (Fig. 4A & 4C) considering the high excess of oxidants used here in comparison with previous experiments performed with an intact GRXS16. On the contrary, the Cys¹⁵⁸ was almost fully oxidized in the presence of all oxidants, predominantly as oxidized monomers in the presence of GSSG and GSNO and as oxidized dimers after oxidation by H₂O₂ (Fig. 4B). The pronounced and consistent sensitivity of Cys¹⁵⁸ to oxidants was somehow expected because this residue corresponds to the catalytic cysteine in GRXs possessing a

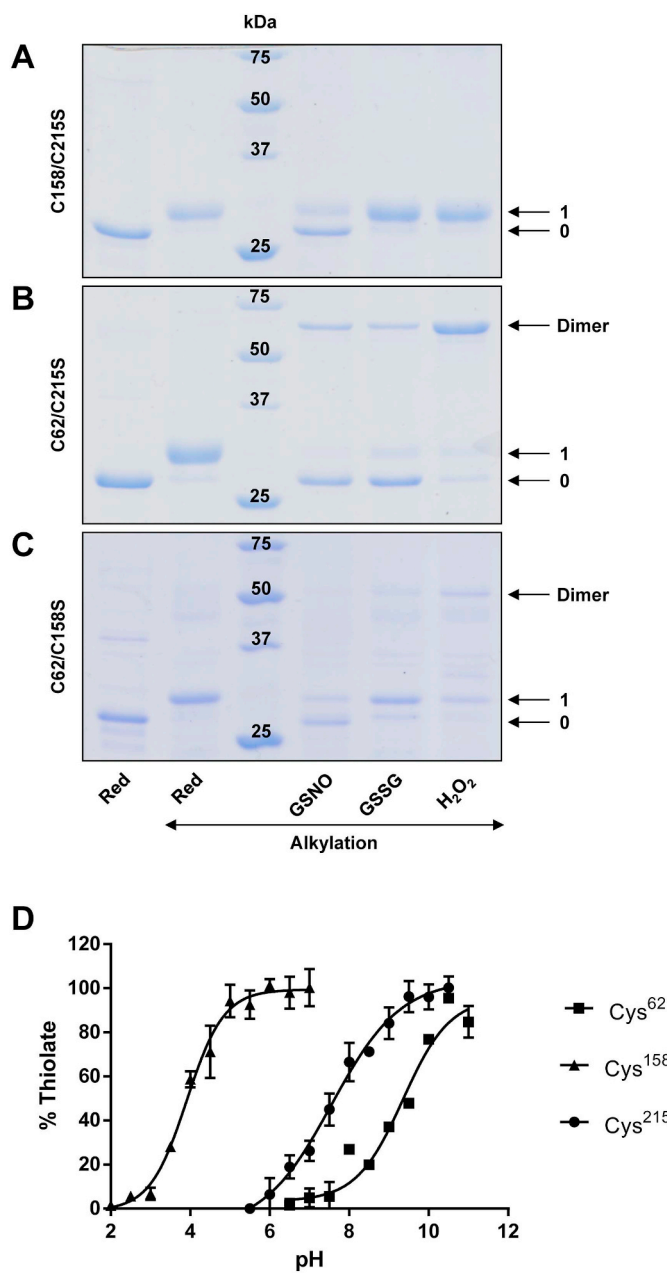


Fig. 4. The pK_a of GRXS16 cysteines correlates with their oxidation sensitivity. Non-reducing SDS-PAGE of 5 μ M reduced GRXS16 C158S/C215S (A), C62S/C215S (B) and C62S/C158S (C) variants subjected to oxidation by a 80-fold excess of either GSSG, GSNO or H_2O_2 for 1 h, and subsequently alkylated with 2 kDa mPEG maleimide prior to separation on non-reducing SDS-PAGE. Non-alkylated control samples are always shown in the left lane. The numbers on the right correspond to the number of thiols that remained reduced upon treatment with oxidants and thus were alkylated. D. The pK_a values of sulphhydryl group Cys⁶², Cys¹⁵⁸ and Cys²¹⁵ was determined by incubating 10 μ M of reduced GRXS16 C158/C215S, C62/C215S and C62/C158S variants in buffers ranging from pH 2.0 to 11.0 in the presence of 200 μ M fluorescein-IAM which reacts with thiolates. The thiolate groups were labeled by fluorescein-IAM and the resulting fluorescence emission was expressed as a % of maximal fluorescence and fitted to the pH value of the solution. The obtained pK_a values are the mean \pm SD of three separate experiments.

regular reductase activity. However, the results obtained with the other variants did not point to differences in their reactivity, at least in a buffer with pH 8.0 as used here. Hence, we sought to determine precisely the pK_a of all three cysteines using an alkylation method relying on 5-iodoacetamido-fluorescein (fluorescein IAM), a fluorescent

molecule that reacts with thiolates but not thiols. The pH-dependent reaction of each variant, retaining a single cysteine residue, with fluorescein IAM was followed by incubating reduced proteins with fluorescein IAM in different buffers ranging from pH 2.0 to 11.0. From the titration curves, we obtained pK_a values of 9.4 ± 0.2 for Cys⁶², 3.9 ± 0.1 for Cys¹⁵⁸ and 7.6 ± 0.1 for Cys²¹⁵ (Fig. 4D). Without considering other factors, this indicated that, at physiological pH of the chloroplast (*i.e.* between 7 and 8), the catalytic cysteine Cys¹⁵⁸ will be predominantly present as thiolate, Cys⁶² in the protonated thiol form and Cys²¹⁵ in a mixture of thiolate and thiol forms. Incidentally, these results suggested that the putative intramolecular disulfide bond formed in GRXS16 after oxidative treatment likely involves Cys¹⁵⁸ as the primary oxidation site and Cys²¹⁵ acting as the recycling cysteine.

3.4. GRXS16 forms an intramolecular Cys¹⁵⁸-Cys²¹⁵ disulfide

To validate this assumption, we first analyzed the changes in the redox state of the C62S variant after oxidative treatment with 5-fold excess of oxidants and subsequent alkylation (Fig. 5A). In accordance with results obtained for GRXS16 (Fig. 3B), the oxidation profile of the GRXS16 C62S variant corresponded to the loss of 2 free thiols upon treatment with GSSG and GSNO. In contrast, incubation with H_2O_2 resulted only in poor oxidation (Fig. 5A). Furthermore, on non-reducing SDS-PAGE, the reduced non-alkylated protein and the oxidized monomeric form display different migration profiles (Fig. 5A). It was due to the redox shift between oxidized and reduced non-alkylated proteins as it was no more visible on reducing SDS-PAGE (Fig. 5B).

To firmly establish what are their oxidation forms, GRXS16 and GRXS16 C62S were either reduced with DTT or incubated with GSSG and subsequently analyzed by mass spectrometry (Supplementary Figs. 1 & 2). First, a single species was obtained with both reduced proteins but they presented a mass decrease of *ca* 131 Da compared to the theoretical molecular masses (Table 1). It does undoubtedly correspond to the cleavage of the first methionine as expected from the presence of an alanine at the second position. Both GSSG-oxidized proteins were exclusively detected as monomeric forms with a decrease of their molecular masses of around 1.7 Da compared to the reduced forms, corresponding to the loss of two protons (Table 1). Hence, these results confirmed the formation of a Cys¹⁵⁸-Cys²¹⁵ intramolecular disulfide bond, in accordance with previous alkylation experiments (Figs. 3B & 4). Using a His-tagged version of GRXS16, previous work suggested the existence of an intramolecular Cys⁶²-Cys¹⁵⁸ disulfide bond that inhibited the endonuclease activity of the protein [29]. Hence, we have also analyzed the redox state of GRXS16 C215S treated with GSSG by ESI-MS (Supplementary Fig. 3). However, only a reduced monomeric form and a disulfide-bridged dimer were detected (Table 1) indicating first that no intramolecular disulfide bond is formed between Cys⁶²-Cys¹⁵⁸ (at least in the presence of GSSG) and second that an intermolecular disulfide bond, likely involving Cys¹⁵⁸, is formed in the absence of Cys²¹⁵. The confirmation that dimer formation originated from the attack of a glutathionylated Cys¹⁵⁸ of one monomer by the reduced Cys¹⁵⁸ of another monomer was obtained by analyzing a GSSG-treated GRXS16 C62S/C215S variant for which we indeed detected a mixture of reduced monomer, glutathionylated monomer (mass increment of 305.1 Da) and disulfide-bridged dimer (Table 1, Supplementary Fig. 4). Overall, these results conflict with the previous study [29], as we neither observed a Cys⁶²-Cys¹⁵⁸ oxidized form (even in the absence of Cys²¹⁵), nor did we find a redox regulation of the endonuclease activity of GRXS16 as assayed with lambda DNA as substrate (Supplementary Fig. 5).

3.5. GRXS16 is reduced by a TRX- but not a GSH-regeneration system

Next, we sought to determine the redox midpoint potential of the intramolecular Cys¹⁵⁸-Cys²¹⁵ disulfide bond. Initial titration with GSH/GSSG redox buffers was unsuccessful. We thus continued with a DTT_{red}/

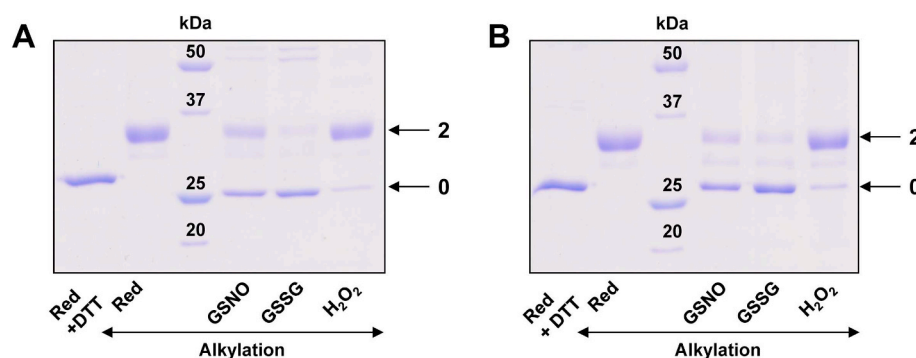


Fig. 5. Cys¹⁵⁸ and Cys²¹⁵ form an intramolecular disulfide bond on GRXS16. Reduced GRXS16 C62S was subjected to a 1 h oxidative treatment with a 5-fold excess GSSG, GSNO or H₂O₂, and subsequently alkylated with 2 kDa mPEG maleimide prior to separation on non-reducing (A) or reducing (B) SDS-PAGE. Non-alkylated control samples are always shown in the left lane. To avoid reoxidation of GRXS16 C62S during electrophoresis, DTT was added to the non-alkylated sample before electrophoresis. The numbers on the right correspond to the number of thiols that remained reduced during the oxidative treatment and thus were alkylated.

DTT_{ox} redox buffer and found an unexpectedly low E_m value of -296 ± 1 mV at pH 7.0 (Fig. 6A). This prompted us to test various reducing systems for their ability to reduce GRXS16, which was detected using the same *in vitro* alkylation method. Consistent with the results of the redox potential titration, GSH, either alone or in combination with NADPH and GR to obtain a fully reduced glutathione pool, was clearly inefficient in the complete reduction of oxidized GRXS16 (Fig. 6B). Adding the chloroplastic GRXS12 in the complete system did not improve much the reduction. Interestingly, the cytosolic TRXh1 fully reduced the oxidized GRXS16 in the presence of NADPH and NTR. In order to test some plastidial TRXs, which are not reducible by NTR but by FTR, we have reconstituted a light-independent system established before for the reduction of TRXz by coupling NADPH, *Chlamydomonas* FNR and *Synechocystis* FDX and FTR [31]. We verified that none of these proteins reduced oxidized GRXS16 in the absence of TRX. Adding either TRXF or TRXM led to GRXS16 reduction although not to the same extent as TRXz. These *in vitro* data indicated that the cellular reduction of the plastidial AtGRXS16 likely does not depend on the GSH system but on light and the FTR/TRX system (Fig. 6C).

3.6. The resolving Cys²¹⁵ modulates both the reductase and oxidase activity of GRXS16

Given the presence of the intramolecular Cys¹⁵⁸-Cys²¹⁵ disulfide, we sought to examine the requirement of other cysteine residues, notably Cys²¹⁵, for GRXS16 activity. First of all, GRXS16 C158S variant was inactive in both the reduction and oxidation of roGFP2 whereas GRXS16 C62S variant displayed an activity profile similar to GRXS16. Interestingly, the GRXS16 C215S variant oxidized roGFP2 more efficiently than GRXS16. Moreover, the mutated variant acquired the novel capacity to reduce roGFP2 (Fig. 7). This indicates that the resolving Cys²¹⁵ interferes with the transfer of glutathione from roGFP2 to the catalytic cysteine of GRXS16. Accordingly, a stable glutathione adduct can be detected on Cys¹⁵⁸ in the GRXS16 C62S/C215S variant (Table 1). Finally, since a TRX system can serve for the regeneration of an oxidized GRXS16, similar roGFP2 reduction experiments have been performed by adding NADPH/NTR/TRXh1 but keeping GSH, which is

mandatory for roGFP2 reduction. Nevertheless, for unclear reasons, this did not allow reduction of roGFP2, the observed slight increase of roGFP2 reduction being due to the action of TRXh1 protein alone (Supplementary Fig. 6). Overall, this indicated that Cys⁶² does not influence the redox activity of GRXS16, that Cys¹⁵⁸ is indispensable for the oxidoreductase activity and that Cys²¹⁵ modulates the glutathione-dependent reductase/oxidase activity of GRXS16 by promoting the formation of an intramolecular Cys¹⁵⁸-Cys²¹⁵ disulfide bridge.

4. Discussion

Delineating the activity and catalytic mechanism of class II GRXs is currently the subject of intense research. For the peculiar GRXS16, a previous study reported the existence of an intramolecular Cys⁶²-Cys¹⁵⁸ disulfide bond, which modulated the activity of the N-terminal endonuclease domain [29]. However, the reduction system for this oxidized form was not investigated. On the other hand, *C. reinhardtii* GRX6, the GRXS16 ortholog possessing only the cysteine residue of the CGFS signature, was shown to form a covalent homodimer that is only very poorly reduced by GSH [39]. All these observations prompted us to investigate the biochemical properties of AtGRXS16 in more details.

4.1. A Cys¹⁵⁸-Cys²¹⁵ intramolecular disulfide is formed in GRXS16

Using an untagged recombinant protein, we initially observed that GRXS16 migrated as a single band of ~26 kDa in reducing SDS-PAGE but as a double band in non-reducing SDS-PAGE, even after a pre-reduction step. This pointed to the existence of at least two redox forms. Coupling GSSG or GSNO treatments of cysteine-mutated variants to an alkylation approach and mass spectrometry analyses, we determined unambiguously that an intramolecular Cys¹⁵⁸-Cys²¹⁵ disulfide was formed. In accordance with their respective pK_a values of 3.9 and 7.9, Cys¹⁵⁸ is glutathionylated in the first step, followed by a nucleophilic attack of the resolving Cys²¹⁵. The high pK_a value of Cys⁶² (9.4) likely precludes its reactivity even if it would be in sufficiently close proximity for attacking the glutathionylated Cys¹⁵⁸.

The existence of an intramolecular disulfide bridge between the

Table 1
Electrospray ionization mass spectrometry analysis of reduced and GSSG-treated GRXS16 and its mutated variants lacking Cys⁶².

Protein	Theoretical mass (Da)	Theoretical mass without Met (Da)	DTT _{red} treatment	GSSG treatment	Mass difference (Da)
GRXS16	25,428.0	25,296.8	25,297.0	25,295.3	-1.7
GRXS16 C62S	25,411.9	25,280.7	25,281.1	25,279.4	-1.7
GRXS16 C215S	25,411.9	25,280.7	25,280.7	25,280.9	+0.2
GRXS16 C62S C215S	25,395.9	25,264.7	25,264.8	50,561.3 25,264.7 25,569.8 50,529.6	x2 -0.1 +305.1 x2

The mass accuracy is generally ± 0.5 Da.

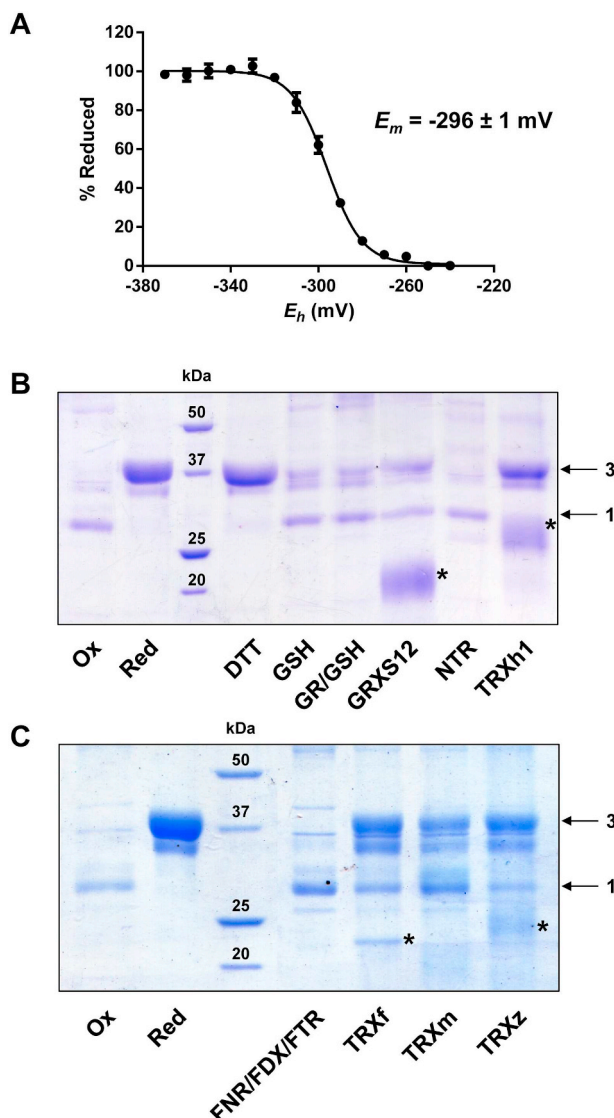


Fig. 6. The GRXS16 disulfide is reduced by thioredoxins but not glutathione. **A**, Representative redox titration curve for GRXS16. The titration was carried out using a total DTT concentration of 2 mM for 2 h at pH 7.0. Free thiol groups were labeled by mBBr and the resulting fluorescence emission was expressed as % of maximal fluorescence and fitted to the redox potential of the solution. The obtained E_m value is the mean \pm SD of three replicates. **B** and **C**, The oxidized GRXS16 was treated for 15 min with DTT, with GSH either alone or in the presence of NADPH and GR. When using poplar GRXS12, poplar TRXh1, pea TRXf, *Chlamydomonas* TRXm and poplar TRXz, the adequate regeneration system was included *i.e.*, NADPH/GR/GSH for GRXS12, NADPH/NTR for TRXh1 and NADPH/FNR/FDX/FTR for TRXf, m and z. After alkylation with 2 kDa mPEG maleimide, proteins were separated on non-reducing SDS-PAGE. Reduced (Red) or oxidized (Ox) proteins served as controls. The stars indicate the alkylated forms of the reducing oxidoreductases in the respective regeneration systems when visible.

catalytic cysteine and the cysteine located in the C-terminal GGCD motif was demonstrated for *C. reinhardtii* GRX3, the GRXS14 ortholog, and for yeast Grx5 [8,40]. This might also be true for *E. coli* Grx4 although the resolving cysteine has not been unambiguously determined [6,41]. Consistent with the existence of a comparable reaction mechanism, the corresponding cysteines in ScGrx5 have pK_a values of 5.0 for Cys⁶⁰ and 8.2 for Cys¹¹⁷ [40]. However, significant differences exist. The first one is the sensitivity to oxidation as only 3 μ M GSSG is sufficient to oxidize 50% of GRXS16 whereas 98 μ M is needed to oxidize ScGrx5 to the same extent [40]. Another difference is the redox

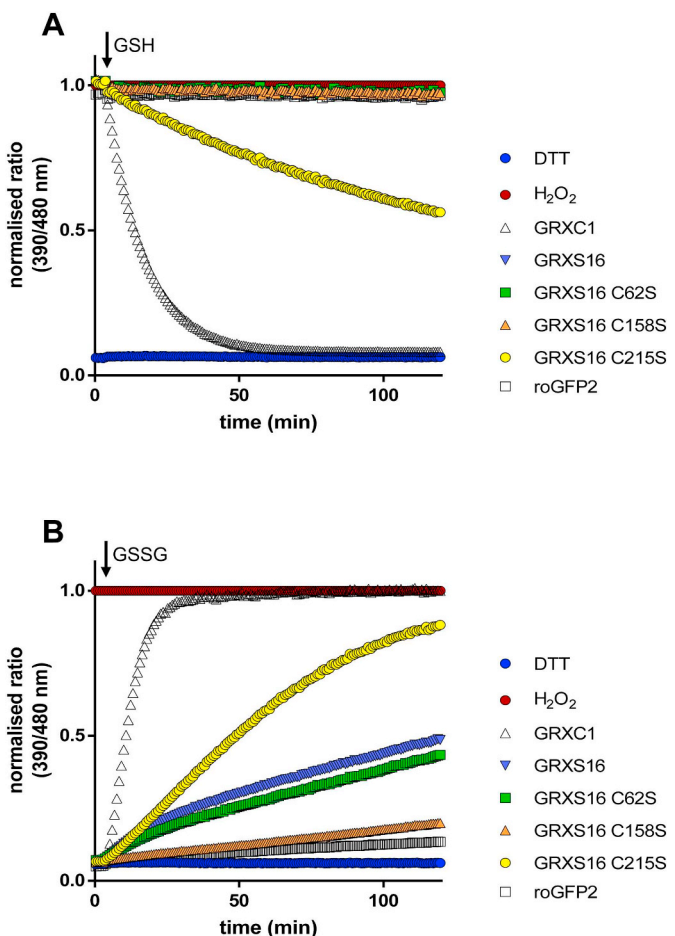


Fig. 7. The resolving Cys²¹⁵ of GRXS16 modulates the oxidation/reduction of roGFP2. GSH-dependent reduction kinetics of 1 μ M oxidized roGFP2 (**A**) and GSSG-dependent oxidation kinetics of 1 μ M reduced roGFP2 (**B**) in presence of GRXS16 or of mutated variants lacking specific cysteines. Control proteins and experiments and fluorescence detection as in Fig. 2.

potential of the disulfide as GRXS16 displays an atypical negative E_m value of -296 mV at pH 7.0 compared to the -175 mV obtained for ScGrx5 [40]. The value obtained for GRXS16 is close to the redox potentials obtained for CrGRX3 (-323 mV at pH 7.9) [8], but also for some *Arabidopsis* plastidial TRXs [42]. On the contrary, it is lower than those determined for class I poplar dithiol GRXs that varied from -233 mV to -263 mV at pH 7.0 [17]. In the latter case, the disulfide involves both cysteines of the CxxC signature and is reduced by GSH. In GRXS12, a monothiol class I GRX, the glutathione adduct has a redox potential of -315 mV at pH 7.0 [21]. All these observations indicate that the inability of GSH to regenerate class II GRXs is very likely not related to the E_m value of the disulfide.

4.2. Recycling of oxidized GRXS16

The quest for the regeneration system of class II GRXs is not completely solved either. Indeed, it was reported that the intramolecular disulfide of human GRX2 or of *E. coli* Grx4 can be reduced respectively by mammalian or *E. coli* NTR and the disulfide of CrGRX3 by FTR [6–8]. Similarly to CrGRX6 [39], the reduction of GRXS16 is not directly mediated by FTR or NTR on their own, but requires the presence of a TRX. It may actually be that the thylakoid preparation used for testing the regeneration of CrGRX3 by FTR contained some residual amounts of TRXs. For instance, m-type TRXs or other redoxins are known to participate in photosystem biogenesis and might be attached to thylakoids [43,44]. To clarify this point, it would be interesting to test the

reduction of CrGRX3 and its *Arabidopsis* ortholog GRXS14 with purified enzymes as we did in this study.

Although all the aforementioned class II GRX isoforms, which are regenerated by thioredoxin reductases and TRX, have an additional C-terminal cysteine residue, numerous other class II GRX isoforms possess only the catalytic cysteine. The question of their redox state and physiological regeneration system remains unsolved. For example, within the GRXS16 subgroup, the C-terminal cysteine is only present in isoforms from angiosperms whereas orthologs present in sequenced chlorophytes, mosses or fern lack this residue. This is an important difference as the recombinant CrGRX6 forms a covalent dimer that is not efficiently reduced by GSH [39]. Among other plant class II GRXs, most members of the mitochondrial GRXS15 subgroup contain only a single cysteine or at least lack the semi-conserved C-terminal cysteine. AtGRXS15 is unable to catalyze the reduction of HED, DHA or roGFP2 even in the presence of physiological concentrations of fully reduced GSH [24,38]. This is puzzling because the GRXS16 C215S variant investigated in this work mimics GRXS15 by possessing only the catalytic cysteine, but was clearly capable of reducing roGFP2. Another surprising observation is that the *C. reinhardtii* ortholog of GRXS15, CrGRX5, which has four cysteine residues, including the one present in the C-terminal GGCD motif, also forms covalent dimers *in vitro* [39]. Hence, a systematic analysis of all GRX isoforms seems necessary to identify the catalytic properties of class II GRXs and the molecular mechanisms involved in their reduction, especially for those with a single cysteine.

It is interesting to note that the C-terminal cysteine residue is also conserved in some class I GRXs [17]. In this case, however, the function seems to be different from the role in GRXS16 as it is not involved in the catalytic mechanism. For example, in poplar GRXC1 and GRXC2, this residue is prone to oxidation leading to the formation of a covalent dimer with an intermolecular disulfide bond that is efficiently reduced by GSH [17].

4.3. Oxidoreductase activity of GRXS16

The absence of a regular GSH-dependent reductase activity for AtGRXS16 when using classical GRX substrates such as HED does not preclude, however, that GRXS16 could possess deglutathionylation activities in addition to the glutathionylation activity reported here. Indeed, *in vitro* deglutathionylation activities have been reported for ScGRX5, CrGRX3 and AtGRXS17 using specific protein substrates, carbonic anhydrase, A₄ glyceraldehyde-3-phosphate dehydrogenase and BOLA2, respectively [8,28,40] whereas a glutathionylation/oxidation activity was described for AtGRXS15 using roGFP2 [38]. In the absence of known redox-regulated partners, we demonstrated that AtGRXS16 was unable to reduce roGFP2 in the presence of GSH whatever the conditions used. The use of a NADPH/NTRB/TRXh1 reducing system in addition to GSH was also inefficient although it would have in principle allowed some turnover of the enzyme. Indeed, reduction of roGFP2 is likely initiated by a nucleophilic attack of GSH on the intramolecular disulfide of roGFP2, followed by a nucleophilic attack of Cys¹⁵⁸ on the glutathionylated roGFP2 allowing its deglutathionylation. The resulting glutathione adduct formed on Cys¹⁵⁸ should be recycled by another GSH molecule in the GRXS16 C215S variant whereas an intramolecular disulfide, not reduced by GSH but by TRX, is preferentially formed in GRXS16 (Fig. 6). Incidentally, this result indicated that GSH is able to sustain the recycling of a glutathionylated GRXS16. This has to be discussed in the light of the recent study comparing the enzymatic mechanism used by class I and class II GRXs. It was proposed that class I GRXs require two distinct glutathione interaction sites for efficiently catalyzing deglutathionylation reactions [38]. A so-called scaffold site would interact with the glutathione moiety of glutathionylated substrates whereas an activator site would activate glutathione for the second step *i.e.*, GRX deglutathionylation. It was reported that AtGRXS15, used as a class II representative, contains

a partially functional glutathione-scaffold site but an altered glutathione activator site [38]. In GRXS16, a functional activator site may be present but the presence of Cys²¹⁵ at the vicinity of residues defining the scaffold site (Fig. 1A) might preclude the interaction with glutathionylated target proteins. Hence, the nucleophilic attack of GRXS16 onto glutathionylated roGFP2 may be the limiting step and might explain why GRXS16 is unable to reduce roGFP2.

Concerning the opposite reaction, AtGRXS16 mediates roGFP2 oxidation in the presence of GSSG, as observed with AtGRXC1 and AtGRXS15 [38]. Such an activity was also reported for AtGRXC2 that catalyzes the glutathionylation of the BRI1-associated receptor kinase 1 *in vitro* [45]. Considering that the first step of roGFP2 oxidation is the transfer of a glutathione moiety from GRX to roGFP2, it is expected that the presence of a recycling cysteine limits the efficiency of the reaction, the GSH transfer to roGFP2 competing with the reduction of glutathionylated catalytic cysteine. Accordingly, mutating Cys²¹⁵ in GRXS16 increased substantially its oxidase activity that is best interpreted by the fact that a stable glutathione adduct, formed on Cys¹⁵⁸ upon reaction with GSSG, is transferred efficiently to the reduced roGFP2 instead of being resolved into an intramolecular disulfide, an oxidized form which is not or less efficiently able to catalyze roGFP2 oxidation. However, the fact that GRXS16 mediated roGFP2 oxidation indicates that the recycling step by Cys²¹⁵ is not very efficient and may be rate-limiting. Coupled with the high reactivity of reduced GRXS16 towards GSSG, this supports the possibility that it could mediate protein glutathionylation *in vivo* in response to small variations of the GSH/GSSG pool that can occur in some conditions.

4.4. Who does what among plastidial GRXs?

In *A. thaliana*, four plastidial GRXs are present in plastids, two belonging to the class I, GRXC5 and GRXS12, and two belonging to the class II, GRXS14 and GRXS16. Except GRXS12, all are able to bind Fe-S clusters at least *in vitro* [19,22]. Moreover, both class I GRXs possess GSH-dependent deglutathionylation activity in their apoforms [14,19] whereas GRXS14 and GRXS16 do not or very poorly, at least with the substrates tested so far. Hence, considering that GRXC5 is only found in Brassicaceae, GRXS12 should be the predominant isoform controlling deglutathionylation reactions in most terrestrial species.

The question of how protein glutathionylation occurs in this compartment is more uncertain. It could be somehow spontaneous in situations where sulfenic acids formed upon reaction of cysteines with molecules such as hydrogen peroxide, react with GSH [46]. But this could be also mediated by GRXs. For instance, considering its reactivity towards GSSG or GSNO, AtGRXS16 could catalyze the glutathionylation of target proteins. Considering that AtGRXC1 is more efficient than AtGRXS16 for roGFP2 oxidation and that class I GRXs appear to react equally well with these oxidized glutathione forms [17,19], the plastidial class I GRXs may be again the best candidates for this type of reaction. Indeed, although the capacity of AtGRXS12 to catalyze glutathionylation reactions has not been specifically addressed, *in vitro* evidence for a stable glutathionylated state were provided using the poplar ortholog [21]. Overall, class I GRXs should be the predominant actors controlling glutathionylation/deglutathionylation cycles in plastids but the glutathionylation activity of class II GRXs may be relevant for promoting the oxidation of specific partners or in specific conditions or organisms as in algae. Indeed, *Ostreococcus* species have no class I GRXs and the only plastidial isoforms found in *C. reinhardtii* are the class II GRXs, GRX3 and GRX6. This raises the question of how glutathionylation/deglutathionylation reactions are controlled in plastids of these species taking into account that TRXs do not seem to be efficient catalysts for these reactions [8].

It is important to notice that, for both deglutathionylation/glutathionylation reactions, GRXs have to be initially reduced in order to perform the nucleophilic attack of either oxidized glutathione forms or glutathionylated targets. Hence, if the chloroplastic NTR-TRX hybrid

protein, NTRc, does not reduce them, class II GRXs should only be reduced in light conditions. The question of the physiological redox state of plastidial class II GRXs and of GRXS16 in particular is also important for the binding of Fe-S clusters. Indeed, by analogy with the mitochondrial GRXS15 counterpart [24], the assumed role of GRXS16 in the maturation of Fe-S proteins is to transfer preformed Fe-S clusters to partner proteins, either final client proteins or other SUF components [47]. This transfer function implies that class II GRXs are under a reduced state to transiently bind the Fe-S clusters. As for the oxidoreductase property, this indicates that the function of class II GRXs in Fe-S cluster biogenesis may not be operational in stress conditions or in the dark. In the latter case, this may be counterintuitive because an attractive hypothesis is that Fe-S cluster biogenesis occurs during the night, a period during which the levels of reactive oxygen species, that potentially damages Fe-S clusters, are lower.

5. Author contribution statement

R.B., molecular biology
 F.Z., A.M., T.D., biochemical analysis
 J.C., N.R., A.J.M., experiment design, data analysis and writing manuscript.

Acknowledgments

The authors are grateful to Pr Jean-Pierre Jacquot for careful and critical reading of the manuscript. Technical support from Fabien Lachaud of the “Service Commun de Spectrométrie de Masse et Chromatographie” of the Université de Lorraine is gratefully acknowledged.

Funding information

This study and the PhD salary of F.Z. were funded by grants of the French National Research Agency (ANR) as part of the “Investissements d’Avenir” program (ANR-11-LABX-0002-01, Lab of Excellence ARBRE) and of the ANR 2010 BLAN_1616 contract.

Financial support from the Deutsche Forschungsgemeinschaft (DFG) to A.J.M. through grants ME1567/9-1 and 9-2 within the Priority Program SPP1710 is gratefully acknowledged.

Appendix A. Supplementary data

Supplementary data to this article can be found online at <https://doi.org/10.1016/j.bbagen.2018.11.014>.

References

- [1] J. Couturier, J.P. Jacquot, N. Rouhier, Evolution and diversity of glutaredoxins in photosynthetic organisms, *Cell. Mol. Life Sci.* 66 (2009) 2539–2557.
- [2] J. Couturier, J. Przybyla-Toscano, T. Roret, C. Didierjean, N. Rouhier, The roles of glutaredoxin ligating Fe-S clusters: Sensing, transfer or repair functions? *Biochim. Biophys. Acta* 1853 (2015) 1513–1527.
- [3] F. Zannini, T. Roret, J. Przybyla-Toscano, T. Dhalleine, N. Rouhier, J. Couturier, Mitochondrial *Arabidopsis thaliana* TRXo Isoforms Bind an Iron – Sulfur Cluster and Reduce NFU Proteins in Vitro, *Antioxidants (Basel)* 7 (2018).
- [4] J.P. Jacquot, H. Eklund, N. Rouhier, P. Schurmann, Structural and evolutionary aspects of thioredoxin reductases in photosynthetic organisms, *Trends Plant Sci.* 14 (2009) 336–343.
- [5] N. Rouhier, Plant glutaredoxins: pivotal players in redox biology and iron-Sulphur Centre assembly, *New Phytol.* 186 (2010) 365–372.
- [6] A.P. Fernandes, M. Fladvad, C. Berndt, C. Andresen, C.H. Lillig, P. Neubauer, M. Sunnerhagen, A. Holmgren, A. Vlamis-Gardikas, A novel monothiol glutaredoxin (Grx4) from *Escherichia coli* can serve as a substrate for thioredoxin reductase, *J. Biol. Chem.* 280 (2005) 24544–24552.
- [7] C. Johansson, C.H. Lillig, A. Holmgren, Human mitochondrial glutaredoxin reduces S-glutathionylated proteins with high affinity accepting electrons from either glutathione or thioredoxin reductase, *J. Biol. Chem.* 279 (2004) 7537–7543.
- [8] M. Zaffagnini, L. Michelet, V. Massot, P. Trost, S.D. Lemaire, Biochemical characterization of glutaredoxins from *Chlamydomonas reinhardtii* reveals the unique properties of a chloroplastic CGFS-type glutaredoxin, *J. Biol. Chem.* 283 (2008) 8868–8876.
- [9] E. Gelhaye, N. Rouhier, J.P. Jacquot, Evidence for a subgroup of thioredoxin h that requires GSH/Grx for its reduction, *FEBS Lett.* 555 (2003) 443–448.
- [10] C.S. Koh, N. Navrot, C. Didierjean, N. Rouhier, M. Hirasawa, D.B. Knaff, G. Wingsle, R. Samian, J.P. Jacquot, C. Corbier, E. Gelhaye, An atypical catalytic mechanism involving three cysteines of thioredoxin, *J. Biol. Chem.* 283 (2008) 23062–23072.
- [11] H. Zhang, Y. Du, X. Zhang, J. Lu, A. Holmgren, Glutaredoxin 2 reduces both thioredoxin 2 and thioredoxin 1 and protects cells from apoptosis induced by auranofin and 4-hydroxyonenal, *Antioxid. Redox Signal.* 21 (2014) 669–681.
- [12] R. Alves, E. Vilaprinjo, A. Sorribas, E. Herrero, Evolution based on domain combinations: the case of glutaredoxins, *BMC Evol. Biol.* 9 (2009) 66.
- [13] N. Rouhier, S.D. Lemaire, J.P. Jacquot, The role of glutathione in photosynthetic organisms: emerging functions for glutaredoxins and glutathionylation, *Annu. Rev. Plant Biol.* 59 (2008) 143–166.
- [14] J. Couturier, C.S. Koh, M. Zaffagnini, A.M. Winger, J.M. Gualberto, C. Corbier, P. Decottignies, J.P. Jacquot, S.D. Lemaire, C. Didierjean, N. Rouhier, Structure-function relationship of the chloroplastic glutaredoxin S12 with an atypical WCSYS active site, *J. Biol. Chem.* 284 (2009) 9299–9310.
- [15] M.J. Saaranen, K.E. Salo, M.K. Latvala-Ranta, V.L. Kinnula, L.W. Ruddock, The C-terminal active site cysteine of *Escherichia coli* glutaredoxin 1 determines the glutathione specificity of the second step of peptide deglutathionylation, *Antioxid. Redox Signal.* 11 (2009) 1819–1828.
- [16] M.M. Gallogly, D.W. Starke, J.J. Miyehal, Mechanistic and kinetic details of catalysis of thiol-disulfide exchange by glutaredoxins and potential mechanisms of regulation, *Antioxid. Redox Signal.* 11 (2009) 1059–1081.
- [17] J. Couturier, J.P. Jacquot, N. Rouhier, Toward a refined classification of class I dithiol glutaredoxins from poplar: biochemical basis for the definition of two subclasses, *Front. Plant Sci.* 4 (2013) 518.
- [18] J. Couturier, C. Didierjean, J.P. Jacquot, N. Rouhier, Engineered mutated glutaredoxins mimicking peculiar plant class III glutaredoxin bind iron-sulfur centers and possess reductase activity, *Biochem. Biophys. Res. Commun.* 403 (2010) 435–441.
- [19] J. Couturier, E. Stroher, A.N. Albetel, T. Roret, M. Muthuramalingam, L. Tarrago, T. Seidel, P. Tsan, J.P. Jacquot, M.K. Johnson, K.J. Dietz, C. Didierjean, N. Rouhier, *Arabidopsis* chloroplastic glutaredoxin C5 as a model to explore molecular determinants for iron-sulfur cluster binding into glutaredoxins, *J. Biol. Chem.* 286 (2011) 27515–27527.
- [20] N. Rouhier, H. Unno, S. Bandyopadhyay, L. Masip, S.K. Kim, M. Hirasawa, J.M. Gualberto, V. Lattard, M. Kusunoki, D.B. Knaff, G. Georgiou, T. Hase, M.K. Johnson, J.P. Jacquot, Functional, structural, and spectroscopic characterization of a glutathione-ligated [2Fe-2S] cluster in poplar glutaredoxin C1, *Proc. Natl. Acad. Sci. U. S. A.* 104 (2007) 7379–7384.
- [21] M. Zaffagnini, M. Bedhomme, C.H. Marchand, J.R. Couturier, X.H. Gao, N. Rouhier, P. Trost, S.P. Lemaire, Glutaredoxin s12: unique properties for redox signaling, *Antioxid. Redox Signal.* 16 (2012) 17–32.
- [22] S. Bandyopadhyay, F. Gama, M.M. Molina-Navarro, J.M. Gualberto, R. Claxton, S.G. Naik, B.H. Huynh, E. Herrero, J.P. Jacquot, M.K. Johnson, N. Rouhier, Chloroplast monothiol glutaredoxins as scaffold proteins for the assembly and delivery of [2Fe-2S] clusters, *EMBO J.* 27 (2008) 1122–1133.
- [23] J. Knuesting, C. Riondet, C. Maria, I. Kruse, N. Becuwe, N. Konig, C. Berndt, S. Tourrette, J. Guilleminot-Montoya, E. Herrero, F. Gaymard, J. Balk, G. Belli, R. Scheibe, J.P. Reichheld, N. Rouhier, P. Rey, *Arabidopsis* glutaredoxin S17 and its partner, the nuclear factor Y subunit C11/negative cofactor 2alpha, contribute to maintenance of the shoot apical meristem under long-day photoperiod, *Plant Physiol.* 167 (2015) 1643–1658.
- [24] A. Moseler, I. Aller, S. Wagner, T. Nietzel, J. Przybyla-Toscano, U. Muhlenhoff, R. Lill, C. Berndt, N. Rouhier, M. Schwarzslander, A.J. Meyer, The mitochondrial monothiol glutaredoxin S15 is essential for iron-sulfur protein maturation in *Arabidopsis thaliana*, *Proc. Natl. Acad. Sci. U. S. A.* 112 (2015) 13735–13740.
- [25] S. Inigo, A.N. Durand, A. Ritter, S. Le Gall, M. Termathe, R. Klassen, T. Tohge, B. De Coninck, J. Van Leene, R. De Clercq, B.P. Cammue, A.R. Fernie, K. Gevaert, G. De Jaeger, S.A. Leidel, R. Schaffrath, M. Van Lijsebettens, L. Pauwels, A. Goossens, Glutaredoxin GRXS17 Associates with the Cytosolic Iron-Sulfur Cluster Assembly Pathway, *Plant Physiol.* 172 (2016) 858–873.
- [26] P. Rey, N. Becuwe, S. Tourrette, N. Rouhier, Involvement of *Arabidopsis* glutaredoxin S14 in the maintenance of chlorophyll content, *Plant Cell Environ.* 40 (2017) 2319–2332.
- [27] E. Stroher, J. Grassl, C. Carrie, R. Fenske, J. Whelan, A.H. Millar, Glutaredoxin S15 is involved in Fe-S Cluster transfer in mitochondria Influencing Lipoic Acid-Dependent Enzymes, Plant Growth, and Arsenic Tolerance in *Arabidopsis*, *Plant Physiol.* 170 (2016) 1284–1299.
- [28] J. Couturier, H.C. Wu, T. Dhalleine, H. Pegeot, D. Sudre, J.M. Gualberto, J.P. Jacquot, F. Gaymard, F. Vignols, N. Rouhier, Monothiol glutaredoxin-Bola interactions: redox control of *Arabidopsis thaliana* Bola2 and SuffE1, *Mol. Plant* 7 (2014) 187–205.
- [29] X. Liu, S. Liu, Y. Feng, J.Z. Liu, Y. Chen, K. Pham, H. Deng, K.D. Hirschi, X. Wang, N. Cheng, Structural insights into the N-terminal GIY-YIG endonuclease activity of *Arabidopsis* glutaredoxin AtGRXS16 in chloroplasts, *Proc. Natl. Acad. Sci. U. S. A.* 110 (2013) 9565–9570.
- [30] M. Behm, J.P. Jacquot, Isolation and characterization of thioredoxin h from poplar xylem, *Plant Physiol. Biochem.* 38 (2000) 363–369.
- [31] K. Chibani, L. Tarrago, P. Schurmann, J.P. Jacquot, N. Rouhier, Biochemical properties of poplar thioredoxin z, *FEBS Lett.* 585 (2011) 1077–1081.
- [32] D.A. Glauser, F. Bourquin, W. Manieri, P. Schürmann, Characterization of ferredoxin:thioredoxin reductase modified by site-directed mutagenesis, *J. Biol. Chem.* 279 (2004) 16662–16669.
- [33] M. Hodges, M. Miginac-Maslow, P. Decottignies, J.P. Jacquot, M. Stein, L. Lepiniec,

- C. Cretin, P. Gadal, Purification and characterization of pea thioredoxin f expressed in *Escherichia coli*, *Plant Mol. Biol.* 26 (1994) 225–234.
- [34] J.P. Jacquot, R. Rivera-Madrid, P. Marinho, M. Kollarova, P. Le Marechal, M. Miginiac-Maslow, Y. Meyer, *Arabidopsis thaliana* NAPHP thioredoxin reductase, cDNA characterization and expression of the recombinant protein in *Escherichia coli*, *J Mol Biol* 235 (1994) 1357–1363.
- [35] A.J. Meyer, T. Brach, L. Marty, S. Kreye, N. Rouhier, J.P. Jacquot, R. Hell, Redox-sensitive GFP in *Arabidopsis thaliana* is a quantitative biosensor for the redox potential of the cellular glutathione redox buffer, *Plant J.* 52 (2007) 973–986.
- [36] M. Stein, J.P. Jacquot, E. Jeannette, P. Decottignies, M. Hodges, J.M. Lancelin, V. Mittard, J.M. Schmitter, M. Miginiac-Maslow, *Chlamydomonas reinhardtii* thioredoxins: structure of the genes coding for the chloroplastic m and cytosolic h isoforms; expression in *Escherichia coli* of the recombinant proteins, purification and biochemical properties, *Plant Mol. Biol.* 28 (1995) 487–503.
- [37] F. Zannini, J. Couturier, O. Keech, N. Rouhier, In Vitro Alkylation Methods for Assessing the Protein Redox State, *Methods Mol Biol.* 1653, (2017), pp. 51–64.
- [38] P. Begas, L. Liedgens, A. Moseler, A.J. Meyer, M. Deponte, Glutaredoxin catalysis requires two distinct glutathione interaction sites, *Nat. Commun.* 8 (2017) 14835.
- [39] X.H. Gao, M. Zaffagnini, M. Bedhomme, L. Michelet, C. Cassier-Chauvat, P. Decottignies, S.D. Lemaire, Biochemical characterization of glutaredoxins from *Chlamydomonas reinhardtii*: kinetics and specificity in deglutathionylation reactions, *FEBS Lett.* 584 (2010) 2242–2248.
- [40] J. Tamarit, G. Belli, E. Cabisco, E. Herrero, J. Ros, Biochemical characterization of yeast mitochondrial Grx5 monothiol glutaredoxin, *J. Biol. Chem.* 278 (2003) 25745–25751.
- [41] M. Fladvad, M. Bellanda, A.P. Fernandes, S. Mammi, A. Vlamis-Gardikas, A. Holmgren, M. Sunnerhagen, Molecular mapping of functionalities in the solution structure of reduced Grx4, a monothiol glutaredoxin from *Escherichia coli*, *J. Biol. Chem.* 280 (2005) 24553–24561.
- [42] K. Yoshida, S. Hara, T. Hisabori, Thioredoxin selectivity for thiol-based redox regulation of target proteins in chloroplasts, *J. Biol. Chem.* 290 (2015) 19540.
- [43] P. Wang, J. Liu, B. Liu, D. Feng, Q. Da, S. Shu, J. Su, Y. Zhang, J. Wang, H.B. Wang, Evidence for a role of chloroplastic m-type thioredoxins in the biogenesis of photosystem II in *Arabidopsis*, *Plant Physiol.* 163 (2013) 1710–1728.
- [44] Y. Zhu, M. Liberton, H.B. Pakrasi, A Novel Redoxin in the Thylakoid Membrane Regulates the Titer of Photosystem I, *J. Biol. Chem.* 291 (2016) 18689–18699.
- [45] K.W. Bender, X. Wang, G.B. Cheng, H.S. Kim, R.E. Zielinski, S.C. Huber, Glutaredoxin AtGRXC2 catalyses inhibitory glutathionylation of *Arabidopsis* BRI1-associated receptor-like kinase 1 (BAK1) in vitro, *Biochem. J.* 467 (2015) 399–413.
- [46] M. Zaffagnini, M. Bedhomme, C.H. Marchand, S. Morisse, P. Trost, S.D. Lemaire, Redox regulation in photosynthetic organisms: focus on glutathionylation, *Antioxid. Redox Signal.* 16 (2012) 567–586.
- [47] J. Przybyla-Toscano, M. Roland, F. Gaymard, J. Couturier, N. Rouhier, Roles and maturation of iron-sulfur proteins in plastids, *J. Biol. Inorg. Chem.* 23 (2018) 545–566.

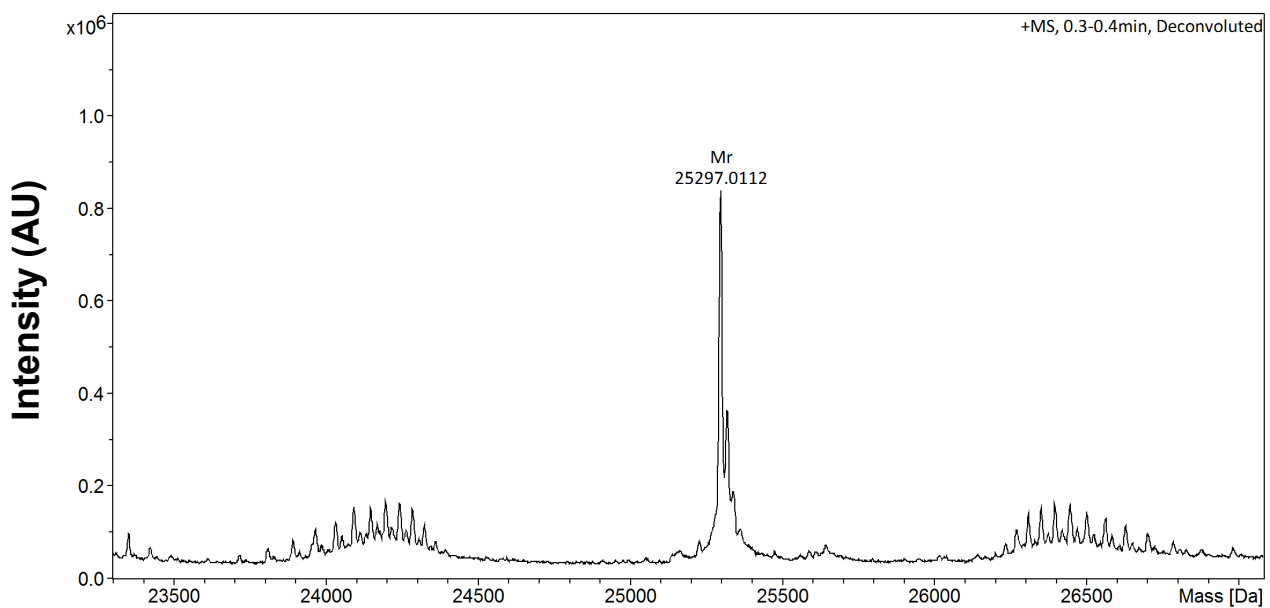
Supplementary Table 1. Primers used for cloning and site-directed mutagenesis experiments.

The *Nco*I and *Bam*HI restriction sites used for cloning are underlined in the primers. The mutagenic codons are in bold.

Name	Sequence
GRXS16 for	5' CCCCC <u>CATGG</u> CTTCCGCCGTCAAATCTCTAACG 3'
GRXS16 rev	5' CCCCG <u>GGATCC</u> CCTAGTTCAAGATATTGGC 3'
GRXS16 C62S for	5' TCTGTGCCGGAGCTTCTGGCTCCGTTAAGGTT 3'
GRXS16 C62S rev	5' AACCTTAACGGAGCC A AAAGCTCCGGCACAGA 3'
GRXS16 C158S for	5' AGGAGTGCTCCTCAAT T GGATTCTCACAGAGA 3'
GRXS16 C158S rev	5' TCTCTGTGAGAAT CC CAGATTGAGGAGCACTCCT 3'
GRXS16 C215S for	5' GAACTTGTAGGAGGAT CT GATATTGACCTCA 3'
GRXS16 C215S rev	5' TGAGGTCAA AA ATAT C AGATCCTCCTACAAGTTC 3'

Figure S1

A



B

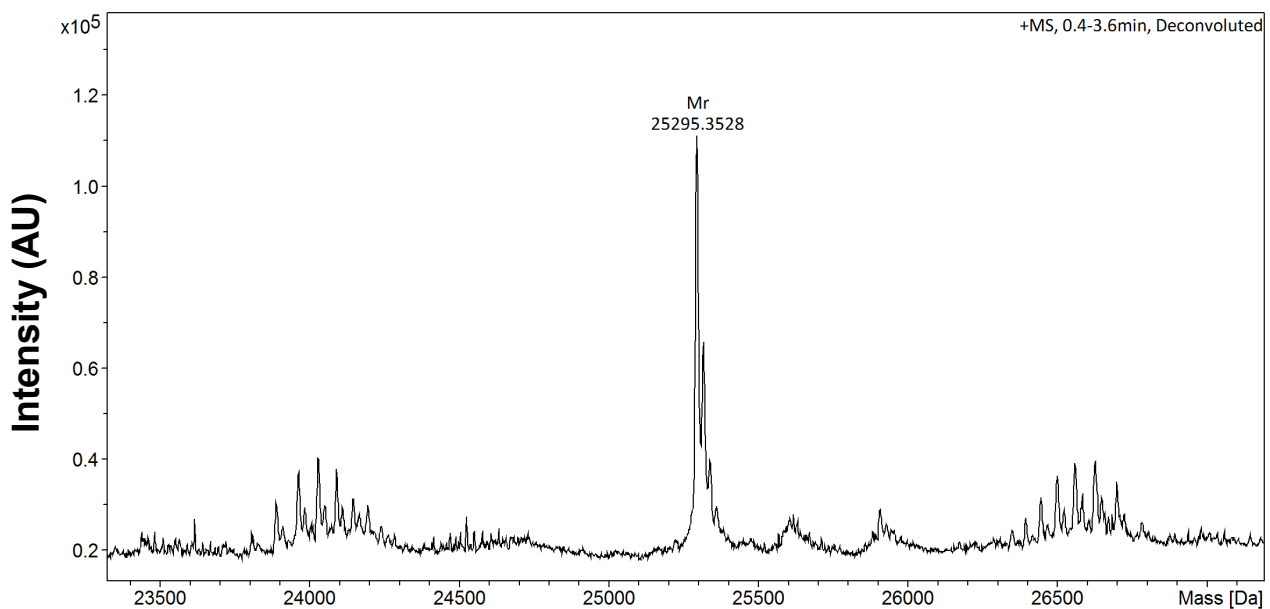
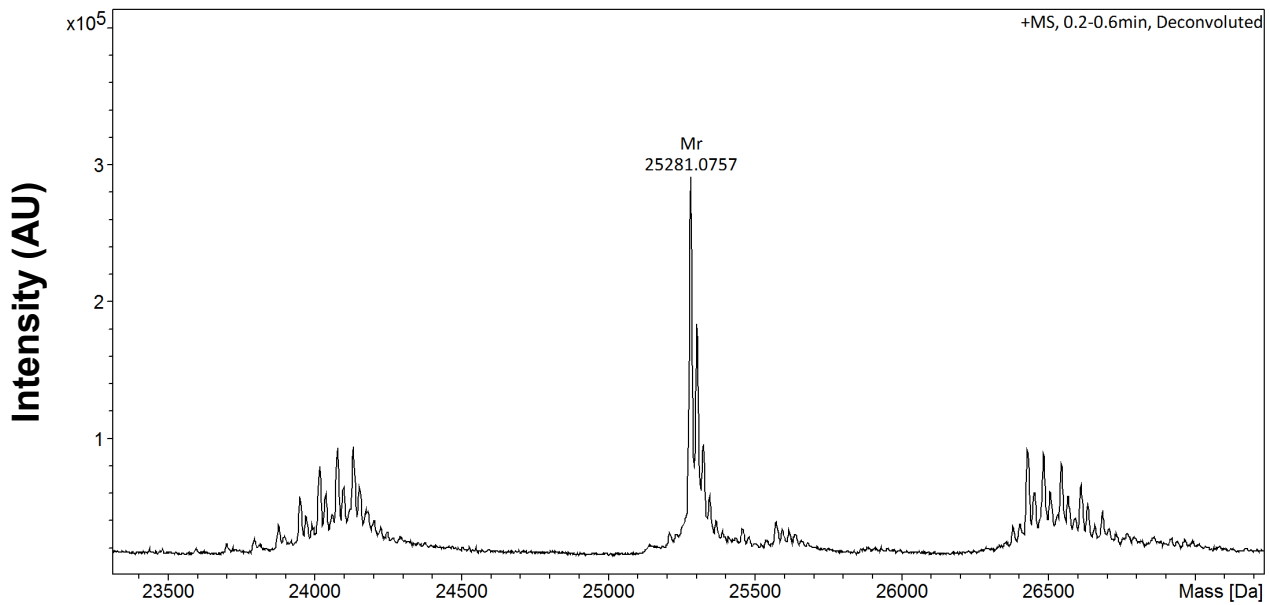


Figure S2

A



B

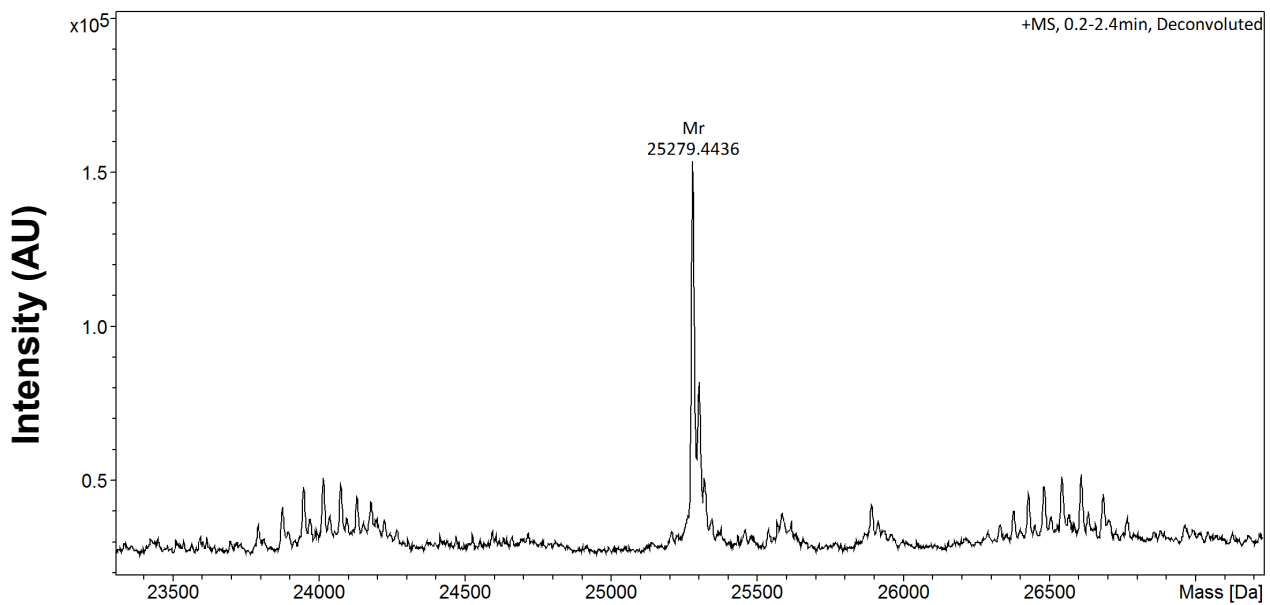
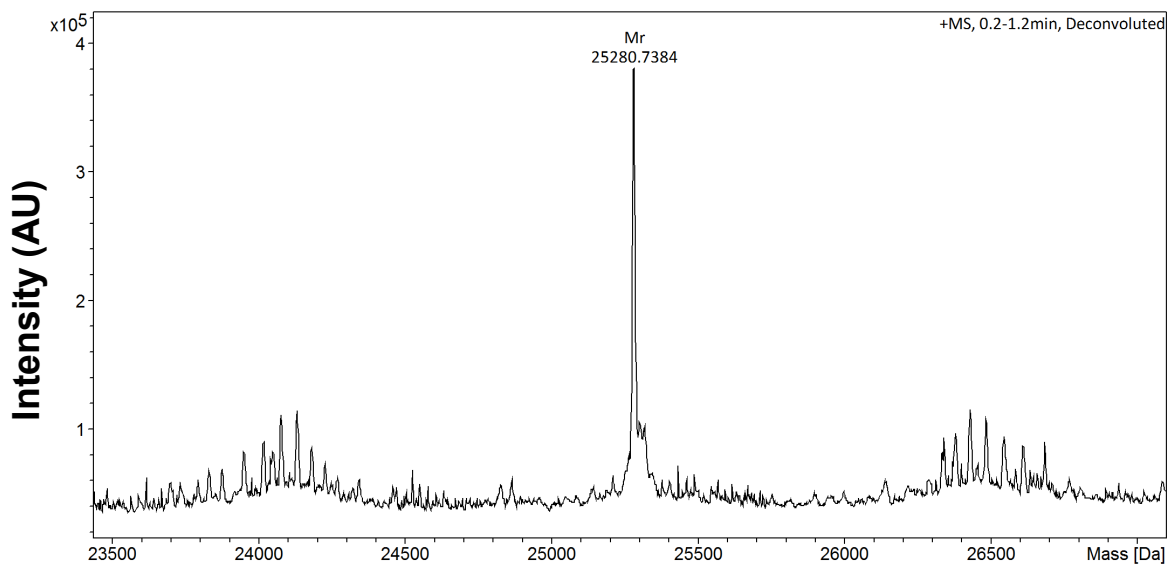
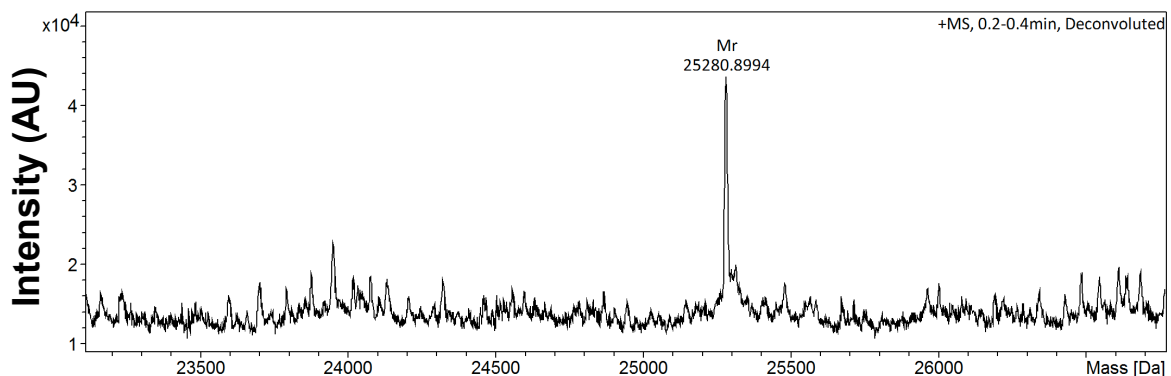


Figure S3

A



B



C

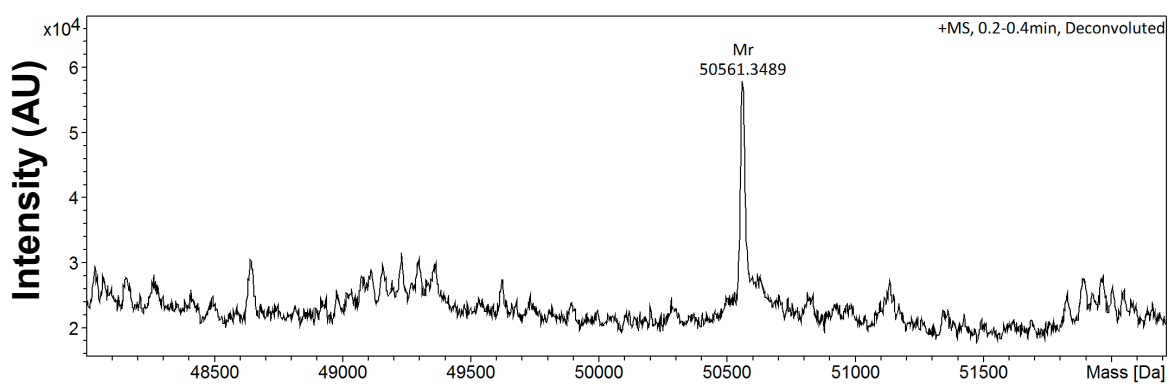
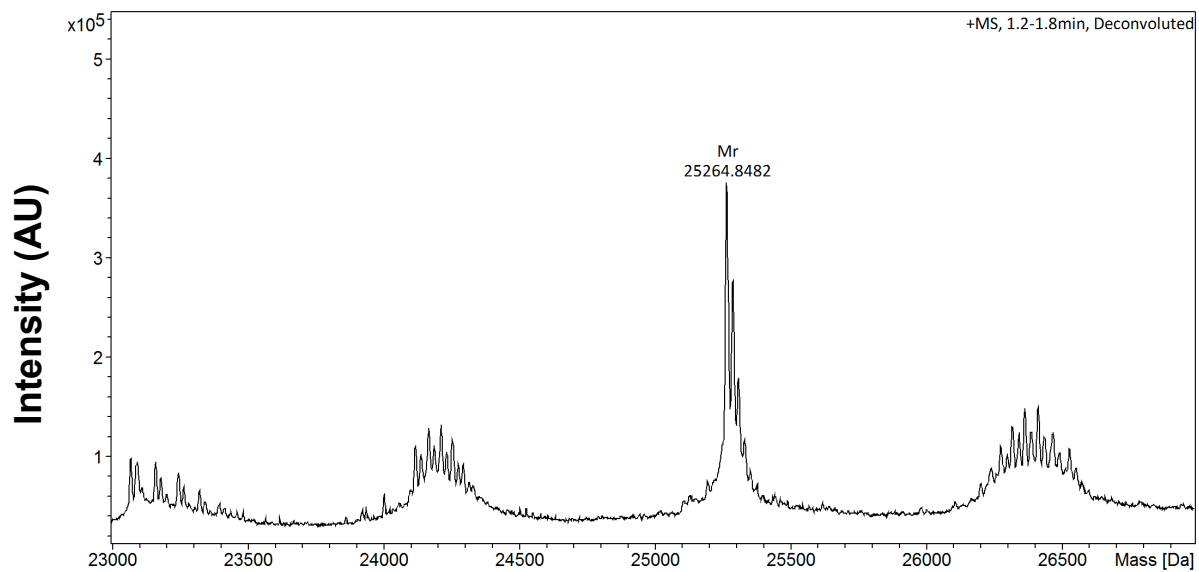
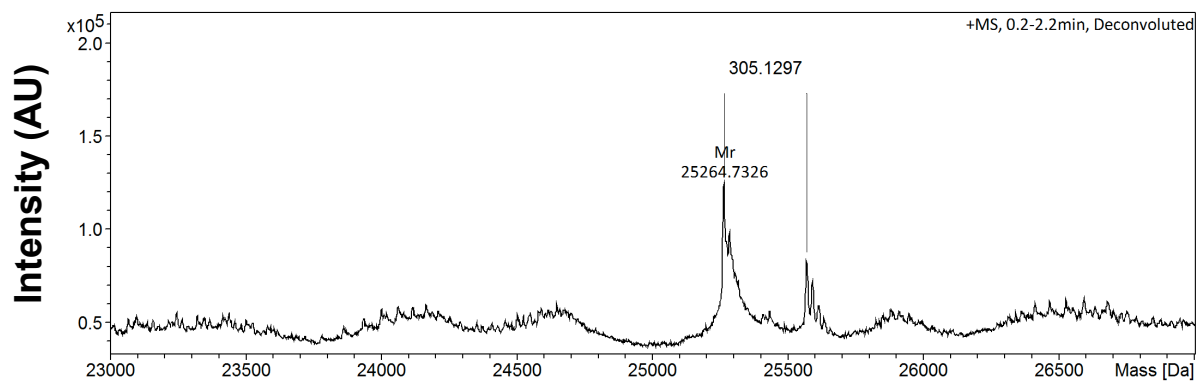


Figure S4

A



B



C

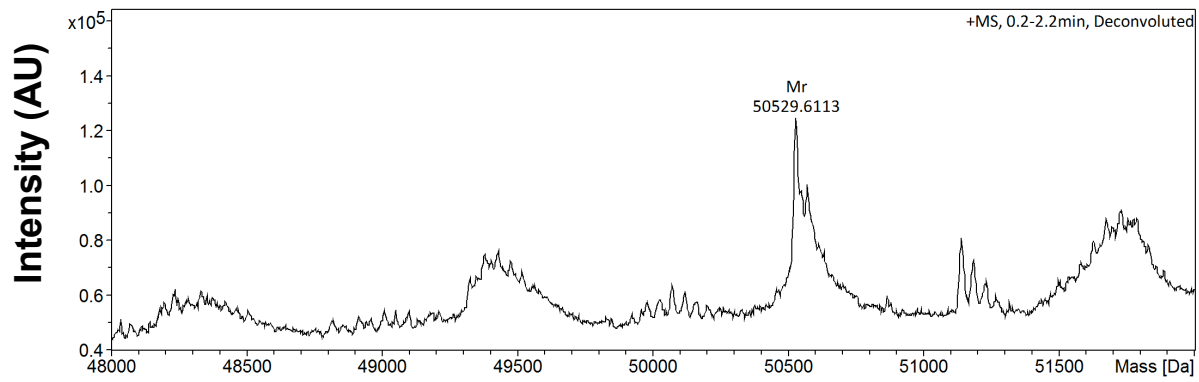


Figure S5

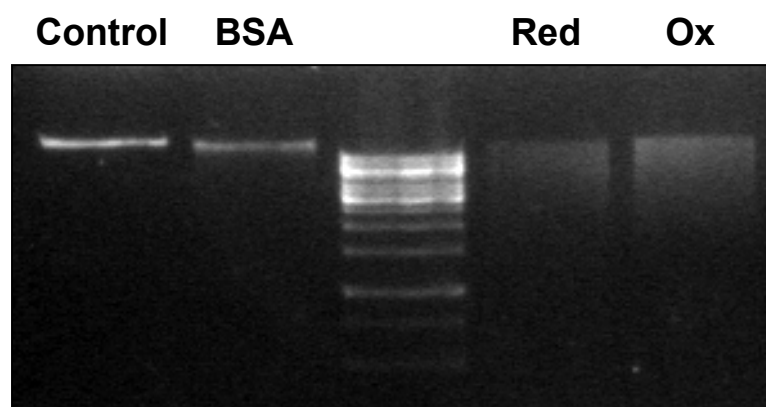


Figure S6

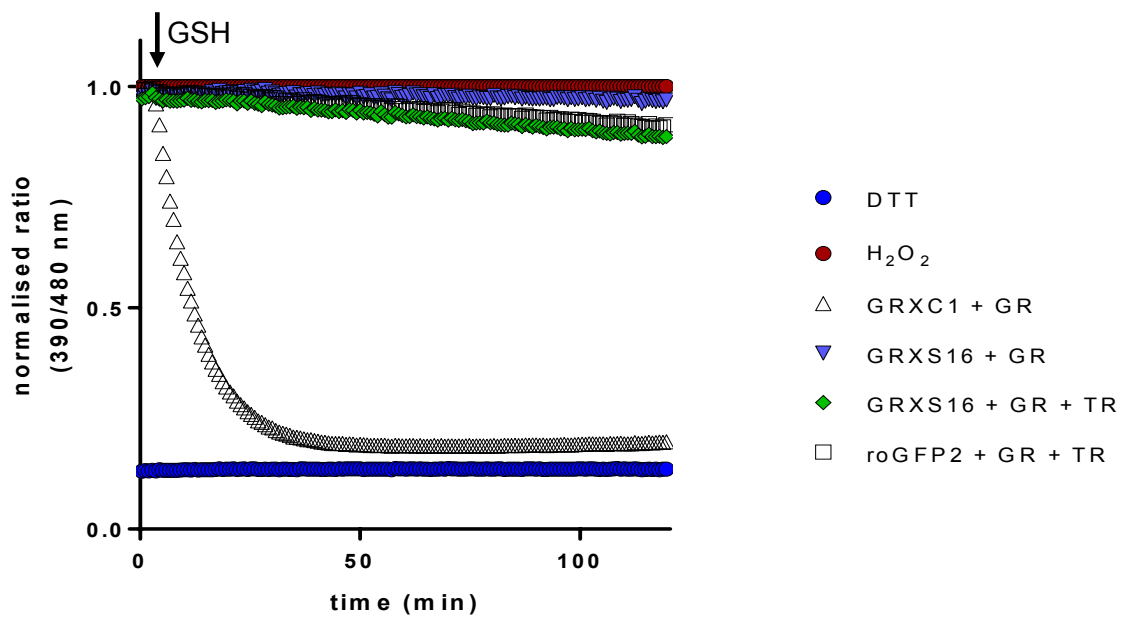
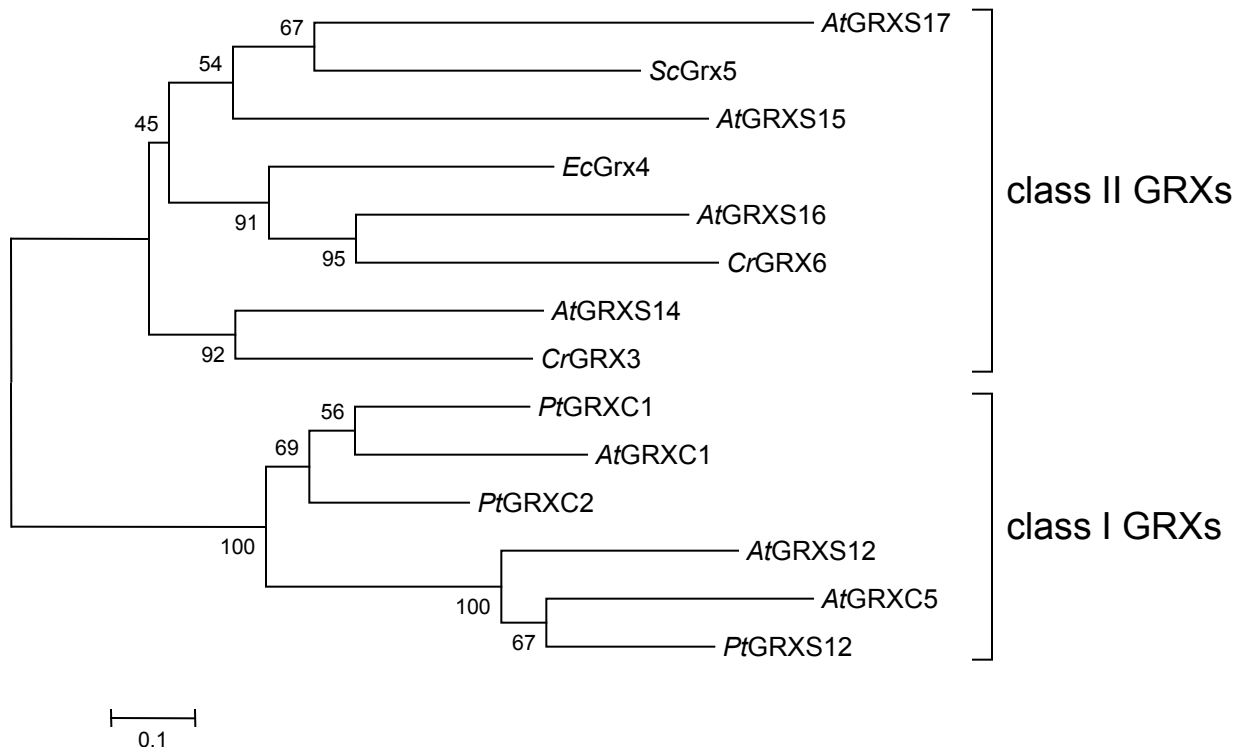


Figure S7



Mitochondrial *Arabidopsis thaliana* TRXo isoforms bind an iron-sulfur cluster and reduce NFU proteins in vitro

Flavien Zannini¹, Thomas Roret^{1,2}, Jonathan Przybyla-Toscano^{1,3}, Tiphaine Dhalleine¹,

Nicolas Rouhier¹ and Jérémie Couturier^{1*}

¹ Université de Lorraine, Inra, IAM, F-54000 Nancy, France

² CNRS, LBI2M, Sorbonne Universités, F-29680 Roscoff, France

³ Department of Plant Physiology, Umeå Plant Science Centre, Umeå University, S-90187 Umea, Sweden

Article publié dans Antioxidants

Chez les organismes photosynthétiques, les TRXs forment une famille multigénique d'environ 40 membres mais peu sont retrouvées dans les mitochondries (TRX h2 et TRX o). Contrairement à la plupart des autres plantes, *Arabidopsis thaliana* possède deux isoformes TRXo. Ces travaux avaient pour objectif de caractériser leurs propriétés biochimiques respectives. De manière surprenante, il est apparu que les deux isoformes lient *a priori* un centre fer-soufre (Fe-S) de type [4Fe-4S] coordonné au sein d'un homodimère par les deux cystéines du site actif WCGPC de chaque monomère après expression dans un système hétérologue bactérien ou lors d'expériences de reconstitution de centre Fe-S *in vitro*. Malgré des différences structurales, ces deux TRX sous forme apo sont capables de réduire les protéines NFU4/5 *in vitro*, protéines préalablement identifiées comme partenaires de TRXo1 et impliquées dans la maturation des protéines Fe-S dans les mitochondries. Ces résultats pourraient indiquer des connections avec la maturation des protéines Fe-S, les TRX o pouvant notamment participer à la réduction de certains facteurs de maturation si ceux-ci se retrouvaient transitoirement oxydés.



Article

Mitochondrial *Arabidopsis thaliana* TRXo Isoforms Bind an Iron–Sulfur Cluster and Reduce NFU Proteins In Vitro

Flavien Zannini ¹, Thomas Roret ^{1,2}, Jonathan Przybyla-Toscano ^{1,3}, Tiphaine Dhalleine ¹, Nicolas Rouhier ¹ and Jérémie Couturier ^{1,*}

¹ Université de Lorraine, Inra, IAM, F-54000 Nancy, France; flavien.zannini@univ-lorraine.fr (F.Z.); thomas.roret@sb-roscott.fr (T.R.); przybylajonathan@orange.fr (J.P.-T.); tiphaine.dhalleine@univ-lorraine.fr (T.D.); nicolas.rouhier@univ-lorraine.fr (N.R.)

² CNRS, LBI2M, Sorbonne Universités, F-29680 Roscoff, France

³ Department of Plant Physiology, Umeå Plant Science Centre, Umeå University, S-90187 Umeå, Sweden

* Correspondence: jeremy.couturier@univ-lorraine.fr; Tel.: +33-372-745-159

Received: 11 August 2018; Accepted: 9 October 2018; Published: 13 October 2018



Abstract: In plants, the mitochondrial thioredoxin (TRX) system generally comprises only one or two isoforms belonging to the TRX h or o classes, being less well developed compared to the numerous isoforms found in chloroplasts. Unlike most other plant species, *Arabidopsis thaliana* possesses two TRXo isoforms whose physiological functions remain unclear. Here, we performed a structure–function analysis to unravel the respective properties of the duplicated TRXo1 and TRXo2 isoforms. Surprisingly, when expressed in *Escherichia coli*, both recombinant proteins existed in an apo-monomeric form and in a homodimeric iron–sulfur (Fe-S) cluster-bridged form. In TRXo2, the [4Fe-4S] cluster is likely ligated in by the usual catalytic cysteines present in the conserved Trp-Cys-Gly-Pro-Cys signature. Solving the three-dimensional structure of both TRXo apo-forms pointed to marked differences in the surface charge distribution, notably in some areas usually participating to protein–protein interactions with partners. However, we could not detect a difference in their capacity to reduce nitrogen-fixation-subunit-U (NFU)-like proteins, NFU4 or NFU5, two proteins participating in the maturation of certain mitochondrial Fe-S proteins and previously isolated as putative TRXo1 partners. Altogether, these results suggest that a novel regulation mechanism may prevail for mitochondrial TRXs o, possibly existing as a redox-inactive Fe-S cluster-bound form that could be rapidly converted in a redox-active form upon cluster degradation in specific physiological conditions.

Keywords: mitochondria; thioredoxin; iron–sulfur cluster; redox regulation

1. Introduction

Mitochondria are important organelles being notably the site of production of cellular energy in the form of adenosine triphosphate (ATP) through the process of oxidative phosphorylation and being also an important site for the amino acid and lipid metabolisms and for the biosynthesis of many crucial vitamins and cofactors. For instance, mitochondria are crucial for the synthesis of the iron–sulfur (Fe-S) clusters found in numerous essential proteins present in the matrix but also in the cytosol and the nucleus [1–3]. Despite the existence of several energy-dissipating systems, the over-reduction of the mitochondrial electron transport chain (ETC) releases reactive oxygen species (ROS) notably at the level of the complexes I and III [4]. Scavenging enzymes for the superoxide ion and H₂O₂ are present in the mitochondrial matrix. This includes superoxide dismutases and ascorbate- and thiol-dependent peroxidases belonging to the peroxiredoxin (PRX) or glutathione-peroxidase-like

(GPXL) families [4]. These thiol peroxidases use reactive cysteine residues for catalysis and rely either on a glutathione/glutaredoxin (GSH/GRX) system or on a thioredoxin (TRX) system for their regeneration [5–8]. Despite the existence of these scavenging systems, ROS-mediated protein oxidation occurs in this compartment. At the level of some sensitive protein cysteine residues, this leads to reversible modifications such as the formation of sulfenic acid, of disulfide bonds, or of glutathionylated or nitrosylated cysteines. In this respect, it is surprising that the systems devoted to the reduction of these oxidized cysteine forms are not very developed in mitochondria. Among the 30 genes coding for GRXs [9] and the 30 to 45 genes encoding TRX or TRX-like proteins in angiosperms [10,11], only one GRX named GRXS15 [12] and one or two TRXs are found in mitochondria, the majority being present in plastids and in the cytosol/nucleus. The mitochondrial TRX isoforms belong to the TRX_h or TRX_o classes [13,14]. Unlike most other plant species, *A. thaliana* possesses two TRX_o isoforms which add to TRX_{h2} [15]. Their regeneration should be in principle dependent on the nicotinamide adenine dinucleotide phosphate reduced (NADPH)-thioredoxin reductase (NTR) A and/or B [13,16]. Concerning GRXS15, no in vitro GSH-dependent reductase activity was observed for GRXS15 so far whereas it possesses an oxidase activity being able to oxidize the reduction-oxidation sensitive green fluorescent protein 2 (roGFP2) at the expense of oxidized glutathione (GSSG) [17]. The physiological relevance of this activity is unclear because it is rather thought that GRXS15 participates to the maturation of Fe-S proteins serving as a transfer protein for the exchange of Fe-S clusters from scaffold proteins, on which de novo synthesis occurs, either to other maturation factors or directly to acceptor proteins [12,18]. Hence, TRX_o and _h likely represent the major disulfide reductases in plant mitochondria.

Both *A. thaliana* TRX_os have the typical characteristics of TRXs i.e., a molecular weight around 13 kDa and a conserved WCGPC motif that comprises the catalytic cysteines. In their reduced forms, TRX_os are rather competent for reducing disulfide bonds in target proteins. Nevertheless, as demonstrated for some peculiar TRX_os, they might also reduce S-nitrosylated or S-glutathionylated proteins [19,20]. If TRX_os also possessed such a property, this would help understanding the absence of GRXs with deglutathionylation activity in mitochondria. The molecular function of these TRX_os is unclear and only *A. thaliana* TRX_{o1} and pea TRX_o were studied so far. TRX_os may function in the regeneration of peroxiredoxin IIF [7,8], in the activation by reduction of citrate synthase [21], alternative oxidase (AOX) [22,23], and isocitrate dehydrogenase [24], but also in the deactivation of both mitochondrial succinate dehydrogenase and fumarase [25]. However, at the macromolecular level, the phenotypes of *A. thaliana* mutants for *trxo1* and *trxo2* single mutants or for the double mutant are extremely mild. In one study, no growth defect was observed for these mutants grown on soil under long-day conditions for four weeks [26]. In other studies, the *A. thaliana* *trxo1* mutant showed an accelerated germination in the presence of salt [27], and a significant reduction in the fresh weight of shoots was visible during the first four weeks of growth whereas the root growth was not affected [25]. At the cellular level, the activity of enzymes of the tricarboxylic acid (TCA) cycle, or associated with it, is deregulated in the *A. thaliana* *trxo1* mutant and this is accompanied by changes in the amounts of some metabolites, notably citrate, malate, and pyruvate [25]. In fact, several experiments aiming at identifying mitochondrial partners of TRX_os identified more than 100 putative targets including all enzymes of the TCA cycle and enzymes involved in many other processes [22,23,28]. In addition, one should also consider as putative partners, proteins forming intra- or intermolecular disulfide bridges [29], and proteins subject to other redox post-translational modifications (sulfenylation, nitrosylation, glutathionylation) as recently repertoried for photorespiratory and associated enzymes [30].

In order to understand whether the two mitochondrial TRX_os from *A. thaliana* could be distinguished by their biochemical properties, we have performed a structure–function analysis of both isoforms. We observed that both proteins bind an Fe-S cluster when expressed as recombinant proteins in *Escherichia coli*. The Fe-S cluster ligation in TRX_{o2} depends on the cysteines found in the conserved WCGPC motif. The physiological relevance of this observation remains unclear. Another observation that may give hints towards a possible connection with the mitochondrial Fe-S cluster

assembly machinery is that apo-TRXs o have the capacity to reduce oxidized NFU4 or NFU5, proteins previously isolated as putative TRX partners and known to participate in the maturation of certain mitochondrial Fe-S proteins [1–3]. Although solving their respective 3D structures indicated that marked differences in the surface charge distribution exist between both proteins, no difference between TRXo1 and TRXo2 was observed in the capacity to reduce NFU proteins.

2. Materials and Methods

2.1. Cloning and Site-Directed Mutagenesis

The sequences coding for the presumed mature form (i.e., devoid of N-terminal targeting sequences) of *A. thaliana* TRXo1 (At2g35010) and TRXo2 (At1g31020) were cloned into the *Nde*I and *Bam*HI restriction sites of both pET12a and pET15b. The cysteines of TRXo2 were individually substituted into serines by site-directed mutagenesis by primer extension using two complementary mutagenic primers [31,32]. In a first round of PCR, two fragments with overlapping ends are generated using TRXo2 forward and mutagenic reverse primers and TRXo2 reverse and mutagenic forward primers, respectively. For the second round of PCR, these fragments were mixed with TRXo2 forward and reverse primers added after 10 PCR cycles to obtain the final product with the desired mutation. The corresponding variants were named TRXo2 C37S and C40S. The sequences coding for the presumed mature forms of AtNFU4 (At3g20970) and AtNFU5 (At1g51390) were cloned into the *Nco*I and *Bam*HI restriction sites of pET3d and the sequence coding for *E. coli* IscS was cloned into the *Nde*I and *Bam*HI restriction sites of pET12a. All primers used in this study are listed in Table S1.

2.2. Heterologous Expression in *Escherichia coli* and Purification of Recombinant Proteins

For protein production, the *E. coli* BL21 (DE3) strain containing the pSBET plasmid, which allows expression of the transfer ribonucleic acid (tRNA) needed to recognize the AGG and AGA rare codons [33], was co-transformed with recombinant pET3d and pET12a plasmids to produce untagged proteins and with recombinant pET15b plasmids to produce N-terminal His-tagged proteins. The volumes of cultures of *E. coli* transformed cells were progressively increased up to 2.4 L in LB medium at 37 °C supplemented with 50 µg/mL of ampicillin and kanamycin. Protein expression was induced at exponential phase by adding 100 µM isopropyl β-D-thiogalactopyranoside for 4 h at 37 °C. Cultures were then centrifuged for 20 min at 6318 g and the cell pellets were resuspended in about 20 mL of Tris NaCl (30 mM Tris-HCl pH 8.0, 200 mM NaCl) for untagged proteins or Tl NaCl (50 mM Tris-HCl pH 8.0, 10 mM imidazole, 300 mM NaCl) for His-tagged proteins and conserved at –20 °C. Cell lysis was performed by sonication (3 × 1 min with intervals of 1 min) and the soluble and insoluble fractions were separated at 4 °C by centrifugation for 30 min at 27,216× g.

For His-tagged TRXs o, the soluble fraction was loaded on Ni²⁺ affinity columns (Sigma-Aldrich, St Louis MO, USA). After extensive washing, proteins were eluted by adding 50 mM Tris-HCl pH 8.0, 300 mM NaCl, 250 mM imidazole. The recombinant proteins were concentrated by ultrafiltration under nitrogen pressure and dialyzed (Amicon, YM10 membrane, Merck, Berlington MA, USA) and stored in a 30 mM Tris-HCl pH 8.0 buffer supplemented with 50% glycerol at –20 °C. The purification of His-tagged proteins was performed in aerobic or anaerobic conditions. Anaerobic manipulations were performed in a Jacobex glovebox under a nitrogen atmosphere with oxygen levels below 1 ppm.

For untagged proteins, the soluble fraction was first precipitated by ammonium sulfate from 0 to 40% and then to 80% of the saturation. Both TRXo and NFU proteins precipitated mostly between 40 and 80% of ammonium sulfate saturation and *E. coli* IscS between 0 and 40%. The fractions of interest were subjected to size exclusion chromatography (ACA44 for TRXo and NFU proteins, ACA34 for IscS) equilibrated with a Tris NaCl buffer. After dialysis against a 30 mM Tris-HCl pH 8.0 buffer and concentration, the interesting fractions were loaded to a DEAE (diethylaminoethyl) sepharose column equilibrated with the same buffer. The recombinant TRXo proteins that passed through the DEAE column, were concentrated by ultrafiltration under nitrogen pressure (Amicon cells, YM10 membrane),

and were stored in the same buffer in the presence of 50% glycerol at -20°C . On the contrary, NFU and IscS proteins were retained and eluted using a linear 0–0.4 M NaCl gradient. The purest fractions as judged by sodium dodecyl sulfate polyacrylamide gel electrophoresis (SDS-PAGE) analysis were pooled and dialyzed against 30 mM Tris-HCl pH 8.0 buffer as described above.

Protein concentrations were determined spectrophotometrically using a molecular extinction coefficient at 280 nm of $11,585 \text{ M}^{-1} \text{ cm}^{-1}$ for TRXo1, TRXo2, and NFU5; of $11,460 \text{ M}^{-1} \text{ cm}^{-1}$ for TRXo2 cysteine variants; of $13,075 \text{ M}^{-1} \text{ cm}^{-1}$ for NFU4; and of $41,495 \text{ M}^{-1} \text{ cm}^{-1}$ for IscS, as determined from the molar extinction coefficients of individual tyrosines, tryptophans, and cystines (1490, 5500, and $125 \text{ M}^{-1} \text{ cm}^{-1}$, respectively) [34].

The other recombinant proteins used in this work e.g., NTRB and GRXS15 from *A. thaliana* have been purified as described previously [35,36].

2.3. Preparation of Apo-TRXs o and IscS-Mediated In Vitro Fe-S Cluster Reconstitution of TRXs o

Under strictly anaerobic conditions in a glove box, 200 μM untagged apo-TRXo isoforms (proteins obtained after aerobic purification) were incubated with 100-fold excess of dithiothreitol (DTT) in Tris NaCl buffer for 1 h. The Fe-S cluster reconstitution was then initiated by the addition of catalytic amount of EcIscS (0.05 fold, 10 μM), five-fold excess of ferrous ammonium sulfate citrate (1 mM) and finally five-fold excess of L-cysteine (1 mM). After 30 min of incubation, the Fe-S cluster-loaded TRXo proteins were desalting on a G25 column equilibrated with Tris NaCl buffer.

2.4. Determination of the Oligomerization State

The oligomerization state of TRXo isoforms was analyzed by size-exclusion chromatography. Samples containing 100 to 300 μg of protein were loaded onto Superdex S200 10/300 columns equilibrated with 30 mM Tris-HCl pH 8.0, 200 mM NaCl and connected to an Äkta purifier system (GE Healthcare). The flow rate was fixed at 0.5 mL min^{-1} , and detection was recorded at 280 and 420 nm. The column was calibrated using a molecular weight standard from Sigma. Protein names, molecular weights and elution volumes are as follows: thyroglobulin 669 kDa, 8.47 mL; apoferritin 443 kDa, 10.51 mL; β -amylase 200 kDa, 11.92 mL; bovine serum albumin 66 kDa, 13.56 mL; carbonic anhydrase 29 kDa, 15.54 mL; cytochrome c 12.4 kDa, 16.82 mL and aprotinin 6.5 kDa, 18.16 mL.

2.5. GRX- and TRX-Mediated Reduction of NFUs

Around 3 mg of NFU proteins were reduced using 10 mM DTT in 200 μL of 30 mM Tris-HCl pH 8.0 buffer for 1 h at 25°C . The reduced proteins were then desalting on a G25 column pre-equilibrated with 30 mM Tris-HCl pH 8.0 buffer. The redox state of untreated and reduced NFUs was determined by electrospray ionization mass spectrometry analysis as described previously [37], and by a cysteine alkylation assay, which also served for assessing reduction by the TRX and GRX reducing systems. The TRX system reconstituted in vitro comprised 200 μM NADPH, 100 nM NTRB, and 1 or 10 μM untagged TRXo1 or o2. The GSH/GRX system was composed of 200 μM NADPH, 0.1 units GR from bakers' yeast (Sigma-Aldrich, St Louis MO, USA), 1 mM GSH and 1 or 10 μM GRXS15. Each reducing system was incubated at 25°C for 15 min prior addition of 10 μM of oxidized NFU4/5 in 50 μL of 30 mM Tris-HCl pH 8.0 buffer. The reaction was stopped after 15 min by the addition of one volume of 20% TCA. Protein free thiol groups have been alkylated with methoxyl-PEG (mPEG)-maleimide of 2 kDa as described previously [38], before separating the protein mixtures on non-reducing 15% SDS-PAGE.

2.6. Crystallization, Diffraction Data Collection, Processing, Structure Solution, and Refinement

Crystallization at 4°C was performed by a microbatch-under-oil method, in which 1 μL of the protein solutions were mixed with an equal volume of the precipitant solution containing 100 mM HEPES pH 7.5 and 20% PEG 8000 for TRXo1 and 100 mM citrate buffer pH 5.6, 30% PEG 4000 and 100 mM ammonium sulfate for TRXo2. Solutions of TRXo1 and TRXo2 had concentrations of

20 mg mL⁻¹ and 13 mg mL⁻¹, respectively. Suitable crystals were soaked briefly in crystallization solution supplemented with 20% glycerol and then flash-frozen immediately in a nitrogen stream before data collection. X-ray diffraction experiments were carried out at 100 K on the French Beamline for Investigation of Proteins–Beam Magnet 30A (FIP-BM30A) at the European Synchrotron Radiation Facility, Grenoble, France. The data sets at 1.80 and 1.50 Å for TRXo1 and TRXo2, respectively, were indexed and processed using XDS [39], and scaled and merged with Aimless from the CCP4 program package [40]. The initial protein model of TRXo2 was built in ARP/wARP [41]. The crystal structure of TRXo1 was solved by molecular replacement with the CCP4 suite program (MOLREP) [42], using the structure of TRXo2 as a search model. Structures were refined (Table 1) with phenix.refine implemented in the PHENIX package [43], with visual inspection and manual correction in Coot [44]. Structures of TRXo1 and TRXo2 were refined to a crystallographic R_{work} and R_{free} of 0.22/0.24 and 0.17/0.18, respectively, by using standard protocols, in which 5% of the reflections were used to continuously monitor the R_{free}. The refined structures maintained excellent geometry and showed no outlier in Ramachandran plots. The validation of the crystal structures was performed with MolProbity [45].

Table 1. Data collection and refinement statistics.

Data Collection	AtTRXo1	AtTRXo2
Beam line	FIP-BM30A	
Space group	P2 ₁ 2 ₁ 2 ₁	P6 ₅
Cell dimensions		
a, b, c (Å)	37.15; 39.24; 79.34	70.81; 70.81; 35.75
α, β, γ (°)	α = β = γ = 90°	α = β = 90° γ = 120°
Resolution (Å)	39.67–1.80 (1.84–1.80)	35.40–1.50 (1.53–1.50)
R _{merge}	0.122 (0.242)	0.070 (0.432)
R _{meas}	0.131 (0.283)	0.075 (0.500)
R _{pim}	0.049 (0.145)	0.028 (0.251)
No. unique reflections	11,316 (653)	16,473 (814)
Mean I/σI	13.1 (3.7)	20.0 (3.1)
CC _{1/2}	0.996 (0.961)	0.997 (0.942)
Completeness (%)	100.0 (100.0)	99.4 (100.0)
Average redundancy	11.4 (7.0)	12.0 (7.3)
<i>Refinement</i>		
Resolution (Å)	39.67–1.80	35.40–1.50
R _{free} /R _{work}	23.96/21.96	17.93/16.74
Total number of atoms	1848	1882
Water	130	92
Crystallographic B-factor		
Overall B-factor (Å ²)	29.16	35.36
B-factor: molecule (Å ²)	28.88	35.35
B-factor: water (Å ²)	32.89	35.47
<i>R.m.s deviations</i>		
Bonds	0.002	0.003
Angles	0.474	0.528
<i>MolProbity analysis</i>		
Clashscore, all atoms	2.91 (99%)	0.00 (100%)
MolProbity score	1.40 (96%)	0.50 (100%)
Protein Data Bank entry	6G61	6G62

Values in parentheses refer to data in the highest-resolution shell. AtTRXo: *Arabidopsis thaliana* thioredoxin-o; FIP-BM30A: French beamline for Investigation of Proteins-Bending Magnet section.

3. Results

3.1. *Arabidopsis thaliana* TRXo Isoforms Exist in Two Forms upon Expression in *E. coli*

To characterize the structure–function relationship of TRXo1 and TRXo2, the mature forms of these proteins were expressed in *E. coli* as untagged and His-tagged recombinant proteins by removing respectively 82 and 47 residues at the N-terminus constituting their putative mitochondrial targeting sequence. As observed for several related proteins of the GRX family [37,46], lysed bacterial cells exhibited a slight but visible brownish color typical of the presence of an Fe-S cluster. After purification in aerobic conditions, His-tagged recombinant proteins purified in one step displayed a residual brownish color unlike untagged versions (data not shown). The reason was obviously associated to the oxygen lability of the cluster and to the length of the purification procedure. These observations prompted us to purify both His-tagged TRXs in anaerobic conditions to avoid chromophore degradation. TRXo2 exhibited an UV-vis absorption spectrum comprising a broad shoulder centered at around 400 nm and a band at around 300 nm that prolonged the polypeptide absorption band at 280 nm (Figure 1A). This spectrum is usually typical of the presence of a [4Fe-4S] cluster [47,48]. Analytical gel filtration analyses demonstrated that TRXo2 (theoretical molecular mass of ca 14.5 kDa) separated into two peaks, a major one with an estimated molecular mass of 12.9 kDa and a minor one of 27.7 kDa suggesting that the purified protein solution contained both monomeric and dimeric forms (Figure 1B). Furthermore, the Fe-S cluster, detected by the absorbance at 420 nm, was only associated with the dimeric form (Figure 1B). Using a similar protocol, TRXo1 displayed a nearly identical UV-vis absorption spectrum, albeit absorption bands in the visible region were much less intense (Figure 1C). Moreover, TRXo1 (theoretical mass of ca 14.6 kDa) also separated into two peaks when analyzed by analytical gel filtration, a major one with an estimated molecular mass of 12.9 kDa and a minor one of 24.8 kDa which corresponded to a apomonomer and a holodimer form, respectively (Figure 1D). Altogether, these results indicate that both TRXo isoforms incorporate an Fe-S cluster after heterologous expression in *E. coli*. Despite these similarities, it seems that the Fe-S cluster in TRXo1 is either less-well matured by the *E. coli* Fe-S cluster assembly machineries or more oxygen-labile as cell lysis is performed in the presence of oxygen.

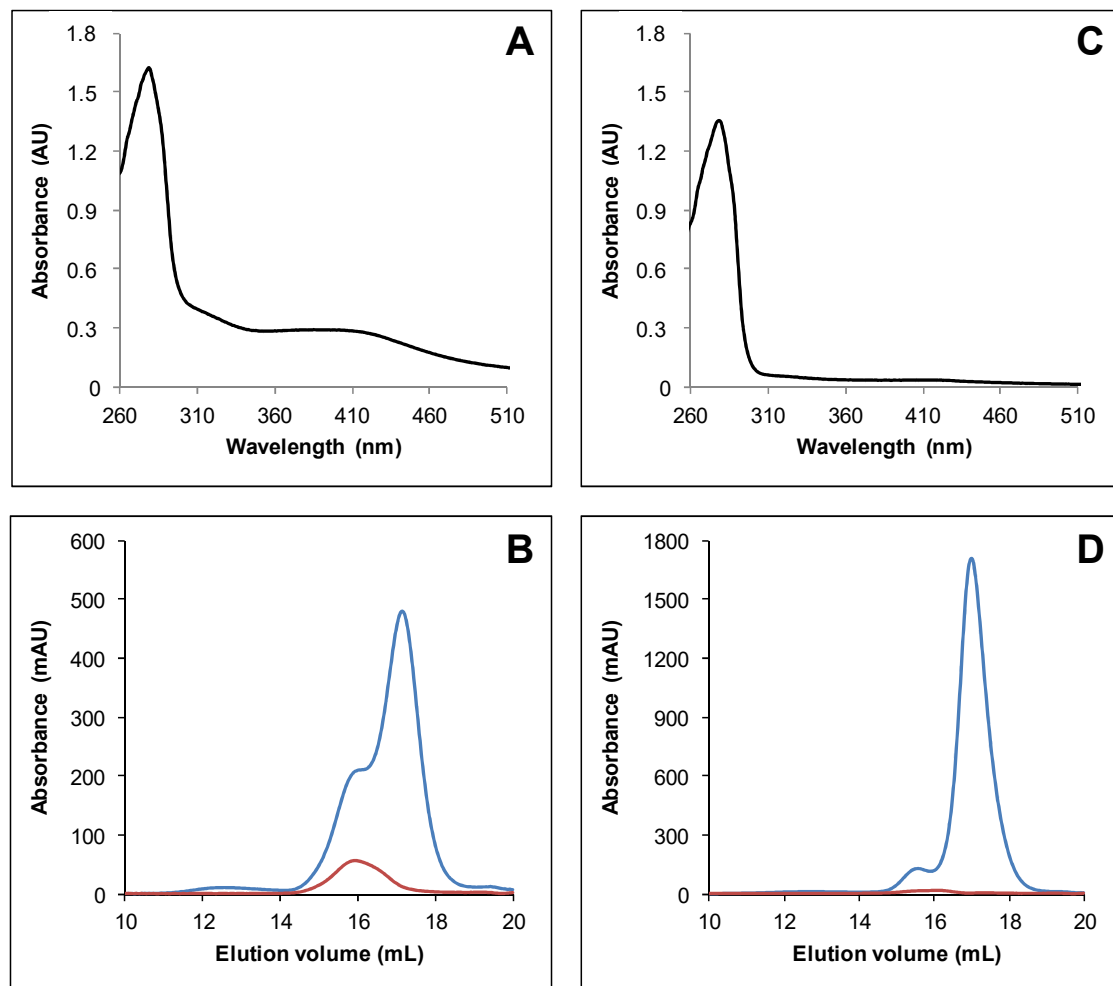


Figure 1. *Arabidopsis TRXo (thioredoxin-*o*) isoforms incorporate an Fe-S cluster after heterologous expression in *E. coli*. UV-visible absorption spectra of His-tagged recombinant TRXo2 (**A**) and TRXo1 (**C**). Spectra were recorded after an anaerobic purification in 30 mM Tris-HCl pH 8.0. Analytical gel filtration of His-tagged recombinant TRXo2 (**B**) and TRXo1 (**D**), purified in anaerobic conditions, was performed by loading 100 to 300 μ g of protein onto a Superdex S200 10/300 column. The presence of the polypeptide and of the Fe-S cluster have been detected by the absorbance at 280 nm (blue line) and 420 nm (red line), respectively.*

3.2. *IscS*-Mediated In Vitro Fe-S Cluster Reconstitution in *Arabidopsis* TRXo Isoforms

As purified recombinant *Arabidopsis* TRXo isoforms existed predominantly under apoforms, we sought to prepare samples by performing in vitro enzymatic Fe-S cluster reconstitution experiments in the presence of the *E. coli* cysteine desulfurase *IscS*. Untagged apo-TRXo1 and TRXo2 (Figure S1) were incubated anaerobically with an excess of L-cysteine and ferrous ammonium sulfate, and a catalytic amount of *IscS* for 1 h. Both reconstituted TRXo1 and TRXo2 exhibited an UV-visible absorption spectrum (Figure 2A,B) similar to the one observed for as-purified proteins but with more intense absorption bands around 300 and 400 nm relative to the one at 280 nm. Analytical gel filtration analyses demonstrated that both TRXo1 and TRXo2 still separated into two peaks, one with an estimated molecular mass of 25 kDa and another one of 12.9 kDa (Figure 2C,D). The smaller peak around 14 mL corresponds to *IscS* protein as deduced from the comparison with the analytical gel filtration performed with an *IscS* concentration similar to the one used for reconstitution (Figure S2). Although the peak containing the dimeric TRX holoforms was more prominent, monomeric forms were still present in the reconstituted samples. The presence of an absorbance at 420 nm associated with the monomeric TRXo1 may be due to the fact that thiol groups of DTT present in the reconstitution

mixture served as ligands. These results indicated that IscS-mediated in vitro reconstitution increased the content of Fe-S clusters in both TRXo isoforms but we could not find conditions to get fully-repleted Fe-S cluster-loaded forms that would allow an accurate analytical titration of Fe and labile sulfide contents. A rough evaluation of the Fe-S cluster content in TRXs o was performed from the absorption band at 410 nm by comparison with data obtained with a fully replete ferredoxin-thioredoxin reductase (FTR) an enzyme, which also contains a [4Fe-4S] center. Indeed, the UV-visible absorption spectra of FTRs purified from different organisms consistently exhibited an A_{410}/A_{280} ratio of 0.42 and molar extinction coefficient values at 410 nm of 17,400 and $15,000 \text{ M}^{-1} \text{ cm}^{-1}$ were determined for spinach and corn FTRs [49]. From the comparable A_{410}/A_{280} ratio in the UV-visible absorption spectra of TRXs o and FTR and an averaged molar extinction coefficient value at 410 nm of $16,000 \text{ M}^{-1} \text{ cm}^{-1}$ as determined for FTRs, we could deduce that there is ca $30 \mu\text{M}$ of Fe-S cluster in each TRX o sample formed by a mixture of monomer and dimer. On the other hand, using the theoretical molar extinction coefficients at 280 nm, we estimated that TRX o samples contained approximately $85\text{--}90 \mu\text{M}$ TRXo monomers (Figure 2A,B). Hence, considering that the Fe-S cluster is bridged into TRX o dimers, we concluded that about two-thirds of the proteins are replete with an Fe-S cluster.

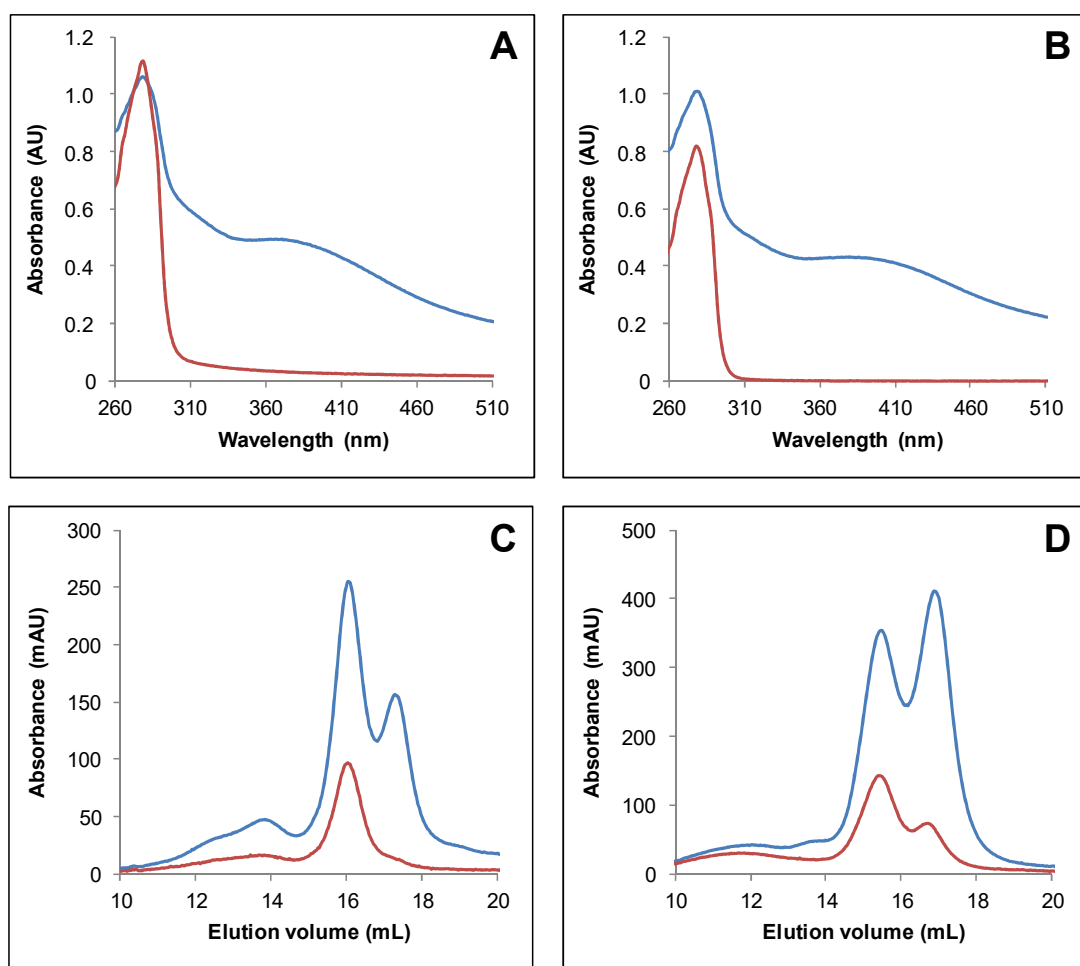


Figure 2. IscS-mediated in vitro Fe-S cluster reconstitution of Arabidopsis TRXo isoforms. UV-visible absorption spectra of TRXo2 (A) and TRXo1 (C) before (red line) and after (blue line) an anaerobic reconstitution performed in the presence of IscS in Tris NaCl buffer. Analytical gel filtration of reconstituted TRXo2 (B) and TRXo1 (D) was performed by loading 100 to 300 μg of protein (including 10 μM of EclscS) onto a Superdex S200 10/300 column. The presence of the polypeptide and of the Fe-S cluster have been detected by the absorbance at 280 nm (blue line) and 420 nm (red line), respectively.

3.3. Both Active Site Cysteines of TRXo2 Are Required for Fe-S Cluster Incorporation

The existence of Fe-S cluster-bridged TRX isoforms were previously observed for the atypical TRX isoform (IsTRP) from the human pathogen *Echinococcus granulosus* [50], and *E. coli* TrxA variants with CACC and CACA active site motifs [51]. The cysteines of the active site signature of IsTRP proved to be essential for cluster binding. Among potential Fe-S cluster ligands, both TRXs o have in common the two active site cysteines but no extra cysteine. To investigate the role of these cysteines for Fe-S cluster ligation, His-tagged C37S and C40S variants of TRXo2 were purified under anaerobiosis. Unlike TRXo2, no coloration was visible on as-purified TRXo2 C37S and C40S variants and accordingly no other absorption band than the one centered at 280 nm was detected on their UV-vis absorption spectra (Figure 3A). Analytical gel filtration experiments revealed that the TRXo2 C37S variant separated as a single peak with an apparent molecular mass of 12.2 kDa likely corresponding to an apomonomer, whereas a small additional peak (15.8 mL, 24.9 kDa) was observed for the TRXo2 C40S variant, which likely contained a covalent dimeric form with Cys³⁷ of two monomers forming an intermolecular disulfide (Figure 3B,C). Altogether these results suggest that the substitution of Cys³⁷ and Cys⁴⁰ hampered Fe-S cluster incorporation in TRXo2 underlying that both cysteines are required for Fe-S cluster binding.

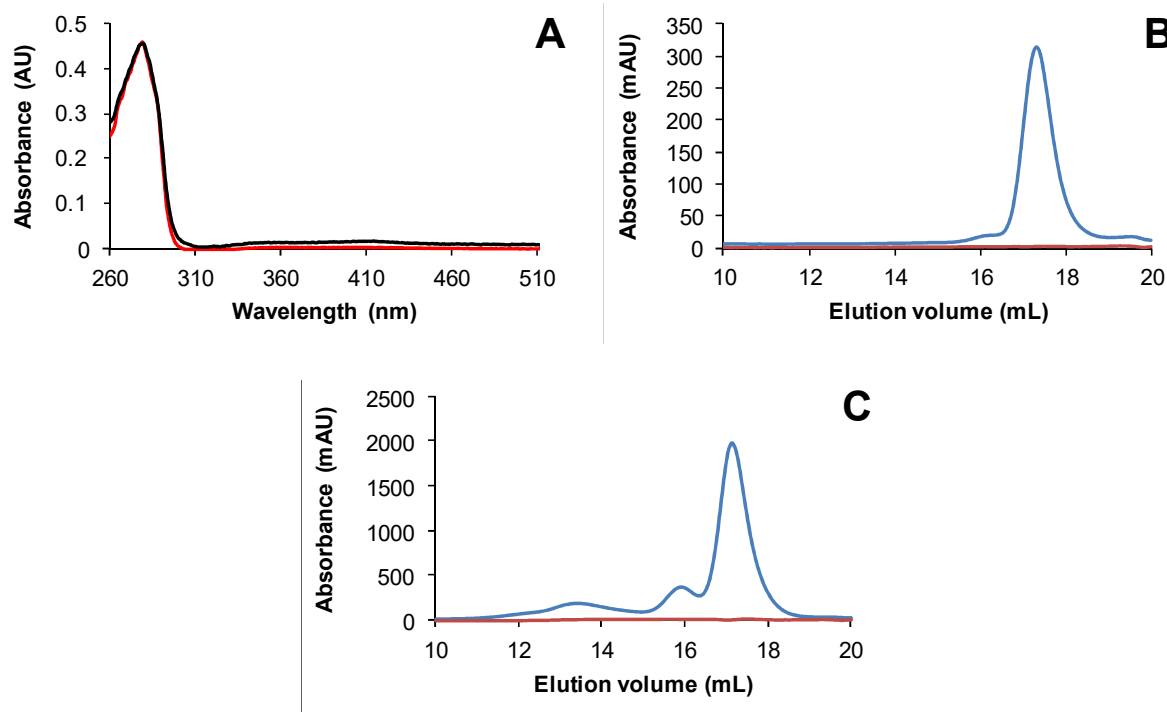


Figure 3. Monocysteinic variants of *Arabidopsis* TRXo2 isoform are mostly apo-monomers. UV-visible absorption spectra of His-tagged recombinant TRXo2 C37S (red line) and C40S (black line) (A) recorded after an anaerobic purification in 30 mM Tris-HCl pH 8.0. Analytical gel filtration of His-tagged recombinant TRXo2 C37S (B) and C40S (C) purified in anaerobic conditions, was performed by loading 100 to 300 µg of protein onto a Superdex S200 10/300 column. The presence of the polypeptide and of the Fe-S cluster have been detected by the absorbance at 280 nm (blue line) and 420 nm (red line), respectively.

3.4. TRXo1 and TRXo2 Possess the Structural Properties of TRX Family Members

To definitely confirm the identity of the Fe-S cluster ligands and decipher the other structural features of TRXo isoforms for which there is no known 3D structure solved so far, we tried to crystallize under nitrogen atmosphere both TRXo1 and TRXo2 holoforms. Crystals have been obtained for both proteins but it turned out that they were not colored and contained only apoforms. TRXo1 crystallized in the orthorhombic space group $P2_12_12_1$ whereas TRXo2 crystallized in the hexagonal system and belonged to space group $P6_5$. Well-diffracting crystals of TRXo1 and TRXo2 were obtained with one molecule per asymmetric unit (a.s.u) with Matthews's coefficient (V_m) values of $2.3 \text{ \AA}^3 \text{ Da}^{-1}$ and $2.0 \text{ \AA}^3 \text{ Da}^{-1}$ corresponding to solvent contents of 46% and 40%, respectively. Their structures were determined by molecular replacement at high resolution of 1.80 and 1.50 Å, respectively. In both protein structures, almost all residues were well defined in the electron density map, except the first two residues (Met¹ and Glu²) of TRXo1, which were disordered (amino acid numbering refers to the mature protein without its mitochondrial presequence).

Both proteins adopt the overall TRX fold ($\beta\alpha\beta\alpha\beta\alpha\beta\beta\alpha$) with all regular secondary structure elements preserved and consisting of a central core with a twisted five-stranded β -sheet in which $\beta 4$ is antiparallel to the others (Figure 4A,B). This β -sheet is capped on one side by $\alpha 1$ and $\alpha 3$ helices and on the other side by $\alpha 2$ and $\alpha 4$ helices (Figure 4B). All secondary structures of these proteins (TRXo1 numbering) are $\beta 1$ (Val⁵-Val⁸), $\alpha 1$ (Ser¹⁰-Gln²²), $\beta 2$ (Ser²⁸-Thr³³), $\alpha 2$ (Gly³⁸-Tyr⁵⁴), $\beta 3$ (Thr⁵⁸-Asp⁶³), $\alpha 3$ (Gly⁶⁸-Leu⁷⁶), $\beta 4$ (Thr⁸³-Lys⁸⁸), $\beta 5$ (Ser⁹¹-Val⁹⁷), and $\alpha 4$ (Asp¹⁰⁰-Lys¹¹³). TRXs generally contain a buried Asp³¹ near Cys⁴⁰ residue, which is replaced by Tyr³¹ in *Arabidopsis* TRXo isoforms as in *Anabaena* Trx2 [52]. The position of the sidechain hydroxyl of Tyr³¹ corresponds very closely to a water-mediated hydrogen bonding between the classical Asp and the Cys⁴⁰ Sγ. In TRXo1 and TRXo2 X-ray structures, the distance between the sidechain hydroxyl of the Tyr³¹ and the Cys⁴⁰ Sγ atom are 3.76 and 5.51 Å, respectively, too far away for an interaction.

The Cys³⁷ and Cys⁴⁰ residues are found at the end of the $\alpha 2$ -helix, the Cys⁴⁰ residue being buried compared to Cys³⁷. Close examination of the resultant Fo-Fc electron density maps revealed a negative density between Cys³⁷ and Cys⁴⁰ in TRXo2, and additional positive density in the opposite sides of Sγ atoms. Refinements, using PHENIX and Coot in an iterative manner, indicated that this effect is an artifact of data collection (radiation damage), due to partial reduction of the disulfide bond by the X-ray beam during data collection. The distances between Cys³⁷ and Cys⁴⁰ Sγ atoms are 2.03 and 2.05 Å in TRXo1 and TRXo2, respectively. They represent the typical length of disulfide bonds, suggesting that both TRXo isoforms were crystallized in an oxidized form. Hence, we modeled all the cysteine pairs as forming intramolecular disulfide bonds (Figure 4C).

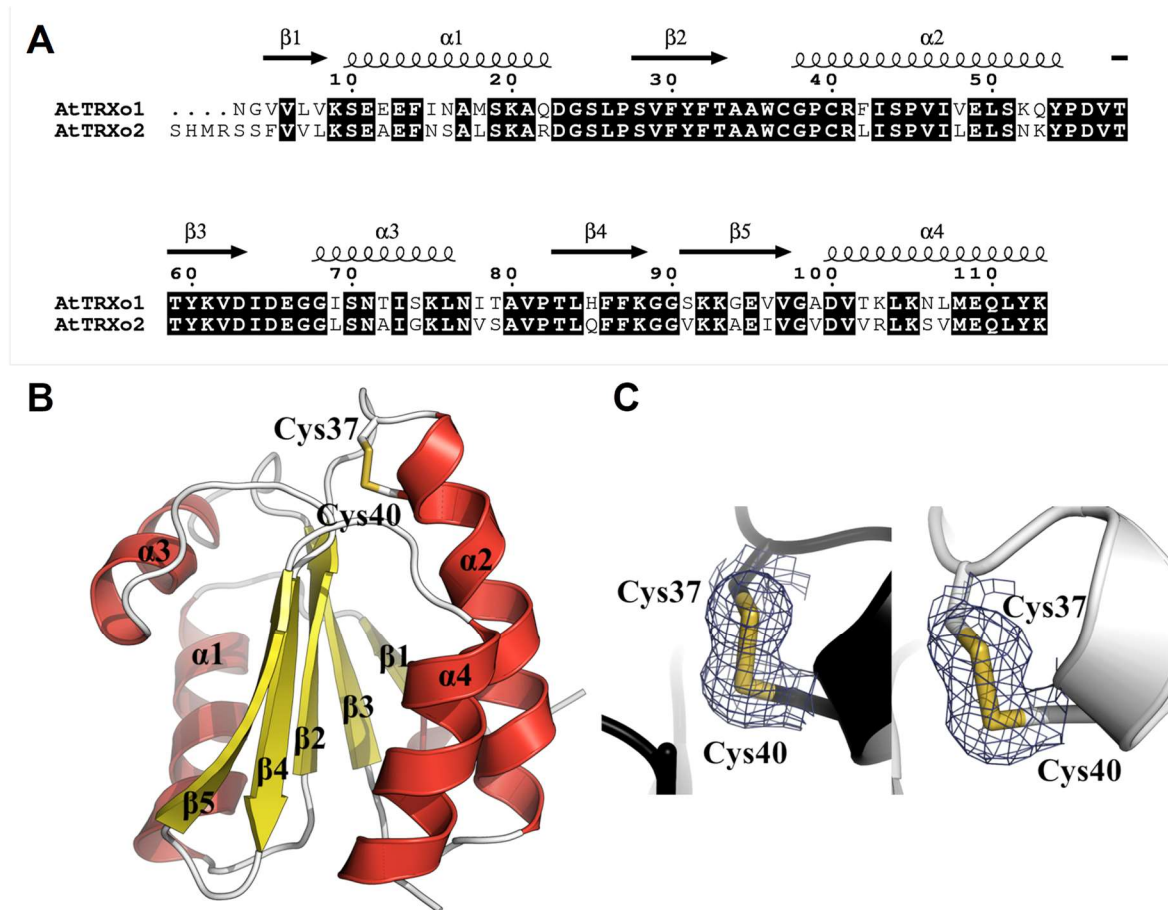


Figure 4. Three-dimensional structure and sequence conservation of oxidized Arabidopsis TRXo isoforms. (A) Structure-based sequence alignment of Arabidopsis TRXo isoforms. Conserved residues are highlighted in black. (B) Three-dimensional structure of AtTRXo2 at 1.50 Å resolution. The X-ray structure of AtTRXo2 is shown as a ribbon representation with helices in red and strands in yellow. In addition, the side chains of Cys³⁷ and Cys⁴⁰ residues are shown as sticks. (C) Electron density around the Cys³⁷-Cys⁴⁰ disulfide bond. The maps shown are σA-weighted $2mF_o-DF_c$ maps contoured at 1.2σ (0.07 and 0.38 e/Å³ for AtTRXo1 and AtTRXo2, respectively). AtTRXo1 and AtTRXo2 are colored in white and black, respectively.

3.5. TRXo1 and TRXo2 Structures Are Not Strictly Superimposable

TRXo1 and TRXo2 share high levels of sequence identity and similarity (74% and 97%, respectively) (Figure 4A) and their crystal structures are quite similar and overlay well (RMSD of 0.9 Å) (Figure 5A). Nevertheless, a fine comparison of both structures revealed two regions presenting significant structural differences. The first area corresponds to the active site loop, which protrudes on one side of the molecule to the N-terminus of α2-helix (Figure 5A). The region containing Trp³⁶-Phe⁴² residues including the WCGPC signature in TRXo1 has a different conformation to that in TRXo2 and is shifted by approximately 1.9 Å. Trp³⁶ and Arg⁴¹ residues are involved in contacts with symmetric molecules through hydrogen bond stabilization. In both proteins, the carbonyl oxygen of Trp³⁶ forms a hydrogen bond with the Nζ atom of Lys¹⁰⁵ (2.81 Å in TRXo1 and 3.15 Å in TRXo2). The NH1 guanidinium nitrogen of Arg⁴¹ is hydrogen-bonded to the carbonyl oxygen of Ser⁷⁴ (2.85 Å) in TRXo1 and to the carbonyl oxygen of Ala¹² (3.50 Å) in TRXo2. This regional difference around the active site is near crystal contacts and may be attributable to different crystal packing interactions. On another note, the fully refined TRXo1 structure contains 130 water molecules whereas the TRXo2 structure includes 92 water molecules, of which 51 have equivalent positions in TRXo1. Despite the high degree of conservation of both primary and tertiary structures between TRXo1 and TRXo2, only 39% and

55% of the water molecule positions are conserved indicating probable differences in the charge state distribution. Even though TRXo1 was crystallized at pH 7.5 whereas TRXo2 was crystallized at pH 5.6, which may explain differences in the solvation shell, TRXo2 would be more positively charged than TRXo1 in a pH range between 5 and 10 (Figure 5B). With a pH value of 8.1 ± 0.2 for the mitochondrial matrix of *A. thaliana* [53], the global charge of TRXo1 and TRXo2 in vivo should be quite different with values of -1 and $+2$, respectively. The differences in the distribution of the electrostatic potential on the TRXo1 and TRXo2 surfaces at pH 8.1 are however not located in the area surrounding the active site (Figure 5C). The second divergent area involves Gly⁶⁸-Thr⁷⁹ residues (Figure 5A) with an RMSD of 2.6 Å. This area surrounds the α 3-helix upstream of the conserved *cis*-Pro⁸² residue, which is located at the N-terminus of β 4-strand. The increase of the crystallographic B-factor along the amino acid chain for TRXo1 (65.33 \AA^2) and TRXo2 (68.91 \AA^2) (Figure 5D), indicates that this part is flexible. Altogether, this may hint to a capacity of TRXo isoforms to interact with different partner proteins.

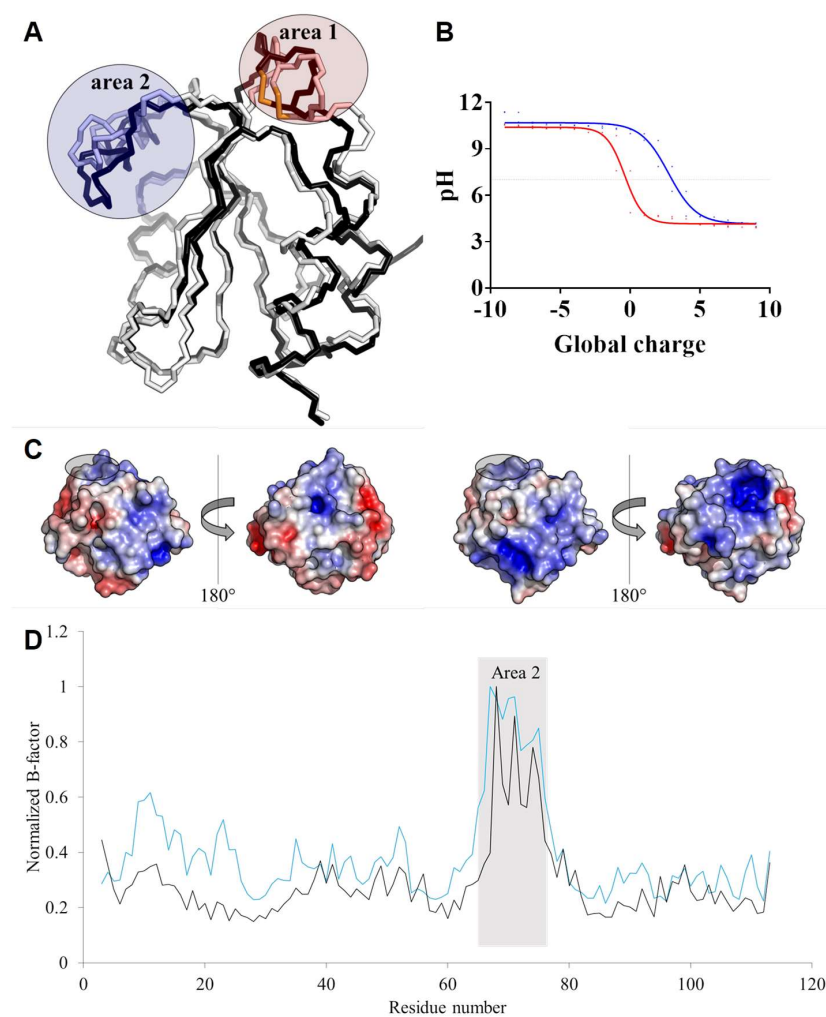


Figure 5. Structural features *vs.* charge and crystallographic B-factor distribution. (A) Structure superposition of the backbone trace of Arabidopsis TRXo isoforms. AtTRXo1 and AtTRXo2 are colored in white and black, respectively. The two divergent areas are circled in red and blue, respectively. (B) Global protein charge of AtTRXo1 (red) and AtTRXo2 (blue) as a function of pH as indicated by the PDB2PQR Server [54]. The dot line corresponds to pH 7.0. (C) Electrostatic potential mapped onto AtTRXo1 (left) and AtTRXo2 (right) structures at pH 8.1. The WCGPC signature residues are circled in black. (D) Flexibility of AtTRXo1 (black) and AtTRXo2 (blue) related to the crystallographic B-factor.

3.6. Oxidized NFU4 and NFU5 Are Reduced by TRXo Isoforms but Not by GRXS15

With the aim of confirming novel TRXo partners, we examined the 101 putative TRXo1 partners identified in a previous proteomic analysis performed by affinity chromatography using a TRXo1 C40S variant and mitochondrial protein extracts [22]. The DTT-dependent elution of these proteins suggests that these TRX partners were trapped because they existed under oxidized forms, which led to the formation of mixed-disulfide intermediates with the TRXo1 variant. Among these proteins, we focused our attention on two proteins, NFU4 and NFU5, involved in the late steps of the maturation of Fe-S proteins and acting as Fe-S cluster transfer proteins. These proteins possess a CxxC motif, the cysteines of which being responsible of the transient ligation of the Fe-S cluster. Thus, they have to be reduced to receive the Fe-S cluster from other maturation factors.

The mature forms of both NFU proteins have been expressed in *E. coli* and purified aerobically. As expected, signs for the presence of an Fe-S cluster were initially visible, but both NFU4 and NFU5 were found as apoproteins at the end of the purification. They have three cysteines including those of the CxxC motif. To determine their oxidation state, mass spectrometry analyses were performed with NFU4 and NFU5 either untreated or reduced by a DTT excess and dialyzed (Figures S3 and S4). A single species was obtained for both untreated proteins but it presented a mass decrease of ca 131 Da compared to their theoretical molecular masses (Table 2). This difference corresponds undoubtedly to the cleavage of the first methionine as expected from the presence of an alanine at the second position. An increase of around 2 Da in the molecular masses of reduced proteins likely corresponded to the gain of two protons indicating the existence of an intramolecular disulfide bond in as-purified proteins (Table 2).

Table 2. Electrospray ionization mass spectrometry analysis of untreated and reduced NFU proteins

Protein	Theoretical Size (Da)	Theoretical Size without Met (Da)	Untreated	Treated with DTT	Mass Difference upon Reduction (Da)
NFU4	22,167.9	22,036.7	22,035.1	22,037.4	+2.3
NFU5	21,823.5	21,692.3	21,690.9	21,693.0	+2.1

The mass accuracy is generally ± 0.5 Da.

To examine the ability of the various reducing systems found in mitochondria to reduce oxidized NFU proteins, untreated NFU4 and NFU5 were incubated with TRX or GSH/GRX reducing systems. Subsequent alkylation of thiol groups with 2 kDa mPEG maleimide and separation on non-reducing SDS-PAGE allowed visualizing the redox state of the proteins (Figure 6). After 15 min reaction, the NADPH/GR/GSH system was clearly unable to reduce oxidized NFU proteins and adding the sole mitochondrial GRX, GRXS15, did not improve the reduction. On the contrary, in the presence of NADPH and NTR, both TRXo isoforms reduced completely oxidized NFU proteins when added at equimolar concentrations (Figure 6). Adding more catalytic amounts of TRXs o by decreasing the relative concentrations of TRXs o vs. NFUs to 1:10 still allowed an efficient reduction of both NFUs, although this was not complete (Figure S5). In the presence of a NADPH/NTR regeneration system, GRXS15 was still not able to reduce oxidized NFUs (Figure S5). These *in vitro* data indicated that the reduction of oxidized mitochondrial NFU isoforms, would this oxidation occur under specific physiological conditions, would depend on the TRX system but not on GSH/GRX or NTR/GRX systems. No difference between both TRXs o was visible using this assay.

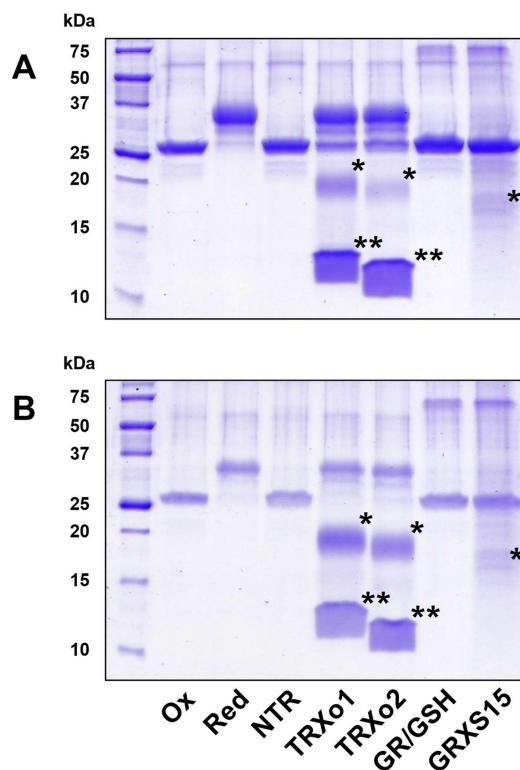


Figure 6. The disulfide bridge of mitochondrial NFUs (nitrogen-fixation-subunit-Us) is reduced by TRXs o but not GRXS15. The reduction of as-purified, oxidized forms of NFU4 (A) or NFU5 (B) was assessed after a 15 min incubation in the presence of the following reducing systems: NTR: NADPH + NTR; TRXo1: NADPH + NTR + TRXo1; TRXo2: NADPH + NTR + TRXo2; GR/GSH: NADPH + GR + GSH ; GRXS15: NADPH + GR + GSH + GRXS15. After alkylation with 2 kDa mPEG maleimide, proteins were separated on non-reducing SDS-PAGE (sodium dodecyl sulfate polyacrylamide gel electrophoresis). Reduced (Red) and oxidized (Ox) proteins served as controls. The stars indicate the alkylated (*) and non-alkylated (**) forms of the oxidoreductases in the respective regeneration systems when visible.

4. Discussion and Conclusions

Compared to plastidial TRX isoforms, the molecular and physiological roles of mitochondrial TRXo isoforms are uncertain although numerous mitochondrial proteins are known or assumed to undergo reversible redox post-translational modifications and a hundred of putative TRXo1 partners have been identified [22]. In *A. thaliana*, TRXo1 is the major TRXo isoform but *A. thaliana* *trxo1* and *trxo2* single and double mutants have no pronounced phenotype [25,26]. Because previous studies did not provide information about the redundancy or specificity of these isoforms, we have decided to investigate the biochemical and structural properties of both proteins. Given that TRXo1 and TRXo2 have been previously purified as recombinant proteins [22], and possess the regular WCGPC signature found in many TRXs, it was completely unexpected that both recombinant proteins formed homodimers bridging a [4Fe-4S] cluster using cysteines of the active site signature either upon expression in *E. coli* or upon in vitro Fe-S cluster reconstitution experiments. To our knowledge, this is the first report that a non-modified TRX incorporates a [4Fe-4S] cluster. Up to now, only a few reports pointed to the capacity of proteins of the TRX superfamily to bind an Fe-S cluster but never a [4Fe-4S] cluster in regular TRXs. A thioredoxin-related protein from the human pathogen *Echinococcus granulosus*, IsTRP, was shown to bind a [2Fe-2S] cluster using cysteines present in an atypical active site signature (NCFAC) [50]. Two atypical PDI-A isoforms from poplar and *Arabidopsis*, formed by a single domain and possessing a WCKHC signature, are able to bind a [2Fe-2S] cluster into a homodimer using the cysteines present in this active site signature [55,56]. Several glutaredoxins can

bind a [2Fe-2S] cluster into homodimers using the first cysteine of the CxxC/S signature and the thiol group of two glutathione molecules [37,46,57–59]. Interestingly, *S. cerevisiae* GRX5 also binds a [4Fe-4S] cluster in the absence of glutathione, using a cysteine present in the C-terminal part [48].

Besides these naturally-existing isoforms, several variants of *E. coli* or human TRX1 were shown to bind various types of Fe-S cluster. By introducing two mutations, W28C and I75C, a mononuclear [FeS4] cluster can be incorporated in *E. coli* Trx1 both in vitro and in vivo using also the two active site cysteines, Cys³² and Cys³⁵ [60]. By searching proteins that could restore disulfide bond formation when exported to the periplasm of strains lacking the entire periplasmic oxidative pathway, two *E. coli* Trx1 variants with CACC and CACA active site motifs were shown to form Fe-S cluster-bridged homodimers with the cysteines forming the CxC motif being essential for cluster ligation [51]. The structure of an apo Trx1 CACA variant, where the cysteines thought to serve as ligands of the Fe-S cluster are engaged in two intermolecular disulfide bonds, has been solved [61]. It seems that the exposure of the second active site cysteine, generally buried in TRXs, caused by the unraveling of α 2 helix may be sufficient to enable Fe-S cluster binding. Whether a similar change occurs in the structures of TRXo is unknown. Last but not least, a [4Fe-4S] cluster can be assembled into the hydrophobic core of a monomeric *E. coli* Trx1 [62]. The polypeptide contained several substitutions for introducing the Fe-S cluster binding residues (L24C, L42C, V55C, and L99C) and removing the two catalytic cysteines. The incorporation was achieved into a fully reduced, partially unfolded protein (2 M urea treatment) from a synthetic, preformed tetranuclear Fe-S cluster. In other words, it required drastic changes and conditions. Very interestingly, in human TRX1, which possesses a regular WCGPC signature, the simple mutation of the *cis*-Pro (P75S/T/A) found in the active site of most TRX superfamily members is sufficient to allow incorporation of a [2Fe-2S] cluster into homodimers [63]. Among the five cysteines present in human TRX1, it seems that Cys³² and the specific Cys⁷³ are important for iron atom binding. Introducing a glutaredoxin active site (CSYC) into human TRX1, without substituting the *cis*-Pro, allowed Fe-S cluster incorporation. Hence, all these mutagenesis studies performed using *E. coli* Trx1 and human TRX1 suggested that the combination of a WCGPC active site motif and a *cis*-Pro prevented the active site cysteines from binding an Fe-S cluster. However, both Arabidopsis TRXs o have these two features and the capacity to bind an Fe-S cluster indicating that other factors come into play. In order to understand the structural factors that favor Fe-S cluster incorporation into TRXs o, we sought to solve their structures but could only get information on the apoforms so far.

Although both TRXs o display globally similar structures, interesting observations have been made when the 28 residues varying between Arabidopsis TRXo isoforms were mapped onto AtTRXo1 X-ray structure. These non-conserved residues are solvent exposed and outside the highly conserved area (Figure 7A) comprising the WCGPC active site motif and residues that surround it. However, half of these non-conserved residues is potentially involved in protein–protein interactions (Figure 7B) as determined by a comparison with already characterized complexes involving thioredoxin homologs. These 14 non-conserved residues are mainly located on the same face of the protein (comprising α 3-helix, the loop between α 3 and β 4, β 5-strand, and α 4-helix) with marked differences in the surface charge distribution (Figure 5C, left panels). The fact that (i) this region is involved in the interaction between TRXs and other proteins [64], (ii) that at mitochondrial pH, TRXo1 (calculated pI of 6.22) would be negatively charged whereas TRXo2 (calculated pI of 10.12) would be positively charged and (iii) that interactions between TRX and their partners are mostly electrostatic could point to a distinct ability of both TRXs o to interact with their partners. However, whether TRXo2 could have specific partners is unknown as only TRXo1 was used to isolate putative partners so far and both isoforms have not been systematically tested with the same proteins. Using the two identified mitochondrial Fe-S cluster maturation factors, NFU4 and NFU5, we could not demonstrate a difference between TRXo1 and TRXo2, both being able to efficiently reduce the intramolecular disulfide formed on NFUs, unlike GRXS15. However, regardless whether a specificity exists, the fact that several ISC factors (NFS1, ISCA4, ISU1) involved in the maturation of Fe-S proteins in mitochondria were identified as putative partners of TRXo1 [22], raises the question of whether TRXo isoforms are involved in the reduction of

these proteins in specific conditions where they can become oxidized. Indeed, most proteins involved in the maturation of Fe-S proteins, including NFU4 and NFU5, possess critical cysteine residues that have to be under a reduced state to bind their Fe-S cluster. Interestingly, the recent work that aimed at isolating TRX partners in *Chlamydomonas reinhardtii* identified several proteins belonging to the Fe-S cluster assembly machinery in chloroplasts (SUF machinery) such as NFU1/2/3, SUFB/C/D, and SUFS but also the mitochondrial NFS1 and several Fe-S proteins [65]. This may be fortuitous because these proteins have exposed and reactive cysteines when they do not bind Fe-S clusters but a control of their redox state by TRX isoforms might add a light-dependent regulation to the maturation of Fe-S proteins in chloroplasts. For instance, the reduction of an oxidized form of Arabidopsis GRXS16, a presumed SUF component, is achieved by the plastidial FTR/TRX system [66]. Hence, a TRX-dependent control of the redox state of proteins involved in Fe-S cluster biogenesis may be a unified picture among organelles and organisms.

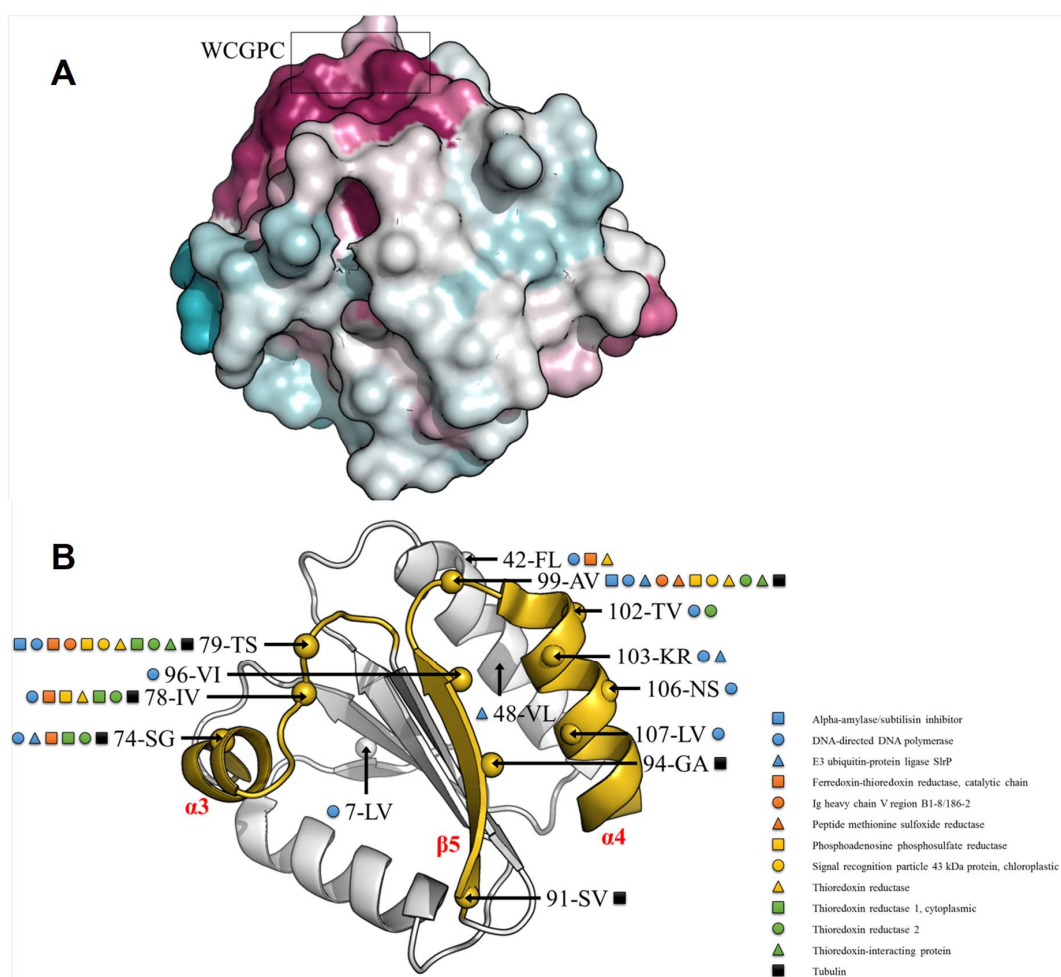


Figure 7. Thioredoxin interfacing residues. (A) Residue conservation among 500 thioredoxin orthologs of AtTRXo1 and AtTRXo2 using the ConSurf server [67] with the UniRef90 database (www.uniprot.org/uniref/). Residues are colored in white to purple, for least to most conserved residues. The conserved WCGPC motif is circled in black. (B) AtTRXo1 and AtTRXo2 sequences were blasted against the PDB to find protein–protein interactions involving thioredoxin homologs. 44 complexes were found using an E-Value Cutoff of 0.001. AtTRXo1 and AtTRXo2 non-conserved residues potentially involved in protein–protein interactions were mapped onto the X-ray structure of AtTRXo1. In each case the residue position, and the amino acids in one letter code for AtTRXo1 and AtTRXo2 are shown (ex: 78-IV; position 78, isoleucine and valine found in AtTRXo1 and AtTRXo2, respectively). The area comprising α_3 -helix, the loop between α_3 and β_4 , β_5 -strand, and α_4 -helix is colored in yellow.

In summary, this study might point to a connection between TRXo isoforms and the ISC assembly machinery. Although the *E. coli* ISC machinery seems able to perform the maturation of a [4Fe-4S] cluster on both Arabidopsis TRXs o, the maturation is not complete, even though these TRXs are expressed at moderate levels, at least comparable to some Fe-S proteins that are completely maturated. Evidence that the plant ISC system is also competent for this maturation and that an Fe-S cluster is present on these TRXs in a cellular context are now necessary to give more credence to a physiological role of holoforms of TRXs o. The capacity to interact with NFU4/5 and ISCA2 [22], which are the maturation factors responsible for the delivery and insertion of preformed [4Fe-4S] clusters into client proteins, is already a good indication. As the catalytic cysteines constitute the ligands of the Fe-S cluster, TRXo holoforms should not exhibit reductase activity, which was confirmed for IsTRP that is unable to reduce efficiently insulin [52]. Thus, as previously proposed for human Grx2 [68], the formation of an Fe-S cluster on TRXs o may be a convenient regulation mechanism of their reductase activity, at least for a certain pool of proteins. In the absence of a light control as for chloroplastic TRXs, having an inactive pool of labile Fe-S cluster-bridged TRXs may be a rapid and convenient way to adjust the redox metabolism during adverse conditions. In addition to other confirmed stress-responsive proteins—such as PRX IIF [7] and AOX [22]—targets that require TRXo reduction may include ISC maturation factors as NFU4/5.

Supplementary Materials: The following are available online at <http://www.mdpi.com/2076-3921/7/10/142/s1>, FigureS1: Purity of recombinant AtTRXo1 and AtTRXo2, Figure S2: Analytical gel filtration of *E. coli* IscS, Figure S3: Electrospray ionization mass spectrometry analysis of NFU4, Figure S4: Electrospray ionization mass spectrometry analysis of NFU5, Figure S5: The disulfide bridge of mitochondrial NFUs is reduced by NTR/TRXo system but not by NTR/GRXS15 system, Table S1: Primers used for cloning and site-directed mutagenesis experiments.

Author Contributions: Conceptualization, N.R. and J.C.; Investigation, F.Z., T.R., J.P.-T., and T.D.; Supervision, N.R. and J.C.; Writing—Original draft, F.Z. and T.R.; Writing—Review & Editing, N.R. and J.C.

Funding: This work was supported by a grant overseen by the French National Research Agency (ANR) as part of the "Investissements d'Avenir" program (ANR-11-LABX-0002-01, Lab of Excellence ARBRE).

Acknowledgments: Technical support from Fabien Lachaud of the "Service Commun de Spectrométrie de Masse et Chromatographie" of the Université de Lorraine is gratefully acknowledged.

Conflicts of Interest: The authors declare no conflict of interest.

References

1. Couturier, J.; Touraine, B.; Briat, J.F.; Gaymard, F.; Rouhier, N. The iron–sulfur cluster assembly machineries in plants: Current knowledge and open questions. *Front. Plant Sci.* **2013**, *4*, 259. [[CrossRef](#)] [[PubMed](#)]
2. Braymer, J.J.; Lill, R. Iron–sulfur cluster biogenesis and trafficking in mitochondria. *J. Biol. Chem.* **2017**, *292*, 12754–12763. [[CrossRef](#)] [[PubMed](#)]
3. Ciofi-Baffoni, S.; Nasta, V.; Banci, L. Protein networks in the maturation of human iron–sulfur proteins. *Metallomics* **2018**, *10*, 4972. [[CrossRef](#)] [[PubMed](#)]
4. Navrot, N.; Rouhier, N.; Gelhaye, E.; Jacquot, J.P. Reactive oxygen species generation and antioxidant systems in plant mitochondria. *Physiol. Plant.* **2007**, *129*, 185–195. [[CrossRef](#)]
5. Navrot, N.; Collin, V.; Gualberto, J.; Gelhaye, E.; Hirasawa, M.; Rey, P.; Knaff, D.B.; Issakidis, E.; Jacquot, J.P.; Rouhier, N. Plant glutathione peroxidases are functional peroxiredoxins distributed in several subcellular compartments and regulated during biotic and abiotic stresses. *Plant Physiol.* **2006**, *142*, 1364–1379. [[CrossRef](#)] [[PubMed](#)]
6. Gama, F.; Keech, O.; Eymery, F.; Finkemeier, I.; Gelhaye, E.; Gardeström, P.; Dietz, K.J.; Rey, P.; Jacquot, J.P.; Rouhier, N. The mitochondrial type II peroxiredoxin from poplar. *Physiol. Plant* **2007**, *129*, 196–206. [[CrossRef](#)]
7. Finkemeier, I.; Goodman, M.; Lamkemeyer, P.; Kandlbinder, A.; Sweetlove, L.J.; Dietz, K.J. The mitochondrial type II peroxiredoxin F is essential for redox homeostasis and root growth of *Arabidopsis thaliana* under stress. *J. Biol. Chem.* **2005**, *280*, 12168–12180. [[CrossRef](#)] [[PubMed](#)]
8. Barranco-Medina, S.; Krell, T.; Bernier-Villamor, L.; Sevilla, F.; Lázaro, J.J.; Dietz, K.J. Hexameric oligomerization of mitochondrial peroxiredoxin PrxIIF and formation of an ultrahigh affinity complex with its electron donor thioredoxin Trx-o. *J. Exp. Bot.* **2008**, *59*, 3259–3269. [[CrossRef](#)] [[PubMed](#)]

9. Couturier, J.; Jacquot, J.P.; Rouhier, N. Evolution and diversity of glutaredoxins in photosynthetic organisms. *Cell. Mol. Life Sci.* **2009**, *66*, 2539–2557. [CrossRef] [PubMed]
10. Chibani, K.; Wingsle, G.; Jacquot, J.P.; Gelhaye, E.; Rouhier, N. Comparative genomic study of the thioredoxin family in photosynthetic organisms with emphasis on *Populus trichocarpa*. *Mol. Plant* **2009**, *2*, 308–322. [CrossRef] [PubMed]
11. Plomion, C.; Aury, J.M.; Amselem, J.; Leroy, T.; Murat, F.; Duplessis, S.; Faye, S.; Francillonne, N.; Labadie, K.; Le Provost, G.; et al. Oak genome reveals facets of long lifespan. *Nat. Plants* **2018**, *1*. [CrossRef] [PubMed]
12. Moseler, A.; Aller, I.; Wagner, S.; Nietzel, T.; Przybyla-Toscano, J.; Mühlhoff, U.; Lill, R.; Berndt, C.; Rouhier, N.; Schwarzländer, M.; et al. The mitochondrial monothiol glutaredoxin S15 is essential for iron–sulfur protein maturation in *Arabidopsis thaliana*. *Proc. Natl. Acad. Sci. USA* **2015**, *112*, 13735–13740. [CrossRef] [PubMed]
13. Laloi, C.; Rayapuram, N.; Chartier, Y.; Grienberger, J.M.; Bonnard, G.; Meyer, Y. Identification and characterization of a mitochondrial thioredoxin system in plants. *Proc. Natl. Acad. Sci. USA* **2001**, *98*, 14144–14149. [CrossRef] [PubMed]
14. Gelhaye, E.; Rouhier, N.; Jacquot, J.P. The thioredoxin h system of higher plants. *Plant Physiol. Biochem.* **2004**, *42*, 265–271. [CrossRef] [PubMed]
15. Meng, L.; Wong, J.H.; Feldman, L.J.; Lemaux, P.G.; Buchanan, B.B. A membrane-associated thioredoxin required for plant growth moves from cell to cell, suggestive of a role in intercellular communication. *Proc. Natl. Acad. Sci. USA* **2010**, *107*, 3900–3905. [CrossRef] [PubMed]
16. Reichheld, J.P.; Meyer, E.; Khafif, M.; Bonnard, G.; Meyer, Y. AtNTRB is the major mitochondrial thioredoxin reductase in *Arabidopsis thaliana*. *FEBS Lett.* **2005**, *579*, 337–342. [CrossRef] [PubMed]
17. Begas, P.; Liedgens, L.; Moseler, A.; Meyer, A.J.; Deponte, M. Glutaredoxin catalysis requires two distinct glutathione interaction sites. *Nat. Commun.* **2017**, *8*, 14835. [CrossRef] [PubMed]
18. Ströher, E.; Grassl, J.; Carrie, C.; Fenske, R.; Whelan, J.; Millar, A.H. Glutaredoxin S15 Is Involved in Fe-S Cluster Transfer in Mitochondria Influencing Lipoic Acid-Dependent Enzymes, Plant Growth, and Arsenic Tolerance in *Arabidopsis*. *Plant Physiol.* **2016**, *170*, 1284–1299. [CrossRef] [PubMed]
19. Bedhomme, M.; Adamo, M.; Marchand, C.H.; Couturier, J.; Rouhier, N.; Lemaire, S.D.; Zaffagnini, M.; Trost, P. Glutathionylation of cytosolic glyceraldehyde-3-phosphate dehydrogenase from the model plant *Arabidopsis thaliana* is reversed by both glutaredoxins and thioredoxins in vitro. *Biochem. J.* **2012**, *445*, 337–347. [CrossRef] [PubMed]
20. Kneeshaw, S.; Gelineau, S.; Tada, Y.; Loake, G.J.; Spoel, S.H. Selective protein denitrosylation activity of thioredoxin-h5 modulates plant immunity. *Mol. Cell* **2014**, *56*, 153–162. [CrossRef] [PubMed]
21. Schmidmann, E.; König, A.C.; Orwat, A.; Leister, D.; Hartl, M.; Finkemeier, I. Redox regulation of *Arabidopsis* mitochondrial citrate synthase. *Mol. Plant* **2014**, *7*, 156–169. [CrossRef] [PubMed]
22. Yoshida, K.; Noguchi, K.; Motohashi, K.; Hisabori, T. Systematic exploration of thioredoxin target proteins in plant mitochondria. *Plant Cell Physiol.* **2013**, *54*, 875–892. [CrossRef] [PubMed]
23. Martí, M.C.; Olmos, E.; Calvete, J.J.; Díaz, I.; Barranco-Medina, S.; Whelan, J.; Lázaro, J.J.; Sevilla, F.; Jiménez, A. Mitochondrial and nuclear localization of a novel pea thioredoxin: Identification of its mitochondrial target proteins. *Plant Physiol.* **2009**, *150*, 646–657. [CrossRef] [PubMed]
24. Yoshida, K.; Hisabori, T. Mitochondrial isocitrate dehydrogenase is inactivated upon oxidation and reactivated by thioredoxin-dependent reduction in *Arabidopsis*. *Front. Environ. Sci.* **2014**, *2*, 38. [CrossRef]
25. Daloso, D.M.; Müller, K.; Obata, T.; Florian, A.; Tohge, T.; Bottcher, A.; Riondet, C.; Bariat, L.; Carrari, F.; Nunes-Nesi, A.; et al. Thioredoxin, a master regulator of the tricarboxylic acid cycle in plant mitochondria. *Proc. Natl. Acad. Sci. USA* **2015**, *112*, E1392–E1400. [CrossRef] [PubMed]
26. Yoshida, K.; Hisabori, T. Adenine nucleotide-dependent and redox-independent control of mitochondrial malate dehydrogenase activity in *Arabidopsis thaliana*. *Biochim. Biophys. Acta* **2016**, *1857*, 810–818. [CrossRef] [PubMed]
27. Ortiz-Espín, A.; Iglesias-Fernández, R.; Calderón, A.; Carbonero, P.; Sevilla, F.; Jiménez, A. Mitochondrial AtTrxO1 is transcriptionally regulated by AtbZIP9 and AtAZF2 and affects seed germination under saline conditions. *J. Exp. Bot.* **2017**, *68*, 1025–1038. [CrossRef] [PubMed]
28. Balmer, Y.; Vensel, W.H.; Tanaka, C.K.; Hurkman, W.J.; Gelhaye, E.; Rouhier, N.; Jacquot, J.P.; Manieri, W.; Schürmann, P.; Droux, M.; et al. Thioredoxin links redox to the regulation of fundamental processes of plant mitochondria. *Proc. Natl. Acad. Sci. USA* **2004**, *101*, 2642–2647. [CrossRef] [PubMed]

29. Winger, A.M.; Taylor, N.L.; Heazlewood, J.L.; Day, D.A.; Millar, A.H. Identification of intra- and intermolecular disulphide bonding in the plant mitochondrial proteome by diagonal gel electrophoresis. *Proteomics* **2007**, *7*, 4158–4170. [CrossRef] [PubMed]
30. Keech, O.; Gardeström, P.; Kleczkowski, L.A.; Rouhier, N. The redox control of photorespiration: From biochemical and physiological aspects to biotechnological considerations. *Plant Cell Environ.* **2017**, *40*, 553–569. [CrossRef] [PubMed]
31. Higuchi, R.; Krummel, B.; Saiki, R.K. A general method of in vitro preparation and specific mutagenesis of DNA fragments: Study of protein and DNA interactions. *Nucleic Acids Res.* **1988**, *16*, 7351–7367. [CrossRef] [PubMed]
32. Ho, S.N.; Hunt, H.D.; Horton, R.M.; Pullen, J.K.; Pease, L.R. Site-directed mutagenesis by overlap extension using the polymerase chain reaction. *Gene* **1989**, *77*, 51–59. [CrossRef]
33. Schenk, P.M.; Baumann, S.; Mattes, R.; Steinbiss, H.H. Improved high-level expression system for eukaryotic genes in *Escherichia coli* using T7 RNA polymerase and rare ArgtRNAs. *Biotechniques* **1995**, *19*, 196–200. [PubMed]
34. Gill, S.C.; von Hippel, P.H. Calculation of protein extinction coefficients from amino acid sequence data. *Anal. Biochem.* **1989**, *182*, 319–326. [CrossRef]
35. Jacquot, J.P.; Rivera-Madrid, R.; Marinho, P.; Kollarova, M.; Le Marechal, P.; Miginiac-Maslow, M.; Meyer, Y. *Arabidopsis thaliana* NAPH thioredoxin reductase. cDNA characterization and expression of the recombinant protein in *Escherichia coli*. *J. Mol. Biol.* **1994**, *235*, 1357–1363. [CrossRef] [PubMed]
36. Bandyopadhyay, S.; Gama, F.; Molina-Navarro, M.M.; Gualberto, J.M.; Claxton, R.; Naik, S.G.; Huynh, B.H.; Herrero, E.; Jacquot, J.P.; Johnson, M.K.; et al. Chloroplast monothiol glutaredoxins as scaffold proteins for the assembly and delivery of [2Fe-2S] clusters. *EMBO J.* **2008**, *27*, 1122–1133. [CrossRef] [PubMed]
37. Couturier, J.; Stroher, E.; Albetel, A.N.; Roret, T.; Muthuramalingam, M.; Tarrago, L.; Seidel, T.; Tsan, P.; Jacquot, J.P.; Johnson, M.K.; et al. Arabidopsis chloroplastic glutaredoxin C5 as a model to explore molecular determinants for iron–sulfur cluster binding into glutaredoxins. *J. Biol. Chem.* **2011**, *286*, 27515–27527. [CrossRef] [PubMed]
38. Zannini, F.; Couturier, J.; Keech, O.; Rouhier, N. In Vitro Alkylation Methods for Assessing the Protein Redox State. *Methods Mol. Biol.* **2017**, *1653*, 51–64. [CrossRef] [PubMed]
39. Kabsch, W. XDS. *Acta Crystallogr. D Biol. Crystallogr.* **2010**, *66*, 125–132. [CrossRef] [PubMed]
40. Winn, M.D.; Ballard, C.C.; Cowtan, K.D.; Dodson, E.J.; Emsley, P.; Evans, P.R.; Keegan, R.M.; Krissinel, E.B.; Leslie, A.G.; McCoy, A.; et al. Overview of the CCP4 suite and current developments. *Acta Crystallogr. D Biol. Crystallogr.* **2011**, *67*, 235–242. [CrossRef] [PubMed]
41. Langer, G.; Cohen, S.X.; Lamzin, V.S.; Perrakis, A. Automated macromolecular model building for X-ray crystallography using ARP/wARP version 7. *Nat. Protoc.* **2008**, *3*, 1171–1179. [CrossRef] [PubMed]
42. Vagin, A.; Teplyakov, A. Molecular replacement with MOLREP. *Acta Crystallogr. D Biol. Crystallogr.* **2010**, *66*, 22–25. [CrossRef] [PubMed]
43. Adams, P.D.; Afonine, P.V.; Bunkoczi, G.; Chen, V.B.; Davis, I.W.; Echols, N.; Headd, J.J.; Hung, L.W.; Kapral, G.J.; Grosse-Kunstleve, R.W.; et al. PHENIX: A comprehensive Python-based system for macromolecular structure solution. *Acta Crystallogr. D Biol. Crystallogr.* **2010**, *66*, 213–221. [CrossRef] [PubMed]
44. Emsley, P.; Lohkamp, B.; Scott, W.G.; Cowtan, K. Features and development of Coot. *Acta Crystallogr. D Biol. Crystallogr.* **2010**, *66*, 486–501. [CrossRef] [PubMed]
45. Chen, V.B.; Arendall, W.B.; Headd, J.J.; Keedy, D.A.; Immormino, R.M.; Kapral, G.J.; Murray, L.W.; Richardson, J.S.; Richardson, D.C. MolProbity: All-atom structure validation for macromolecular crystallography. *Acta Crystallogr. D Biol. Crystallogr.* **2010**, *66*, 12–21. [CrossRef] [PubMed]
46. Rouhier, N.; Unno, H.; Bandyopadhyay, S.; Masip, L.; Kim, S.K.; Hirasawa, M.; Gualberto, J.M.; Lattard, V.; Kusunoki, M.; Knaff, D.B.; et al. Functional, structural, and spectroscopic characterization of a glutathione-ligated [2Fe-2S] cluster in poplar glutaredoxin C1. *Proc. Natl. Acad. Sci. USA* **2007**, *104*, 7379–7384. [CrossRef] [PubMed]
47. Gao, H.; Subramanian, S.; Couturier, J.; Naik, S.G.; Kim, S.K.; Leustek, T.; Knaff, D.B.; Wu, H.C.; Vignols, F.; Huynh, B.H.; et al. *Arabidopsis thaliana* Nfu2 accommodates [2Fe-2S] or [4Fe-4S] clusters and is competent for in vitro maturation of chloroplast [2Fe-2S] and [4Fe-4S] cluster-containing proteins. *Biochemistry* **2013**, *52*, 6633–6645. [CrossRef] [PubMed]

48. Zhang, B.; Bandyopadhyay, S.; Shakamuri, P.; Naik, S.G.; Huynh, B.H.; Couturier, J.; Rouhier, N.; Johnson, M.K. Monothiol glutaredoxins can bind linear $[Fe_3S_4]^+$ and $[Fe_4S_4]^{2+}$ clusters in addition to $[Fe_2S_2]^{2+}$ clusters: spectroscopic characterization and functional implications. *J. Am. Chem. Soc.* **2013**, *135*, 15153–15164. [CrossRef] [PubMed]
49. Droux, M.; Jacquot, J.P.; Miginac-Maslow, M.; Gadal, P.; Huet, J.C.; Crawford, N.A.; Yee, B.C.; Buchanan, B.B. Ferredoxin-thioredoxin reductase, an iron–sulfur enzyme linking light to enzyme regulation in oxygenic photosynthesis: Purification and properties of the enzyme from C3, C4, and cyanobacterial species. *Arch. Biochem. Biophys.* **1987**, *252*, 426–439. [CrossRef]
50. Bisio, H.; Bonilla, M.; Manta, B.; Graña, M.; Salzman, V.; Aguilar, P.S.; Gladyshev, V.N.; Comini, M.A.; Salinas, G. A new class of thioredoxin-related protein able to bind iron–sulfur clusters. *Antioxid. Redox Signal.* **2015**, *24*, 205–216. [CrossRef] [PubMed]
51. Masip, L.; Pan, J.L.; Haldar, S.; Penner-Hahn, J.E.; DeLisa, M.P.; Georgiou, G.; Bardwell, J.C.; Collet, J.F. An engineered pathway for the formation of protein disulfide bonds. *Science* **2004**, *303*, 1185–1189. [CrossRef] [PubMed]
52. Saarinen, M.; Gleason, F.K.; Eklund, H. Crystal structure of thioredoxin-2 from *Anabaena*. *Structure* **1995**, *3*, 1097–1108. [CrossRef]
53. Shen, J.; Zeng, Y.; Zhuang, X.; Sun, L.; Yao, X.; Pimpl, P.; Jiang, L. Organelle pH in the *Arabidopsis* endomembrane system. *Mol. Plant* **2013**, *6*, 1419–1437. [CrossRef] [PubMed]
54. Dolinsky, T.J.; Czodrowski, P.; Li, H.; Nielsen, J.E.; Jensen, J.H.; Klebe, G.; Baker, N.A. PDB2PQR: Expanding and upgrading automated preparation of biomolecular structures for molecular simulations. *Nucleic Acids Res.* **2007**, *35*, 522–525. [CrossRef] [PubMed]
55. Selles, B.; Zannini, F.; Couturier, J.; Jacquot, J.P.; Rouhier, N. Atypical protein disulfide isomerases (PDI): Comparison of the molecular and catalytic properties of poplar PDI-A and PDI-M with PDI-L1A. *PLoS ONE* **2017**, *12*, e0174753. [CrossRef] [PubMed]
56. Remelli, W.; Santabarbara, S.; Carbonera, D.; Bonomi, F.; Ceriotti, A.; Casazza, A.P. Iron Binding Properties of Recombinant Class A Protein Disulfide Isomerase from *Arabidopsis thaliana*. *Biochemistry* **2017**, *56*, 2116–2125. [CrossRef] [PubMed]
57. Feng, Y.; Zhong, N.; Rouhier, N.; Hase, T.; Kusunoki, M.; Jacquot, J.P.; Jin, C.; Xia, B. Structural insight into poplar glutaredoxin C1 with a bridging iron–sulfur cluster at the active site. *Biochemistry* **2006**, *45*, 7998–8008. [CrossRef] [PubMed]
58. Johansson, C.; Roos, A.K.; Montano, S.J.; Sengupta, R.; Filippakopoulos, P.; Guo, K.; von Delft, F.; Holmgren, A.; Oppermann, U.; Kavanagh, K.L. The crystal structure of human GLRX5: Iron–sulfur cluster co-ordination, tetrameric assembly and monomer activity. *Biochem. J.* **2011**, *433*, 303–311. [CrossRef] [PubMed]
59. Banci, L.; Brancaccio, D.; Ciofi-Baffoni, S.; Del Conte, R.; Gadepalli, R.; Mikolajczyk, M.; Neri, S.; Piccioli, M.; Winkelmann, J. [2Fe-2S] cluster transfer in iron–sulfur protein biogenesis. *Proc. Natl. Acad. Sci. USA* **2014**, *111*, 6203–6208. [CrossRef] [PubMed]
60. Benson, D.E.; Wisz, M.S.; Liu, W.; Hellinga, H.W. Construction of a novel redox protein by rational design: conversion of a disulfide bridge into a mononuclear iron–sulfur center. *Biochemistry* **1998**, *37*, 7070–7076. [CrossRef] [PubMed]
61. Collet, J.F.; Peisach, D.; Bardwell, J.C.; Xu, Z. The crystal structure of TrxA(CACA): Insights into the formation of a [2Fe-2S] iron–sulfur cluster in an *Escherichia coli* thioredoxin mutant. *Protein Sci.* **2005**, *14*, 1863–1869. [CrossRef] [PubMed]
62. Coldren, C.D.; Hellinga, H.W.; Caradonna, J.P. The rational design and construction of a cuboidal iron–sulfur protein. *Proc. Natl. Acad. Sci. USA* **1997**, *94*, 6635–6640. [CrossRef] [PubMed]
63. Su, D.; Berndt, C.; Fomenko, D.E.; Holmgren, A.; Gladyshev, V.N. A conserved cis-proline precludes metal binding by the active site thiolates in members of the thioredoxin family of proteins. *Biochemistry* **2007**, *46*, 69036910. [CrossRef] [PubMed]
64. Berndt, C.; Schwenn, J.D.; Lillig, C.H. The specificity of thioredoxins and glutaredoxins is determined by electrostatic and geometric complementarity. *Chem. Sci.* **2015**, *6*, 7049–7058. [CrossRef] [PubMed]
65. Pérez-Pérez, M.E.; Mauriès, A.; Maes, A.; Tourasse, N.J.; Hamon, M.; Lemaire, S.D.; Marchand, C.H. The Deep Thioredoxome in *Chlamydomonas reinhardtii*: New Insights into Redox Regulation. *Mol. Plant* **2017**, *10*, 1107–1125. [CrossRef] [PubMed]

66. Zannini, F.; Moseler, A.; Bchini, R.; Dhalleine, T.; Meyer, A.J.; Rouhier, N.; Couturier, J. The thioredoxin-mediated recycling of *Arabidopsis thaliana* GRXS16 relies on a conserved C-terminal cysteine. *BBA General Subj.* under revision.
67. Landau, M.; Mayrose, I.; Rosenberg, Y.; Glaser, F.; Martz, E.; Pupko, T.; Ben-Tal, N. ConSurf 2005: The projection of evolutionary conservation scores of residues on protein structures. *Nucleic Acids Res.* **2005**, *33*, W299–W302. [[CrossRef](#)] [[PubMed](#)]
68. Lillig, C.H.; Berndt, C.; Vergnolle, O.; Lönn, M.E.; Hudemann, C.; Bill, E.; Holmgren, A. Characterization of human glutaredoxin 2 as iron–sulfur protein: a possible role as redox sensor. *Proc. Natl. Acad. Sci. USA* **2005**, *102*, 8168–8173. [[CrossRef](#)] [[PubMed](#)]



© 2018 by the authors. Licensee MDPI, Basel, Switzerland. This article is an open access article distributed under the terms and conditions of the Creative Commons Attribution (CC BY) license (<http://creativecommons.org/licenses/by/4.0/>).

FigureS1. Purity of recombinant AtTRXo1 and AtTRXo2. Sample proteins (10 µg) were separated by 15% SDS-PAGE and stained with Coomassie Brilliant Blue.



Figure S2. Analytical gel filtration of *E. coli* IscS. This analysis was performed by loading 100 µg of protein onto a Superdex S200 10/300 column. The presence of the polypeptide and of the PLP cofactor have been detected by the absorbance at 280 nm (blue line) and 420 nm (red line), respectively.

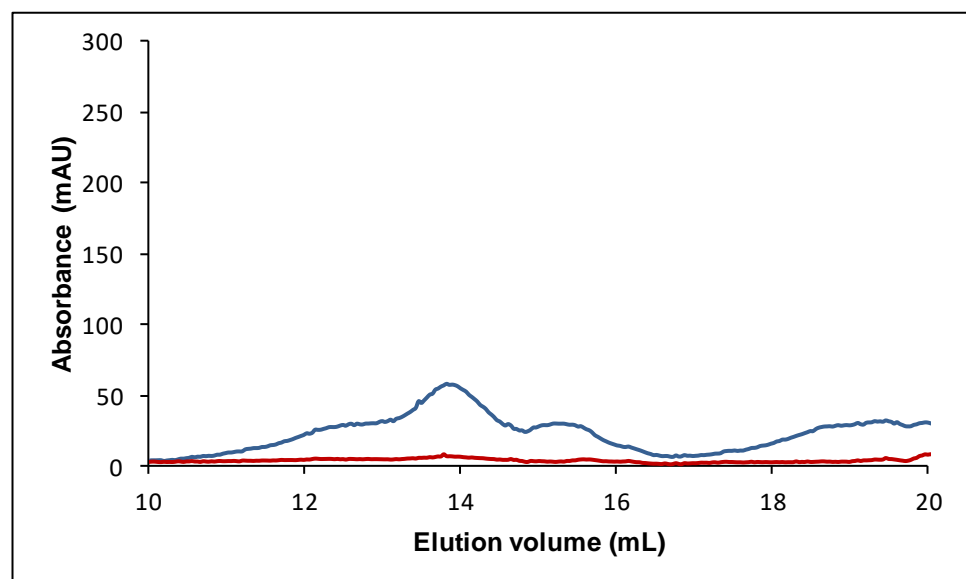


Figure S3. Electrospray ionization mass spectrometry analysis of NFU4. Mass spectrum of NFU4 protein determined for an untreated (A) or a reduced protein (B) as described in the “Materials and Methods” section. Species with a mass of 22,035.1 and 22,037.4 Da represent oxidized and reduced forms, respectively. Other species with sodium or Tris adduct are visible (species with a mass of 22,056.8 and 22,057.6 Da).

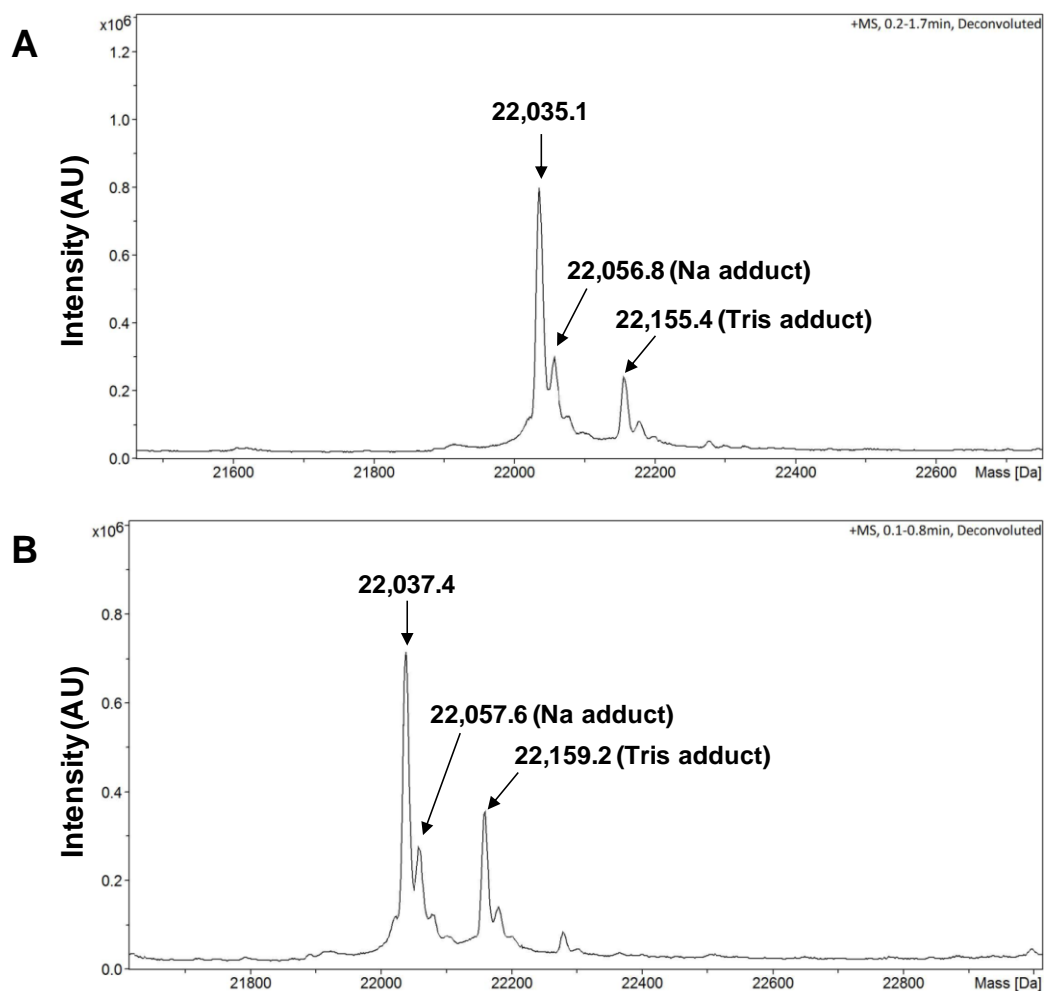


Figure S4. Electrospray ionization mass spectrometry analysis of NFU5. Mass spectrum of NFU5 protein determined for an untreated (A) or reduced protein (B) as described in the “Materials and Methods” section. Species with a mass of 21,690.9 and 21693.0 Da represent oxidized and reduced forms, respectively. Other species with sodium or Tris adduct are visible (species with a mass of 21,714.7 Da, 21,812.5 and 21,813.3 Da).

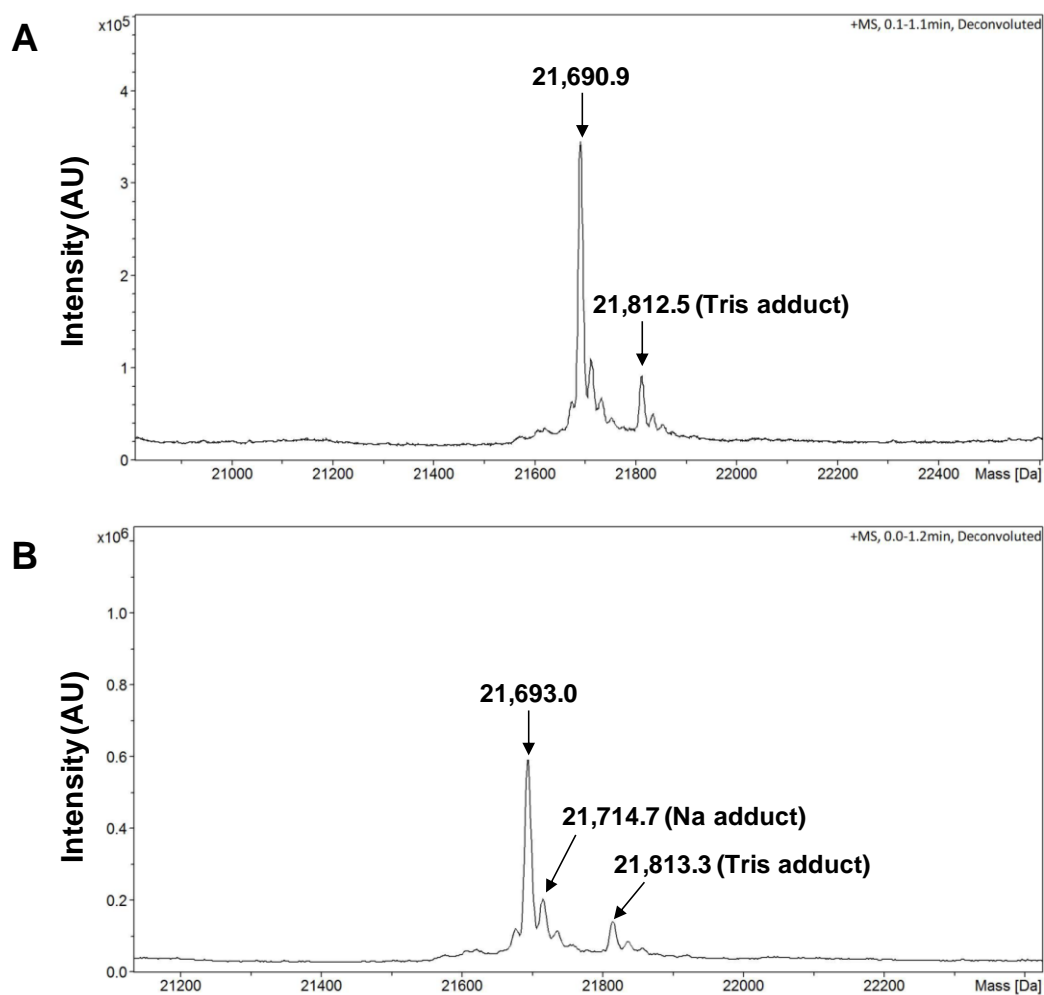


Figure S5. The disulfide bridge of mitochondrial NFUs is reduced by NTR/TRXo system but not by NTR/GRXS15 system. The reduction of as-purified, oxidized forms of NFU4 (A) or NFU5 (B) was assessed after a 15 min incubation in the presence of the following reducing systems: NTR: NADPH + NTR ; TRXo1: NADPH + NTR + TRXo1 ; TRXo2: NADPH + NTR + TRXo2 ; GRXS15: NADPH + NTR + GRXS15. The ability of these three oxidoreductases to reduce NFU proteins was evaluated using either 1 μ M or 10 μ M. After alkylation with 2 kDa mPEG maleimide, proteins were separated on non-reducing SDS-PAGE. Reduced (Red) and oxidized (Ox) proteins served as controls. The stars indicate the alkylated (*) forms of the oxidoreductases in the respective regeneration systems when visible.

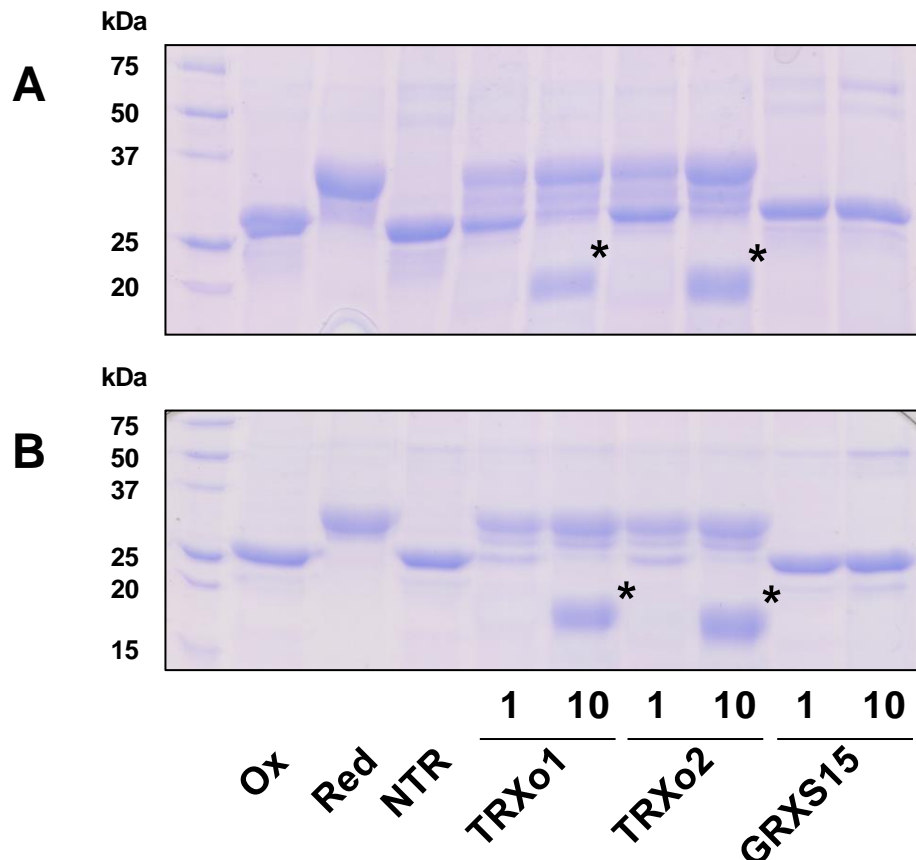


Table S1. Primers used for cloning and site-directed mutagenesis experiments. The *Nco*I, *Nde*I and *Bam*HI restriction sites used for cloning are underlined in the primers. The mutagenic codons are in bold.

Name	Sequence
TRXo1 for	5' <u>CCCCCCCCCATATGGAAAATGGTGTGTTCTA</u> 3'
TRXo1 rev	5' <u>CCCCGGATCCTCACTTGTAGAGCTGTT</u> 3'
TRXo2 for	5' <u>CCCCCCCCCATATGCGATCCAGCTTGTAGTG</u> 3'
TRXo2 rev	5' <u>CCCCGGATCCTCACTTGTAGAGTTGTT</u> 3'
TRXo2 C37S for	5' TTCACTGCCGCATGGTCTGGACCTGCAGGCTT 3'
TRXo2 C37S rev	5' AAGCCTGCAAGGTCCAGACCATGCGGCAGTGAA3'
TRXo2 C40S for	5' GCATGGTGTGGACCTAGCAGGCTTATCTCTCCT3'
TRXo2 C40S rev	5' AGGAGAGATAAGCCTGCTAGGTCCACACCATGC3'
NFU4 for	5' <u>CCCCCATGGTTTATCCAACCCAATCA</u> 3'
NFU4 rev	5' <u>CCCCGGATCCCTACTCTACTCTCATCTC</u> 3'
NFU5 for	5' <u>CCCCCATGGTTTATCCAACC</u> 3'
NFU5 rev	5' <u>CCCCGGATCCTCACTCCATTGGACCAGA</u> 3'
IscS for	5' <u>CCCCCCCCCATATGTACGGAGTTATAGAGCA</u> 3'
IscS rev	5' <u>CCCCGGATCCTTAATGATGAGCCCATT</u> 3'

Atypical protein disulfide isomerase (PDI): Comparison of the molecular and catalytic properties of poplar PDI-A and PDI-M with PDI-L1A

Benjamin Selles, Flavien Zannini, Jérémie Couturier, Jean-Pierre Jacquot et Nicolas Rouhier*

UMR 1136 Interactions Arbres/Microorganismes, Université de Lorraine/ INRA, Faculté des Sciences et Technologies, Vandoeuvre-lès-Nancy, France

Article publié dans PLOS-One

Chez les plantes supérieures, des analyses phylogénétiques ont permis d'identifier 9 classes de protéine disulfure isomérasées (PDI) qui diffèrent par leur organisation structurale et la présence de domaines spécifiques. Cette étude présente la caractérisation biochimique de trois PDIs chez *Populus trichocarpa* ayant des organisations structurales bien distinctes et appartenant à trois classes différentes de PDIs. La PDI-A est composée d'un seul module catalytique appelé domaine a comportant un repliement TRX avec un site actif WCKHC, tandis que les PDI-M et PDI-L1a présentent respectivement une organisation a'-b-b'-a et a^o-a-b. Les deux isoformes PDI-L1a et PDI-M possèdent une activité oxydase et réductase vis-à-vis de différents substrats classiquement utilisés pour l'étude de cette famille protéique. Par contre, aucune activité n'a été mise en évidence pour l'isoforme PDI-A. De manière inattendue, cette protéine incorpore un centre de type [2Fe-2S] au sein d'un homodimère après expression dans *Escherichia coli*. La signification physiologique de cette spécificité et un lien avec la fonction *in vivo* de cette isoforme sont inconnus. Enfin, des analyses biochimiques approfondies démontrent l'importance des domaines a et b (nombre et position) sur les propriétés redox et la reconnaissance des substrats respectifs de ces PDIs.

RESEARCH ARTICLE

Atypical protein disulfide isomerases (PDI): Comparison of the molecular and catalytic properties of poplar PDI-A and PDI-M with PDI-L1A

Benjamin Selles^a, Flavien Zannini, Jérémie Couturier, Jean-Pierre Jacquot, Nicolas Rouhier*

^a UMR 1136 Interactions Arbres/Microorganismes, Université de Lorraine/INRA, Faculté des Sciences et Technologies, Vandoeuvre-lès-Nancy, France

✉ Current address: Epigenetic regulations and Seed Development, UMR232, IRD Montpellier, Montpellier, France
 * nicolas.rouhier@univ-lorraine.fr



OPEN ACCESS

Citation: Selles B, Zannini F, Couturier J, Jacquot J-P, Rouhier N (2017) Atypical protein disulfide isomerases (PDI): Comparison of the molecular and catalytic properties of poplar PDI-A and PDI-M with PDI-L1A. PLoS ONE 12(3): e0174753. <https://doi.org/10.1371/journal.pone.0174753>

Editor: Luis Eduardo Soares Netto, Universidade de São Paulo Instituto de Biociências, BRAZIL

Received: February 8, 2017

Accepted: March 14, 2017

Published: March 31, 2017

Copyright: © 2017 Selles et al. This is an open access article distributed under the terms of the [Creative Commons Attribution License](#), which permits unrestricted use, distribution, and reproduction in any medium, provided the original author and source are credited.

Data Availability Statement: All relevant data are within the paper.

Funding: The UMR1136 is supported by a grant overseen by the French National Research Agency (ANR) as part of the "Investissements d'Avenir" program (ANR-11-LABX-0002-01, Lab d'Excellence ARBRE). The funders had no role in study design, data collection and analysis, decision to publish, or preparation of the manuscript.

Competing interests: The authors have declared that no competing interests exist.

Abstract

Protein disulfide isomerases are overwhelmingly multi-modular redox catalysts able to perform the formation, reduction or isomerisation of disulfide bonds. We present here the biochemical characterization of three different poplar PDI isoforms. PDI-A is characterized by a single catalytic Trx module, the so-called *a* domain, whereas PDI-L1a and PDI-M display an *a-b-b'-a'* and *a°-a-b* organisation respectively. Their activities have been tested *in vitro* using purified recombinant proteins and a series of model substrates as insulin, NADPH thioredoxin reductase, NADP malate dehydrogenase (NADP-MDH), peroxiredoxins or RNase A. We demonstrated that PDI-A exhibited none of the usually reported activities, although the cysteines of the WCKHC active site signature are able to form a disulfide with a redox midpoint potential of -170 mV at pH 7.0. The fact that it is able to bind a [Fe₂S₂] cluster upon *Escherichia coli* expression and anaerobic purification might indicate that it does not have a function in dithiol-disulfide exchange reactions. The two other proteins were able to catalyze oxidation or reduction reactions, PDI-L1a being more efficient in most cases, except that it was unable to activate the non-physiological substrate NADP-MDH, in contrast to PDI-M. To further evaluate the contribution of the catalytic domains of PDI-M, the dicysteinic motifs have been independently mutated in each *a* domain. The results indicated that the two *a* domains seem interconnected and that the *a'* module preferentially catalyzed oxidation reactions whereas the *a* module catalyzed reduction reactions, in line with the respective redox potentials of -170 mV and -190 mV at pH 7.0. Overall, these *in vitro* results illustrate that the number and position of *a* and *b* domains influence the redox properties and substrate recognition (both electron donors and acceptors) of PDI which contributes to understand why this protein family expanded along evolution.

Introduction

Oxidative protein folding is an essential process, occurring generally in oxidizing sub-cellular compartments, and which is required, in particular, for the maturation and assembly of newly synthesized secreted and membrane proteins. In the periplasm of prokaryotes, the proteins responsible for the formation and isomerisation of disulfide bonds belong to the Dsb (DiSulfide Bonds) protein family. This protein family is composed of several members referred to as DsbA to DsbL [1, 2]. The major actors, conserved in many bacteria, are the DsbA-DsbB couple which is involved in oxidation reactions, the DsbC-DsbD couple in isomerisation reactions, DsbE or CcmG in cytochrome c maturation and DsbG in the reduction of sulfenic acids [2–4]. In eukaryotes, the proteins responsible of the oxidative protein folding are essentially found in the endoplasmic reticulum (ER) and in the intermembrane mitochondrial space. In the ER, the proteins involved belong mostly to the endoplasmic reticulum oxidase (ERO) and protein disulfide isomerase (PDI) families [5]. In addition, proteins named quiescin sulphydryl oxidases (QSOX) displaying oxidase activity *in vitro* are also present in this compartment and various physiological functions were proposed for QSOX [6–8]. In the mitochondrial intermembrane space, the oxidation of cysteines is ensured by the Mia40-Erv1 disulfide relay [9].

All PDI, as well as some Dsb members, belong to the thioredoxin (Trx) superfamily displaying a common structural fold named the Trx fold [10, 11]. All PDI possess at least one Trx domain referred to as *a* or *b* domain which consists of about 100 amino acids and adopts a Trx fold. The difference is that *a* modules exhibit a catalytic active site (most frequently WCGHC) whereas *b* modules do not possess the typical CxxC catalytic motifs but instead are thought to be important for substrate recognition [12, 13]. The isoforms usually differ by the number and the positions of *a* and *b* domains and by the active site signature of *a* domains. The classical PDI isoforms, which are present in all eukaryotic organisms, possess four modules with an *a-b-b'-a'* organisation. Several PDI isoforms possess a more limited number of domains as well as additional domains that have been evolutionary added and which likely confer specific functions to the isoforms possessing them [5].

PDI constitute a multigenic family composed of 5 genes in yeast and up to 20 genes in human [14, 15]. In photosynthetic organisms, PDI cluster into 9 classes (A, B, C, D, E, F, L, M and S), 3 are specific to algae (D, E, F), 1 is specific to land plants (A) and the 5 others are present in both phyla [5, 16–19]. Land plants possess around 10 members [5]. Some soybean PDI isoforms belonging to classes L, M and S play essential roles in seed and pollen maturation and development [17–22]. The plastidial form of a *Chlamydomonas reinhardtii* PDI-L is involved in the redox-dependent transcriptional regulation in the chloroplast [23]. A maize PDI-A protein is accumulated in response to an ER stress, but, in contrast to classical PDI, it might not reside in the ER or only transiently [16]. It was also recently proposed that the *Hordeum vulgare* PDI5.1 isoform, a PDI-A, is involved in the susceptibility toward various bymoviruses and particularly the barley yellow mosaic virus [24]. However, very little is known concerning the biochemical and physiological properties of many plant PDI.

Thus, the aim of this study was to compare the biochemical properties of three poplar PDI (PDI-A, PDI-L1a and PDI-M) exhibiting different domain organisations and belonging to three different classes, by examining in particular their *in vitro* reductase and oxidase/isomerase activities using both physiological and non-physiological substrates. For poplar PDI-M, a deeper analysis was performed using proteins with mutated active site cysteines in order to investigate the importance of each catalytic domain for the oxidation or reduction of disulfide bonds. The data indicated that, although the redox potentials of the two modules of PDI-M are

very close, each Trx module preferentially performed specific reactions, the α° domain being rather competent for oxidation and the α domain for reduction.

Material and methods

Cloning, site-directed mutagenesis, production and purification of recombinant proteins

The sequences encoding poplar PDI-L1a (Potri.002G082100.1), PDI-M (Potri.014G160000.1), PDI-A (Potri.009G004500.2) were amplified from leaf cDNAs of *Populus trichocarpa* x *Populus deltoides* for PDI-L1a and *P. trichocarpa* for PDI-M and PDI-A, and cloned into pET3d for PDI-L1a or into pET-15b for PDI-M and PDI-A. In order to express proteins in their mature forms, the 21, 23 and 26 N-terminal amino acids corresponding to the putative ER targeting sequences in PDI-L1a, PDI-M and PDI-A respectively were removed. The primers used for cloning and site-directed mutagenesis (PDI-A K56G, PDI-M C36/C39S and C165/C168S) are listed in Table 1. Recombinant plasmids were used to transform the *Escherichia coli* BL21 (DE3) pSBET strain. The culture conditions were as described in [25]. The purification of PDI-L1a consisted in a succession of ammonium sulfate precipitation, ACA44 gel filtration and DEAE Sephadex chromatography as described [25]. The purification of His-tagged PDI-M and PDI-A variants was performed by affinity chromatography on IMAC columns (Sigma Aldrich) from the soluble fraction obtained after a 30 min centrifugation (27,000 x g) of cells lysed by sonication. The washing buffer was 30 mM Tris-HCl pH 8.0, 300 mM NaCl, 10 mM imidazole and the elution buffer was 30 mM Tris-HCl pH 8.0, 300 mM NaCl, 250 mM imidazole. All proteins were finally dialyzed against a 30 mM Tris-HCl pH 8.0, 1 mM EDTA, 200 mM NaCl buffer by ultrafiltration on YM10 membranes and concentrated. The same procedure was applied for the anaerobic purification of PDI-A in the glove box except that imidazole was removed by desalting on a G25 column and the protein was concentrated using 500 μL centriprep centrifugal filters omitting EDTA in the buffer. Protein concentrations were determined using molar extinction coefficients at 280 nm of 39,100 M⁻¹ cm⁻¹ for PDI-L1a, 55,265 M⁻¹ cm⁻¹ for PDI-M, 55,140 M⁻¹ cm⁻¹ for PDI-M C36/C39S and PDI-M C165/C168S, 21,220 M⁻¹ cm⁻¹ for PDI-A and PDI-A K56G.

Table 1. Oligonucleotides used in this study for cloning and site-directed mutagenesis experiments.

name	sequences
PDI-L1a for	5' CCCCCCATGGCTGAGGATGAATCAAAGGAGTAC 3'
PDI-L1a rev	5' <u>CCCCGGATCCT</u> CAAAGTCATCTTAGCTGT 3'
PDI-M for	5' CCCCCCCCCATATGCTATATGGGCCTTCATCTCC 3'
PDI-M rev	5' <u>CCCCGGATCCT</u> TATAACTCATCCTTGCTTC 3'
PDI-M C36/39S for	5' GCACCATGGTCTGGGCACTCTAAAGCTCTC 3'
PDI-M C36/39S rev	5' GAGAGCTTAGAGTGCCCAGACCATGGTGC 3'
PDI-M C165/168S for	5' GCACCTGGTCGGGCACTCTAAAGAACTGGCT 3'
PDI-M C165/168S rev	5' AGCCAGTTCTTAGAGTGACCCGACCAAGGTGC 3'
PDI-A for	5' CCCCCCCCCATATGGTTATAACCTTAACCTCC 3'
PDI-A rev	5' <u>CCCCGGATCCT</u> CACAAATCTTATCATAGCC 3'
PDI-A K56G for	5' TGTGTTCCCTGGGTGTGGGCATTGTAAGAATTG 3'
PDI-A K56G rev	5' CAAATTCTACAATGCCACACCAGGAAACACA 3'

Restriction sites are underlined.

<https://doi.org/10.1371/journal.pone.0174753.t001>

Oligomerization state determination of PDI-A

The oligomerization state of PtPDI-A was analyzed using an ÄKTA Purifier system equipped with a Sephadex75 10–300 column (GE Healthcare). 100 µg of fresh anaerobically-purified proteins reduced in the presence of a 10-fold DTT excess at room temperature was loaded on the column at a flow rate 0.5 ml min⁻¹, and detection was recorded at 280 and 420 nm. The columns were calibrated using the 29–700 kDa molecular weight standards (Sigma).

Determination of the redox midpoint potential

Oxidation-reduction titrations using the fluorescence of adducts formed between the protein and monobromobimane (mBr) were carried out at ambient temperature as described previously [26, 27]. The 500 µl reaction mixtures contained 100 µg protein in 100 mM HEPES-NaOH buffer pH 7.0, together with defined mixtures of oxidized and reduced glutathione to set the ambient potential (E_h) with an overall concentration in glutathione of 2 mM. After 2 h incubation at 25°C, excess mBr was added and incubated in the dark for 1 h. mBr labelled proteins were precipitated with TCA 20% (v/v), incubated 15 min on ice and centrifuged 15 min at 13,000 rpm. Pellets were washed with 1 volume of 2% TCA by centrifugation (15 min, 13,000 rpm) and then resuspended in 300 µl Tris-HCl 1 M, SDS 2% during 30 min. Protein solutions were then diluted to a final volume of 2.2 ml and mBr fluorescence emission was measured at 480 nm using a Cary Eclipse spectrofluorimeter after excitation at 350 nm. Fluorescence emission values were then plotted against Eh value for each sample with QtiPlot software and fitted with Boltzmann sigmoid preset parameters.

RNase A oxidative refolding

RNase A reduction and denaturation was performed in 200 µl of 100 mM Tris-HCl pH 8.0 containing 6 M guanidine, 73 mM DTT and 7.3 mM native bovine RNase A (Sigma Aldrich), for 1 h at 37°C. Excess DTT was removed with a desalting column (Sephadex G25) equilibrated with 30 mM Tris-HCl pH 8.0, 1 mM EDTA and 1% acetic acid. The RNase A concentration was determined using a molar extinction coefficient at 280 nm of 9,800 M⁻¹. cm⁻¹. The effective full reduction of RNase A was confirmed with DTNB (5,5'-dithio-bis-2-nitrobenzoic acid, 13,600 M⁻¹ cm⁻¹) confirming the expected number of 8 thiols per RNase A molecule. RNase A refolding was assessed by incubating 50 µM of reduced and denatured RNase A for 15 min in a 300 µl mixture containing 30 mM Tris-HCl pH 8.0, 1 mM EDTA, 1 mM GSH, 0.2 mM GSSG with or without 3 µM PDI. For RNase A activity measurement, 50 µl of refolding mixture were added every 5 min to 450 µl of 30 mM Tris-HCl pH 8.0, 1 mM EDTA containing 2.5 mM cytidine 2',3'-cyclic monophosphate (cCMP). RNase A recovered activity was estimated by following the increase of absorbance at 296 nm resulting from the hydrolysis of cCMP to CMP [28].

Insulin and 5,5'-Dithio-Bis-2-Nitrobenzoic Acid (DTNB) reduction

Insulin reduction was measured using 5 µM poplar Trx h1 or PDI as in [29]. The non-enzymatic reduction of insulin by DTT was used as a control. The ability of PDI to catalyze the reduction of DTNB in the presence of *Arabidopsis thaliana* NADPH-thioredoxin reductase B (AtNTRB) was measured at 25°C by monitoring the increase in absorbance at 412 nm caused by the release of thionitrobenzoate (TNB⁻). The reaction medium contained 30 mM Tris-HCl pH 8.0, 1 mM EDTA, 200 µM NADPH, 2 µM AtNTRB, 100 µM DTNB and 0.2 µM PDI.

PDI-mediated recycling of 2-Cys Peroxiredoxin (Prx)

The PDI-dependent recycling of *A. thaliana* 2-Cys Prx was measured using a NADPH-coupled spectrophotometric method at 25°C as described previously [30]. The assays were carried out in a total volume of 500 µl containing 30 mM Tris-HCl pH 8.0, 1 mM EDTA, 200 µM NADPH, 1 µM AtNTRB, 5 µM At2-Cys Prx, 100 µM H₂O₂ and 2.5 µM PDI. The decrease in absorbance was followed at 340 nm. The peroxidase activity was determined after subtracting the spontaneous reduction rate observed in the absence of PDI.

NADP-Malate Dehydrogenase (NADP-MDH) activation

The purification and activation test of NADP-MDH from *Sorghum bicolor* are as described in [31]. The activation mixture (200 µl) contained 500 µM DTT, 5 µM PDI or Trx h1 used as a control and 10 µg recombinant NADP-MDH in 100 mM Tris-HCl pH 8.0 buffer. It was incubated at 25°C for 15 min. Every 5 min, an aliquot of 20 µl was added to 480 µl of standard reaction mixture containing 100 mM Tris-HCl pH 8.0, 190 µM oxaloacetate, and 800 µM NADPH. Activities were measured by following the decrease in absorbance at 340 nm.

Quantification of iron and sulfide contents

Protein concentrations of PDI-A have been estimated using the bicinchoninic acid (BCA) protein assay (Interchim) using bovine serum albumin as a standard. For iron measurements, known concentrations of PDI-A prepared in 130 µl are mixed with 90 µl of 1 M perchloric acid (PCA). After 15 min incubation at room temperature, the reaction mixtures are centrifuged at 10,000 x g for 5 min. Then, 144 µl of 3.15 mM bathophenanthroline-disulfonic acid, 72 µl of 192 mM sodium ascorbate and 152 µl of 6.2 M ammonium acetate are sequentially added to 180 µl of the supernatant. The reaction mixtures are incubated 30 min at room temperature and centrifuged at 10,000 x g for 5 min. The absorbance ratio between 535 and 680 nm is determined for each sample including the standard curve (from 0 to 150 µM) made using a 500 µM ammonium iron(II) sulfate solution prepared by a 1/20 dilution from a 10 mM solution prepared in 1 N HCl.

For sulfide measurements, known concentrations of PDI-A prepared in 100 µl are mixed with 300 µl of 1% zinc acetate, immediately followed by the addition of 15 µl of NaOH 3N. The solution is vigorously mixed and incubated at room temperature for 10 min. Then, 75 µl of a 0.1% N,N-dimethyl-p-phenylenediamine (DMPD) solution prepared in HCl 5N are added, immediately followed by the addition of 16 µl of a 23 mM iron chloride solution prepared in HCl 1.2 N, and the mixture is vigorously mixed. The reaction mixture is then incubated for 30 min (standard curve) or 3h (samples) at 4°C. All samples are centrifuged 5 min at 10,000 x g and the sulfide concentration is determined by measuring the absorbance at 670 nm. The standard curve (0 to 100 µM) is prepared from a 200 µM Li₂S solution prepared by a 1/100e dilution from a 20 mM stock solution prepared in 0.3 N NaOH.

Results

The three selected poplar PDI have particular sequence characteristics and domain organisations

In order to analyze the biochemical properties of PDI with different domain organisations, three poplar isoforms referred to as PDI-L1a, PDI-M and PDI-A have been selected for an in-depth analysis [5]. PDI-L1a and PDI-M are multi-modular proteins composed of 4 and 3 domains respectively but both proteins possess two *a* domains containing the conventional WCGHC active site signature (Fig 1A and 1B). On the contrary, PDI-A exhibits a single *a*

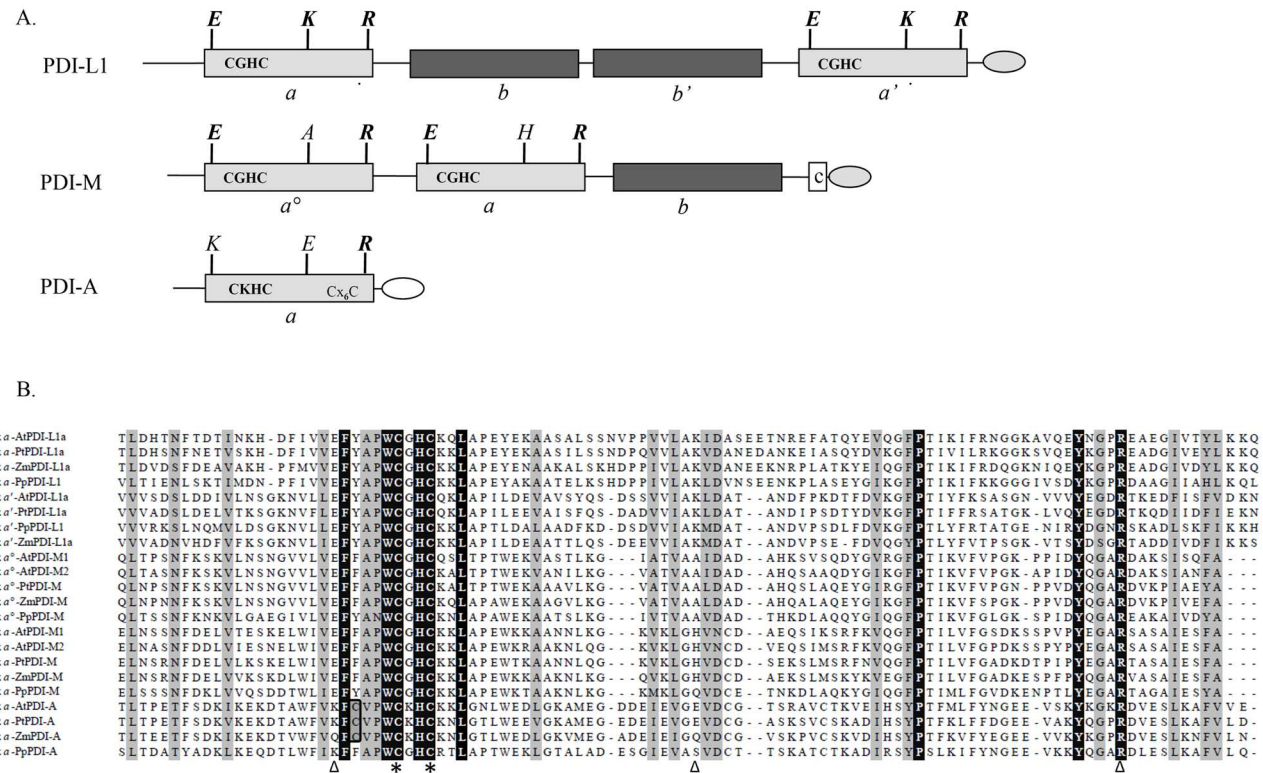


Fig 1. Sequence characteristics and domain organisation of characterized poplar PDI isoforms and their plant orthologs. A.

Modular organisation of poplar PDI-L1a, PDI-M and PDI-A. Boxes in light grey and dark grey indicate redox active (a° , a' or a) and inactive (b or b') Trx modules. Additional letters indicate the amino acids important for the redox properties. The presence of classical (KDEL) ER retention signals are represented in a light grey egg-shaped form. The unusual DK[D/E]L C-terminal sequence found in PDI-A is represented in white. B. Amino acid sequence alignment of the catalytic a modules from PDI-L1a, PDI-M and PDI-A isoforms belonging to At, *Arabidopsis thaliana* (AtPDI-A, At1g07960; AtPDI-L1a, At1g21750; AtPDI-M1, At1g04980; AtPDI-M2, At2g32920); Pp, *Physcomitrella patens* (PpPDI-A, Phpat.006G010400; PpPDI-L1, Phpat.015G023600; PpPDI-M, Phpat.004G043700); Pt, *Populus trichocarpa* (PtPDI-A, Potri.009G04500; PtPDI-L1a, Potri.002G082100; PtPDI-M, Potri.014G160000) and Zm, *Zea mays* (ZmPDI-A, GRMZM2G373628; ZmPDI-L1a, GRMZM2G091481; ZmPDI-M, GRMZM2G389173). The Trx modules were delimited according to Pfam only database (<http://pfam.sanger.ac.uk>) and the alignment was built using ClustalW algorithm at the NPSA web portal (<http://npsa-pbil.ibcp.fr>). Output of this alignment was made with the ESPript web portal (<http://escript.ibcp.fr/EScript/cgi-bin/EScript.cgi>). Amino acids strictly conserved appear in black whereas partially conserved amino acids are indicated in light grey. Cysteines of the active site signature are indicated with stars. The E, K, R residues also represented in the panel A and possibly involved in the modulation of the cysteine pKa are indicated by triangles.

<https://doi.org/10.1371/journal.pone.0174753.g001>

domain with a modified WCKHC signature, which is also found in land plant orthologs. It is interesting to note that ancestral PDI-A relatives found in *Selaginella moellendorffii* and *Physcomitrella patens* have the regular WCGHC signature.

Besides active site residues, there are 5 additional strictly conserved residues, a Phe and a Leu at positions -5 and +6 compared to the catalytic Cys, the cis-Pro conserved in all oxidoreductases having a Trx fold, and a Tyr and an Arg in the C-terminal part. This Arg was proposed to modulate the pKa of the C-terminal active site Cys, necessary for the PDI reoxidation step, by moving into and out of the active site, depending on the catalytic step [32]. Two other residues, a Glu and a Lys, highlighted in Fig 1A and 1B, are involved in the modulation of the N-terminal active site cysteine pKa at least in *E. coli* Trx1 [33]. Whereas they are strictly conserved in poplar PDI-L1a (E₅₂/K₈₆ and E₃₉₇/K₄₃₁), only the Glu is conserved in the two a domains of PDI-M, the Lys being replaced by an Ala (A₈₅) or a His (H₂₁₃) in the a° and a modules respectively. None of them is conserved in PDI-A. All these observations raise the

question of whether the redox properties of the atypical PDI-A and PDI-M are influenced by these variations in sequence and domain organisation.

Among atypical PDI, PDI-A is inactive and PDI-M is less efficient than the regular PDI-L1a

After producing in *E. coli* all three proteins devoid of their putative N-terminal ER targeting sequences and purifying them to homogeneity, the classical test used for measuring PDI activity *i.e.*, the oxidative refolding of a reduced and denatured RNase A, has been used for an initial comparison of their respective activity. PDI-L1a was the most efficient protein, as, after an incubation time of 15 min, it allowed the recovery of *ca* 90% of the activity relatively to the one observed with native RNase A ([Fig 2A](#)). At the same time, RNase A activity recovery was only 60% in the presence of PDI-M whereas the results obtained with PDI-A were similar to the reaction achieved by omitting PDI, indicating that the latter did not promote oxidation reactions, at least with RNase A.

Then, the capacity of all these PDI to catalyze the reduction of disulfide bridges instead of promoting their formation was analyzed by measuring insulin reduction, which is accompanied by its precipitation as measured by recording absorbance at 650 nm. In this test, PDI-L1a was the most efficient protein, even more than poplar Trx h1, with the reduction starting after 0.5 and 4 min respectively at concentrations of 5 μM ([Fig 2B](#)). PDI-M can also perform insulin reduction but, as in the previous assay, it was less efficient than PDI-L1a or Trx h1. PDI-A was not able to reduce insulin at all. Considering the presence of two catalytic domains in PDI-L1a and PDI-M, the better reducing activity of PDI-L1a compared to PDI-M could suggest that both catalytic domains of PDI-L1a possess reductase activity whereas only one PDI-M domain may be efficient. Moreover, independently of the rate of the reaction, the fact that the turbidity was lower is the case of both PDI compared to Trx h1 might indicate that not all insulin disulfide bonds are reduced by PDI.

Finally, since a variety of PDI can be efficiently reduced by a NADPH/NADPH thioredoxin reductase (NTR) system, we examined whether PDI can be reduced by the *A. thaliana* NTRB isoform using DTNB as an electron acceptor. Although this is presumably not the physiological reductant of ER-targeted PDI, PDI-A does not have the typical ER-retention signal contrary to PDI-L1a and PDI-M and such a system would be extremely convenient afterwards for measuring the reducing capacity of PDI by using usual Trx targets. As in the other assays, PDI-L1a was more efficient than PDI-M and PDI-A was inactive ([Fig 2C](#)).

Atypical PDI have redox midpoint potentials adequate for an oxidoreductase activity

Besides structural considerations, the redox properties of oxidoreductases are also governed by the pKa of the catalytic cysteines and the redox potential of the catalytic disulfides. Since PDI-A was inactive in all assays and possessed a particular active site signature and differences are observed among PDI, we sought to evaluate the redox potentials of both atypical PDI, PDI-A and PDI-M. It is well documented that the nature of the spacing residues between the two cysteine residues influences the redox potential values of proteins of the Trx superfamily [[34, 35](#)]. Hence, for PDI-A, a K56G variant, the active site sequence of which was changed from WCKHC to the regular WCGHC signature, has been produced and characterized. The E_m value of PDI-A was determined to be $-170 \text{ mV} \pm 5 \text{ mV}$ whereas the one measured for PDI-A K56G was $-150 \text{ mV} \pm 5 \text{ mV}$ ([Fig 3A](#)). However, the observed 20 mV increase for the PDI-A K56G variant did not allow acquiring oxidoreductase activity since it was also inactive

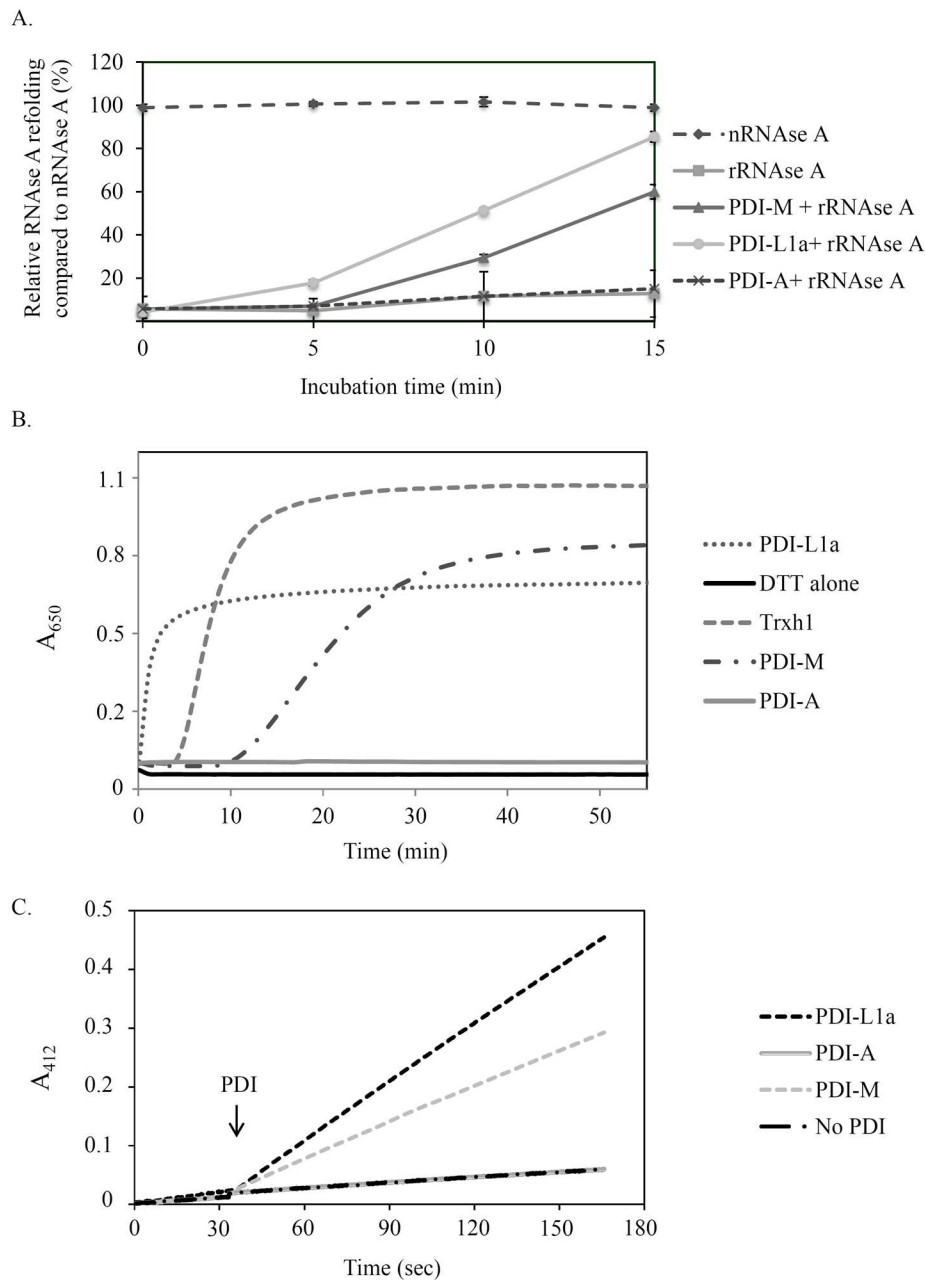
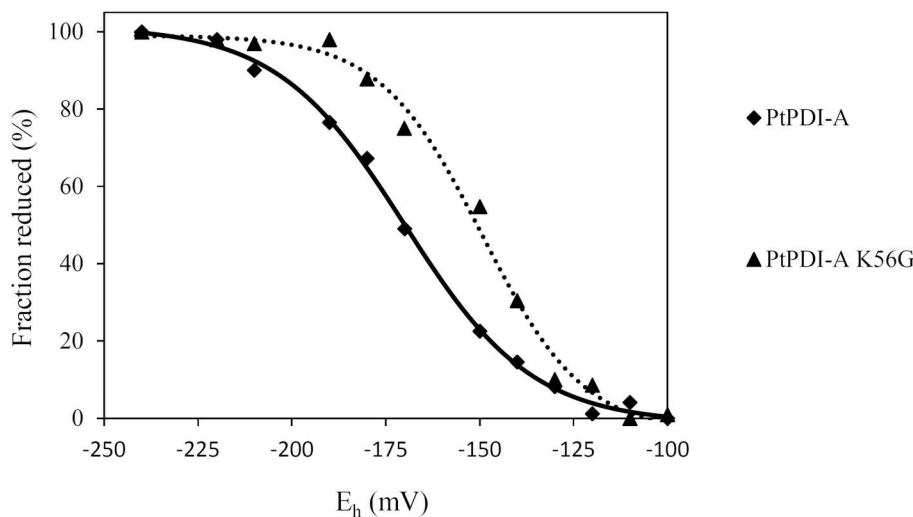


Fig 2. Comparative analysis of the oxidoreductase activities of poplar PDI isoforms. A. Oxidative refolding of RNase A. Results are represented as percentages of activity relative to the activity of native RNase A (nRNase A). The reduced RNase A (rRNase A) was tested alone or upon incubation with PDI-L1a, PDI-M or PDI-A for the indicated times. Measurements were made in triplicate and error bars indicate standard deviation. B. Insulin reduction. It was assessed by measuring the turbidity at 650 nm caused by the precipitation of insulin upon reduction with DTT alone or supplemented with 5 μM PDI-L1a, PDI-M, PDI-A or Trxh1. The reaction curve shown is representative of at least three independent repetitions. C. PDI reduction by AtNTRB. DTNB reduction was followed at 412 nm in the presence of NADPH, AtNTRB alone or with PDI-L1a, PDI-M or PDI-A. The PDI have been added after 30 seconds. The reaction curve shown is representative of at least three independent repetitions.

<https://doi.org/10.1371/journal.pone.0174753.g002>

A.



B.

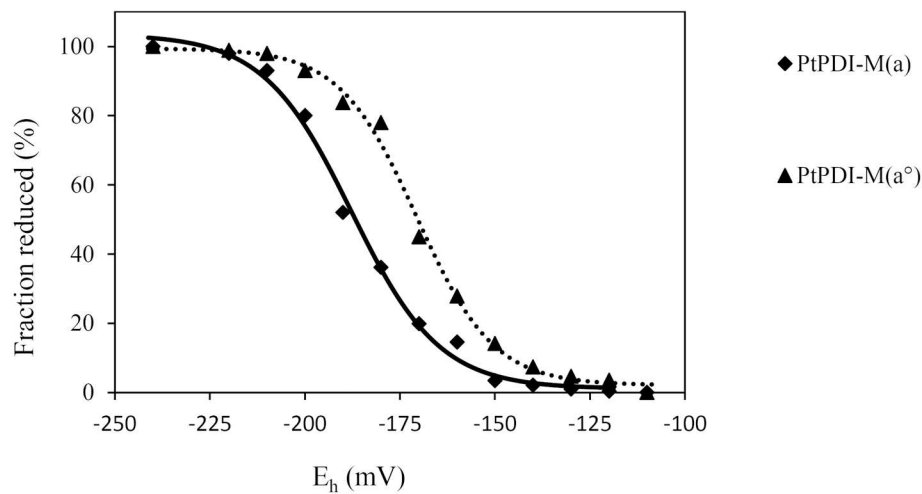


Fig 3. Redox midpoint potential of the catalytic domains of poplar PDI-A and PDI-M. A. Redox midpoint potential of PDI-A (solid line) and PDI-A K56G (dotted line). B. Redox midpoint potential of the *a* (solid line) and *a*° (dotted line) modules of PDI-M measured using the PDI-M C36/39S and PDI-M C165/168S variants respectively. The titrations were carried out using a total glutathione concentration of 2 mM in the redox buffer and with a redox equilibration time of 2 h, before labelling free protein thiols by mBBr.

<https://doi.org/10.1371/journal.pone.0174753.g003>

in all assays used previously (RNase A refolding, insulin and DTNB reduction) (data not shown).

For PDI-M, the redox potentials of the disulfide formed by the cysteine residues found in both *a* domains was measured after producing two variants corresponding to the full-length protein but where the dicysteinic WCGHC motif of each *a* domain was substituted by a WSGHS motif. Using PDI-M C165/168S and PDI-M C36/39S variants, E_m values of -170 mV \pm 5 mV and of -190 mV \pm 5 mV have been determined for the catalytic disulfides found in the *a*° and *a* domains respectively (Fig 3B). The PDI-M C165/168S variant will be thereafter

referred to as PDI-M(a°) since only the a° domain possesses cysteines susceptible to provide the oxidoreductase activity and the PDI-M C36/39S variant as PDI-M(a) for the same reasons.

PDI-A incorporates a [Fe₂S₂] cluster upon expression in *E. coli*

The absence of activity for PDI-A was intriguing. By comparing *E. coli* cell pellets after centrifugation, we observed a darker colour for the one expressing PDI-A. For this reason, the protein was purified under anaerobic conditions. The UV-visible absorption spectrum of the purified brownish protein exhibited two peaks around 320 and 420 nm and a shoulder at 460 nm which are likely characteristic of the presence of an iron-sulfur (Fe-S) cluster of the [Fe₂S₂] type (Fig 4A). The analytical measurement of iron and sulfide contents revealed 1.28 ± 0.13 Fe atoms and 1.10 ± 0.05 S atoms per monomer. Analytical gel filtration experiments showed a small part of aggregated protein and two major, not well separated, peaks with elution volumes at 7.91, 12.65 and 15.5 ml respectively (Fig 4B). Considering the theoretical molecular mass of PDI-A of *ca* 15 kDa, the peak at 12.65 ml corresponding to an apparent volume of *ca* 115 kDa may be interpreted as an octameric form and the one at 15.5 ml corresponding to an apparent volume of *ca* 27 kDa may be interpreted as a dimeric form. Both peaks contained PDI-A with Fe-S cluster as attested by the presence of the absorbance at 420 nm. Altogether, although, PDI-A seems to exist under various oligomeric forms, these results could be consistent with PDI-A binding a [Fe₂S₂] cluster into a dimer. The association of dimers may lead to this higher oligomeric form. Further spectroscopic analyses are however needed for a definitive assessment of the type(s) of cluster that PDI-A can incorporate.

The two catalytic domains of PDI-M do not possess equivalent oxidoreductase properties

In subsequent experiments, we focused our effort on the atypical PDI-M. Using PDI-M(a°) and PDI-M(a) variants, we have investigated the contribution of each catalytic domain to the PDI-M redox properties using the same assays *i.e.*, RNase A oxidative refolding, DTNB and insulin reduction, but also by testing activities typical of Trx *i.e.*, the capacity to activate the chloroplastic NADP-MDH, a well-characterized redox-regulated chloroplastic protein catalyzing the conversion of oxaloacetate to malate, and to sustain the peroxidase activity of a chloroplastic Prx belonging to the 2-Cys Prx subgroup by regenerating the reduced active form of the protein.

In the RNase A refolding assay, PDI-M(a°) presented an efficiency comparable to the one of PDI-M whereas PDI-M(a) exhibited only 50 to 60% of this activity after 15 minutes (Fig 5). This suggested that the a° module is likely the major contributor for the oxidase activity measured with the intact protein and that there may be a partial compensation by the second domain in the absence of the catalytic cysteines of the a° module.

Then, the reductase activity of the respective PDI-M domains was tested by assessing their capacity to reduce insulin and to activate NADP-MDH in the presence of DTT. In the insulin reduction assay, PDI-M(a) was more efficient than PDI-M(a°) (Fig 6A). In this case, the fact that the activity of both domains was decreased compared to the activity of PDI-M suggests that both domains contribute to the reductase activity of PDI-M although with different efficiencies. In the NADP-MDH activation assay, we observed that PDI-M was the only PDI representative able to activate the enzyme since PDI-A (data not shown) and PDI-L1a were unable to do that (Fig 6B). This was quite surprising taking into account the unfavourable thermodynamic barrier, NADP-MDH possesses disulfides with very negative redox potential, around -300 mV at pH 7.0 [36]. However, the observed activation was less efficient compared to the one observed at identical concentrations with Trx h1 used as a reference. The two

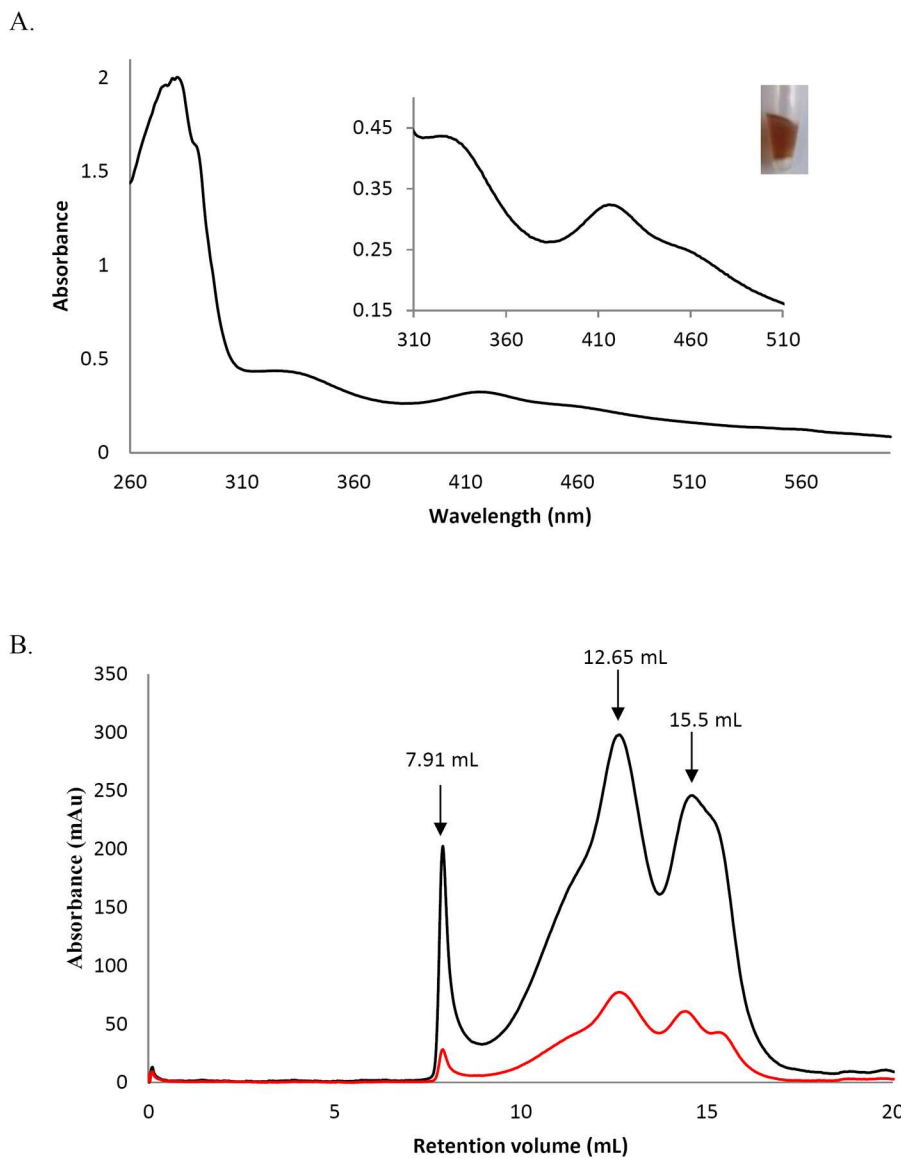


Fig 4. The recombinant PDI-A binds an Fe-S cluster. A. UV-visible absorption spectrum between 260 and 600 nm of anaerobically purified PDI-A. The blow-up shows absorbance bands between 310 and 510 nm characteristics of a [Fe₂-S₂] cluster and a picture of a tube containing the protein in its holoform. B. Analytical size-exclusion chromatography performed on a Sephadex S75 10–300 column using 100 μg and a 30 mM Tris-HCl pH 8.0, 200 mM NaCl buffer. The black curve corresponds to the absorbance at 280 nm and the red curve at 420 nm.

<https://doi.org/10.1371/journal.pone.0174753.g004>

PDI-M domains presented different reactivities toward oxidized NADP-MDH, PDI-M(*a*) was even slightly more active than PDI-M whereas PDI-M(*a*^o) was less active (Fig 6B). Altogether, these data indicated that the *a* module is a more efficient reductant than the *a*^o module.

The properties of PDI-M domains have been further examined using the DTNB assay and AtNTRB as an electron donor. The PDI-M(*a*^o) domain was as efficient as PDI-M whereas PDI-M(*a*) was only very poorly able to promote DTNB reduction (Fig 7A). To check whether this was due to the inability to be reduced by NTR or to reduce DTNB, insulin reduction assays have been performed with the NADPH/NTR system as the electron supplier instead of DTT

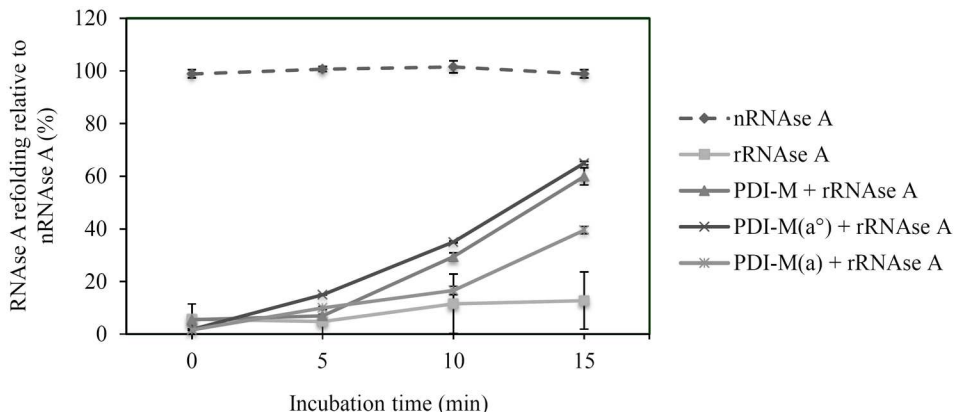


Fig 5. Oxidative refolding of reduced RNase A by the PDI-M catalytic domains. Results are represented as percentages relative to native RNase A (nRNase A) for the indicated time. The activity of the reduced and denatured RNase A (rRNase A) was tested alone or after incubation with PDI-M, PDI-M(a°) or PDI-M(a). Measurements were made in triplicate and error bars indicate standard deviation.

<https://doi.org/10.1371/journal.pone.0174753.g005>

(Fig 7B). The absence of activity for PDI-M(a), which was in fact the most efficient for insulin reduction when DTT was used as a reductant, obviously indicates that the a domain is not or only poorly reduced by NTR and that the catalytic disulfides of PDI-M are asymmetrically targeted by NTR. On the other hand, insulin reduction by PDI-M(a°) was less efficient than by PDI-M (Fig 7B). Since PDI-M(a°) and PDI-M had comparable efficiency for DTNB reduction, these results indicate that mutating the active site cysteines of the a domain may somehow affect the redox properties of the a° module (possibly at the level of the 3D structure or of substrate recognition (here insulin)) which incidentally suggests that these two adjacent domains are connected.

Finally, we have taken advantage of the NADPH-coupled NTR reduction system to examine the reduction of Prx by PDI-M. Indeed, it was shown recently that an ER-targeted human 2-Cys Prx (PrxIV) can accept electrons from two PDI isoforms, P5 and ERp46 [37, 38].

Although there is no evidence yet that a 2-Cys Prx is targeted to the ER in plants, we tested the biochemical capability of PDI-M to reduce the chloroplastic *Arabidopsis* 2-Cys Prx (At2-Cys Prx). As shown in Fig 8, PDI-M promoted the regeneration of At2-Cys Prx in the presence of the NADPH-NTR system as an electron donor. As expected from its poor reduction by AtNTRB, the PDI-M(a) was almost inefficient, only ca 10% activity was retained compared to PDI-M. The PDI-M(a°) retained about 50% activity. Such a decrease may again indicate that having mutated the active site cysteines of the a module impacted the a° module reactivity.

Discussion

Protein disulfide isomerases are versatile proteins catalyzing the reduction, formation and/or isomerisation of disulfide bonds *in vitro* and also possibly *in vivo* depending on the substrates, on their subcellular localizations and/or on the cellular and subcellular redox potentials. In connection with these elements and with the variety of substrates, there are multiple PDI with variable module arrangements which provide the necessary flexibility in the PDI activity pattern [39–41]. For multi-modular proteins, each domain could ensure a “specific” function. As an example, the b' module of mammalian ERp57 or PDI proteins, which is redox inactive, is essential for substrate or chaperone partner recruitment [13, 15, 42, 43]. By comparing the biochemical properties of plant PDI belonging to three different classes and with different

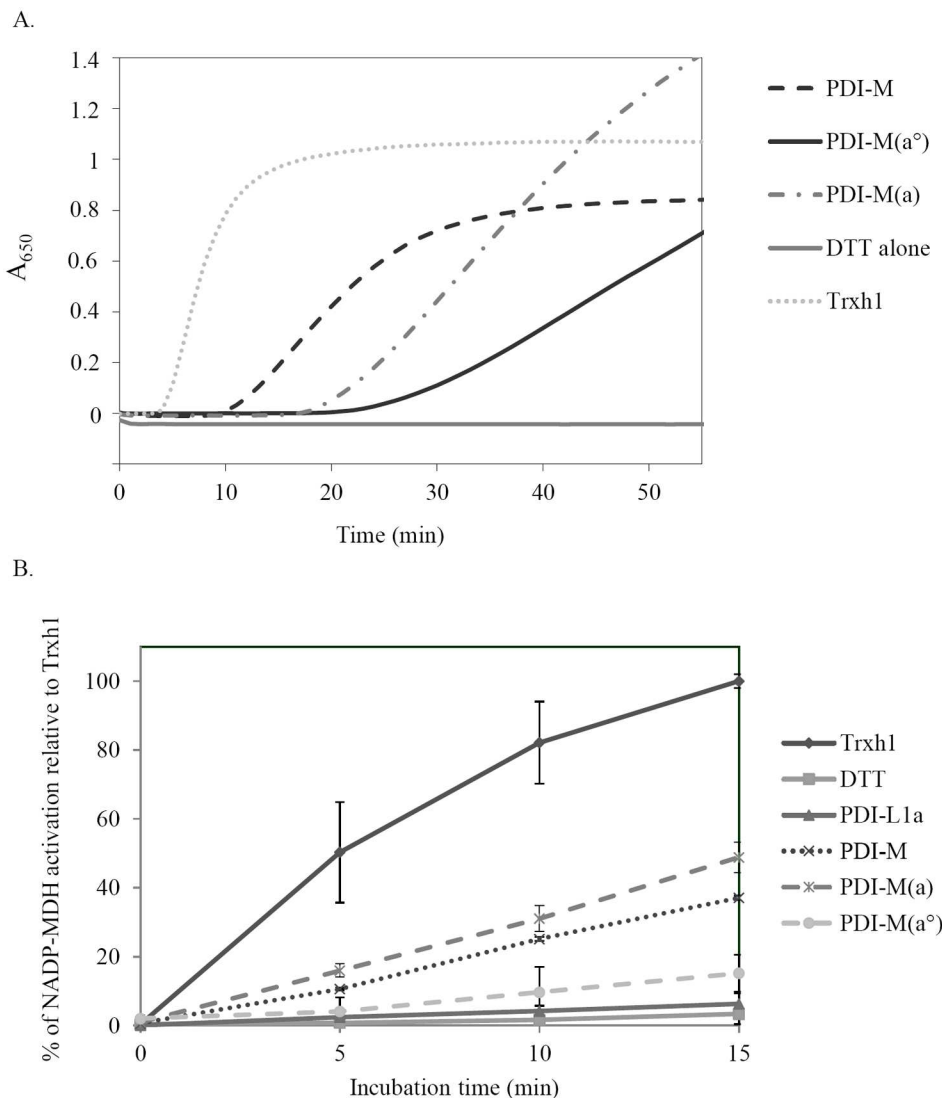


Fig 6. Reductase activity of the PDI-M catalytic domains. A. Insulin reduction was assayed by measuring the turbidity at 650 nm caused by its precipitation upon reduction using DTT alone or in the presence of 5 μM Trxh1, PDI-M, PDI-M(a°), PDI-M(a). As in Figs 3 and 5, PDI-M(a°) and PDI-M(a) refers to the PDI-M C165/168S and PDI-M C36/39S variants respectively. B. Activation of NADP-malate dehydrogenase. The NADP-MDH activity was followed by measuring the NADPH-coupled oxaloacetate conversion at 340 nm after a pre-incubation of the purified recombinant protein with DTT alone (solid line, squares) or in the presence of Trxh1 (solid line, diamonds), PDI-L1a (solid line, triangles), PDI-M (dotted line, crosses), PDI-M(a°) (dashed line, circles) and PDI-M(a') (dashed line, crosses) for the indicated time. The results have been represented as percentages relative to the maximal reactivation obtained with Trxh1 after 15 min. Measurements were made in triplicate and error bars indicate standard deviation.

<https://doi.org/10.1371/journal.pone.0174753.g006>

modular organisation, we also brought elements indicating that the catalytic domains within a given PDI or between PDI do not have the same redox properties.

What is the biochemical function of the single module PDI-A?

Using the battery of substrates tested, we did not detect any oxidase or reductase activity for the atypical mono-module PDI-A, which raises the question of its physiological role and

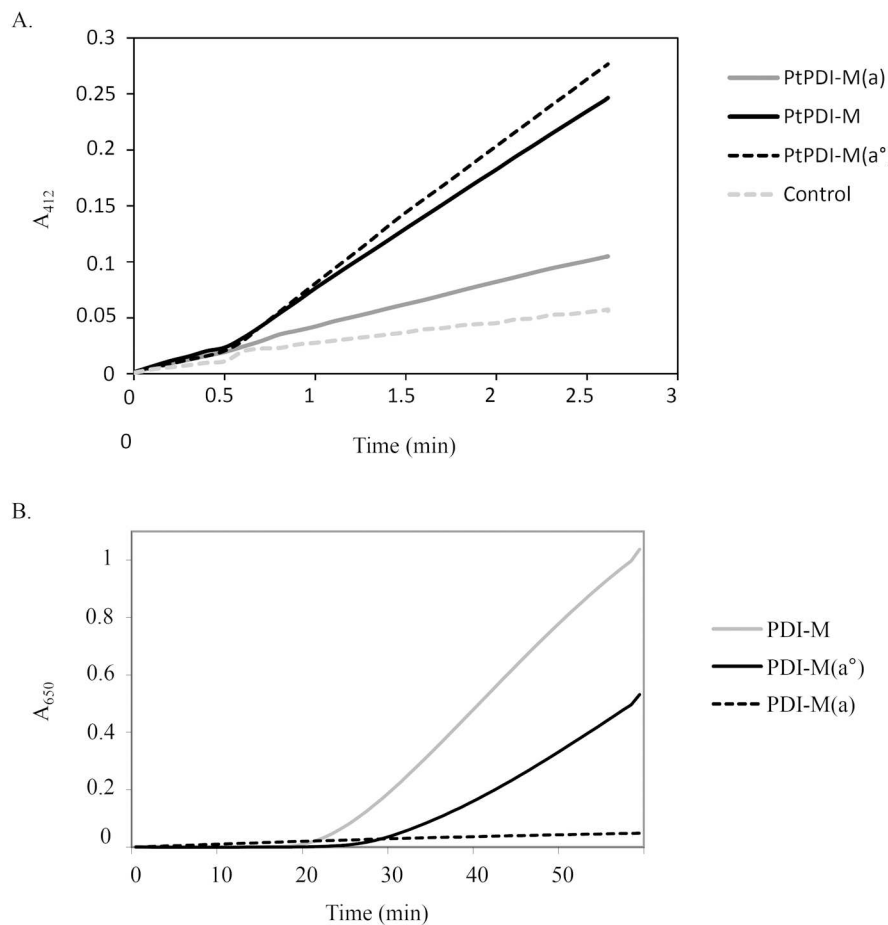


Fig 7. Reduction of the PDI-M catalytic domains by AtNTRB as assayed using DTNB and insulin. A. DTNB reduction assay. Representative kinetic curves obtained in the presence of NADPH and AtNTRB alone or with 0.2 μ M PDI-M, PDI-M(a°) or PDI-M(a). B. Insulin reduction assessed using NADPH/AtNTRB as an electron donor system and 5 μ M of PDI-M, PDI-M(a°) or PDI-M(a).

<https://doi.org/10.1371/journal.pone.0174753.g007>

partners. First, considering the DKDL C-terminal sequence, divergent from classical ER retention signals (very often KDEL or KEEL), the question of its subcellular localization is still open. It is worth mentioning that human ERp18, a small mono-domain PDI was shown to exhibit an oxidase activity on synthetic peptides [44]. However, despite their comparable modular organisation, PDI-A and ERp18 might not be true orthologs, exhibiting only *ca* 15% sequence identity. Proteins involved in oxidation reactions usually exhibit redox potentials ranging from less than -100 mV for some prokaryotic DsbA proteins to -180 mV for the a modules of classical PDI [41, 45, 46]. Hence, the E_m value of -170 mV determined for PDI-A is clearly compatible with oxidation reactions and should not be the reason for the absence of activity. So, why is PDI-A inactive? A first possible explanation could be that the transit peptide has been cleaved at an unfavourable position, eliminating some N-terminal residues essential for activity. However, this seems unlikely since we have cleaved only 26 amino acids in a region which is not conserved and without predicted secondary structure and the protein is fully soluble. Hence, the absence of reactivity is more likely linked to specific differences in the sequence of PDI-A compared to other PDI.

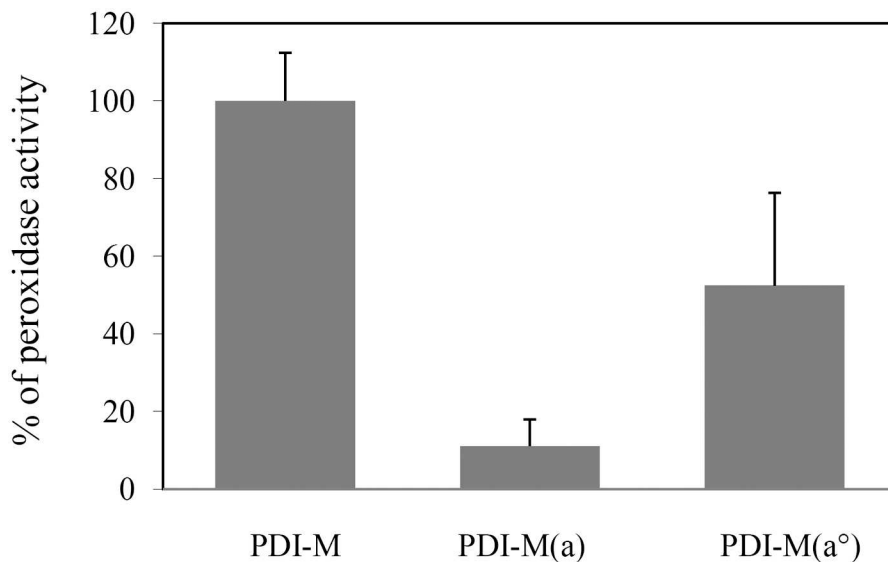


Fig 8. *In vitro* recycling of 2-Cys Prx by PDI-M. The peroxidase activity of *A. thaliana* 2-Cys Prx was assessed using a coupled assay measuring NADPH oxidation. Results obtained for PDI-M(a[°]) or PDI-M(a) are represented as percentages relative to the activity obtained with PDI-M fixed at 100%. Measurements were made in triplicate and error bars indicate standard deviation.

<https://doi.org/10.1371/journal.pone.0174753.g008>

First, the CVPWCKHC active site signature which is conserved in PDI-A orthologs replaces the usual [Y/F]APWCGHC (Fig 1). We initially thought that the presence of a charged residue between the two cysteines might be strongly unfavourable. However, we have observed that the atypical WCKHC, although influencing the redox midpoint potential, was not responsible for the absence of activity. In fact, there are many other sequence variations that would explain the lack of oxidoreductase activity. First, the FA or YA pair, found in the above-mentioned signature and usually quite conserved in PDI, is replaced by a CV pair. Then, among the three residues (Glu, Lys, Arg, highlighted in Fig 1) susceptible of contributing to the lowering the pKa of the catalytic cysteines in some Trxs, only the Arg is present in PDI-A [32, 33, 47]. The two other residues (Glu, Lys) are replaced by residues with an opposite charge (Lys, Glu) in PDI-A (Fig 1A). From its absence in PDI-M and the work performed on *E. coli* Trx1, the Lys does not seem to be as important as the Glu and might thus not be absolutely required [33]. Besides these sequence variations, it is still possible that we have not used proper substrates yet in our *in vitro* assays and that this protein possesses highly specific physiological partners. Alternatively, it may have evolved to play a completely different function, unrelated to dithiol-disulfide exchanges. The observation that PDI-A can incorporate a [Fe₂S₂] cluster was totally unexpected because this has to our knowledge never been observed for a PDI member. It appears a bit less surprising when taking into account that proteins sharing the same thioredoxin fold, *i.e.* some thioredoxins or glutaredoxins, including the ER-targeted GRX6 isoform of *S. cerevisiae*, are able to do this [48–51]. However, the physiological relevance of this observation is unclear and it remains to be investigated whether such cluster is not an artefact linked to *E. coli* expression and can indeed be formed in plant cells. It would also be important to determine the subcellular localization of the protein, because Fe-S cluster maturation systems are only found in organelles and in the cytosol, not in the ER [52].

Does the domain organisation of PDI confer them different biochemical properties?

The second aim of the study was the biochemical characterization of a poplar PDI-M isoform possessing an a^o-a-b domain organisation quite different from the $a-b-b'-a'$ of the classical and well-characterized PDI-L. In particular, the organisation of the catalytic domains in tandem raises the question of their respective contribution to protein reactivity and of their possible connectivity. The latter point is in fact one of the unsolved questions for most PDI, although such cooperativity has been proposed based on the U shape arrangement of the four Trx domains of the yeast PDI1p, very similar to DsbC or DsbG [41]. We have compared the PDI-L1a and PDI-M capacity to reduce insulin and NADP-MDH or to oxidize NTR and RNase-A. It was previously reported that some PDI can act as oxidants of NTR or in other words that NTR can reduce oxidized PDI [53].

Except for the NADP-MDH activation assay, where it was not active at all, PDI-L1a was always more efficient than PDI-M in all other assays measuring reductase or oxidase activities. This difference of activity observed with poplar proteins is similar to what was recently observed with rice orthologs, indicating that this may be a general feature of these two classes [40]. The better efficiency of PDI-L1a, in particular in reduction assays, may be explained by the strict conservation of the charged amino acids required for decreasing the pKa of the N-terminal catalytic cysteine. Indeed, both a modules of PDI-L1a possess the usual Glu and Lys residues, whereas both domains of PDI-M contain the Glu but an Ala and a His in the a^o and a modules respectively (Fig 1). That PDI-L1a was inactive towards NADP-MDH whereas PDI-M exhibited noticeable activities could possibly derive from a natural tendency to interact with non-folded or folded proteins respectively. Indeed, it was shown for mammalian enzymes that PDI-L interact directly with misfolded or unfolded proteins via the mediation of a hydrophobic patch in the b' module, whereas P5 proteins, the mammalian PDI-M orthologs, are partners of the BiP chaperone, a folded protein, which is thought to bring mis-oxidized/misfolded proteins to P5 for their correct oxidative folding [54]. Hence, by analogy and despite a lower “intrinsic” reductase activity compared to PDI-L1a, PDI-M could interact with and promote the activation of native proteins such as NADP-MDH. In agreement with the difference observed in their *in vitro* biochemical properties, it was shown by genetic studies that a rice PDI-M ortholog, OsPDI2.3, and a rice PDI-L ortholog, PDIL1.1 do not have redundant functions in the ER, having for instance different storage proteins as substrates in the endosperm [21].

These dual and opposite oxidase/reductase activities observed *in vitro* raise the question of their physiological relevance and occurrence. The *in vivo* measurement of the redox state of PDI in HEK-293 cells showed for instance a mixture of fully reduced (50%), fully oxidized (16%) and partially oxidized forms of the a or a' modules (18/15%) [55]. These results indicate first that neither of the two domains of this human PDI might exclusively catalyze substrate oxidation or reduction, but also that the protein redox state may be adequate for both reactions. This potential dual function has been nicely illustrated recently by demonstrating that several PDI can reduce ER-resident proteins as 2-Cys Prx (PrxIV) or vitamin K epoxide reductase [37, 56–58]. This alternative route of PDI oxidation which would occur independently of ERO1 protein *i.e.*, without producing H₂O₂, should clearly decrease reactive oxygen species formation in the ER [59].

Are there specific contributions and/or connections between the catalytic domains in multi-domain PDI?

It is documented that the a' module (the C-terminal one) of a human regular PDI-L, which presents the highest redox potential (*ca* -150 mV), possesses a preponderant oxidase activity

toward reduced and scrambled RNase A [41]. Also, it was shown that only one of the catalytic disulfides of this PDI is directly oxidized by Ero1 α and with a slow turnover rate [39]. With the above-mentioned evidence showing the complexity of assessing and interpreting the *in vivo* redox state [55], these elements suggest that the presence of two catalytic a domains might be important for the formation of native disulfides in proteins entering the secretory pathway by ensuring either oxidase or isomerase reactions.

Although experiments have not been achieved with poplar PDI-L1a, we have observed such a duality among the a domains in PDI-M. The a module, having the cysteine pairs with the lowest redox potential (-170 mV) is the most efficient for reduction reactions (insulin, NADP-MDH) (Figs 6 and 7). On the contrary, the a° module, having the cysteine pairs with the highest redox potential (-150 mV), is more efficient for oxidation reaction than the a module, promoting the recovery of RNase A activity similar to PDI-M levels. Accordingly, the a° module of orthologs (rice PDI2,3 and mammalian P5) is also the major contributor in the oxidative refolding of reduced or scrambled RNase A [40, 60]. In line with this observation, the a° module can efficiently oxidize NTR contrary to the a module. The incapacity of the a module to oxidize NTR or RNase A may relate to steric hindrance or unfavourable protein/protein interactions rather than to thermodynamic factors, the redox potentials of both domains being still rather close. The structure of the *E. coli* NTR-Trx complex indicated that Trx interacts with NTR mostly via hydrophobic residues (W33, I60, G74 and I75) and via R73 [61]. By comparing all a domains of PDI-L1a and PDI-M, it is interesting to note that two of these five residues differ in the a domain of PDI-M compared to the three other a domains analyzed where they are all strictly similar (not shown). Hence, it is tempting to attribute the inability of the a domain of PDI-M to interact with NTR to these changes. Another possible explanation could rely on steric factors. In PDI-L1a, if it adopts a regular structure, the two a domains should be found at the extremity of the U-shape structure and thus be very likely accessible to NTR. On the contrary, the fact that the two a domains in PDI-M are adjacent and that the a domain is sandwiched between the a° and b domains may be problematic for the accessibility of NTR which is an homodimer of two identical 35 kDa subunits.

In the course of these experiments and taking advantage of the fact that the a° module of PDI-M is reduced by AtNTRB whereas the a module is not or very poorly, we have observed some sort of cross-talk or interference between both domains. Indeed, PDI-M(a°) is as efficient as PDI-M in the assay with the small DTNB molecule (Fig 7A) whereas it is much less efficient with insulin and 2-Cys Prx, retaining about 50% activity (Fig 7B and 7C). Thus, it may be that the presence of a redox active a module is needed for a maximal efficiency of the a° module with some substrates. Alternatively, introducing cysteine substitutions in the a module may have generated subtle conformational changes which hamper recognition of large substrates by the a° module. These substitutions may have more impact in PDI-M because the two catalytic domains are adjacent.

Author Contributions

Conceptualization: BS JC JPJ NR.

Formal analysis: BS FZ.

Funding acquisition: JPJ NR.

Investigation: BS FZ.

Methodology: BS.

Project administration: JC NR.

Validation: JC NR.

Visualization: BS FZ.

Writing – original draft: BS JPJ NR.

Writing – review & editing: FZ JC.

References

1. Grimshaw JP, Stirnimann CU, Brozzo MS, Malojcic G, Grutter MG, Capitani G, et al. DsBL and DsBL form a specific dithiol oxidase system for periplasmic arylsulfate sulfotransferase in uropathogenic *Escherichia coli*. *J Mol Biol*. 2008; 380(4):667–80. <https://doi.org/10.1016/j.jmb.2008.05.031> PMID: 18565543
2. Inaba K. Disulfide bond formation system in *Escherichia coli*. *J Biochem*. 2009; 146(5):591–7. <https://doi.org/10.1093/jb/mvp102> PMID: 19567379
3. Arts IS, Gennaris A, Collet JF. Reducing systems protecting the bacterial cell envelope from oxidative damage. *FEBS Lett*. 2015; 589(14):1559–68. <https://doi.org/10.1016/j.febslet.2015.04.057> PMID: 25957772
4. Depuydt M, Leonard SE, Vertommen D, Denoncin K, Morsomme P, Wahni K, et al. A periplasmic reducing system protects single cysteine residues from oxidation. *Science*. 2009; 326(5956):1109–11. <https://doi.org/10.1126/science.1179557> PMID: 19965429
5. Selles B, Jacquot JP, Rouhier N. Comparative genomic study of protein disulfide isomerases from photosynthetic organisms. *Genomics*. 2011; 97(1):37–50. <https://doi.org/10.1016/j.ygeno.2010.10.001> PMID: 20951197
6. Alon A, Grossman I, Gat Y, Kodali VK, DiMaio F, Mehlman T, et al. The dynamic disulphide relay of quiescin sulphhydryl oxidase. *Nature*. 2012; 488(7411):414–8. <https://doi.org/10.1038/nature11267> PMID: 22801504
7. Kodali VK, Thorpe C. Oxidative protein folding and the Quiescin-sulphydryl oxidase family of flavoproteins. *Antioxid Redox Signal*. 2010; 13(8):1217–30. <https://doi.org/10.1089/ars.2010.3098> PMID: 20136510
8. Okuda A, Matsusaki M, Higashino Y, Masuda T, Urade R. Disulfide bond formation activity of soybean quiescin sulfhydryl oxidase. *Febs J*. 2014; 281(23):5341–55. <https://doi.org/10.1111/febs.13079> PMID: 25265152
9. Riemer J, Bulleid N, Herrmann JM. Disulfide formation in the ER and mitochondria: two solutions to a common process. *Science*. 2009; 324(5932):1284–7. <https://doi.org/10.1126/science.1170653> PMID: 19498160
10. Collet JF, Messens J. Structure, function, and mechanism of thioredoxin proteins. *Antioxid Redox Signal*. 2010; 13(8):1205–16. <https://doi.org/10.1089/ars.2010.3114> PMID: 20136512
11. Pedone E, Limauro D, D'Ambrosio K, De Simone G, Bartolucci S. Multiple catalytically active thioredoxin folds: a winning strategy for many functions. *Cell Mol Life Sci*. 2010; 67(22):3797–814. <https://doi.org/10.1007/s00018-010-0449-9> PMID: 20625793
12. Wang C, Yu J, Huo L, Wang L, Feng W, Wang CC. Human protein-disulfide isomerase is a redox-regulated chaperone activated by oxidation of domain a'. *J Biol Chem*. 2012; 287(2):1139–49. <https://doi.org/10.1074/jbc.M111.303149> PMID: 22090031
13. Yagi-Utsumi M, Satoh T, Kato K. Structural basis of redox-dependent substrate binding of protein disulfide isomerase. *Sci Rep*. 2015; 5:13909. <https://doi.org/10.1038/srep13909> PMID: 26350503
14. Appenzeller-Herzog C, Ellgaard L. The human PDI family: versatility packed into a single fold. *Biochim Biophys Acta*. 2008; 1783(4):535–48. <https://doi.org/10.1016/j.bbamcr.2007.11.010> PMID: 18093543
15. Kozlov G, Maattanen P, Thomas DY, Gehring K. A structural overview of the PDI family of proteins. *Febs J*. 2010; 277(19):3924–36. <https://doi.org/10.1111/j.1742-4658.2010.07793.x> PMID: 20796029
16. Houston NL, Fan C, Xiang JQ, Schulze JM, Jung R, Boston RS. Phylogenetic analyses identify 10 classes of the protein disulfide isomerase family in plants, including single-domain protein disulfide isomerase-related proteins. *Plant Physiol*. 2005; 137(2):762–78. <https://doi.org/10.1104/pp.104.056507> PMID: 15684019
17. Iwasaki K, Kamauchi S, Wadahama H, Ishimoto M, Kawada T, Urade R. Molecular cloning and characterization of soybean protein disulfide isomerase family proteins with nonclassic active center motifs. *Febs J*. 2009; 276(15):4130–41. <https://doi.org/10.1111/j.1742-4658.2009.07123.x> PMID: 19583593
18. Kamauchi S, Wadahama H, Iwasaki K, Nakamoto Y, Nishizawa K, Ishimoto M, et al. Molecular cloning and characterization of two soybean protein disulfide isomerases as molecular chaperones for seed

- storage proteins. *Febs J.* 2008; 275(10):2644–58. <https://doi.org/10.1111/j.1742-4658.2008.06412.x> PMID: 18422652
19. Wadahama H, Kamauchi S, Ishimoto M, Kawada T, Urade R. Protein disulfide isomerase family proteins involved in soybean protein biogenesis. *Febs J.* 2007; 274(3):687–703. <https://doi.org/10.1111/j.1742-4658.2006.05613.x> PMID: 17181539
20. Onda Y, Kumamaru T, Kawagoe Y. ER membrane-localized oxidoreductase Ero1 is required for disulfide bond formation in the rice endosperm. *Proc Natl Acad Sci U S A.* 2009; 106(33):14156–61. <https://doi.org/10.1073/pnas.0904429106> PMID: 19666483
21. Onda Y, Nagamine A, Sakurai M, Kumamaru T, Ogawa M, Kawagoe Y. Distinct roles of protein disulfide isomerase and P5 sulfhydryl oxidoreductases in multiple pathways for oxidation of structurally diverse storage proteins in rice. *Plant Cell.* 2011; 23(1):210–23. <https://doi.org/10.1105/tpc.110.079509> PMID: 21278127
22. Wadahama H, Kamauchi S, Nakamoto Y, Nishizawa K, Ishimoto M, Kawada T, et al. A novel plant protein disulfide isomerase family homologous to animal P5—molecular cloning and characterization as a functional protein for folding of soybean seed-storage proteins. *Febs J.* 2008; 275(3):399–410. <https://doi.org/10.1111/j.1742-4658.2007.06199.x> PMID: 18167147
23. Kim J, Mayfield SP. The active site of the thioredoxin-like domain of chloroplast protein disulfide isomerase, RB60, catalyzes the redox-regulated binding of chloroplast poly(A)-binding protein, RB47, to the 5' untranslated region of psbA mRNA. *Plant Cell Physiol.* 2002; 43(10):1238–43. PMID: 12407204
24. Yang P, Lupken T, Habekuss A, Hensel G, Steuernagel B, Kilian B, et al. PROTEIN DISULFIDE ISOMERASE LIKE 5–1 is a susceptibility factor to plant viruses. *Proc Natl Acad Sci U S A.* 2014; 111(6):2104–9. <https://doi.org/10.1073/pnas.1320362111> PMID: 24481254
25. Couturier J, Didierjean C, Jacquot JP, Rouhier N. Engineered mutated glutaredoxins mimicking peculiar plant class III glutaredoxins bind iron-sulfur centers and possess reductase activity. *Biochem Biophys Res Commun.* 2010; 403(3–4):435–41. <https://doi.org/10.1016/j.bbrc.2010.11.050> PMID: 21094149
26. Hirasawa M, Schurmann P, Jacquot JP, Manieri W, Jacquot P, Keryer E, et al. Oxidation-reduction properties of chloroplast thioredoxins, ferredoxin:thioredoxin reductase, and thioredoxin f-regulated enzymes. *Biochemistry.* 1999; 38(16):5200–5. <https://doi.org/10.1021/bi982783v> PMID: 10213627
27. Krimm I, Lemaire S, Ruelland E, Miginiac-Maslow M, Jaquot JP, Hirasawa M, et al. The single mutation Trp35→Ala in the 35–40 redox site of *Chlamydomonas reinhardtii* thioredoxin h affects its biochemical activity and the pH dependence of C36-C39 1H-13C NMR. *Eur J Biochem.* 1998; 255(1):185–95. PMID: 9692918
28. Lyles MM, Gilbert HF. Catalysis of the oxidative folding of ribonuclease A by protein disulfide isomerase: pre-steady-state kinetics and the utilization of the oxidizing equivalents of the isomerase. *Biochemistry.* 1991; 30(3):619–25. PMID: 1988051
29. Couturier J, Koh CS, Zaffagnini M, Winger AM, Gualberto JM, Corbier C, et al. Structure-function relationship of the chloroplastic glutaredoxin S12 with an atypical WCSYS active site. *J Biol Chem.* 2009; 284(14):9299–310. <https://doi.org/10.1074/jbc.M807998200> PMID: 19158074
30. Navrot N, Collin V, Gualberto J, Gelhaye E, Hirasawa M, Rey P, et al. Plant glutathione peroxidases are functional peroxiredoxins distributed in several subcellular compartments and regulated during biotic and abiotic stresses. *Plant Physiol.* 2006; 142(4):1364–79. <https://doi.org/10.1104/pp.106.089458> PMID: 17071643
31. Issakidis E, Lemaire M, Decottignies P, Jacquot JP, Miginiac-Maslow M. Direct evidence for the different roles of the N- and C-terminal regulatory disulfides of sorghum leaf NADP-malate dehydrogenase in its activation by reduced thioredoxin. *FEBS Lett.* 1996; 392(2):121–4. PMID: 8772188
32. Lappi AK, Lensink MF, Alanen HI, Salo KE, Lobell M, Juffer AH, et al. A conserved arginine plays a role in the catalytic cycle of the protein disulphide isomerases. *J Mol Biol.* 2004; 335(1):283–95. PMID: 14659757
33. Dyson HJ, Jeng MF, Tenant LL, Slaby I, Lindell M, Cui DS, et al. Effects of buried charged groups on cysteine thiol ionization and reactivity in *Escherichia coli* thioredoxin: structural and functional characterization of mutants of Asp 26 and Lys 57. *Biochemistry.* 1997; 36(9):2622–36. <https://doi.org/10.1021/bi961801a> PMID: 9054569
34. Chibani K, Tarrago L, Gualberto JM, Wingsle G, Rey P, Jacquot JP, et al. Atypical thioredoxins in poplar: the glutathione-dependent thioredoxin-like 2.1 supports the activity of target enzymes possessing a single redox active cysteine. *Plant Physiol.* 2012; 159(2):592–605. <https://doi.org/10.1104/pp.112.197723> PMID: 22523226
35. Ren G, Stephan D, Xu Z, Zheng Y, Tang D, Harrison RS, et al. Properties of the thioredoxin fold superfamily are modulated by a single amino acid residue. *J Biol Chem.* 2009; 284(15):10150–9. <https://doi.org/10.1074/jbc.M809509200> PMID: 19181668

36. Hirasawa M, Ruelland E, Schepens I, Issakidis-Bourguet E, Miginiac-Maslow M, Knaff DB. Oxidation-reduction properties of the regulatory disulfides of sorghum chloroplast nicotinamide adenine dinucleotide phosphate-malate dehydrogenase. *Biochemistry*. 2000; 39(12):3344–50. PMID: [10727227](#)
37. Tavender TJ, Springate JJ, Bulleid NJ. Recycling of peroxiredoxin IV provides a novel pathway for disulphide formation in the endoplasmic reticulum. *Embo J*. 2010; 29(24):4185–97. <https://doi.org/10.1038/emboj.2010.273> PMID: [21057456](#)
38. Zhu L, Yang K, Wang X, Wang CC. A novel reaction of peroxiredoxin 4 towards substrates in oxidative protein folding. *PLoS One*. 2014; 9(8):e105529. <https://doi.org/10.1371/journal.pone.0105529> PMID: [25137134](#)
39. Chambers JE, Tavender TJ, Oka OB, Warwood S, Knight D, Bulleid NJ. The reduction potential of the active site disulfides of human protein disulfide isomerase limits oxidation of the enzyme by Ero1alpha. *J Biol Chem*. 2010; 285(38):29200–7. <https://doi.org/10.1074/jbc.M110.156596> PMID: [20657012](#)
40. Onda Y, Kobori Y. Differential activity of rice protein disulfide isomerase family members for disulfide bond formation and reduction. *FEBS Open Bio*. 2014; 4:730–4. <https://doi.org/10.1016/j.fob.2014.07.007> PMID: [25161881](#)
41. Tian G, Xiang S, Noiva R, Lennarz WJ, Schindelin H. The crystal structure of yeast protein disulfide isomerase suggests cooperativity between its active sites. *Cell*. 2006; 124(1):61–73. <https://doi.org/10.1016/j.cell.2005.10.044> PMID: [16413482](#)
42. Kozlov G, Maattanen P, Schrag JD, Pollock S, Cygler M, Nagar B, et al. Crystal structure of the bb' domains of the protein disulfide isomerase ERp57. *Structure*. 2006; 14(8):1331–9. <https://doi.org/10.1016/j.str.2006.06.019> PMID: [16905107](#)
43. Maattanen P, Kozlov G, Gehring K, Thomas DY. ERp57 and PDI: multifunctional protein disulfide isomerases with similar domain architectures but differing substrate-partner associations. *Biochemistry and cell biology*. 2006; 84(6):881–9. <https://doi.org/10.1139/o06-186> PMID: [17215875](#)
44. Alanen HI, Williamson RA, Howard MJ, Lappi AK, Jantti HP, Rautio SM, et al. Functional characterization of ERp18, a new endoplasmic reticulum-located thioredoxin superfamily member. *J Biol Chem*. 2003; 278(31):28912–20. <https://doi.org/10.1074/jbc.M304598200> PMID: [12761212](#)
45. Hatahet F, Ruddock LW. Protein disulfide isomerase: a critical evaluation of its function in disulfide bond formation. *Antioxid Redox Signal*. 2009; 11(11):2807–50. <https://doi.org/10.1089/ARS.2009.2466> PMID: [19476414](#)
46. Lafaye C, Iwema T, Carpentier P, Jullian-Binard C, Kroll JS, Collet JF, et al. Biochemical and structural study of the homologues of the thiol-disulfide oxidoreductase DsbA in *Neisseria meningitidis*. *J Mol Biol*. 2009; 392(4):952–66. <https://doi.org/10.1016/j.jmb.2009.07.056> PMID: [19631659](#)
47. Menchise V, Corbier C, Didierjean C, Saviano M, Benedetti E, Jacquot JP, et al. Crystal structure of the wild-type and D30A mutant thioredoxin h of *Chlamydomonas reinhardtii* and implications for the catalytic mechanism. *Biochem J*. 2001; 359(Pt 1):65–75. PMID: [11563970](#)
48. Bisio H, Bonilla M, Manta B, Grana M, Salzman V, Aguilar PS, et al. A New Class of Thioredoxin-Related Protein Able to Bind Iron-Sulfur Clusters. *Antioxid Redox Signal*. 2015.
49. Couturier J, Stroher E, Albetel AN, Roret T, Muthuramalingam M, Tarrago L, et al. Arabidopsis chloroplastic glutaredoxin C5 as a model to explore molecular determinants for iron-sulfur cluster binding into glutaredoxins. *J Biol Chem*. 2011; 286(31):27515–27. <https://doi.org/10.1074/jbc.M111.228726> PMID: [21632542](#)
50. Mesecke N, Mittler S, Eckers E, Herrmann JM, Deponte M. Two novel monothiol glutaredoxins from *Saccharomyces cerevisiae* provide further insight into iron-sulfur cluster binding, oligomerization, and enzymatic activity of glutaredoxins. *Biochemistry*. 2008; 47(5):1452–63. <https://doi.org/10.1021/bi7017865> PMID: [18171082](#)
51. Rouhier N, Unno H, Bandyopadhyay S, Masip L, Kim SK, Hirasawa M, et al. Functional, structural, and spectroscopic characterization of a glutathione-ligated [2Fe-2S] cluster in poplar glutaredoxin C1. *Proc Natl Acad Sci U S A*. 2007; 104(18):7379–84. <https://doi.org/10.1073/pnas.0702268104> PMID: [17460036](#)
52. Couturier J, Touraine B, Briat JF, Gaymard F, Rouhier N. The iron-sulfur cluster assembly machineries in plants: current knowledge and open questions. *Front Plant Sci*. 2013; 4:259. <https://doi.org/10.3389/fpls.2013.00259> PMID: [23898337](#)
53. Lundström-Ljung J, Birnbach U, Rupp K, Soling HD, Holmgren A. Two resident ER-proteins, CaBP1 and CaBP2, with thioredoxin domains, are substrates for thioredoxin reductase: comparison with protein disulfide isomerase. *FEBS Lett*. 1995; 357(3):305–8. PMID: [7835433](#)
54. Jessop CE, Watkins RH, Simmons JJ, Tasab M, Bulleid NJ. Protein disulphide isomerase family members show distinct substrate specificity: P5 is targeted to BiP client proteins. *J Cell Sci*. 2009; 122(Pt 23):4287–95. <https://doi.org/10.1242/jcs.059154> PMID: [19887585](#)

55. Appenzeller-Herzog C, Ellgaard L. In vivo reduction-oxidation state of protein disulfide isomerase: the two active sites independently occur in the reduced and oxidized forms. *Antioxid Redox Signal*. 2008; 10(1):55–64. <https://doi.org/10.1089/ars.2007.1837> PMID: 17939758
56. Schulman S, Wang B, Li W, Rapoport TA. Vitamin K epoxide reductase prefers ER membrane-anchored thioredoxin-like redox partners. *Proc Natl Acad Sci U S A*. 2010; 107(34):15027–32. <https://doi.org/10.1073/pnas.1009972107> PMID: 20696932
57. Tavender TJ, Sheppard AM, Bulleid NJ. Peroxiredoxin IV is an endoplasmic reticulum-localized enzyme forming oligomeric complexes in human cells. *Biochem J*. 2008; 411(1):191–9. <https://doi.org/10.1042/BJ20071428> PMID: 18052930
58. Wajih N, Hutson SM, Wallin R. Disulfide-dependent protein folding is linked to operation of the vitamin K cycle in the endoplasmic reticulum. A protein disulfide isomerase-VKORC1 redox enzyme complex appears to be responsible for vitamin K1 2,3-epoxide reduction. *J Biol Chem*. 2007; 282(4):2626–35. <https://doi.org/10.1074/jbc.M608954200> PMID: 17124179
59. Gross E, Kastner DB, Kaiser CA, Fass D. Structure of Ero1p, source of disulfide bonds for oxidative protein folding in the cell. *Cell*. 2004; 117(5):601–10. PMID: 15163408
60. Kikuchi M, Doi E, Tsujimoto I, Horibe T, Tsujimoto Y. Functional analysis of human P5, a protein disulfide isomerase homologue. *J Biochem*. 2002; 132(3):451–5. PMID: 12204115
61. Lennon BW, Williams CH Jr., Ludwig ML. Twists in catalysis: alternating conformations of *Escherichia coli* thioredoxin reductase. *Science*. 2000; 289(5482):1190–4. PMID: 10947986

Erv1 of *Arabidopsis thaliana* can directly oxidize mitochondrial intermembrane space proteins in the absence of redox-active Mia40

Valentina Peleh¹, Flavien Zannini², Sandra Backes¹, Nicolas Rouhier² and Johannes M. Herrmann¹

¹Cell Biology, University of Kaiserslautern, Erwin-Schrödinger-Strasse 13, 67663 Kaiserslautern, Germany

²Université de Lorraine, Inra, IAM, F-54000 Nancy, France.

Article publié dans BMC biology

L'import de la plupart des protéines au sein de l'espace intermembranaire des mitochondries (IMS) est couplé à leur repliement oxydatif, processus catalysé par les protéines MIA40 et ERV1. Les données publiées concernant les orthologues de plantes suggéraient des différences fonctionnelles importantes mais certains résultats, notamment les complémentations de mutants de levure, paraissaient surprenants. Ce travail avait pour but de réexaminer la fonction d'AtERV1. Les résultats obtenus démontrent la capacité de la protéine AtERV1 à complémer partiellement le mutant *erv1* de levure, contrairement à ce qui avait été publié. Cette complémentation partielle est liée à l'incapacité d'AtERV1 à régénérer efficacement ScMia40 *in vivo* bien que les protéines puissent interagir. De manière originale, AtERV1 complémente aussi un mutant *mia40* de levure s'il est exprimé en présence d'une version de MIA40 dépourvue de ses propriétés redox mais conservant sa fonction de chaperon, indiquant qu'AtERV1 est capable d'oxyder certains substrats de MIA40 de levure *in vivo*. Cette particularité pourrait expliquer l'absence de phénotype du mutant *mia40* chez *A. thaliana*. Plus globalement, cette étude met en lumière l'existence de variations fonctionnelles dans le couple MIA40 et ERV1 chez les plantes et étaye un modèle évolutif intermédiaire où MIA40 est présente (contrairement à de nombreux protistes) mais pas essentielle du fait de la singularité biochimique et structurale de l'oxydase ERV1.

RESEARCH ARTICLE

Open Access



Erv1 of *Arabidopsis thaliana* can directly oxidize mitochondrial intermembrane space proteins in the absence of redox-active Mia40

Valentina Peleh¹, Flavien Zannini², Sandra Backes¹, Nicolas Rouhier^{2*} and Johannes M. Herrmann^{1*}

Abstract

Background: Many proteins of the mitochondrial intermembrane space (IMS) contain structural disulfide bonds formed by the mitochondrial disulfide relay. In fungi and animals, the sulfhydryl oxidase Erv1 ‘generates’ disulfide bonds that are passed on to the oxidoreductase Mia40, which oxidizes substrate proteins. A different structural organization of plant Erv1 proteins compared to that of animal and fungal orthologs was proposed to explain its inability to complement the corresponding yeast mutant.

Results: Herein, we have revisited the biochemical and functional properties of *Arabidopsis thaliana* Erv1 by both in vitro reconstituted activity assays and complementation of *erv1* and *mia40* yeast mutants. These mutants were viable, however, they showed severe defects in the biogenesis of IMS proteins. The plant Erv1 was unable to oxidize yeast Mia40 and rather even blocked its activity. Nevertheless, it was able to mediate the import and folding of mitochondrial proteins.

Conclusions: We observed that plant Erv1, unlike its homologs in fungi and animals, can promote protein import and oxidative protein folding in the IMS independently of the oxidoreductase Mia40. In accordance to the absence of Mia40 in many protists, our study suggests that the mitochondrial disulfide relay evolved in a stepwise reaction from an Erv1-only system to which Mia40 was added in order to improve substrate specificity.

Keywords: Disulfide bond formation, Eukaryotic evolution, Intermembrane space, Mitochondria, Oxidative protein folding, Protein translocation

Background

Two compartments of the eukaryotic cell, namely the endoplasmic reticulum (ER) and the mitochondrial intermembrane space (IMS), contain disulfide relays to introduce structural disulfide bonds into proteins and to facilitate oxidative protein folding [1]. In the ER, proteins are oxidized by direct interaction with members of the protein disulfide isomerase (PDI) family, which are maintained in an oxidized state by the sulfhydryl oxidase Ero1

[2]. Thus, PDIs provide substrate specificity whereas Ero1 initially ‘generates’ the disulfides [3, 4].

The function of the mitochondrial disulfide relay is less well understood. The sulfhydryl oxidase of the IMS, Erv1, is a flavoprotein just like Ero1. Although not structurally related, the architecture of the flavodomain of Erv1 family members is similar to that of Ero1, presumably as a result of convergent evolution [5–8]. Unlike PDIs, the mitochondrial oxidoreductase Mia40 has no thioredoxin fold and its structure is entirely different to that of PDI. Mia40 has a hydrophobic substrate-binding cleft that recognizes patterns of hydrophobic residues in helical regions of its substrates, referred to as mitochondrial intermembrane space sorting signal (MISS) or intermembrane space targeting signal (ITS) sequences [9–17]. This interaction drives the

* Correspondence: nicolas.rouhier@univ-lorraine.fr; hannes.herrmann@biologie.uni-kl.de

²Unité Mixte de Recherches 1136 Interactions Arbres-Microorganismes, Université de Lorraine/INRA, Faculté des sciences et technologies, 54500 Vandoeuvre-lès-Nancy, Nancy, France

¹Cell Biology, University of Kaiserslautern, Erwin-Schrödinger-Strasse 13, 67663 Kaiserslautern, Germany

© Herrmann et al. 2017 **Open Access** This article is distributed under the terms of the Creative Commons Attribution 4.0 International License (<http://creativecommons.org/licenses/by/4.0/>), which permits unrestricted use, distribution, and reproduction in any medium, provided you give appropriate credit to the original author(s) and the source, provide a link to the Creative Commons license, and indicate if changes were made. The Creative Commons Public Domain Dedication waiver (<http://creativecommons.org/publicdomain/zero/1.0/>) applies to the data made available in this article, unless otherwise stated.

translocation of IMS proteins across the outer membrane [14, 18, 19]. During or directly following the import reaction, Mia40 forms mixed covalent dimers with its substrates, which can be stable for seconds to minutes [12, 13, 20–25]. This lasting interaction is very different to the very rapid disulfide exchange reaction of PDI with its substrates [26].

Reduced Mia40 is re-oxidized by Erv1 in a reaction that mimics the Mia40-substrate interaction [9]. The Erv1-catalyzed oxidation of Mia40 is highly efficient, such that in vivo Mia40 is predominantly or exclusively present in the oxidized state [20, 25, 27–30]. Reconstitution experiments proved that Mia40 and Erv1 are the only two proteins required to drive efficient oxidation of IMS proteins in vitro [21, 28, 31].

Mia40 is conserved among animals, fungi, and plants but absent in many ‘more primitive’ eukaryotes such as in trypanosomes [32] or in kinetoplastids [33]. Presumably, Mia40 was never present in these groups but it cannot be excluded that certain organisms initially contained Mia40 but secondarily lost it during evolution.

In contrast, genes for Erv1 homologs were identified ubiquitously in genomes of mitochondria-containing eukaryotes [34]. However, the structural organization of Erv1 proteins considerably differs among organisms of different eukaryotic phyla. Studies in *Arabidopsis thaliana* suggested that, in plants, Mia40 (*AtMia40*) is located both in mitochondria and peroxisomes (due to a C-terminal SKL targeting signal) and is dispensable for IMS import [35]. Still, the *A. thaliana* Erv1 (*AtErv1*) was found to be essential and critical for mitochondrial biogenesis.

Since a detailed functional analysis of Erv1 can hardly be performed in plants, we decided to express *AtErv1* in *erv1* and *mia40* yeast mutants lacking a functional disulfide relay in the IMS and to re-examine if and why it could not complement these mutants [35, 36]. While we observed that *AtErv1* did not cooperate with yeast Mia40 but rather blocked its function, it still mediated protein import into the IMS, unexpectedly interacting directly with imported IMS proteins and facilitating their oxidative folding. Thus, upon expression of *AtErv1*, the redox-active CPC motif on the yeast Mia40 became dispensable as the plant Erv1 can fold some client proteins directly. Overall, this suggests that, during evolution, Mia40 was added to an Erv1-only system at a later stage, presumably in order to improve substrate specificity and isomerization of more complex substrates.

Results

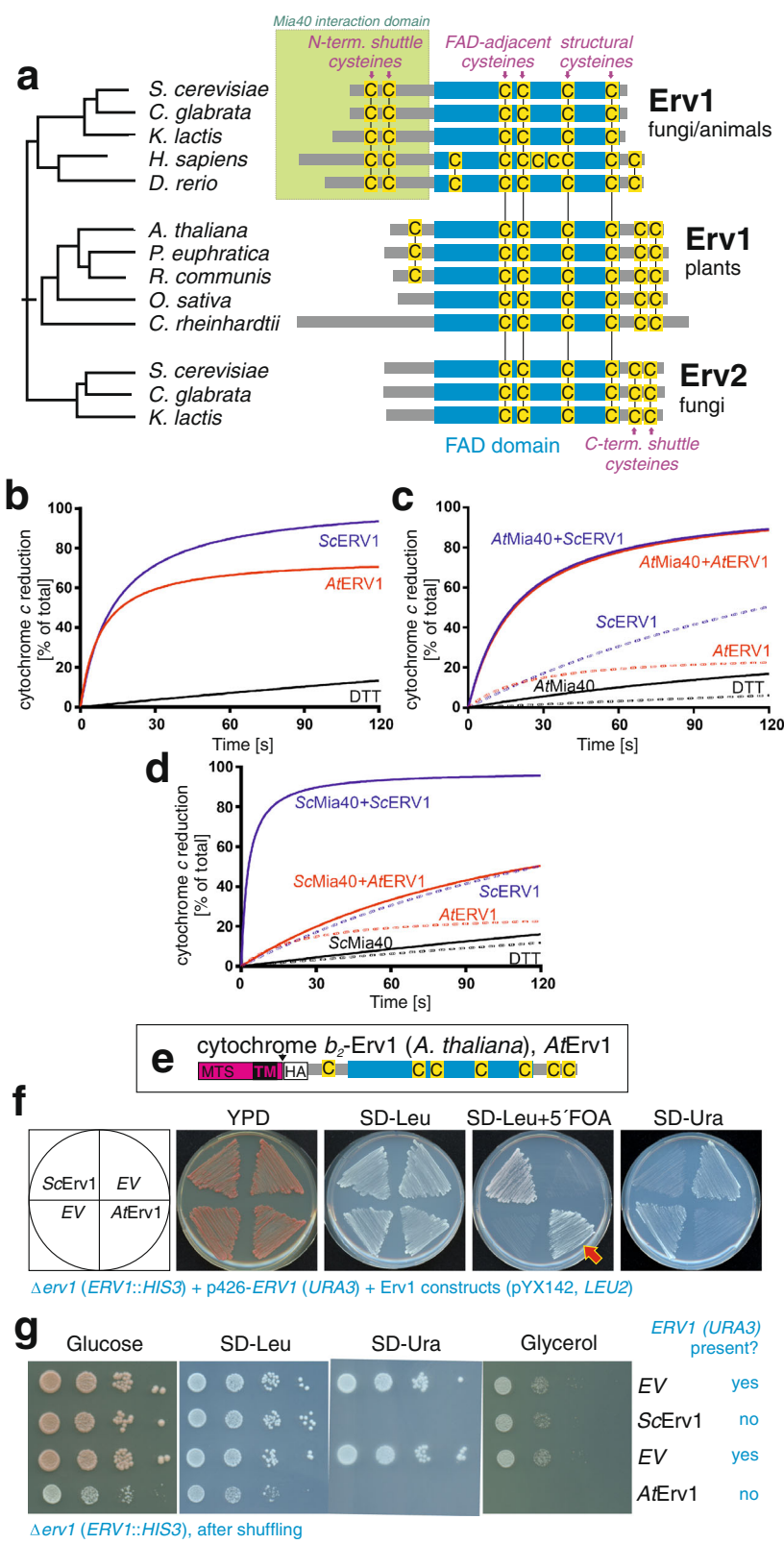
Erv1 proteins of plants, animals, and fungi differ in their domain organization

The Erv1 protein family is characterized by a conserved domain that mediates the electron transfer between a bound FAD cofactor and a surface-exposed CxxC motif

(Fig. 1a, Additional file 1: Figure S1). This domain is present in the Erv1 proteins of mitochondria, in the Erv2 proteins present in the ER of fungi, and in members of the rather diverse QSOX group [37, 38]. However, the regions that flank this conserved FAD domain in these proteins differ considerably. In the Erv1 proteins of fungi and animals, an N-terminal flexible region serves as an essential interaction arm that shuttles electrons between Mia40 and the FAD domain of Erv1 [9, 21]. Erv1 proteins of plants and Erv2 proteins lack this region but contain a C-terminal redox-active disulfide that, at least in the case of Erv2, serves as an electron shuttle [36, 39].

The ability of Erv1 to shuttle electrons from electron donors such as DTT or Mia40 to its electron acceptor cytochrome *c* can be measured by following cytochrome *c* reduction at 550 nm. We purified recombinant yeast Erv1 and *AtErv1* produced in *E. coli* and monitored the reduction of cytochrome *c* over time in the presence of 100 μM DTT (Fig. 1b). Both proteins efficiently accelerated the rate of cytochrome *c* reduction, although the yeast Erv1 showed a somewhat higher efficiency in this reaction. Then, *AtMia40* was introduced in these assays after reducing the DTT concentration to 50 μM to limit its direct reaction with Erv1 while maintaining the Mia40 catalytic disulfide reduced (Fig. 1c). Using *AtMia40*, yeast Erv1 and *AtErv1* could transfer electrons to cytochrome *c* with comparable efficiency. However, when yeast Mia40 was used, only yeast Erv1 was able to catalyze cytochrome *c* reduction (Fig. 1d), suggesting that *AtErv1* cannot efficiently accept electrons from yeast Mia40. Overall, the in vitro measurements indicated that the Erv1 proteins from yeast and *A. thaliana* exhibited comparable in vitro capacity to reduce cytochrome *c* with the notable difference that *AtErv1* does not accept electrons from yeast Mia40.

In order to test whether, despite its different domain organization, plant Erv1 can functionally replace the well-characterized Erv1 protein of yeast, we generated a *LEU2* plasmid for the expression of *AtErv1* fused to the IMS-targeting sequence of cytochrome *b*₂ for adequate targeting followed by a hemagglutinin tag present in the N-terminal region for detection (Fig. 1e). This differs from previous studies that did not verify the correct localization of the proteins and used either an intact sequence or added a shorter cytochrome *b*₂ pre-sequence and fused *AtErv1* with or without a C-terminal His-tag [36]. We transformed this plasmid into a *Δerv1* mutant that contained the yeast *ERV1* gene on a *URA3* plasmid. Through growth on 5' fluoroorotic acid, we counter-selected against the *URA3* plasmid, yielding viable cells. Viable cells were also obtained with the yeast *ERV1* gene on a *LEU2* plasmid but not with the empty plasmid (Fig. 1f). We concluded that *AtErv1* can replace the

**Fig. 1** (See legend on next page.)

(See figure on previous page.)

Fig. 1 The yeast *ERV1* gene can be deleted upon expression of its *Arabidopsis* homolog. **a** Phylogeny and structural comparison of members of the Erv1 family (see Additional file 1: Figure S1 for details). An overview of the protein sequences is shown, in which all cysteine residues are indicated in yellow. **b** Reduction of cytochrome c (40 μM) by purified yeast or *A. thaliana* Erv1 (8 μM) in the presence of 100 μM DTT. A control measurement without Erv1 is shown (DTT). **c** Reduction of cytochrome c (40 μM) by 50 μM DTT alone or in the presence of 20 μM AtMia40, 8 μM AtErv1, 8 μM yeast Erv1 (ScErv1), or 20 μM AtMia40 combined with 8 μM AtErv1 or 8 μM ScErv1. **d** Reduction of cytochrome c (40 μM) by 50 μM DTT alone, or in the presence of 20 μM ScMia40, 8 μM AtErv1, 8 μM ScErv1, or 20 μM ScMia40 combined with 8 μM AtErv1 or 8 μM ScErv1. **e** Schematic representation of the AtErv1 protein used in this study. MTS mitochondrial targeting signal, TM transmembrane domain of cytochrome *b*₂ (residues 1–169) to verify IMS targeting, HA hemagglutinin tag. **f** By use of a plasmid shuffle strategy, a *URA3* plasmid for the expression of yeast Erv1 could be replaced by a *LEU2* plasmid harboring a gene for the synthesis of AtErv1 (red arrow). *EV* empty vector. **g** Strain in which the *URA3* plasmid was replaced by a plasmid expressing yeast Erv1 or AtErv1, grown to log phase. Ten-fold serial dilutions were dropped on the indicated media. Whereas cells expressing the yeast Erv1 were able to respire, the AtErv1 mutant did not grow on non-fermentative carbon sources such as glycerol

Erv1 protein of yeast. However, this strain was unable to grow on glycerol, indicating that it was unable to respire (Fig. 1g). Thus, obviously, although AtErv1 can take over an essential function of Erv1, it is not able to replace the yeast protein in its role in the biogenesis of the respiratory chain.

Mitochondria expressing AtErv1 show severely reduced levels of Mia40 substrates

Next, we assessed whether AtErv1 can replace the yeast Erv1 protein in its function in mitochondrial protein import. To this end, we analyzed the levels of different mitochondrial proteins in whole cells (Fig. 2a) or isolated mitochondria (Fig. 2b) of the different AtErv1-expressing mutants. The levels of matrix-targeted proteins (Ilv5, Oxal, Mrpl40, or Aco1) were similar in these samples. However, in mutants expressing AtErv1 but no yeast Erv1, the levels of Mia40 substrates, such as Atp23, Tim10 or Cmc1, were strongly reduced. In these cells, Sod1 levels were normal in whole cell extracts whereas the protein was almost absent from mitochondria, which confirms that the biogenesis of the IMS-located fraction of Sod1 requires the disulfide relay whereas the cytosolic Sod1 does not [40–42]. Additionally, Mia40 levels were reduced in the AtErv1 mitochondria, highlighting problems in its oxidative folding that may cause an Yme1-mediated instability (Fig. 2b).

Moreover, we expressed AtErv1 in a temperature-sensitive *erv1* mutant (*erv1-ts*) [43] and isolated mitochondria from cells that were shifted to restrictive conditions for 16 h. Again, the levels of the Mia40 substrates Atp23 and Cmc1 were severely reduced, whereas low amounts of the essential IMS protein Tim10 were still detected (Additional file 2: Figure S2A). Thus, the AtErv1 protein can facilitate the import of low levels of small Tim proteins and therefore exhibits the essential function of Erv1. However, AtErv1-expressing mitochondria lack Cmc1, an IMS protein required for the assembly of cytochrome oxidase [44–46]. Accordingly, we observed considerably reduced levels of subunit 2 of cytochrome oxidase (Cox2, Additional file 2: Figure S2B), although this mitochondrially encoded protein was synthesized at normal levels (Additional file 2:

Figure S2C). Thus, the absence of IMS-located biogenesis factors of cytochrome oxidase explains the inability of the AtErv1 mutant to respire.

AtErv1 does not oxidize yeast Mia40 in vivo

The severe defects observed in the AtErv1-expressing mutants and the in vitro activity results prompted us to test whether AtErv1 can oxidize the yeast Mia40 protein in vivo. To this end, we analyzed the redox state of Mia40 in the different mutants by an alkylation shift assay based on the modification of reduced but not oxidized thiols by methyl-polyethylene glycol₂₄-maleimide (mmPEG₂₄, Fig. 2c). In wild-type cells, Mia40 is almost exclusively present in the oxidized state [21, 47] and its six cysteine residues can only be alkylated after reducing its three disulfide bonds with tris(2-carboxyethyl)phosphine, a thiol-free chemical reductant (Fig. 2c, wild-type). In contrast, the two catalytic cysteine residues of Mia40 remained accessible in the AtErv1-expressing mutant and almost no oxidized Mia40 was observed. Thus, AtErv1 is extremely inefficient in oxidizing the yeast Mia40 protein, which may be explained by the fact that the shuttle disulfide of AtErv1 is not part of an amphipathic helix structure (Fig. 2d) that could serve as a Mia40 interaction region.

The inability of AtErv1 to cooperate with yeast Mia40 could point to an incompatibility of the fungal and plant systems. However, neither the decreased levels of Mia40 substrates (Fig. 2e) nor the growth defects on glycerol (Fig. 2f) of the AtErv1-expressing mutant were suppressed by co-expressing AtMia40. Apparently, the AtErv1 protein does not productively cooperate with Mia40.

This is further supported by the observation that the AtErv1-expressing mutant was hypersensitive to DTT (Additional file 3: Figure S3A, B), which counteracts disulfide bond formation by the mitochondrial disulfide relay [21]. Re-oxidation of Erv1 can occur either in a cytochrome *c*-independent reaction in which oxygen is directly reduced to hydrogen peroxide or in a cytochrome *c*-mediated reaction that can also occur under anaerobic conditions [48–50]. Since the AtErv1-expressing mutant grows efficiently also in the absence of oxygen (Additional file 3: Figure S3C), we

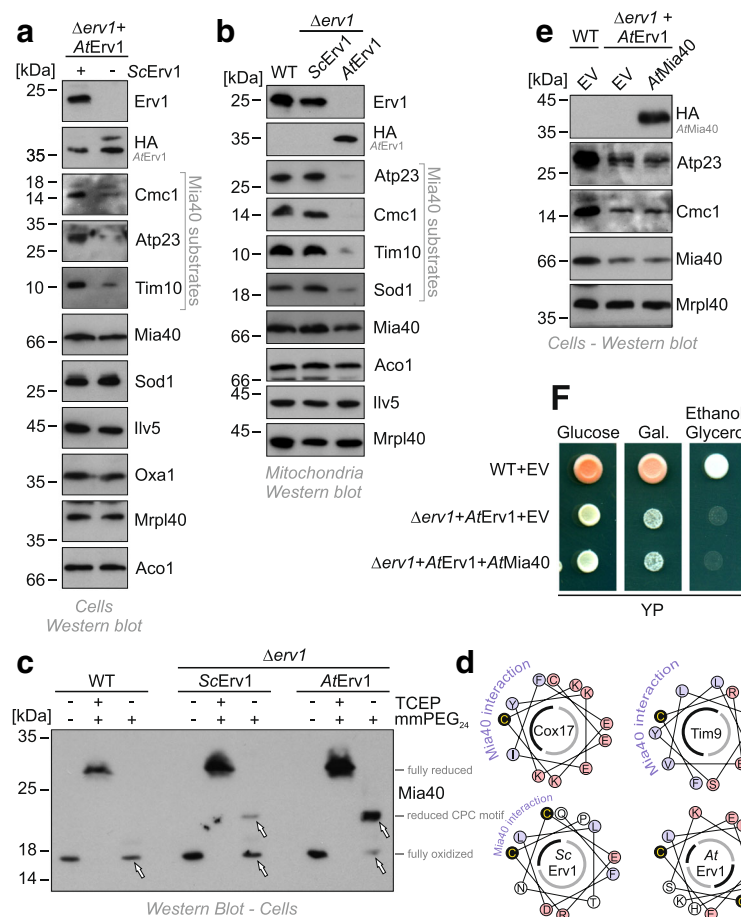


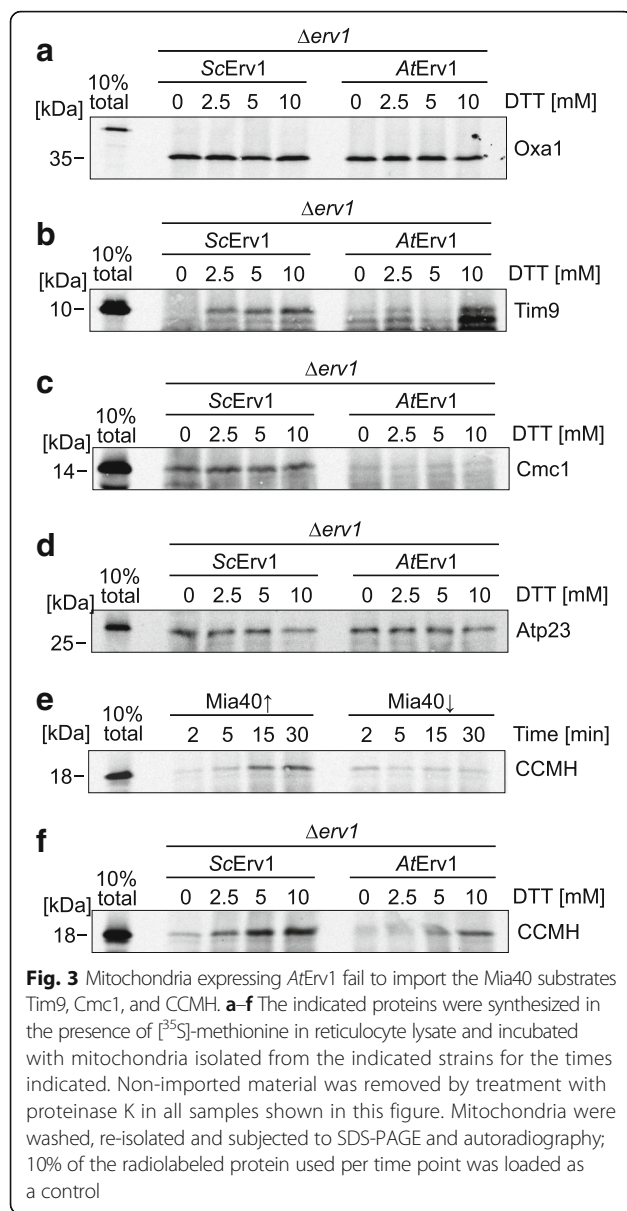
Fig. 2 AtErv1 fails to oxidize the catalytic cysteines in the CPC motif of Mia40. Western blot analysis of extracts of whole cells (**a**) or isolated mitochondria (**b**) of the indicated strains show a strong depletion of Mia40 substrates in strains that express AtErv1 in the absence of yeast Erv1. Panel **a** shows the shuffle strain before and after shuffling out the ScErv1-encoding URA3 plasmid. **c** To monitor the redox state of Mia40 in the different strains, proteins of the indicated strains were TCA-precipitated (in order to ‘freeze’ the redox state of thiol groups), denatured in SDS, treated with the reducing agent tris(2-carboxyethyl)phosphine (TCEP) and the alkylating compound methyl-polyethylene glycol₂₄-maleimide (mmPEG₂₄), and visualized by SDS-PAGE and western blotting. For this experiment a Mia40 variant was used that lacked the long membrane linker, which leads to much more reliable results in this kind of shift assay [18, 25]. TCEP reduced all thiols in Mia40 such that its six cysteines were alkylated, resulting in a shift of approximately 12 kDa (2 kDa per mmPEG₂₄). In wild-type cells, in the absence of TCEP, Mia40 was not shifted since all cysteines were oxidized (arrowhead). Additionally, in the Δerv1 mutant that was complemented by yeast Erv1, the cysteine residues of Mia40 remained largely inaccessible. In the AtErv1-expressing mutant, however, almost no oxidized Mia40 was detectable. The shift by 4 kDa corresponds to the alkylation of the two redox-active cysteines of Mia40, indicative of the reduced form of Mia40. It should be noted that the two structural disulfides that are critical for the formation of the substrate-binding domain of Mia40 were formed in this mutant. **d** Helical wheel representation of the Mia40 interaction region in Cox17, Tim9, yeast Erv1 (Sc), and AtErv1 [9, 10, 14, 17]. The hydrophobic (black) and hydrophilic (grey) faces of the helix are indicated as half circles. Note that the docking cysteines in Cox17 and Tim9, as well as cysteines of the shuttle disulfide in yeast Erv1 (yellow), are part of an amphipathic helix structure whereas cysteines of the shuttle disulfide of AtErv1 are not. **e, f** Levels of IMS proteins were analyzed by western blotting (**e**). Growth of the indicated mutants on non-fermentable medium (**f**). Gal galactose

regard it as unlikely that the defect in this strain is due to an incompatibility of AtErv1 with yeast cytochrome *c*, but rather due to an incompatibility of AtErv1 with Mia40.

Mitochondria of the AtErv1-expressing mutant show defects in the import of IMS proteins

Next, we directly tested the ability of mitochondria from Δerv1 cells that expressed either yeast Erv1 or AtErv1 to import proteins in vitro. To this end, we purified mitochondria and incubated them with radiolabeled

precursor proteins destined for the matrix (Oxa1, Fig. 3a) or the IMS (Tim9, Cmc1, Atp23, Fig. 3b–d) in the presence of different concentrations of DTT. Non-imported material was removed by protease treatment before samples were analyzed by SDS-PAGE and autoradiography. Oxa1 was efficiently imported into both mitochondria, verifying that they were import-competent. However, the import of Tim9 and Cmc1 was almost completely blocked. This confirms previous studies showing that the redox state of Mia40 strongly influences the import



efficiency, even though the oxidation of the catalytic disulfide bond in Mia40 is not essential for the import of Tim9, but only for its subsequent folding and assembly [14, 18, 19, 51]. In contrast to Tim9 and Cmc1, the Mia40 substrate Atp23 was efficiently imported into the AtErv1-expressing mitochondria. Atp23 differs from Tim9 and Cmc1 by the fact that its cysteine residues are not required for its import since a cysteine-free mutant of Atp23 was shown to be still efficiently imported in a strictly Mia40-dependent manner [19, 51, 52]. However, without the structural disulfide bonds, Atp23 is unstable and rapidly degraded by Yme1.

The proteome of plant mitochondria, and presumably also that of their IMS, differs considerably from that of fungi and animals [53, 54]. For example, bacteria, plant mitochondria, and chloroplasts use common systems for

the biogenesis of *c*-type cytochromes, which differs considerably from the *c*-type cytochrome biogenesis machinery of animals and fungi [55]. The plant system, but not that of animals and fungi, contains the protein CCMH, which contributes to the heme incorporation. CCMH has a conserved protein domain exposed into the IMS and contains two cysteines in a CxxC motif [56]. We wondered whether the yeast system could be used to test whether CCMH is a substrate of the mitochondrial disulfide relay. To this end, we incubated radiolabeled *Arabidopsis* CCMH with isolated mitochondria of Mia40-containing and Mia40-depleted mitochondria. We observed that the import of CCMH was strongly reduced in mitochondria in which Mia40 was depleted (Fig. 3e), suggesting that this protein is a substrate of the mitochondrial disulfide relay. Further, this plant substrate was imported much more efficiently in mitochondria expressing the yeast Erv1 than in those expressing AtErv1 (Fig. 3f). Thus, the poor performance of the AtErv1-expressing mutant is not caused by an incompatibility of yeast substrates with AtErv1 but rather by an incompatibility of AtErv1 with Mia40.

AtErv1 binds efficiently to yeast Mia40 but has a dominant-negative activity in yeast mitochondria

The inability of AtErv1 to oxidize yeast Mia40 might be due either to an inability of both proteins to interact or to an unproductive interaction. Co-immunoprecipitation experiments with Mia40-specific antibodies efficiently pulled down a fraction of AtErv1 after stabilization of the interaction with the cleavable crosslinker dithiobis succinimidyl propionate (Fig. 4a). As expected, newly imported radiolabeled Mia40 was efficiently recovered in a complex with AtErv1 (Additional file 4: Figure S4A). From this we concluded that AtErv1 and yeast Mia40 are able to interact and it is apparently not the lack of binding that prevented AtErv1 from functionally replacing yeast Erv1, but AtErv1 rather appears to block Mia40 activity.

In order to mitigate a potentially dominant-negative activity of AtErv1 on Mia40, we transformed the mutants with a plasmid harboring an extra copy of Mia40 (Fig. 4b). Surprisingly, overexpression of yeast Mia40 indeed partially suppressed the negative effect of AtErv1 as it restored the levels of some IMS proteins (Tim10 and Atp23, Fig. 4b) and allowed slow growth of the strains on non-fermentable carbon sources (Fig. 4c).

Furthermore, the dominant-negative effect of AtErv1 was very obvious when the protein was expressed in wild-type mitochondria containing a functional yeast Erv1 protein. The presence of AtErv1 strongly impaired the import of Mia40 substrates such as Cmc1 or Tim9, but not that of the matrix protein Oxa1 (Fig. 4d). In summary, we concluded that AtErv1 did interact with Mia40 but rather blocked its activity, presumably by competitive inhibition of its hydrophobic substrate binding domain.

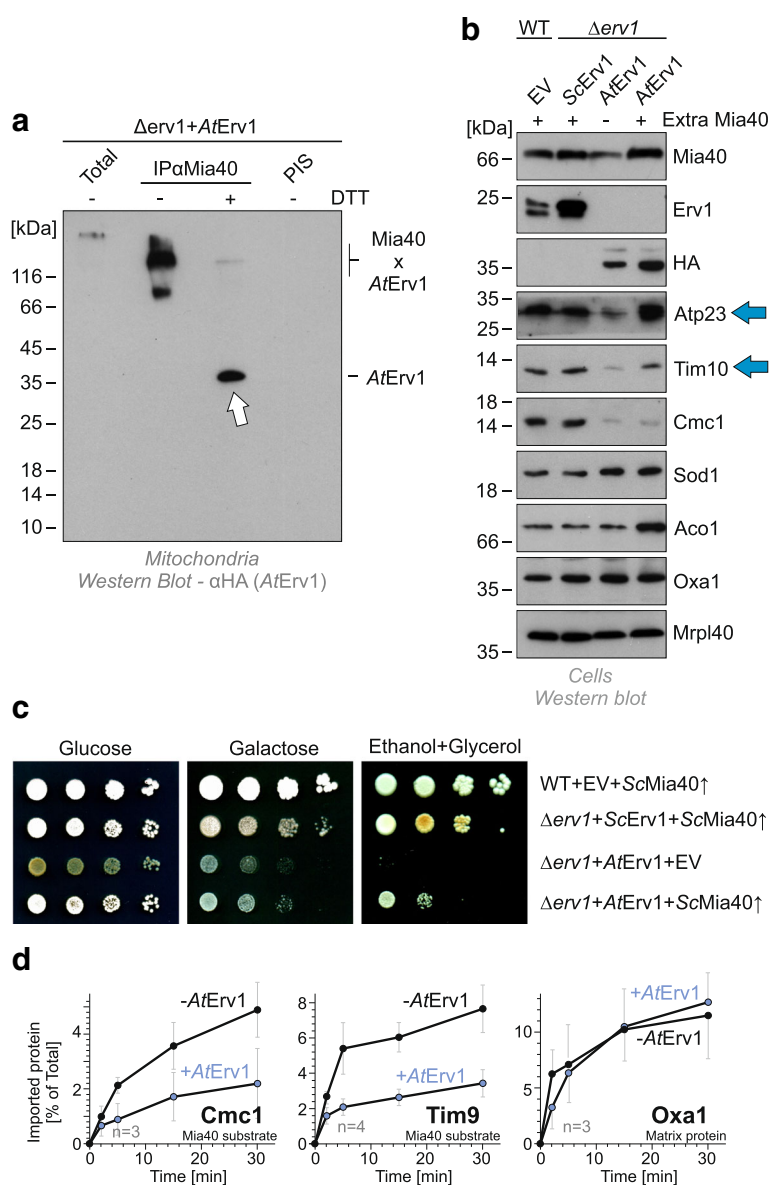
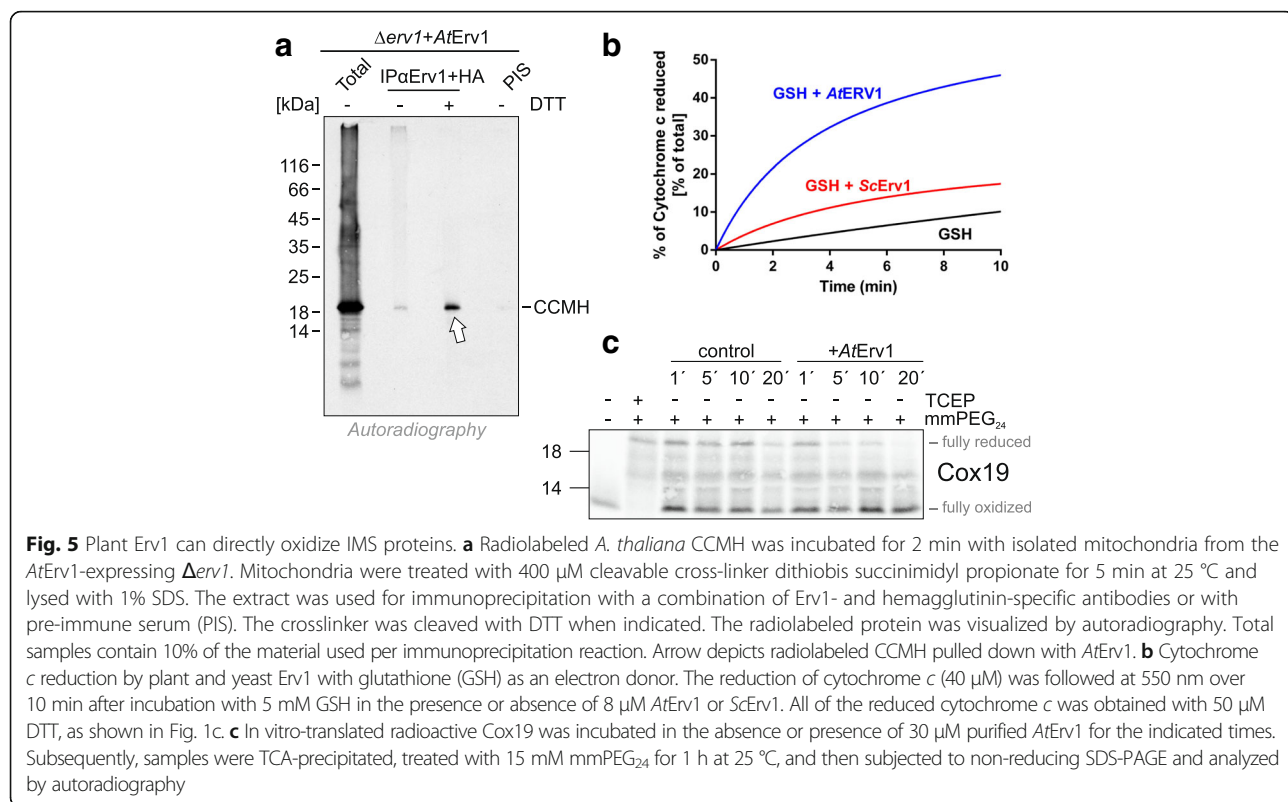


Fig. 4 AtErv1 exhibits a dominant-negative activity on yeast Mia40. **a** Mitochondria isolated from a Δ erv1 strain expressing AtErv1 were treated with 1 mM cleavable cross-linker dithiobis succinimidyl propionate for 15 min at 25 °C and lysed with 1% SDS. The extract was used for immunoprecipitation with Mia40-specific antibodies or with pre-immune serum (PIS). Hemagglutinin-tagged AtErv1 protein was visualized by western blotting. Arrows indicate immunoprecipitated AtErv1. Total samples contain 10% of the material used per immunoprecipitation reaction. **b** A multicopy plasmid carrying the yeast *MIA40* gene was transformed into wild-type or Δ erv1 cells. Whole cell extracts were prepared and analyzed by western blotting. Note that the levels of Atp23 and Tim10 were largely restored upon overexpression of Mia40 despite the absence of yeast Erv1 in these mutants (blue arrows). **c** An extra copy of yeast Mia40 (ScMia40) partially rescues the growth defect of the AtErv1 mutant on non-fermentative medium. **d** Mitochondria were isolated from wild-type cells lacking or carrying an expression plasmid for AtErv1. The Mia40 substrates Cmc1 and Tim9, as well as the matrix protein Oxa1, were incubated with these mitochondria at 25 °C for the times indicated. Non-imported material was removed by protease treatment. The amounts of imported radiolabeled proteins were quantified. Mean values and standard deviations of at least three replicates are shown

AtErv1 can oxidize IMS proteins in the absence of a redox-active Mia40

It is possible that AtErv1 may be able to rescue the Δ erv1 mutant without productively interacting with Mia40 through the direct interaction of Erv1 with incoming polypeptides, bypassing the need for Mia40. To

test this, we immunoprecipitated AtErv1 from mitochondria in which we had imported radiolabeled CCMH. Indeed, CCMH was efficiently pulled down in a DTT-sensitive manner (Fig. 5a), confirming the direct AtErv1-substrate interaction. In contrast, no CCMH was recovered with Mia40-specific antibodies, suggesting that, in



the presence of AtErv1, the import of CCMH occurs independently of Mia40 (Additional file 5: Figure S5). Further, not only CCMH but also the yeast proteins Tim9 and Tim17 were found to interact with AtErv1, although the efficiency of the crosslinking was lower than that of the plant substrate (Additional file 4: Figure S4B, C). Additionally, small amounts of yeast Erv1 were found to be in contact with newly imported Tim9 and Tim17, in line with previous studies showing that small Tim proteins and Tim17 are oxidized in yeast mitochondria that lack redox-active Mia40 [18, 57].

In order to test whether AtErv1 is able to oxidize thiol-containing peptides, we employed the cytochrome *c* assay to monitor the oxidation of glutathione with AtErv1 and yeast Erv1 as a control (Fig. 5b). We observed that AtErv1 oxidized glutathione, resulting in cytochrome *c* reduction. In contrast, the yeast Erv1 protein was extremely inefficient in its interaction with glutathione, suggesting that AtErv1 can directly oxidize this small peptide whereas the yeast Erv1 protein does not or only to a minimal extent.

We then tested whether AtErv1 is able to oxidize a well-established Mia40 substrate. To this end, we incubated radiolabeled Cox19 in the absence or presence of purified AtErv1 (Fig. 5c). At different time points, proteins were precipitated by acid treatment and denatured, and reduced thiols were alkylated with mmPEG₂₄. In the presence of AtErv1, but not in its absence, reduced

Cox19 protein was efficiently depleted from the reaction, indicating that AtErv1 is indeed able to oxidize this yeast protein, at least in vitro. It should be noted that yeast Erv1 has been previously shown to slowly oxidize Cox19 in vitro [18, 21, 23, 58].

Next, we used genetics to test whether AtErv1 was indeed able to bypass the need for Mia40. To this end, we expressed AtErv1 in the temperature-sensitive Mia40 mutants *mia40-3* and *mia40-4* [23]. AtErv1 partially suppressed the growth defect of these strains at restrictive growth conditions (Fig. 6a, Additional file 6: Figure S6A) and restored the levels of Mia40 substrates, such as Cmc1 and Tim10, to some degree (Fig. 6b, Additional file 6: Figure S6B).

Since it cannot be excluded that the Mia40 of the temperature-sensitive *mia40* mutant still has some residual activity even at restrictive conditions, we decided to test whether a redox-active Mia40 can be completely removed in the presence of AtErv1 in the IMS. We therefore performed plasmid shuffling experiments in the absence or presence of a redox-inactive Mia40 mutant in which both cysteines of the CPC motif were replaced by serine residues (Mia40-SPS) [18]. Expression of AtErv1 allowed the loss of *MIA40* as long as Mia40-SPS was co-expressed (Fig. 5d). Thus, a combination of Mia40-SPS, which mediates the import but not the oxidation of proteins [18], and of AtErv1, which subsequently oxidizes imported proteins, is obviously sufficient to promote the biogenesis of IMS proteins

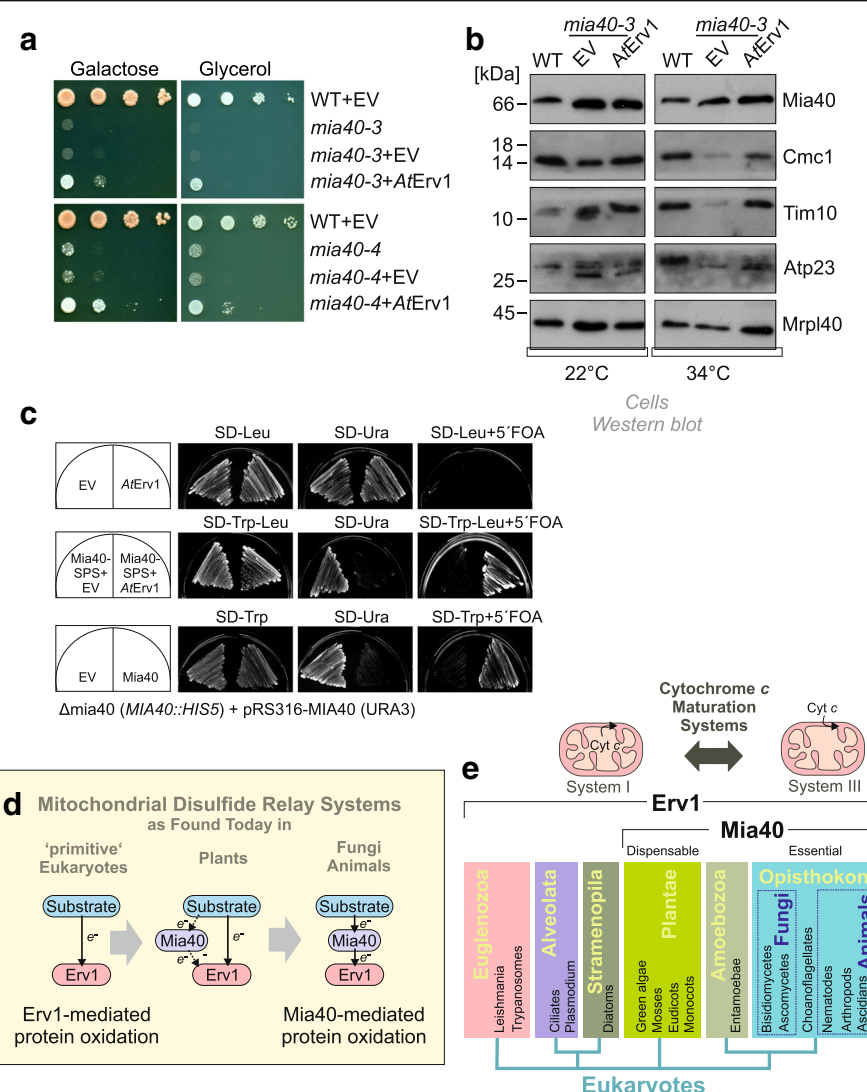


Fig. 6 a, b The expression of AtErv1 in the temperature-sensitive Mia40 strains *mia40-3* and *mia40-4* allows cell growth at a restrictive temperature (a) and restores the level of Mia40 substrates in the IMS of mitochondria (b). **c** *Δmia40* cells containing *MA40* on an *URA3* plasmid were transformed with plasmids to express AtErv1 alone (upper row), AtErv1 in combination with Mia40-SPS (middle row), or wild-type Mia40 as a positive control (lower row). The ability of the strains to grow upon loss of *URA3* plasmid was tested on 5-fluoroorotic acid. Co-expression of AtErv1 and Mia40-SPS resulted in viable cells. **d, e** Many 'primitive' eukaryotic phyla (such as euglenozoa, alveolata, and stramenopila) lack Mia40 and protein oxidation should be carried out by Erv1 directly. In plants, a gene for Mia40 is present but not essential, as substrate oxidation can still occur in a Mia40-independent manner. In opisthokonts, both Erv1 and Mia40 are crucial for protein oxidative folding. We propose that the initial disulfide relay only employed an Erv1-like oxidase and was thus similar to the situation still found in some protists

(Additional file 6: Figure S6C). This demonstrates that AtErv1 can take over the essential function of the mitochondrial disulfide system in the IMS as long as the hydrophobic substrate-binding region of Mia40 facilitates protein translocation across the outer membrane.

Discussion

A. thaliana mutants lacking Mia40 are viable and it was proposed that the mitochondrial disulfide relay system can function without Mia40 or that an additional, not yet characterized, oxidoreductase makes Mia40 dispensable

[35]. The results presented in this study show that AtErv1 can oxidize substrate proteins directly in a Mia40-independent manner. In contrast, Erv1 proteins of fungi and animals were suggested to oxidize substrate proteins predominantly or exclusively via the oxidoreductase Mia40. However, recent studies suggest that also in yeast, Erv1 can oxidize specific substrates such as the inner membrane protein Tim17 [57] and, with low efficiency, typical Mia40 substrates, at least in the background of Mia40 mutants that lack the redox-active cysteine pair [18].

Although the molecular details of this *AtErv1*-mediated protein oxidation have to be better delineated, we report here that *AtErv1* can directly bind to newly imported IMS proteins, thereby forming mixed disulfides. This promotes their import and oxidative folding in the IMS even in strains that lack a functional *Mia40* protein. Thus, the mitochondrial disulfide relay of plants obviously differs from that of fungi and animals as it allows the direct electron flow from substrates to *AtErv1* (Fig. 6d). Possibly, *AtMia40* might still handle specific, non-essential substrates or carry out another function such as the isomerization of IMS proteins. Such a substrate-specific function could explain the decreased complex I activity observed in *Mia40* plant mutant lines [35]. Moreover, a recent study showed that *AtMia40* can form a complex with the mitochondrial phosphatase SLP2 and proposed a regulatory, again substrate-specific, role of *AtMia40* in plant mitochondria [59].

Interestingly, many eukaryotic groups, including ciliates, diatoms, or parasites such as *Leishmania*, *Trypanosoma*, or *Plasmodium*, lack genes for *Mia40* homologs but still contain *Erv1* (Fig. 6e) [32–34, 60]. Thus, the mitochondrial disulfide relay obviously started from an *Erv1*-only system in which *Erv1*, similar to the QSOX proteins of the secretory pathway [38, 61], directly catalyzed protein oxidation (Fig. 5e). *Mia40* was presumably added later, initially as a dispensable player. In fungi and animals, however, *Mia40* became essential and *Erv1* lost its ability to interact directly with IMS proteins. It should be noted that we do not propose that animals and fungi developed from plants; however, given the intermediate stage of the plant system compared to that of protists on the one side and of animals/fungi on the other, we assume that the disulfide relay in animals and fungi developed from a situation that was similar to that still operating in mitochondria of *Arabidopsis*.

Why was *Mia40* added into the mitochondrial disulfide relay during eukaryotic evolution? Oxidoreductases can provide substrate specificity, thereby targeting the oxidative potential of sulfhydryl oxidases to specific clients. This is most obvious for the disulfide relay of the ER, where the sulfhydryl oxidase *Ero1* presumably oxidizes only one single substrate, *PDI*, which oxidizes many different substrate proteins (often employing even additional *PDI* homologs) [3, 4]. The substrate specificity of *Mia40* was well characterized and IMS proteins with disulfide bonds show MISS/ITS signals to ensure their specific recognition by *Mia40* [14, 17]. It is unclear why an increased substrate specificity became necessary during evolution; however, the change in the *c*-type cytochrome biogenesis system coincided with the addition of *Mia40* [55]. Cytochrome *c* is by far the most abundant protein of the IMS. It is characterized by two reduced cysteines in a CxxC motif to which heme is covalently

attached during cytochrome biogenesis. Oxidation of these cysteines prevents cytochrome maturation, and bacteria employ a specific reduction system in order to keep apocytochrome *c* reduced. In mitochondria of protists and plants (as well as in bacteria), cytochrome *c* is secreted across the inner membrane into the IMS and matured by a complex machinery employing many conserved factors (called system-1 and system-2) [62]. Several of these components are mitochondrially encoded due to their hydrophobic nature. In contrast, in fungi and animals, which have a considerably smaller mitochondrial genome, apocytochrome *c* is imported from the cytosol and matured by a single enzyme, cytochrome *c* heme lyase. Perhaps, the increased substrate specificity of *Mia40* made a much simpler maturation system for *c*-type cytochromes possible and allowed the further reduction of the set of mitochondrially encoded genes [62, 63].

The results of this study also nicely demonstrate that, for the mitochondrial disulfide relay, the proper interplay between its two components *Mia40* and *Erv1* is essential. Although the catalytic activity of *AtErv1* in disulfide bond formation is comparable to that of yeast *Erv1* when using DTT, *AtErv1* was unable to productively interact with *Mia40*. *AtErv1* did not efficiently oxidize yeast *Mia40*, which prevented the import of IMS proteins. The observation that overexpression of *Mia40* mitigated the defects of the *AtErv1*-expressing mutant and that the expression of *AtErv1* exhibited a dominant-negative activity despite yeast *Erv1* being present suggests that *AtErv1* arrested the *Mia40* reaction cycle. *AtErv1* binds efficiently to *Mia40* but fails to oxidize it, presumably due to its different domain organization compared with yeast *Erv1*. Thus, the results shown in this study are compatible with a model according to which *AtErv1* acts as a competitive inhibitor of *Mia40*, blocking its substrate-binding site without oxidizing its CPC motif.

It should be noted that the phenotype of the *AtErv1*-expressing mutant cannot be simply explained by the insufficient oxidation of *Mia40* as a *Mia40-SPS* mutant (which lacks the catalytic disulfide) still imports proteins into the IMS, but fails to oxidize them [18]. As a consequence, these unfolded proteins fail to assemble and are rapidly degraded by the IMS-AAA protease *Yme1* [19, 51, 52].

IMS proteins, such as *Cox17* or *Tim9*, bind to *Mia40* via hydrophobic interactions of a helical sequence known as MISS or ITS signal [14, 17]. These signals are characterized by an amphipathic helix, which places the attached cysteine residue within a hydrophobic patch (Fig. 2d). The yeast *Erv1* protein has a similar, though less pronounced, sequence believed to mimic the MISS/ITS signal of *Mia40* substrates (Fig. 2d). In contrast, *AtErv1* lacks such a pattern. Here, the shuttle cysteines are separated by four residues such that a disulfide bond

is not compatible with the formation of a helical structure, which should prevent *AtErv1* to properly align its shuttle disulfide with the CPC motif of Mia40 and thus to oxidize yeast Mia40 (Fig. 2d).

In fungi and animals, Mia40 and Erv1 cooperate in the import and folding of proteins into the IMS. The use of a combination of a Mia40-SPS mutant, which traps import intermediates but is unable to oxidize them, and of the *AtErv1* protein, which promotes substrate oxidation in a Mia40-independent reaction, showed that these two functions of the disulfide relay can be completely separated. This will provide an excellent system in order to dissect the individual reactions of the biogenesis of IMS proteins in mitochondria in greater mechanistic detail.

Conclusions

Disulfide relays stabilize protein structures by oxidative protein folding. The present study shows that the mitochondrial disulfide relay of plants is much simpler than that of previously studied systems and may resemble the oxidation machinery of early eukaryotes; its sulfhydryl oxidase *AtErv1* oxidizes substrates directly, making an oxidoreductase obsolete.

Methods

Yeast strains and plasmids

Yeast strains used in this study were based on the wild-type strains W303 and YPH499. Shuffle strains for *ERV1* and *MIA40*, as well as *erv1-ts*, *mia40-3*, and *mia40-4* mutants, have been previously described [18, 21, 23, 58]. Yeast strains were either grown in synthetic media containing 2% glucose or galactose, or in YP (1% yeast extract, 2% peptone) medium containing 2% galactose, glucose, glycerol, or ethanol [64].

For expression of the *AtErv1* variant, the *AtErv1* sequence was amplified from leaf *Arabidopsis* cDNA using the primers: forward 5' CCCCGGATCCTATCCTTAC-GACGTGCCTGACTACGCCGGTGAGAAGCCATGG-CAGCCAC 3' and reverse 5' CCCCGTCGACTTAAAAGTCCATAGAACGTTCCATG 3', introducing an N-terminal hemagglutinin tag. The amplified fragment was cloned in frame into the *BamHI* and *Sall* restriction sites of the pYX142 vector (Addgene) containing the sequence coding for the amino acids 1–167 of cytochrome *b*₂ (comprising its mitochondrial targeting sequence, the transmembrane domain and the heme-binding domain) into *EcoRI* and *BamHI* restriction sites.

To express *AtMia40*, the sequence corresponding to the protein sequence of residues 2–161 was cloned using *BamHI* and *BstX1* restriction sites in frame into the single copy vectors pRS314, pRS315, or pRS316 harboring *MIA40* promoter and a sequence corresponding to the amino acid residues 1–70 of yeast Mia40 [18]. To over-express yeast Mia40, the entire *MIA40* gene, including

the promoter and terminator, was cloned by PCR between *SacI* and *Sall* restriction sites into the multi-copy vectors pRS424 and pRS426.

For in vitro transcription/translation of CCMH, the sequence corresponding to amino acid residues 1–159 was amplified from an *A. thaliana* cDNA using the primers: forward 5' CCCCGAATTGCCACCATG GAGAAAACAGACGAAGAG 3' and reverse 5' CCCCGGATCCCTACCGGTTGAGCCATCTCC 3' and cloned into the *EcoRI* and *BamHI* sites of a pGEM4 vector (Promega).

Experimental procedures on the isolation of mitochondria, the import of radiolabeled precursor proteins, immunoprecipitation and western blotting have been reported previously [15].

Cloning, expression, and purification of recombinant proteins in *E. coli*

The *AtErv1* sequence (without the region coding for the first 70 amino acids) and the *AtMia40* sequence (without the region coding for the first 55 amino acids) were amplified by PCR from *A. thaliana* leaf cDNA using the following pairs of primers: *AtErv1* forward 5' CCCCCCCCATATGACTGGTCCTGTGACTAAAGAG 3' and *AtErv1* reverse 5' CCCCGGATCCCTAAAAA GTCCATAGAAGT 3' and *AtMia40* forward 5' CCCCCCCCATATGGAGTCTCTTGAAAGCC 3' and *AtMia40* reverse 5' CCCCGGATCCCTAAAGCTTGGA ATTGCC 3' and cloned in pET12a and pET15b plasmids, respectively (Novagen). The pET24a-*ScErv1* and pGEX6-*ScMia40* expression plasmids have been previously described [18, 21, 23, 58]. Protein production was achieved in the *Escherichia coli* BL21(DE3) strain containing pSBET plasmids using a culture protocol previously described [65]. *AtErv1* was purified in three successive steps (ammonium sulfate precipitation, ACA44 gel filtration and DEAE-Sepharose), whereas *AtMia40* and *ScErv1* were purified in a single step on His-Select® Nickel affinity gel (Sigma-Aldrich) from the soluble part of the bacterial extract following procedures already described [65]. After dialysis against a 30 mM Tris-HCl (pH 8.0), 1 mM EDTA buffer, proteins were stored at -20 °C. The purification of the GST-*ScMia40* fusion was performed on Glutathione Sepharose 4B (GE Healthcare, product code 17-0756-01) following the manufacturer's recommendations. The GST-tag cleavage was performed in the a 50 mM Tris-HCl (pH 7.0), 150 mM NaCl, 1 mM EDTA, and 1 mM DTT buffer by adding the recommended amount of Precision Protease on the glutathione sepharose resin for overnight incubation at 4 °C. The cleaved protein was eluted using a 50 mM Tris-HCl (pH 8.0), 1 mM EDTA, and 150 mM NaCl buffer, dialyzed against a 30 mM Tris-HCl (pH 8.0) and 1 mM EDTA buffer, and finally stored at -20 °C in 50% glycerol. All protein concentrations were determined

using the respective theoretical extinction coefficients at 280 nm calculated using the Expasy Protparam tool (<http://web.expasy.org/protparam/>).

Antibodies used in this study were generated in rabbits against recombinantly expressed and purified Erv1 or Mia40 [20, 21] or commercially obtained from Roche (Anti_HA-Peroxidase; Cat. No. 12013819001; Antibody ID AB_390917).

Alkylation shift experiments for redox state detection

To analyze the redox state of cysteine residues in whole cells, mitochondrial proteins were precipitated with TCA, denatured with SDS, and incubated with 15 mM mmPEG₂₄ (Thermo Scientific product # 22713) as described [15].

Reduction of cytochrome c

The reduction of cytochrome c from equine heart (40 μM, SIGMA-Aldrich, product code C7752) was followed by recording changes in absorbance at 550 nm using a Cary 50 Variant-Agilent spectrophotometer. The reactions were performed in a 50 mM phosphate buffer at pH 7.4 and 1 mM EDTA, and started by adding DTT (50 or 100 μM) to the cuvettes containing various combinations of purified recombinant proteins (Erv1 (8 μM) and Mia40 (20 μM) from both *S. cerevisiae* and *A. thaliana*).

Additional files

Additional file 1: Figure S1. Related to Fig. 1. Alignment of members of the Erv1 family. The sequences were compared using Clustal Omega with standard settings of the program. (DOCX 1001 kb)

Additional file 2: Figure S2. Related to Fig. 2. Mitochondria of the AtErv1-expressing *erv1-ts* mutant show strongly reduced levels of Mia40 substrates and no functional cytochrome oxidase. **A** The temperature-sensitive *erv1-ts* mutant was transformed with plasmids to express yeast Erv1 or AtErv1. Cells were shifted to restrictive conditions at 34 °C for 16 h before mitochondria were isolated and analyzed by western blotting. **B** AtErv1-expressing cells show strongly reduced steady-state levels of Cox2, a central, mitochondrially encoded subunit of cytochrome oxidase. **C** Mitochondrial translation products were radiolabeled in cells after blocking cytosolic translation with cycloheximide. Cells were incubated for 15 min at 30 °C in the presence of [³⁵S]-methionine. Radiolabeled proteins were separated by SDS-PAGE and visualized by autoradiography. (EPS 6782 kb)

Additional file 3: Figure S3. Related to Fig. 2. The AtErv1-expressing *Δerv1* mutant shows increased sensitivity to DTT. **A, B** For the experiment shown in panel A, 10 μL of 3 M DTT was added to the filter paper placed in the middle of the plates. For the experiment shown in panel B, the following solutions were used: water, 1 M diamide, 1 M DTT or 3 M DTT (10 μL each) or 30% H₂O₂ (5 μL) as indicated. Cells were grown at 30 °C for 3 days. **C** Wild-type and *Δerv1* cells expressing yeast Erv1 or AtErv1 were incubated on glucose plates in the presence (blue color of the indicator strip) or absence (white color of the indicator strip) of oxygen for 5 days at 30 °C. (EPS 142732 kb)

Additional file 4: Figure S4. Related to Fig. 4. AtErv1 directly interacts with Tim9 and Tim17. **A** Radiolabeled Mia40 was incubated for 2 min with isolated *erv1-ts* mitochondria containing or lacking hemagglutinin (HA)-tagged AtErv1. Mitochondria were re-isolated and lysed with 1% SDS. The extract was used for immunoprecipitation with HA-specific antibodies or with pre-immune serum (PIS). Disulfide bonds were reduced with

DTT when indicated. Radioactive proteins were visualized by SDS-PAGE and autoradiography. Total samples contain 10% of the material used per immunoprecipitation reaction. Arrows depict radiolabeled fractions of Mia40 in a complex with AtErv1 or as a monomer upon reduction with DTT, both pulled down with the HA-tagged AtErv1. **B–E** Radiolabeled Tim9 (B, C) or Tim17 (D, E) were incubated for 2 min with isolated *Δerv1* mitochondria containing ScErv1 (B, D) or AtErv1 (C, E). Mitochondria were treated with 400 μM cleavable cross-linker dithiobis succinimidyl propionate for 5 min at 25 °C, incubated in NEM-containing buffer for 20 min on ice and finally lysed with 1% SDS. The extract was used for immunoprecipitation with Erv1-specific antibodies or with PIS. Disulfide bonds were reduced with DTT. Radioactive proteins were visualized by SDS-PAGE and autoradiography. Total samples contain 10% of the material used per immunoprecipitation reaction. Arrows depict radiolabeled proteins pulled down with Erv1. (EPS 23207 kb)

Additional file 5: Figure S5. Related to Fig. 5 CCMH appears not to interact with Mia40 during import into AtErv1 mitochondria. **A** The experiment was performed as described for Fig. 5a, with the exception that Mia40-specific antibodies were used here. Radiolabeled *A. thaliana* CCMH was incubated for 2 min with isolated mitochondria from the AtErv1-expressing *Δerv1* mutant. Mitochondria were treated with 400 μM cleavable cross-linker dithiobis succinimidyl propionate for 5 min at 25 °C and lysed with 1% SDS. The extract was used for immunoprecipitation with a combination of Mia40-specific antibodies or with pre-immune serum. The crosslinker was cleaved with DTT when indicated. Radiolabeled protein was visualized by autoradiography. Total samples contain 10% of the material used per immunoprecipitation reaction. Note that no CCMH was immunoprecipitated here, in contrast to the significant amounts that were pulled down with AtErv1 (Fig. 5a). (EPS 2090 kb)

Additional file 6: Figure S6. Related to Fig. 5 Plant Erv1 facilitates import and oxidative folding of proteins in temperature-sensitive *mia40* mutants. **A** Wild-type cells and the temperature-sensitive *mia40-3* and *mia40-4* mutants harboring either an empty vector or an AtErv1-expressing plasmid were serially dropped on glucose-, galactose-, or glycerol-containing medium. Plates were incubated for 5 days at the indicated temperatures. The expression of plant Erv1 partially restored the growth defect of *mia40* strains at restrictive temperature. **B** The levels of the intermembrane space (IMS) proteins Mia40 and Cmc1 and of the matrix protein Mrpl40 were analyzed by western blotting in the indicated strains. Cells were cultured at permissive (22 °C) or at restrictive (34 °C) conditions before preparation of the protein extract. **C** Model of the Mia40 reaction cycle in the IMS of *Arabidopsis*. As described in this study, AtErv1 can directly interact with IMS proteins in order to oxidize them independently of Mia40. AtMia40, which is present in plants though non-essential, might improve the import reaction of certain substrates. (EPS 50673 kb)

Abbreviations

ER: endoplasmic reticulum; IMS: intermembrane space; ITS: IMS-targeting signal; MISS: mitochondrial intermembrane space sorting signal; mmPEG₂₄: methyl-polyethylene glycol₂₄-maleimide; PDI: protein disulfide isomerase

Acknowledgements

We thank Sabine Knaus and Janina Laborenz for technical assistance, Jérémie Couturier and Sabrina Seavers for discussions, and Agnieszka Chacinska, Kai Hell, and Roland Lill for providing the yeast strains.

Funding

This study was funded by grants of the Deutsche Forschungsgemeinschaft (He2803/4-2, SPP1710 and IRTG1830), the BioComp initiative of Rheinland-Pfalz, and of the French National Research Agency (ANR) as part of the “Investissements d’Avenir” program (ANR-11-LABX-0002-01, Lab of Excellence ARBRE). The research stay of Nicolas Rouhier in Kaiserslautern was supported by the von Humboldt foundation.

Availability of data and materials

All data generated or analyzed during this study are included in this published article and its supplementary information files.

Authors' contributions

NR and JMH developed the concept for this study. VP, FZ, SB, NR, and JMH generated the mutants, performed the experiments, and interpreted the data. JMH wrote the initial draft of the manuscript. VP, NR, and JMH finalized the manuscript and prepared the figures. NR and JMH acquired the funding. NR and JMH supervised the project. All authors read and approved the final manuscript.

Ethics approval and consent to participate

Not applicable.

Consent for publication

Not applicable.

Competing interests

The authors declare that they have no competing interests.

Publisher's Note

Springer Nature remains neutral with regard to jurisdictional claims in published maps and institutional affiliations.

Received: 1 August 2017 Accepted: 19 October 2017

Published online: 08 November 2017

References

- Riemer J, Bulleid N, Herrmann JM. Disulfide formation in the ER and mitochondria: two solutions to a common process. *Science*. 2009; 324(5932):1284–7.
- Frand AR, Kaiser CA. The *ERO1* gene of yeast is required for oxidation of protein disulfides in the endoplasmic reticulum. *Mol Cell*. 1998;1(2):161–70.
- Solovyov A, Xiao R, Gilbert HF. Sulphydryl oxidation, not disulfide isomerization, is the principal function of protein disulfide isomerase in yeast *Saccharomyces cerevisiae*. *J Biol Chem*. 2004;279(33):34095–100.
- Araki K, Iemura S, Kamiya Y, Ron D, Kato K, Natsume T, et al. Ero1-alpha and PDIs constitute a hierarchical electron transfer network of endoplasmic reticulum oxidoreductases. *J Cell Biol*. 2013;202(6):861–74.
- Gross E, Kastner DB, Kaiser CA, Fass D. Structure of Ero1p, source of disulfide bonds for oxidative protein folding in the cell. *Cell*. 2004;117(5):601–10.
- Gross E, Sevier CS, Vala A, Kaiser CA, Fass D. A new FAD-binding fold and intersubunit disulfide shuttle in the thiol oxidase Erv2p. *Nat Struct Biol*. 2002;9(1):61–7.
- Daithankar VN, Schaefer SA, Dong M, Bahnsen BJ, Thorpe C. Structure of the human sulphydryl oxidase augmenter of liver regeneration and characterization of a human mutation causing an autosomal recessive myopathy. *Biochemistry*. 2010;49(31):6737–45.
- Wu CK, Dailey TA, Dailey HA, Wang BC, Rose JP. The crystal structure of augmenter of liver regeneration: a mammalian FAD-dependent sulphydryl oxidase. *Protein Sci*. 2003;12(5):1109–18.
- Banci L, Bertini I, Calderone V, Cefaro C, Ciofi-Baffoni S, Gallo A, et al. Molecular recognition and substrate mimicry drive the electron-transfer process between Mia40 and ALR. *Proc Natl Acad Sci U S A*. 2011;108(12):4811–6.
- Kawano S, Yamano K, Naoe M, Momose T, Terao K, Nishikawa S, et al. Structural basis of yeast Tim40/Mia40 as an oxidative translocator in the mitochondrial intermembrane space. *Proc Natl Acad Sci U S A*. 2009; 106(34):14403–7.
- Banci L, Bertini I, Cefaro C, Ciofi-Baffoni S, Gallo A, Martinelli M, et al. Mia40 is an oxidoreductase that catalyzes oxidative protein folding in mitochondria. *Nat Struct Mol Biol*. 2009;16(2):198–206.
- Koch JR, Schmid FX. Mia40 targets cysteines in a hydrophobic environment to direct oxidative protein folding in the mitochondria. *Nat Commun*. 2014;5:3041.
- Koch JR, Schmid FX. Mia40 combines thiol oxidase and disulfide isomerase activity to efficiently catalyze oxidative folding in mitochondria. *J Mol Biol*. 2014;426(24):4087–98.
- Sideris DP, Petrakis N, Katrakili N, Mikropoulou D, Gallo A, Ciofi-Baffoni S, et al. A novel intermembrane space-targeting signal docks cysteines onto Mia40 during mitochondrial oxidative folding. *J Cell Biol*. 2009;187(7):1007–22.
- Peleh V, Riemer J, Dancis A, Herrmann JM. Protein oxidation in the intermembrane space of mitochondria is substrate-specific rather than general. *Microbial Cell*. 2014;1(3):81–93.
- von der Malsburg K, Muller JM, Bohnert M, Oeljeklaus S, Kwiatkowska P, Becker T, et al. Dual role of mitoflin in mitochondrial membrane organization and protein biogenesis. *Dev Cell*. 2011;21(4):694–707.
- Milenkovic D, Ramming T, Muller JM, Wenz LS, Gebert N, Schulze-Specking A, et al. Identification of the signal directing Tim9 and Tim10 into the intermembrane space of mitochondria. *Mol Biol Cell*. 2009;20(10):2530–9.
- Peleh V, Cordat E, Herrmann JM. Mia40 is a trans-site receptor that drives protein import into the mitochondrial intermembrane space by hydrophobic substrate binding. *Elife*. 2016;5.
- Weckbecker D, Longen S, Riemer J, Herrmann JM. Atp23 biogenesis reveals a chaperone-like folding activity of Mia40 in the IMS of mitochondria. *EMBO J*. 2012;31(22):4348–58.
- Mesecke N, Terziyska N, Kozany C, Baumann F, Neupert W, Hell K, et al. A disulfide relay system in the intermembrane space of mitochondria that mediates protein import. *Cell*. 2005;121(7):1059–69.
- Bien M, Longen S, Wagener N, Chwalla I, Herrmann JM, Riemer J. Mitochondrial disulfide bond formation is driven by intersubunit electron transfer in Erv1 and proof read by glutathione. *Mol Cell*. 2010;37:516–28.
- Naoe M, Ohwa Y, Ishikawa D, Ohshima C, Nishikawa S, Yamamoto H, et al. Identification of Tim40 that mediates protein sorting to the mitochondrial intermembrane space. *J Biol Chem*. 2004;279(46):47815–21.
- Chacinska A, Pfannschmidt S, Wiedemann N, Kozjak V, Sanjuan Szklarz LK, Schulze-Specking A, et al. Essential role of Mia40 in import and assembly of mitochondrial intermembrane space proteins. *EMBO J*. 2004;23:3735–46.
- Terziyska N, Lutz T, Kozany C, Mokranjac D, Mesecke N, Neupert W, et al. Mia40, a novel factor for protein import into the intermembrane space of mitochondria is able to bind metal ions. *FEBS Lett*. 2005;579:179–84.
- Terziyska N, Grummt B, Kozany C, Hell K. Structural and functional roles of the conserved cysteine residues of the redox-regulated import receptor Mia40 in the intermembrane space of mitochondria. *J Biol Chem*. 2009;284(3):1353–63.
- Koch JR, Schmid FX. Mia40 is optimized for function in mitochondrial oxidative protein folding and import. *ACS Chem Biol*. 2014;9(9):2049–57.
- Böttlinger L, Gornicka A, Czerwinski T, Bragoszewski P, Loniewska-Lwowska A, Schulze-Specking A, et al. In vivo evidence for cooperation of Mia40 and Erv1 in the oxidation of mitochondrial proteins. *Mol Biol Cell*. 2012;23(20):3957–69.
- Tienson HL, Dabir DV, Neal SE, Loo R, Hasson SA, Boontheung P, et al. Reconstitution of the Mia40-Erv1 oxidative folding pathway for the small Tim proteins. *Mol Biol Cell*. 2009;20(15):3481–90.
- Neal SE, Dabir DV, Tienson HL, Horn DM, Glaeser K, Ogozalek Loo RR, et al. Mia40 protein serves as an electron sink in the Mia40-Erv1 import pathway. *J Biol Chem*. 2015;290(34):20804–14.
- Stojanovski D, Milenkovic D, Muller JM, Gabriel K, Schulze-Specking A, Baker MJ, et al. Mitochondrial protein import: precursor oxidation in a ternary complex with disulfide carrier and sulphydryl oxidase. *J Cell Biol*. 2008;183(2):195–202.
- Ang SK, Lu H. Deciphering structural and functional roles of individual disulfide bonds of the mitochondrial sulphydryl oxidase Erv1p. *J Biol Chem*. 2009;284(42):28754–61.
- Basu S, Leonard JC, Desai N, Mavridou DA, Tang KH, Goddard AD, et al. Divergence of Erv1-associated mitochondrial import and export pathways in trypanosomes and anaerobic protists. *Eukaryot Cell*. 2013;12(2):343–55.
- Eckers E, Petrucciani C, Gross D, Riemer J, Hell K, Deponte M. Divergent molecular evolution of the mitochondrial sulphydryl:cytochrome c oxidoreductase Erv in opisthokonts and parasitic protists. *J Biol Chem*. 2013;288(4):2676–88.
- Liu Z, Li X, Zhao P, Gui J, Zheng W, Zhang Y. Tracing the evolution of the mitochondrial protein import machinery. *Comput Biol Chem*. 2011;35(6):336–40.
- Carrie C, Giraud E, Duncan O, Xu L, Wang Y, Huang S, et al. Conserved and novel functions for *Arabidopsis thaliana* Mia40 in assembly of proteins in mitochondria and peroxisomes. *J Biol Chem*. 2010;285(46):36138–48.
- Levitin A, Danon A, Lisowsky T. Unique features of plant mitochondrial sulphydryl oxidase. *J Biol Chem*. 2004;279(19):20002–8.
- Fass D. The Erv family of sulphydryl oxidases. *Biochim Biophys Acta*. 2008; 1783(4):557–66.
- Ilani T, Alon A, Grossman I, Horowitz B, Kartvelishvily E, Cohen SR, et al. A secreted disulfide catalyst controls extracellular matrix composition and function. *Science*. 2013;341(6141):74–6.
- Vitu E, Bentzur M, Lisowsky T, Kaiser CA, Fass D. Gain of function in an ERV/ALR sulphydryl oxidase by molecular engineering of the shuttle disulfide. *J Mol Biol*. 2006;362(1):89–101.
- Reddehase S, Grummt B, Neupert W, Hell K. The disulfide relay system of mitochondria is required for the biogenesis of mitochondrial Ccs1 and Sod1. *J Mol Biol*. 2009;385:331–8.

41. Sturtz LA, Diekert K, Jensen LT, Lill R, Culotta VC. A fraction of yeast Cu, Zn-superoxide dismutase and its metallochaperone, CCS, localize to the intermembrane space of mitochondria. A physiological role for SOD1 in guarding against mitochondrial oxidative damage. *J Biol Chem.* 2001; 276(41):38084–9.
42. Klöppel C, Suzuki Y, Kojer K, Petrungaro C, Longen S, Fiedler S, et al. Mia40-dependent oxidation of cysteines in domain I of Ccs1 controls its distribution between mitochondria and the cytosol. *Mol Biol Cell.* 2011;22(20):3749–57.
43. Becher D, Kricke J, Stein G, Lisowsky T. A mutant for the yeast scERV1 gene displays a new defect in mitochondrial morphology and distribution. *Yeast.* 1999;15(12):1171–81.
44. Dabir DV, Hasson SA, Setoguchi K, Johnson ME, Wongkongkathep P, Douglas CJ, et al. A small molecule inhibitor of redox-regulated protein translocation into mitochondria. *Dev Cell.* 2013;25(1):81–92.
45. Bourens M, Barrientos A. A CMC1-knockout reveals translation-independent control of human mitochondrial complex IV biogenesis. *EMBO Rep.* 2017; 18(3):477–94.
46. Bourens M, Dabir DV, Tienson HL, Sorokina I, Koehler CM, Barrientos A. Role of twin Cys-Xaa₉-Cys motif cysteines in mitochondrial import of the cytochrome c oxidase biogenesis factor Cmc1. *J Biol Chem.* 2012;287(37): 31258–69.
47. Kojer K, Bien M, Gangel H, Morgan B, Dick TP, Riemer J. Glutathione redox potential in the mitochondrial intermembrane space is linked to the cytosol and impacts the Mia40 redox state. *EMBO J.* 2012;31(14):3169–82.
48. Bihlmaier K, Mesecke N, Terzyiska N, Bien M, Hell K, Herrmann JM. The disulfide relay system of mitochondria is connected to the respiratory chain. *J Cell Biol.* 2007;179:389–95.
49. Allen S, Balabanidou V, Sideris DP, Lisowsky T, Tokatlidis K. Erv1 mediates the Mia40-dependent protein import pathway and provides a functional link to the respiratory chain by shuttling electrons to cytochrome c. *J Mol Biol.* 2005;353(5):937–44.
50. Dabir DV, Leverich EP, Kim SK, Tsai FD, Hirasawa M, Knaff DB, et al. A role for cytochrome c and cytochrome c peroxidase in electron shuttling from Erv1. *EMBO J.* 2007;26(23):4801–11.
51. Baker MJ, Mooga VP, Guiard B, Langer T, Ryan MT, Stojanovski D. Impaired folding of the mitochondrial small TIM chaperones induces clearance by the i-AAA protease. *J Mol Biol.* 2012;424(5):227–39.
52. Schreiner B, Westerburg H, Forne I, Imhof A, Neupert W, Mokranjac D. Role of the AAA protease Yme1 in folding of proteins in the intermembrane space of mitochondria. *Mol Biol Cell.* 2012;23(22):4335–46.
53. Huang S, Taylor NL, Narsai R, Eubel H, Whelan J, Millar AH. Experimental analysis of the rice mitochondrial proteome, its biogenesis, and heterogeneity. *Plant Physiol.* 2009;149(2):719–34.
54. Heazlewood JL, Tonti-Filippini JS, Gout AM, Day DA, Whelan J, Millar AH. Experimental analysis of the *Arabidopsis* mitochondrial proteome highlights signaling and regulatory components, provides assessment of targeting prediction programs, and indicates plant-specific mitochondrial proteins. *Plant Cell.* 2004;16(1):241–56.
55. Kranz R, Lill R, Goldman B, Bonnard G, Merchant S. Molecular mechanisms of cytochrome c biogenesis: three distinct systems. *Mol Microbiol.* 1998; 29(2):383–96.
56. Meyer EH, Giege P, Gelhaye E, Rayapuram N, Ahuja U, Thony-Meyer L, et al. AtCCMH, an essential component of the c-type cytochrome maturation pathway in *Arabidopsis* mitochondria, interacts with apocytochrome c. *Proc Natl Acad Sci U S A.* 2005;102(44):16113–8.
57. Ramesh A, Peleh V, Martinez-Caballero S, Wollweber F, Sommer F, van der Laan M, et al. A disulfide bond in the TIM23 complex is crucial for voltage gating and mitochondrial protein import. *J Cell Biol.* 2016;214(4):417–31.
58. Lisowsky T. Dual function of a new nuclear gene for oxidative phosphorylation and vegetative growth in yeast. *Mol Gen Genet.* 1992; 232(1):58–64.
59. Uhrig RG, Labandera AM, Tang LY, Sieben NA, Goudreault M, Yeung E, et al. Activation of mitochondrial protein phosphatase SLP2 by MIA40 regulates seed germination. *Plant Physiol.* 2017;173(2):956–69.
60. Haindrich AC, Boudova M, Vancova M, Diaz PP, Horakova E, Lukes J. The intermembrane space protein Erv1 of *Trypanosoma brucei* is essential for mitochondrial Fe-S cluster assembly and operates alone. *Mol Biochem Parasitol.* 2017;214:47–51.
61. Alon A, Grossman I, Gat Y, Kodali VK, DiMaio F, Mehlman T, et al. The dynamic disulphide relay of quiescin sulphhydryl oxidase. *Nature.* 2012; 488(7411):414–8.
62. Kranz RG, Richard-Fogal C, Taylor JS, Frawley ER. Cytochrome c biogenesis: mechanisms for covalent modifications and trafficking of heme and for heme-iron redox control. *Microbiol Mol Biol Rev.* 2009;73(3):510–28.
63. Gray MW, Burger G, Lang BF. Mitochondrial evolution. *Science.* 1999; 283(5407):1476–81.
64. Peleh V, Ramesh A, Herrmann JM. Import of proteins into isolated yeast mitochondria. *Methods Mol Biol.* 2015;1270:37–50.
65. Couturier J, Wu HC, Dhalleine T, Pegeot H, Sudre D, Gualberto JM, et al. Monothiol glutaredoxin-Bola interactions: redox control of *Arabidopsis thaliana* Bola2 and SufE1. *Mol Plant.* 2014;7(1):187–205.

Submit your next manuscript to BioMed Central and we will help you at every step:

- We accept pre-submission inquiries
- Our selector tool helps you to find the most relevant journal
- We provide round the clock customer support
- Convenient online submission
- Thorough peer review
- Inclusion in PubMed and all major indexing services
- Maximum visibility for your research

Submit your manuscript at
www.biomedcentral.com/submit



Oxidation of *Arabidopsis thaliana* MIA40 substrates by the combined action of ERV1 and glutathione

Flavien Zannini, Jérémie Couturier and Nicolas Rouhier

Université de Lorraine, Inra, IAM, F-54000 Nancy, France.

Cet article, en cours de préparation, sera soumis à the Journal of Biological Chemistry dans un format « Accelerated communications ».

Nos précédents travaux ont révélé la capacité de la protéine *At*ERV1 à oxyder certains substrats de MIA40 chez la levure, permettant la complémentation fonctionnelle du mutant *mia40*. Nous avons évalué la capacité des protéines ERV1 et MIA40 à oxyder COX19 *in vitro* en présence ou en absence d'un mélange de glutathion réduit et oxydé reflétant les concentrations et potentiels redox mesurés *in vivo*. Les résultats indiquent que la protéine ERV1 est capable d'oxyder COX19 en absence de MIA40 si du glutathion est présent. En outre, les protéines ERV1-MIA40 n'oxydent pas l'apo-cytochrome réductase, CCMH, ce qui expliquerait pourquoi aucune réductase de CCMH n'a été identifiée à ce jour. Ces résultats confirment la particularité du système ERV1-MIA40 chez les plantes supérieures et soulignent l'importance du GSH dans le processus d'oxydation des protéines au sein de l'IMS. Cependant, bien que le format de ces articles soit court (5 figures/tableaux maximum), nous envisageons d'inclure des expériences supplémentaires, notamment la détermination du potentiel redox des couples dithiol-disulfure correspondants aux motifs CPC de MIA40 et CEQKSC d'ERV1 et des cinétiques de réduction de ces protéines par le glutathion. De plus, il sera nécessaire d'analyser l'activité d'oxydation d'ERV1 dans des environnements plus ou moins réducteurs et d'essayer de prouver que l'oxydation des substrats par ERV1 fait appel à une activité de glutathionylation.

1 **Oxidation of *Arabidopsis thaliana* MIA40 substrates by the combined action of ERV1 and**
2 **glutathione**

3

4 Flavien Zannini, Jérémie Couturier, and Nicolas Rouhier

5

6 Université de Lorraine, Inra, IAM, F-54000 Nancy, France.

7

8 **Running title:** Bypassing AtMIA40 by GSH

9

10 **Abstract**

11 Protein import and oxidative folding into the intermembrane space of mitochondria (IMS) relies
12 on the MIA40-ERV1 couple. The MIA40 oxidoreductase usually performs substrate recognition
13 and oxidation and is then regenerated by the FAD-dependent oxidase ERV1. In most eukaryotes,
14 both proteins are essential, but MIA40 is dispensable in *Arabidopsis thaliana*. Previous
15 complementation experiments of a yeast *mia40* mutant expressing a redox inactive, but import-
16 competent version of yeast Mia40 by *Arabidopsis* ERV1 suggested that AtERV1 catalyzed
17 oxidation of MIA40 substrates. We assessed the capacity of both yeast and *Arabidopsis* MIA40
18 and ERV1 recombinant proteins to oxidize the cytochrome c oxidase assembly protein COX19, a
19 typical MIA40 substrate, and the apo-cytochrome reductase CCMH in the presence or absence of
20 glutathione using *in vitro* alkylation assays. The results pointed to fundamental biochemical
21 differences between *Arabidopsis* and yeast ERV1 in catalyzing the COX19 and CCMH
22 oxidation. The presence of glutathione used at physiological concentration and redox potential
23 was sufficient to support the oxidation of a MIA40 substrate by AtERV1 providing a likely
24 explanation why MIA40 is not essential for the import and oxidative folding of IMS-located
25 proteins in *Arabidopsis*.

26

27 **Keywords:** MIA40, ERV1, glutathione, oxidative folding, mitochondrial inter-membrane space

28

29 **Introduction**

30

31 Mitochondria are essential organelles, sustaining many crucial cellular pathways such as ATP
32 production, apoptosis, iron-sulfur (Fe-S) cluster biogenesis, and ion homeostasis. Mitochondria
33 are formed by two aqueous compartments, the matrix and the inter-membrane space (IMS)
34 separated by two biological membranes, the outer membrane (OM) and the inner membrane
35 (IM). Among the 1000 proteins present in this organelle, 51 and 127 proteins have been
36 reported as present in the IMS of yeast and human mitochondria respectively (Hung et al., 2014;
37 Morgenstern et al., 2017; Vögtle et al., 2012). After their translation in the cytosol, the import of
38 IMS-located proteins relies at least on three distinct pathways (Neupert and Herrmann, 2007;
39 Riemer et al., 2009). The predominant pathway allows both import and oxidative folding
40 (Neupert and Herrmann, 2007). Many of the proteins concerned are characterized by the presence
41 of two repeated Cx₃C (for TIM proteins) or Cx₉C (for COX proteins) motifs (Longen et al., 2009;
42 Peleh et al., 2016) but other proteins (Atp23, CCS1, MICU, SLP2) with particular cysteine motifs
43 have proven to be also imported using this pathway (Gabriel et al., 2007; Gross et al., 2011;
44 Petrungaro et al., 2015; Suzuki et al., 2013; Uhrig et al., 2017). The import and oxidative folding
45 of these protein substrates are ensured by a pair of proteins referred to as the oxidoreductase
46 Mitochondrial Intermembrane space import and Assembly protein 40 (MIA40) and Essential for
47 the Respiration and Vegetative growth (ERV1) (Meyer et al., 2019). The former introduces
48 disulfide bonds and is regenerated by the latter. The core structure of MIA40 is formed by two
49 disulfide-bridged helices forming a hydrophobic cleft important for substrate recognition and an
50 N-terminal flexible arm where the catalytic cysteines present in a CPC motif are found (Banci et
51 al., 2009; Chacinska et al., 2004; Peleh et al., 2016). Three different models have been proposed
52 to describe the molecular interactions between MIA40 and their substrates (Hansen and
53 Herrmann, 2019). In the folding trap model, protein translocation into the IMS is dependent on
54 the formation of disulfides on MIA40 substrates, preventing back-translocation into the cytosol.
55 In the two trans-site receptor models, substrate trapping is ensured initially by the hydrophobic
56 domain of MIA40 but requires the MIA40 oxidase activity either concomitantly or in a further
57 separated step (Hansen and Herrmann, 2019; Peleh et al., 2016). The hydrophobic cleft interacts
58 with specific recognition sequences present in MIA40 substrates referred to as MISS or ITS
59 (respectively for Mitochondrial IMS–Sorting Signal and Intermembrane space Targeting Signal)

60 (Erdogan and Riemer, 2017; Milenkovic et al., 2009; Sideris et al., 2009). These specific motifs
61 formed by hydrophobic and aromatic amino acids are situated in close proximity of the Cx₃C or
62 Cx₉C motifs. After this initial step of recognition, the substrates are oxidized by the catalytic
63 cysteine pair of MIA40, promoting their folding and retention in the IMS (Koch and Schmid,
64 2014; Peleh et al., 2016).

65 Whatever the model considered, MIA40 is *in fine* released under reduced form after
66 catalyzing its oxidation reaction. Its re-oxidation is achieved by the homodimeric FAD-dependent
67 thiol oxidase, ERV1. ERV1 isoforms possess two conserved cysteine pairs forming
68 intramolecular disulfides. An exposed disulfide (shuttle disulfide) catalyzes the oxidation of the
69 CPC disulfide of MIA40 (Hell, 2008; Lionaki et al., 2010; Rissler et al., 2005; Stojanovski et al.,
70 2012) and is then regenerated by the disulfide present in the central domain of the second
71 monomer. Electrons are then shuttled to the FAD cofactor, to cytochrome c and cytochrome c
72 oxidase (Bihlmaier et al., 2007; Herrmann and Riemer, 2010; Kojer and Riemer, 2014; Tienson
73 et al., 2009; Vitu et al., 2006). While the core domain of ERV1 proteins from different species is
74 relatively well conserved, a noticeable difference exists among ERV1 proteins. In opisthokonts,
75 the catalytic disulfide is formed by cysteines present in a Cx₂C motif found in the N-terminal part
76 of ERV1 whereas it is formed between cysteines located found in a Cx₃₋₅C motif in the C-
77 terminal part in isoforms from plant and protists (Leviton et al., 2004; Specht et al., 2018).
78 Proteins from protists have an additional KISS domain located between the FAD central domain
79 and the catalytic domain (Allen et al., 2008). In Opisthokonts, both MIA40 and ERV1 have
80 proven to be essential as yeast mutants are lethal in respiratory conditions and mutations affecting
81 these proteins in human induce severe diseases such as myopathy and neuronal cell degeneration
82 (Chacinska et al., 2004; Fischer and Riemer, 2013; Lisowsky, 1992; Polimeno et al., 2013;
83 Rissler et al., 2005). Mutation of Erv1 is also lethal in *Arabidopsis thaliana* and in the protist
84 *Leishmania infantum* (Leviton et al., 2004; Specht et al., 2018). However, several protists
85 including apicomplexan and kinetoplastid parasites lack Mia40 and an *Arabidopsis mia40* mutant
86 displays no growth phenotype despite a slight decrease in complex I activity (Allen et al., 2008;
87 Carrie et al., 2010). From a functional point of view, ERV1 proteins from these parasites could
88 not functionally substitute the essential Erv1 in yeast (Eckers et al., 2013) whereas *Arabidopsis*
89 ERV1 only partially complements the yeast *erv1* mutant (Peleh et al., 2017). It was shown that
90 *At*ERV1 and *Sc*Mia40 interact together *in vivo* but that *At*ERV1 is unable to oxidize *Sc*Mia40

properly (Peleh et al., 2017). These incompatibilities have been explained by the structural divergence between ERV1 isoforms (Levitin et al., 2004; Peleh et al., 2017). Accordingly, chimeric ERV1 proteins combining the N-terminal domain of yeast ERV1 to the core domain of *Leishmania tarentolae* Erv1 thus mimicking the yeast Erv1 structural architecture, were able to complement the yeast *erv1* mutant (Specht et al., 2018). The question whether parasite and plant Erv1 proteins might exert the function of Mia40 was addressed by complementing *mia40* yeast cells. Whereas none of the tested truncated, chimeric or mutated Erv1 constructs from *L. tarentolae* were able to rescue these cells, *AtERV1* did it when a redox inactive but chaperone competent MIA40 protein was co-expressed (Peleh et al., 2017). Altogether, these observations suggested that *AtERV1* was able to some extent to oxidize directly MIA40 substrates as long as they are imported.

In order to obtain such a confirmation, we have compared the capacity of the *A. thaliana* and *S. cerevisiae* ERV1 to oxidize the Arabidopsis cytochrome c oxidase biogenesis factor COX19 in the presence or absence of the respective MIA40 proteins but also CCMH, a reductase dedicated to the reduction of apo-cytochrome c in the IMS. Moreover, from the reports indicating that glutathione improves protein import both *in vivo* and *in vitro* by counteracting in particular the formation of long-lived or unproductive MIA40-substrate covalent intermediates (Bien et al., 2010; Fischer et al., 2013), a possible contribution of glutathione was examined in these *in vitro* assays.

110

111 Materials and Methods

112

113 ***Cloning, production and purification of recombinant proteins***

The open reading frame of *A. thaliana* COX19 (AT1G69750.1) has been amplified from leaf cDNAs using the following primers (restriction sites underlined), AtCOX19 for 5' CCCCCCCCATATGAGTACAGGTGGAGCATT 3' and AtCOX19 rev 5' CCCGGATCCTCAATGTTGATACTCTCTGT 3' and cloned into pET15b between NdeI and BamHI restriction sites allowing the production of an N-terminal His-tagged protein. The protein was expressed in the *E. coli* Origami2 strain cultivated at 37°C in LB medium and protein production was induced at exponential phase by adding 100 µM IPTG (isopropyl-β-D-thiogalactopyranoside) for 4h before collecting bacteria cells, which were resuspended into a 50

122 mM Tris-HCl pH 8.0, 300 mM NaCl, 10 mM imidazole buffer. Cell lysis and IMAC protein
123 purification of His-tagged COX19 was performed using a procedure similar to the one described
124 previously (Selles et al., 2017).

125 The recombinant *S. cerevisiae* and *A. thaliana* ERV1 and MIA40 and *A. thaliana* CCMH
126 have been expressed in *E. coli* BL21(DE3) from pET24a-ScErv1, pGEX6-ScMia40, pET12a-
127 AtMIA40, pET12a-AtERV1 and pQE60-AtCCMH plasmids following procedures described
128 previously (Bien et al., 2010; Chacinska et al., 2004; Meyer et al., 2005; Peleh et al., 2016;
129 Tienson et al., 2009). Peleh 2017). Protein concentrations were determined
130 spectrophotometrically using the respective molar extinction coefficients at 280 nm calculated
131 from the amino acid sequences using the ProtParam server tool (*AtMIA40*: $7365 \text{ M}^{-1}.\text{cm}^{-1}$,
132 *AtERV1*: $50063 \text{ M}^{-1}.\text{cm}^{-1}$, *ScMia40*: $11835 \text{ M}^{-1}.\text{cm}^{-1}$, *ScErv1*: $42315 \text{ M}^{-1}.\text{cm}^{-1}$, *AtCCMH*: 3105
133 $\text{M}^{-1}.\text{cm}^{-1}$, *AtCOX19*: $3230 \text{ M}^{-1}.\text{cm}^{-1}$).

134

135 ***Reduction of COX19 and CCMH proteins***

136 Before each test, around 1 mg of COX19 and CCMH proteins was reduced using a 50-
137 fold excess dithiothreitol (DTT) during 4 hours at room temperature, then desalted against 50
138 mM phosphate buffer pH 7.4 using Sephadex-G25 column (Sigma-Aldrich).

139

140 ***Reduction of cytochrome c***

141 The reduction of 20 μM cytochrome c from equine heart (SIGMA-Aldrich, product code
142 C7752) was followed spectrophotometrically by recording the absorbance changes at 550 nm
143 over time, usually 60 min (Cary 50 Variant-Agilent). The reaction was performed in 500 μL of
144 50 mM phosphate buffer at pH 7.4, in presence of 40 μM reduced Arabidopsis COX19 or CCMH
145 and various combinations of *A. thaliana* and *S. cerevisiae* ERV1 and MIA40 at 4 μM . The
146 positive control was obtained in the presence of 40 μM DTT. All experiments have been repeated
147 at least three times and the data shown are representative of the results obtained.

148

149 ***Alkylation shift experiment for redox state detection***

150 For all tests, 40 μM of reduced proteins were incubated with 4 μM of ERV1 alone or in
151 presence of 4 μM of MIA40 for different times in 50 μL of 50 mM phosphate buffer pH 7.4.
152 After a precipitation with 10% TCA, reduced cysteines are alkylated with methyl-polyethylene

153 glycol-maleimide of 1.2 kDa (mmPEG₂₄) or 2 kDa (mPEG₂₀₀₀) and 2.5 µg of proteins are loaded
154 on non-reducing SDS-PAGE gel 17% as described previously (Zannini et al., 2017). The
155 oxidation of AtCOX19 was also assessed in the presence of an 8 mM GSH/GSSG mixture
156 corresponding to a redox potential of - 274 mV at pH 7.4. In fact, this solution corresponded to a
157 freshly prepared GSH solution in which we have estimated that 0.25% GSSG was present. This
158 estimate was determined from a spectrophotometric detection in an assay containing 200 µM
159 NADPH, and 0.5 unit baker yeast glutathione reductase (GR, SIGMA).

160

161 **Results and discussion**

162

163 **ERV1 alone or with a redox inactive MIA40 is not able to oxidize COX19 *in vitro***

164 Upon expression in the more oxidizing cytoplasm compartment of the *E. coli* origami
165 strain, AtCOX19 was purified in a fully oxidized form as were the yeast and Arabidopsis MIA40
166 and ERV1 proteins expressed in the regular *E. coli* BL21(DE3) strain. AtCOX19 possesses four
167 cysteinyl residues forming two intramolecular disulfides. Its reduction was achieved with a 50-
168 fold excess of DTT for 4 hours as it has proven to be resistant to reduction and to re-oxidize quite
169 quickly. In order to assess the capacity of Arabidopsis ERV1, but also of yeast ERV1 for
170 comparison, to oxidize a reduced AtCOX19, we have carried out two types of *in vitro* assays. The
171 first method measured AtCOX19 oxidation in a coupled assay measuring cytochrome *c* reduction
172 at 550 nm over time with catalytic amounts of ERV1 and/or MIA40. Using similar reaction
173 mixtures, the second method assessed AtCOX19 redox state after cysteine alkylation and
174 separation on non-reducing SDS-PAGE. In this assay, only reduced cysteine residues are
175 accessible to modification. This results in a change of the migration behavior that allows
176 distinguishing different redox forms, *i.e.* completely reduced or with one or two intramolecular
177 disulfides.

178 In the cytochrome *c* reduction assay, it became apparent that AtERV1 has no or a very
179 poor capacity to oxidize AtCOX19 (Fig. 1A), the presence of AtMIA40 being crucial to reach a
180 good oxidation efficiency as compared to the control test performed using DTT instead of
181 AtCOX19 and both AtERV1 and AtMIA40 proteins. The same conclusion arose from the
182 alkylation shift assay (Fig. 1B). In the presence of AtERV1 alone, there are only minimal
183 amounts of completely oxidized AtCOX19 up to 45 min but rather the formation of a partially

184 oxidized intermediate with one disulfide. Only after 1h, higher amounts of completely oxidized
185 AtCOX19 were accumulated. On the contrary, the combined presence of AtMIA40 promoted a
186 near complete AtCOX19 oxidation at the end of the 1h reaction. Globally, similar results have
187 been obtained when yeast Mia40 and Erv1 proteins were used (Fig. 1C and D), ScErv1 alone
188 cannot oxidize efficiently *At*COX19 in the absence of ScMia40. In both assays, the reaction was
189 even more efficient with a complete COX19 oxidation after 30 min. This difference in efficiency
190 between the plant and yeast oxidation systems might be due to an intrinsic difference between
191 both ERV1 proteins as observed previously when their activity was tested in the cytochrome c
192 reduction assay performed in the absence of MIA40 (Peleh et al., 2017). In addition, these results
193 point to an indispensable contribution of MIA40 for COX19 oxidation in these *in vitro*
194 conditions.

195 Previous studies performed in yeast demonstrated that expressing a redox-inactive
196 ScMia40 version was sufficient to allow substrate import into IMS (Peleh et al., 2016). This
197 suggested that the sole presence of the hydrophobic cleft on Mia40 sustaining its chaperone
198 function allowed trapping the substrates which would be oxidized by ERV1. Hence, to examine
199 whether the oxidase activity of MIA40 from *A. thaliana* is required for COX19 oxidation, we
200 have purified a MIA40 variant mutated for both cysteines of the redox motif (SPS) and
201 performed the same experiments. The cytochrome *c* reduction assay indicated that the level of
202 reduced cytochrome *c* is not noticeably increased in the presence of the AtMIA40 SPS variant as
203 compared to *At*ERV1 alone and well below the assay with a non-mutated AtMIA40 (Fig. 1E).
204 Accordingly, the alkylation shift assays (Fig. 1F) showed that only minimal amounts of fully
205 oxidized *At*COX19 were formed in an assay comprising this AtMIA40 SPS variant.
206

207 **Arabidopsis MIA40 oxidase activity is modulated upon interaction with ScERV1**

208 Unlike yeast and human, the maturation of *c* type cytochromes in the IMS of plant
209 mitochondria requires a reducing component called CCMH (Sanders et al., 2010). This protein
210 possesses a Cx₂CH motif allowing apo-cytochrome *c* reduction before heme incorporation and
211 this catalytic pair of cysteines is found in the IMS (Meyer et al., 2005). Hence, as a second step,
212 we have analyzed whether MIA40/ERV1 couples can oxidize CCMH. The observation that the
213 yeast Mia40/Erv1 couple was more efficient in oxidizing AtCOX19 suggested that these proteins
214 have different redox properties. Using the same read-outs (cysteine alkylation and cytochrome *c*

reduction assays) (Fig. 2A and B), we have observed that AtERV1 was unable to oxidize AtCCMH and adding AtMIA40 resulted in very poorly efficient reaction as most AtCCMH remained in a reduced state after 1 hour. On the contrary, a complete oxidation of AtCCMH was visible in less than 5 min in both assays using yeast counterparts (Figure 2C and D). This oxidation requires the presence of both proteins as ScErv1 alone does not have the capacity to oxidize efficiently AtCCMH. These data indicated that one of the yeast oxidases has particular redox properties that the plant ortholog does not have and prompted us to perform a test where AtMIA40 was combined with ScErv1. The other combination cannot be tested as we previously observed that *At*ERV1 does not have the capacity to oxidize *Sc*Mia40 (Peleh et al., 2017). In this combination, AtMIA40 was now able to oxidize *At*CCMH efficiently, although the reaction appeared slightly less efficient than with the complete yeast system (Figs. 2E and F). This unexpected observation should not (or not only) correspond to a better efficiency of ScErv1 to oxidize AtMIA40. Rather it indicates that ScErv1 participates in the oxidation reaction by acting on AtCCMH, AtMIA40 or both, thus promoting MIA40 activity. It has been proposed in some studies that ternary complexes are formed in yeast involving Erv1, Mia40 and the substrate (Böttinger et al., 2012; Stojanovski et al., 2008). This will have to be investigated for plant proteins.

Arabidopsis ERV1 oxidizes COX19, a MIA40 substrate, in the presence of GSH

Although previous observations indicated that AtERV1 was able to complement a yeast *mia40* mutant expressing a redox-inactive Mia40 and suggested an oxidase activity of ERV1, the *in vitro* results shown in Figure 1 pointed to the requirement of a redox-active AtMIA40 for AtCOX19 oxidation by AtERV1. Previous studies reported that elevated glutathione concentrations (5 to 13 mM) are present in the IMS with measured redox potentials comprised between -255 and -300 mV in yeast cells and of *ca* -290 mV in human cells (Fischer et al., 2013; Hu et al., 2008; Kojer et al., 2012; Østergaard et al., 2004). Moreover, it was shown that the glutathione pool of the IMS equilibrated with the cytosol glutathione pool due to the passive exchange of GSH via porins (Kojer et al., 2012). Such redox component could be the missing factor in our *in vitro* assay as compared to the yeast cellular context. Indeed, the GSH pool influences Mia40 redox state, although MIA40 is only slowly reduced by GSH (Bien et al., 2010; Kojer et al., 2012). With the report that low amounts of Grx2 are present in the mitochondrial

246 IMS of yeast, it was proposed that Grx2 mediates this GSH effect (Calabrese et al., 2017; Kojer
247 et al., 2015). Hence, the presence of these components may ensure some sort of proofreading
248 activity for misfolded proteins or avoiding protein misfolding at the import step (Bien et al.,
249 2010) in a way somehow similar with oxidative folding in the ER where protein disulfide
250 isomerase (PDI) activity is assisted by GSH (Appenzeller-Herzog, 2011).

251 The impact of glutathione on AtCOX19 oxidation was thus examined over a longer
252 period, typically 3 hours, using a concentration of 8 mM and a GSH/GSSG ratio corresponding to
253 a redox potential of -274 mV at pH 7.4, the timeframe and average values for glutathione were
254 chosen based on previous studies (see above) and somehow imposed by the presence of 0.25%
255 GSSG in freshly prepared GSH solutions. At these values, a significant oxidation of AtCOX19
256 occurred when only glutathione was present, the fully oxidized form representing *ca* 40% of the
257 total AtCOX19 at the end of this experiment (Fig. 3A). Hence, the low amounts of GSSG and/or
258 the combination of GSH and O₂ is sufficient to introduce both disulfides in AtCOX19. Then, the
259 impact of this GSH/GSSG buffer was assayed in presence of the yeast (Fig. 3B) and Arabidopsis
260 (Fig. 3C) MIA40/ERV1 couples. ScErv1 was unable to oxidize AtCOX19 in the presence of
261 glutathione and the reaction still required ScMia40 (around 90 % of AtCOX19 oxidation after 30
262 min as observed in Figure 1). On the contrary, AtERV1 was able to oxidize AtCOX19 in the
263 presence of glutathione (80% of oxidized AtCOX19 after 3 hours) and the reaction is not
264 improved by the presence of AtMIA40 (Fig. 3C). Overall, unlike yeast proteins, there is a clear
265 effect of GSH on Arabidopsis MIA40/ERV1 oxidizing properties, GSH or GSSG supporting an
266 ERV1 oxidase activity and maybe counteracting MIA40 activity.

267

268 **Model for the oxidation of COX19 by AtERV1 in the presence of GSH**

269

270 We have previously observed in a cytochrome reduction assay that AtERV1 oxidized reduced
271 glutathione or in other words that AtERV1 is reduced by GSH whereas ScERV1 had a poor
272 capacity to do so (Peleh et al., 2017). As already mentioned, these proteins differ by the position
273 of their so-called shuttle disulfide (N-terminal for ScErv1 *vs* C-terminal for AtERV1) and
274 cysteine spacing residues (2 residues for ScErv1 *vs* 4 residues for AtERV1) whereas the signature
275 and position of the catalytic disulfide are in principle unchanged. Hence, the difference in redox
276 properties is likely due to the shuttle disulfide. In the yeast protein, the midpoint redox potential

277 of this dithiol-disulfide couple was measured to be -320 mV at pH 7.0 whereas the one of the
278 catalytic pair of cysteines was - 150 mV (Dabir et al., 2007). Hence, it is now mandatory to
279 measure the redox potential of the disulfides present in AtERV1 and notably the one for the
280 shuttle disulfide, with the expectation to get a less negative value. In absence of this information,
281 we have built a hypothetical model proposing that, in the absence of MIA40 but presence of
282 reduced glutathione, an oxidized AtERV1 mediates substrate glutathionylation (Figure 4). In this
283 model, GSH reacts with the shuttle disulfide of AtERV1 generating a glutathionylated ERV1
284 intermediate that can react with the substrate thiols to form an intramolecular disulfide and
285 releasing GSH but not disulfide glutathione. Complete substrate oxidation could then proceed via
286 oxygen as proposed previously (Banci et al., 2009) or via another turnover involving AtERV1.
287 Note that in the assay without cytochrome, AtERV1 should pass electrons to molecular oxygen to
288 get re-oxidized. An alternative mechanism may be considered where GSH participates in the
289 reduction of disulfides formed between ERV1 and MIA40 substrates. A recognition of MIA40
290 substrates by ERV1 would make sense based on the very similar 3D structures adopted by
291 MIA40 and their substrates.

292 The absence of additive effect of MIA40 in the ERV1- and GSH-mediated oxidation of
293 AtCOX19 using Arabidopsis proteins as compared to the yeast proteins (Figure 3) also suggests
294 that the MIA40 redox properties differ between both organisms. The redox potential of the CPC
295 dithiol-disulfide couple was determined to be -200 mV and -290 mV for the human and yeast
296 protein respectively (Banci et al., 2009; Tienson et al., 2009). This more negative value for the
297 yeast protein may explain why GSH does not reduce it very well (Bien et al., 2010). Coupled to
298 the weak isomerase activity of yeast MIA40, it was proposed that GSH is involved in the
299 reduction/isomerisation of misfolded proteins (Bien et al., 2010; Hudson and Thorpe, 2015).
300 Nevertheless, while some *in vivo* and *in vitro* studies indeed showed positive effects of GSH
301 (Bien et al., 2010; Fischer et al., 2013), other studies have the opposite conclusion that GSH
302 inhibits the import and/or oxidation of some Mia40 substrates (Neal et al., 2015). This indicates
303 that changes in the concentrations and redox state of glutathione are likely critical factors *in vivo*
304 but also for *in vitro* assays. There is also an urgent need to determine whether a dithiol GRX is
305 present in the mitochondrial IMS of plants and measure the redox potential of the MIA40
306 catalytic disulfide. By comparing it with the one of glutathione in the IMS of plant mitochondria,
307 it may help determining to which extent MIA40 is oxidized in plant cells. A recent study

308 concluded that the *in vivo* redox state of Mia40 at steady state in yeast cells is about 70%
309 oxidized and that it is influenced both by ERV1 and glutathione (Kojer et al., 2012).

310

311 **Conclusions**

312

313 The results presented in this study highlight the specificity of the plant ERV1-MIA40 pathway
314 towards GSH and two IMS proteins, COX19 and CCMH. It is first interesting to note that the
315 Arabidopsis ERV1-MIA40 couple is poorly able to oxidize CCMH. This may explain why no
316 reducing system has been identified in plants so far unlike in bacteria such as *E. coli* where
317 reduction of the periplasmic ortholog is assisted by CCMG using electrons coming the cytoplasm
318 and transferred by the membrane CcdA protein (Verissimo et al., 2017) . One of the difference
319 between these systems is the presence of high GSH concentrations in the IMS and eventually of
320 glutaredoxins although this remain to be established for plants. The next step will be to verify *in*
321 *vitro* the capacity of GSH alone or with glutaredoxin to reduce CCMH. The second important
322 conclusion is the observation that the *in vitro* requirement of MIA40 for COX19 oxidation is
323 abolished when ERV1 and physiological concentrations of glutathione provided at a
324 physiological redox potential are present. The capacity of *At*ERV1 to bypass MIA40 function in
325 this context may actually explain why *At*ERV1 was able to complement a yeast *mia40* mutant,
326 restoring the amount of MIA40 substrates (Peleh et al., 2017) and why the role of *At*MIA40 is
327 dispensable in *A. thaliana* but not in other organisms.

328

329 **References**

330 Allen, J.W.A., Ferguson, S.J., and Ginger, M.L. (2008). Distinctive biochemistry in the
331 trypanosome mitochondrial intermembrane space suggests a model for stepwise evolution of the
332 MIA pathway for import of cysteine-rich proteins. FEBS Lett. 582, 2817–2825.

333 Appenzeller-Herzog, C. (2011). Glutathione- and non-glutathione-based oxidant control in the
334 endoplasmic reticulum. J. Cell. Sci. 124, 847–855.

335 Banci, L., Bertini, I., Cefaro, C., Ciofi-Baffoni, S., Gallo, A., Martinelli, M., Sideris, D.P.,
336 Katrakili, N., and Tokatlidis, K. (2009). MIA40 is an oxidoreductase that catalyzes oxidative
337 protein folding in mitochondria. Nature Structural & Molecular Biology 16, 198–206.

338 Bien, M., Longen, S., Wagener, N., Chwalla, I., Herrmann, J.M., and Riemer, J. (2010).
339 Mitochondrial Disulfide Bond Formation Is Driven by Intersubunit Electron Transfer in Erv1 and
340 Proofread by Glutathione. Molecular Cell 37, 516–528.

- 341 Bihlmaier, K., Mesecke, N., Terziyska, N., Bien, M., Hell, K., and Herrmann, J.M. (2007). The
342 disulfide relay system of mitochondria is connected to the respiratory chain. *The Journal of Cell*
343 *Biology* 179, 389–395.
- 344 Böttlinger, L., Gornicka, A., Czerwic, T., Bragoszewski, P., Loniewska-Lwowska, A., Schulze-
345 Specking, A., Truscott, K.N., Guiard, B., Milenkovic, D., and Chacinska, A. (2012). In vivo
346 evidence for cooperation of Mia40 and Erv1 in the oxidation of mitochondrial proteins. *Mol.*
347 *Biol. Cell* 23, 3957–3969.
- 348 Calabrese, G., Morgan, B., and Riemer, J. (2017). Mitochondrial Glutathione: Regulation and
349 Functions. *Antioxid. Redox Signal.* 27, 1162–1177.
- 350 Carrie, C., Giraud, E., Duncan, O., Xu, L., Wang, Y., Huang, S., Clifton, R., Murcha, M.,
351 Filipovska, A., Rackham, O., et al. (2010). Conserved and Novel Functions for *Arabidopsis*
352 *thaliana* MIA40 in Assembly of Proteins in Mitochondria and Peroxisomes. *Journal of Biological*
353 *Chemistry* 285, 36138–36148.
- 354 Chacinska, A., Pfannschmidt, S., Wiedemann, N., Kozjak, V., Sanjuán Szklarz, L.K., Schulze-
355 Specking, A., Truscott, K.N., Guiard, B., Meisinger, C., and Pfanner, N. (2004). Essential role of
356 Mia40 in import and assembly of mitochondrial intermembrane space proteins. *The EMBO*
357 *Journal* 23, 3735–3746.
- 358 Dabir, D.V., Leverich, E.P., Kim, S.-K., Tsai, F.D., Hirasawa, M., Knaff, D.B., and Koehler,
359 C.M. (2007). A role for cytochrome c and cytochrome c peroxidase in electron shuttling from
360 Erv1. *EMBO J.* 26, 4801–4811.
- 361 Eckers, E., Petrungaro, C., Gross, D., Riemer, J., Hell, K., and Deponte, M. (2013). Divergent
362 molecular evolution of the mitochondrial sulfhydryl:cytochrome C oxidoreductase Erv in
363 opisthokonts and parasitic protists. *J. Biol. Chem.* 288, 2676–2688.
- 364 Erdogan, A.J., and Riemer, J. (2017). Mitochondrial disulfide relay and its substrates:
365 mechanisms in health and disease. *Cell and Tissue Research* 367, 59–72.
- 366 Fischer, M., and Riemer, J. (2013). The mitochondrial disulfide relay system: roles in oxidative
367 protein folding and beyond. *Int J Cell Biol* 2013, 742923.
- 368 Fischer, M., Horn, S., Belkacemi, A., Kojer, K., Petrungaro, C., Habich, M., Ali, M., Küttner, V.,
369 Bien, M., Kauff, F., et al. (2013). Protein import and oxidative folding in the mitochondrial
370 intermembrane space of intact mammalian cells. *Mol. Biol. Cell* 24, 2160–2170.
- 371 Gabriel, K., Milenkovic, D., Chacinska, A., Müller, J., Guiard, B., Pfanner, N., and Meisinger, C.
372 (2007). Novel Mitochondrial Intermembrane Space Proteins as Substrates of the MIA Import
373 Pathway. *Journal of Molecular Biology* 365, 612–620.
- 374 Gross, D.P., Burgard, C.A., Reddehase, S., Leitch, J.M., Culotta, V.C., and Hell, K. (2011).
375 Mitochondrial Ccs1 contains a structural disulfide bond crucial for the import of this
376 unconventional substrate by the disulfide relay system. *Mol. Biol. Cell* 22, 3758–3767.

- 377 Hansen, K.G., and Herrmann, J.M. (2019). Transport of Proteins into Mitochondria. *The Protein*
378 *Journal* *38*, 330–342.
- 379 Hell, K. (2008). The Erv1–Mia40 disulfide relay system in the intermembrane space of
380 mitochondria. *Biochimica et Biophysica Acta (BBA) - Molecular Cell Research* *1783*, 601–609.
- 381 Herrmann, J.M., and Riemer, J. (2010). The Intermembrane Space of Mitochondria. *Antioxidants*
382 & Redox Signaling *13*, 1341–1358.
- 383 Hu, J., Dong, L., and Outten, C.E. (2008). The Redox Environment in the Mitochondrial
384 Intermembrane Space Is Maintained Separately from the Cytosol and Matrix. *Journal of*
385 *Biological Chemistry* *283*, 29126–29134.
- 386 Hudson, D.A., and Thorpe, C. (2015). Mia40 is a facile oxidant of unfolded reduced proteins but
387 shows minimal isomerase activity. *Arch. Biochem. Biophys.* *579*, 1–7.
- 388 Hung, V., Zou, P., Rhee, H.-W., Udeshi, N.D., Cracan, V., Svinkina, T., Carr, S.A., Mootha,
389 V.K., and Ting, A.Y. (2014). Proteomic mapping of the human mitochondrial intermembrane
390 space in live cells via ratiometric APEX tagging. *Mol. Cell* *55*, 332–341.
- 391 Koch, J.R., and Schmid, F.X. (2014). Mia40 targets cysteines in a hydrophobic environment to
392 direct oxidative protein folding in the mitochondria. *Nature Communications* *5*.
- 393 Kojer, K., and Riemer, J. (2014). Balancing oxidative protein folding: The influences of reducing
394 pathways on disulfide bond formation. *Biochimica et Biophysica Acta (BBA) - Proteins and*
395 *Proteomics* *1844*, 1383–1390.
- 396 Kojer, K., Bien, M., Gangel, H., Morgan, B., Dick, T.P., and Riemer, J. (2012). Glutathione
397 redox potential in the mitochondrial intermembrane space is linked to the cytosol and impacts the
398 Mia40 redox state: E_{GSH} of the IMS is maintained by the cytosol. *The EMBO Journal* *31*, 3169–
399 3182.
- 400 Kojer, K., Peleh, V., Calabrese, G., Herrmann, J.M., and Riemer, J. (2015). Kinetic control by
401 limiting glutaredoxin amounts enables thiol oxidation in the reducing mitochondrial
402 intermembrane space. *Molecular Biology of the Cell* *26*, 195–204.
- 403 Levitan, A., Danon, A., and Lisowsky, T. (2004). Unique Features of Plant Mitochondrial
404 Sulphydryl Oxidase. *Journal of Biological Chemistry* *279*, 20002–20008.
- 405 Lionaki, E., Aivaliotis, M., Pozidis, C., and Tokatlidis, K. (2010). The N-terminal Shuttle
406 Domain of Erv1 Determines the Affinity for Mia40 and Mediates Electron Transfer to the
407 Catalytic Erv1 Core in Yeast Mitochondria. *Antioxidants & Redox Signaling* *13*, 1327–1339.
- 408 Lisowsky, T. (1992). Dual function of a new nuclear gene for oxidative phosphorylation and
409 vegetative growth in yeast. *Mol. Gen. Genet.* *232*, 58–64.

- 410 Longen, S., Bien, M., Bihlmaier, K., Kloeppe, C., Kauff, F., Hammermeister, M., Westermann,
411 B., Herrmann, J.M., and Riemer, J. (2009). Systematic analysis of the twin cx(9)c protein family.
412 *J. Mol. Biol.* **393**, 356–368.
- 413 Meyer, A.J., Riemer, J., and Rouhier, N. (2019). Oxidative protein folding: state-of-the-art and
414 current avenues of research in plants. *New Phytol.* **221**, 1230–1246.
- 415 Meyer, E.H., Giege, P., Gelhaye, E., Rayapuram, N., Ahuja, U., Thony-Meyer, L.,
416 Grienberger, J.-M., and Bonnard, G. (2005). AtCCMH, an essential component of the c-type
417 cytochrome maturation pathway in *Arabidopsis* mitochondria, interacts with apocytochrome c.
418 *Proceedings of the National Academy of Sciences* **102**, 16113–16118.
- 419 Milenkovic, D., Ramming, T., Müller, J.M., Wenz, L.-S., Gebert, N., Schulze-Specking, A.,
420 Stojanovski, D., Rospert, S., and Chacinska, A. (2009). Identification of the Signal Directing
421 Tim9 and Tim10 into the Intermembrane Space of Mitochondria. *Molecular Biology of the Cell*
422 **20**, 2530–2539.
- 423 Morgenstern, M., Stiller, S.B., Lübbert, P., Peikert, C.D., Dannenmaier, S., Drepper, F., Weill,
424 U., Höß, P., Feuerstein, R., Gebert, M., et al. (2017). Definition of a High-Confidence
425 Mitochondrial Proteome at Quantitative Scale. *Cell Rep* **19**, 2836–2852.
- 426 Neal, S.E., Dabir, D.V., Tienson, H.L., Horn, D.M., Glaeser, K., Ogozalek Loo, R.R., Barrientos,
427 A., and Koehler, C.M. (2015). Mia40 Protein Serves as an Electron Sink in the Mia40-Erv1
428 Import Pathway. *J. Biol. Chem.* **290**, 20804–20814.
- 429 Neupert, W., and Herrmann, J.M. (2007). Translocation of proteins into mitochondria. *Annu.*
430 *Rev. Biochem.* **76**, 723–749.
- 431 Østergaard, H., Tachibana, C., and Winther, J.R. (2004). Monitoring disulfide bond formation in
432 the eukaryotic cytosol. *The Journal of Cell Biology* **166**, 337–345.
- 433 Peleh, V., Cordat, E., and Herrmann, J.M. (2016). Mia40 is a trans-site receptor that drives
434 protein import into the mitochondrial intermembrane space by hydrophobic substrate binding.
435 *Elife* **5**.
- 436 Peleh, V., Zannini, F., Backes, S., Rouhier, N., and Herrmann, J.M. (2017). Erv1 of *Arabidopsis*
437 *thaliana* can directly oxidize mitochondrial intermembrane space proteins in the absence of
438 redox-active Mia40. *BMC Biology* **15**.
- 439 Petrungaro, C., Zimmermann, K.M., Küttner, V., Fischer, M., Dengjel, J., Bogeski, I., and
440 Riemer, J. (2015). The Ca2+-Dependent Release of the Mia40-Induced MICU1-MICU2 Dimer
441 from MCU Regulates Mitochondrial Ca2+ Uptake. *Cell Metabolism* **22**, 721–733.
- 442 Polimeno, L., Rossi, R., Mastrodonato, M., Montagnani, M., Piscitelli, D., Pesetti, B., De
443 Benedictis, L., Girardi, B., Resta, L., Napoli, A., et al. (2013). Augmenter of liver regeneration, a
444 protective factor against ROS-induced oxidative damage in muscle tissue of mitochondrial
445 myopathy affected patients. *The International Journal of Biochemistry & Cell Biology* **45**, 2410–
446 2419.

- 447 Riemer, J., Bulleid, N., and Herrmann, J.M. (2009). Disulfide formation in the ER and
448 mitochondria: two solutions to a common process. *Science* *324*, 1284–1287.
- 449 Rissler, M., Wiedemann, N., Pfannschmidt, S., Gabriel, K., Guiard, B., Pfanner, N., and
450 Chacinska, A. (2005). The Essential Mitochondrial Protein Erv1 Cooperates with Mia40 in
451 Biogenesis of Intermembrane Space Proteins. *Journal of Molecular Biology* *353*, 485–492.
- 452 Sanders, C., Turkarslan, S., Lee, D.-W., and Daldal, F. (2010). Cytochrome c biogenesis: the
453 Ccm system. *Trends Microbiol.* *18*, 266–274.
- 454 Selles, B., Zannini, F., Couturier, J., Jacquot, J.-P., and Rouhier, N. (2017). Atypical protein
455 disulfide isomerases (PDI): Comparison of the molecular and catalytic properties of poplar PDI-
456 A and PDI-M with PDI-L1A. *PLoS ONE* *12*, e0174753.
- 457 Sideris, D.P., Petrakis, N., Katrakili, N., Mikropoulou, D., Gallo, A., Ciofi-Baffoni, S., Banci, L.,
458 Bertini, I., and Tokatlidis, K. (2009). A novel intermembrane space–targeting signal docks
459 cysteines onto Mia40 during mitochondrial oxidative folding. *The Journal of Cell Biology* *187*,
460 1007–1022.
- 461 Specht, S., Liedgens, L., Duarte, M., Stiegler, A., Wirth, U., Eberhardt, M., Tomás, A., Hell, K.,
462 and Deponte, M. (2018). A single-cysteine mutant and chimeras of essential Leishmania Erv can
463 complement the loss of Erv1 but not of Mia40 in yeast. *Redox Biology* *15*, 363–374.
- 464 Stojanovski, D., Milenkovic, D., Müller, J.M., Gabriel, K., Schulze-Specking, A., Baker, M.J.,
465 Ryan, M.T., Guiard, B., Pfanner, N., and Chacinska, A. (2008). Mitochondrial protein import:
466 precursor oxidation in a ternary complex with disulfide carrier and sulfhydryl oxidase. *J. Cell
467 Biol.* *183*, 195–202.
- 468 Stojanovski, D., Bragoszewski, P., and Chacinska, A. (2012). The MIA pathway: A tight bond
469 between protein transport and oxidative folding in mitochondria. *Biochimica et Biophysica Acta
470 (BBA) - Molecular Cell Research* *1823*, 1142–1150.
- 471 Suzuki, Y., Ali, M., Fischer, M., and Riemer, J. (2013). Human copper chaperone for superoxide
472 dismutase 1 mediates its own oxidation-dependent import into mitochondria. *Nature
473 Communications* *4*.
- 474 Tienson, H.L., Dabir, D.V., Neal, S.E., Loo, R., Hasson, S.A., Boontheung, P., Kim, S.-K., Loo,
475 J.A., and Koehler, C.M. (2009). Reconstitution of the Mia40-Erv1 Oxidative Folding Pathway for
476 the Small Tim Proteins. *Molecular Biology of the Cell* *20*, 3481–3490.
- 477 Uhrig, R.G., Labandera, A.-M., Tang, L.-Y., Sieben, N.A., Goudreault, M., Yeung, E., Gingras,
478 A.-C., Samuel, M.A., and Moorhead, G.B.G. (2017). Activation of Mitochondrial Protein
479 Phosphatase SLP2 by MIA40 Regulates Seed Germination. *Plant Physiology* *173*, 956–969.
- 480 Verissimo, A.F., Khalfaoui-Hassani, B., Hwang, J., Steimle, S., Selamoglu, N., Sanders, C.,
481 Khatchikian, C.E., and Daldal, F. (2017). The thiorreduction component CcmG confers efficiency
482 and the heme ligation component CcmH ensures stereo-specificity during
483 cytochrome maturation. *J. Biol. Chem.* *292*, 13154–13167.

- 484 Vitu, E., Bentzur, M., Lisowsky, T., Kaiser, C.A., and Fass, D. (2006). Gain of Function in an
485 ERV/ALR Sulfhydryl Oxidase by Molecular Engineering of the Shuttle Disulfide. *Journal of*
486 *Molecular Biology* *362*, 89–101.
- 487 Vögtle, F.-N., Burkhardt, J.M., Rao, S., Gerbeth, C., Hinrichs, J., Martinou, J.-C., Chacinska, A.,
488 Sickmann, A., Zahedi, R.P., and Meisinger, C. (2012). Intermembrane space proteome of yeast
489 mitochondria. *Mol. Cell Proteomics* *11*, 1840–1852.
- 490 Zannini, F., Couturier, J., Keech, O., and Rouhier, N. (2017). In Vitro Alkylation Methods for
491 Assessing the Protein Redox State. *Methods Mol. Biol.* *1653*, 51–64.

492

493

494 **Figure legends**

495

496 **Figure 1. *In vitro* oxidation of *Arabidopsis* COX19 protein by the ERV1-MIA40 couple
497 from *Arabidopsis thaliana* and *Saccharomyces cerevisiae*.**

498 Capacity of ERV1 alone or in the presence of MIA40 to oxidize the *Arabidopsis* COX19 protein
499 using *A. thaliana* (A, B, E, and F) and *S. cerevisiae* (C and D) proteins. In E and F, an *AtMIA40*
500 variant lacking the catalytic cysteines of the CPC motif (*AtMIA40* SPS) has been used. In A, C,
501 E, COX19 (40 µM) oxidation was followed over time by cysteine alkylation using mmPEG₂₄ and
502 SDS PAGE separation after incubation with 4 µM ERV1 alone or in presence of 4 µM of
503 MIA40. In B, D, F the electron transfer from reduced COX19 (40 µM, grey line) was followed
504 by recording the reduction of 20 µM cytochrome c at 550 nm over time in the presence of 4 µM
505 of ERV1 alone (red line) or with 4 µM of MIA40 (blue line). A reference was made using 40 µM
506 of DTT as an electron donor (black line).

507

508 **Figure 2. *In vitro* oxidation of *Arabidopsis* CCMH by the ERV1-MIA40 couple from
509 *Arabidopsis thaliana* and *Saccharomyces cerevisiae*.**

510 Capacity of *A. thaliana* (A, B) and *S. cerevisiae* (C and D) ERV1/MIA40 couples to oxidize
511 *Arabidopsis* CCMH using cysteine alkylation using mPEG₂₀₀₀ or mmPEG₂₄ and SDS PAGE
512 separation or cytochrome c reduction as described in figure 1. In all these assays, 40 µM CCMH
513 was incubated with 4 µM ERV1 alone or in presence of 4 µM of MIA40. In E and F, the same

514 tests were performed using an hybrid system comprising *S. cerevisiae* ERV1 and *A. thaliana*
515 MIA40.

516

517 **Figure 3. *In vitro* oxidation of Arabidopsis COX19 protein by the ERV1-MIA40 couple**
518 **from *Arabidopsis thaliana* and *Saccharomyces cerevisiae* in the presence of glutathione.**

519 The oxidation of AtCOX19 (40 μ M) was followed over time by the cysteine alkylation assay
520 (mmPEG₂₄ alkylation and SDS PAGE separation) in the presence of a total glutathione
521 concentration of 8 mM adjusted to a midpoint redox potential for the GSH/GSSG couple of – 274
522 mV at pH 7.4 (A). The capacity of Arabidopsis or yeast ERV1 alone, or in presence of MIA40,
523 each at a 4 μ M concentration, was tested in the same conditions (B, C). The amount of fully
524 oxidized AtCOX19 relatively to the total AtCOX19 amounts was quantified in each condition.
525 Mean values \pm SD of at least three replicates are shown.

526

527 **Figure 4. Proposed model for the ERV1 and GSH-mediated oxidation of Arabidopsis**
528 **COX19 in the absence of MIA40.**

529 In this scheme, reduced glutathione (GSH) reacts with the shuttle disulfide of ERV1 (Cx_4C)
530 (rather than the catalytic disulfide), leading to the formation of a glutathione adduct on one of
531 these cysteines. The glutathione molecule would then be transferred to one of the cysteine
532 residues forming the more internal disulfide in the substrates to promote disulfide bond formation
533 and the release of GSH. The second disulfide bridge of the substrate could be formed by the same
534 mechanism (ERV1 + GSH) but eventually by the action of O_2 or GSSG. The catalytic Cx_4C motif
535 of ERV1 is subsequently regenerated by transferring electrons to the catalytic Cx_2C motif, FAD
536 and oxygen (O_2) or cytochrome *c* (cyt *c*).

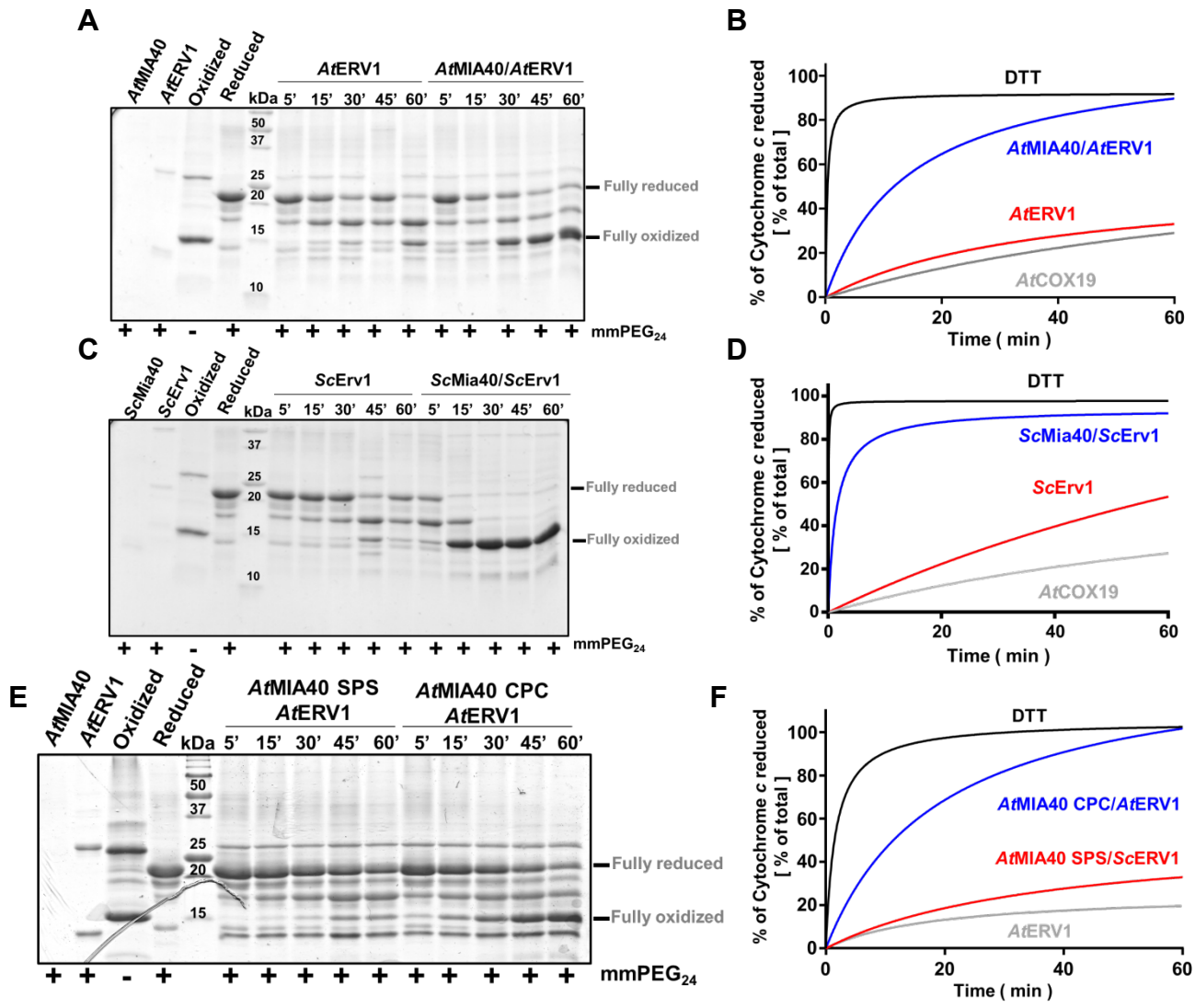
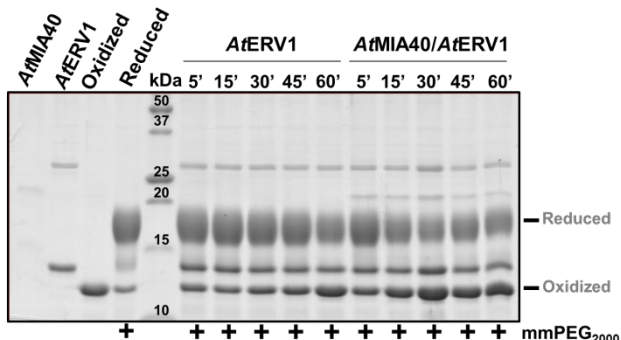
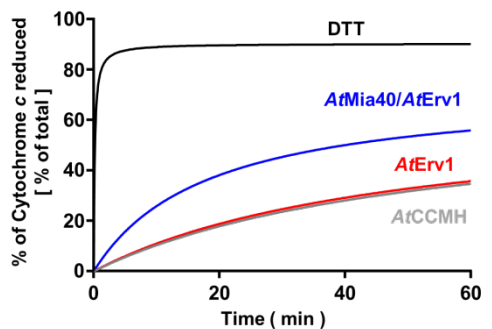
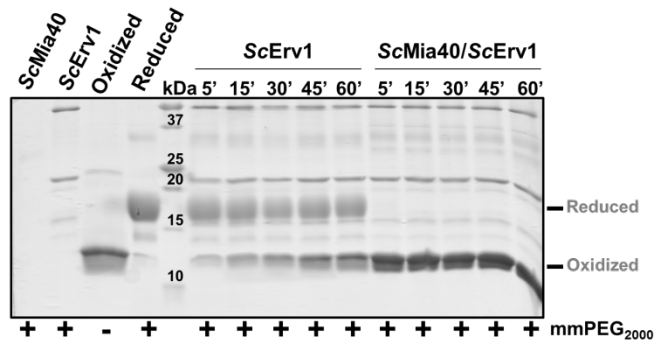
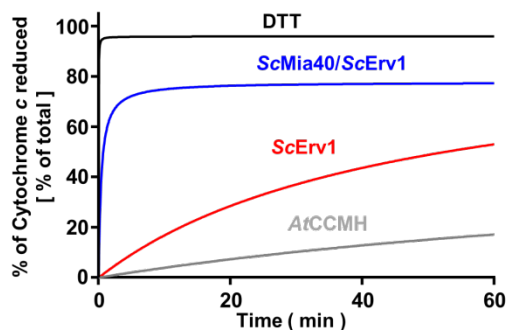
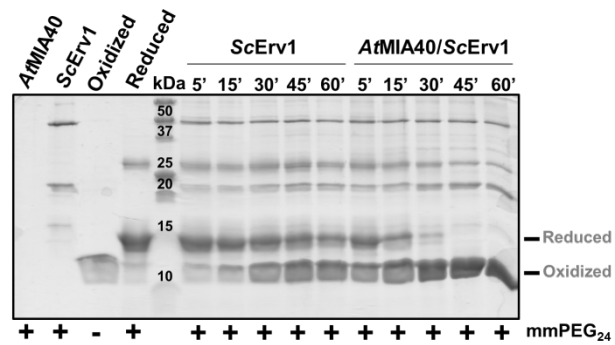
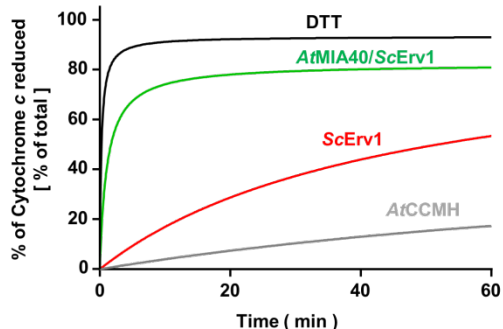
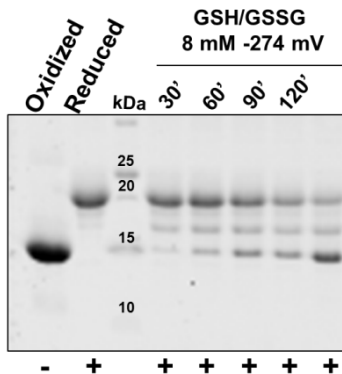
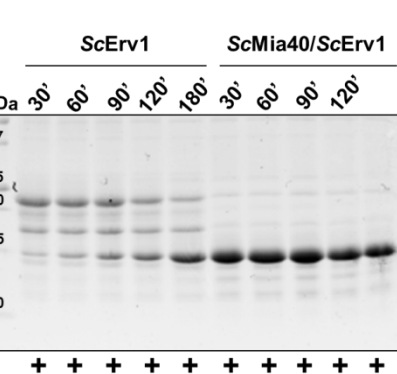
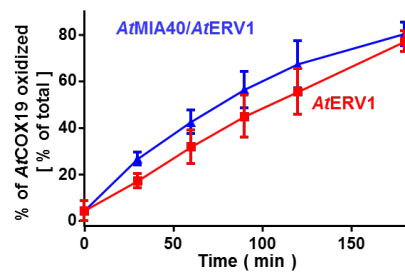
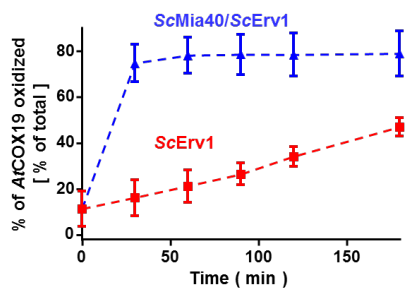
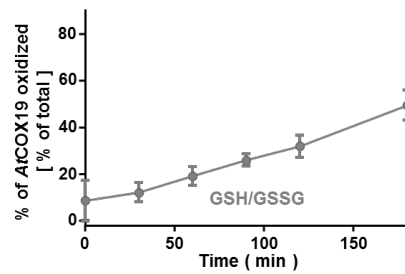
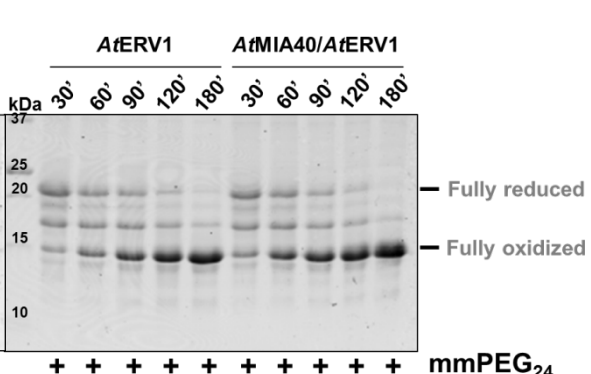


Figure 1

A**B****C****D****E****F****Figure 2**

A**B****C****Figure 3**

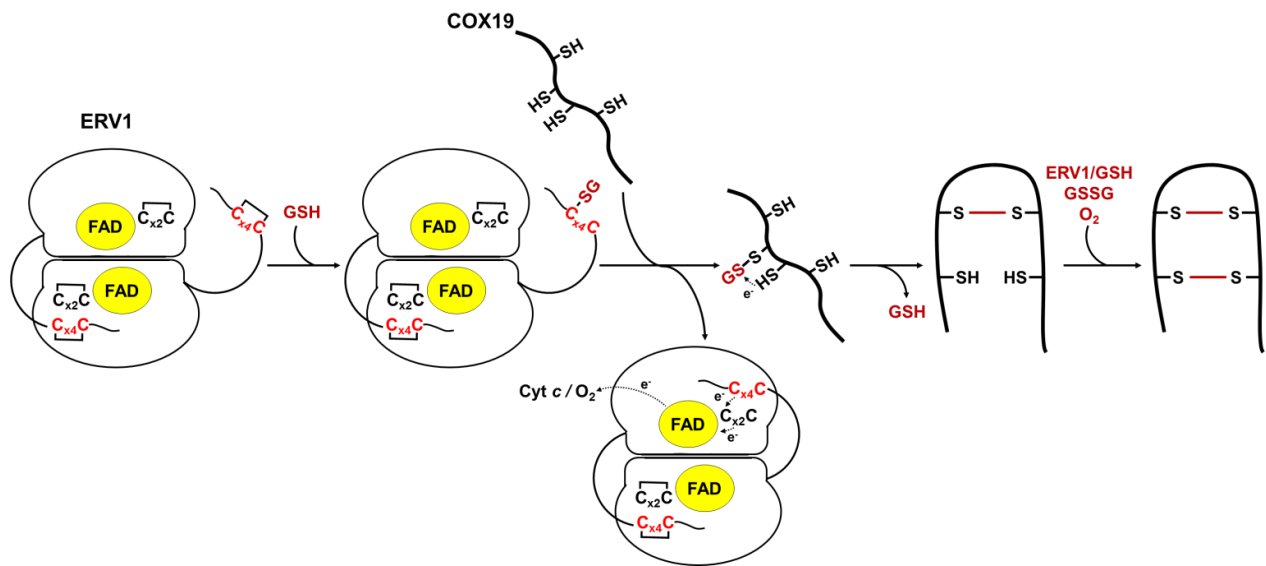


Figure 4

Conclusion générale

Les travaux effectués lors de mon doctorat, financés par le Labex ARBRE (Advanced Research on the Biology of TRee and Forest Ecosystems), ont porté sur l'identification de nouvelles fonctions régulées par des métaux ou par des processus redox chez les plantes. Ce projet avait pour but de définir le rôle de protéines contenant un ou plusieurs motifs CxxC conservés chez les plantes et dont les fonctions étaient inconnues ou incertaines. J'ai donc été amené à travailler sur différentes protéines aux propriétés et fonctions variables: (i) la GRXS16 chloroplastique et (ii) les TRXs o1 et o2 mitochondrielles dont la caractérisation biochimique était parcellaire ; (iii) la PDI-A de peuplier qui n'avait pas été caractérisée (iii) et les protéines MIA40/ERV1 présentes dans l'IMS des mitochondries et pour lesquelles les données fonctionnelles décrites paraissaient questionnables. Les résultats ayant déjà été discutés de manière extensive dans les articles, je ne reprendrai dans cette conclusion générale que les éléments de discussion clés afin de proposer des modèles et des pistes d'études supplémentaires.

I. Impact de la réduction par le système TRX sur le(s) rôle(s) de la GRXS16 chloroplastique

Les GRXs de classe II contiennent un site actif CGFS extrêmement bien conservé. *Arabidopsis thaliana* possède 4 GRXs de classe II, GRXS14 à GRXS17, localisées au sein du chloroplaste (GRXS14 et GRXS16) (Bandyopadhyay et al., 2008), de la mitochondrie (GRXS15) (Moseler et al., 2015; Ströher et al., 2016) et du noyau/cytosol (GRXS17) (Knuesting et al., 2015). À part GRXS15, toutes ces GRXs sont capables de complémenter parfaitement le mutant *grx5* de levure suggérant un rôle dans la maturation des centres Fe-S (Bandyopadhyay et al., 2008; Moseler et al., 2015). Par ailleurs, du fait leur capacité à fixer et transférer des centres Fe-S, le rôle des GRXs de classe II dans la maturation des protéines Fe-S est à présent bien établi même si des évidences manquent encore chez les plantes. À contrario, leur activité oxydoréductase est encore source de questionnement même si la capacité de certaines de ces GRXs à réduire *in vitro* les protéines BOLA2 et SUFE1 glutathionylées a été démontrée (Couturier et al., 2014). Que ce soit pour la déglutathionylation ou la fixation d'un centre Fe-S, il est nécessaire que ces GRXs soient présentes sous une forme réduite ce qui pose la question du ou des mécanismes impliqués dans leur réduction. La caractérisation biochimique de GRXS16 a mis en évidence l'existence d'un pont disulfure intramoléculaire entre les cystéines 158 et 215 du domaine GRX (comme démontré dans la GRX3 de *Chlamydomonas reinhardtii*, l'orthologue de GRXS14) qui peut être formé par réaction avec H₂O₂ mais aussi avec des formes oxydées du glutathion (GSSG,

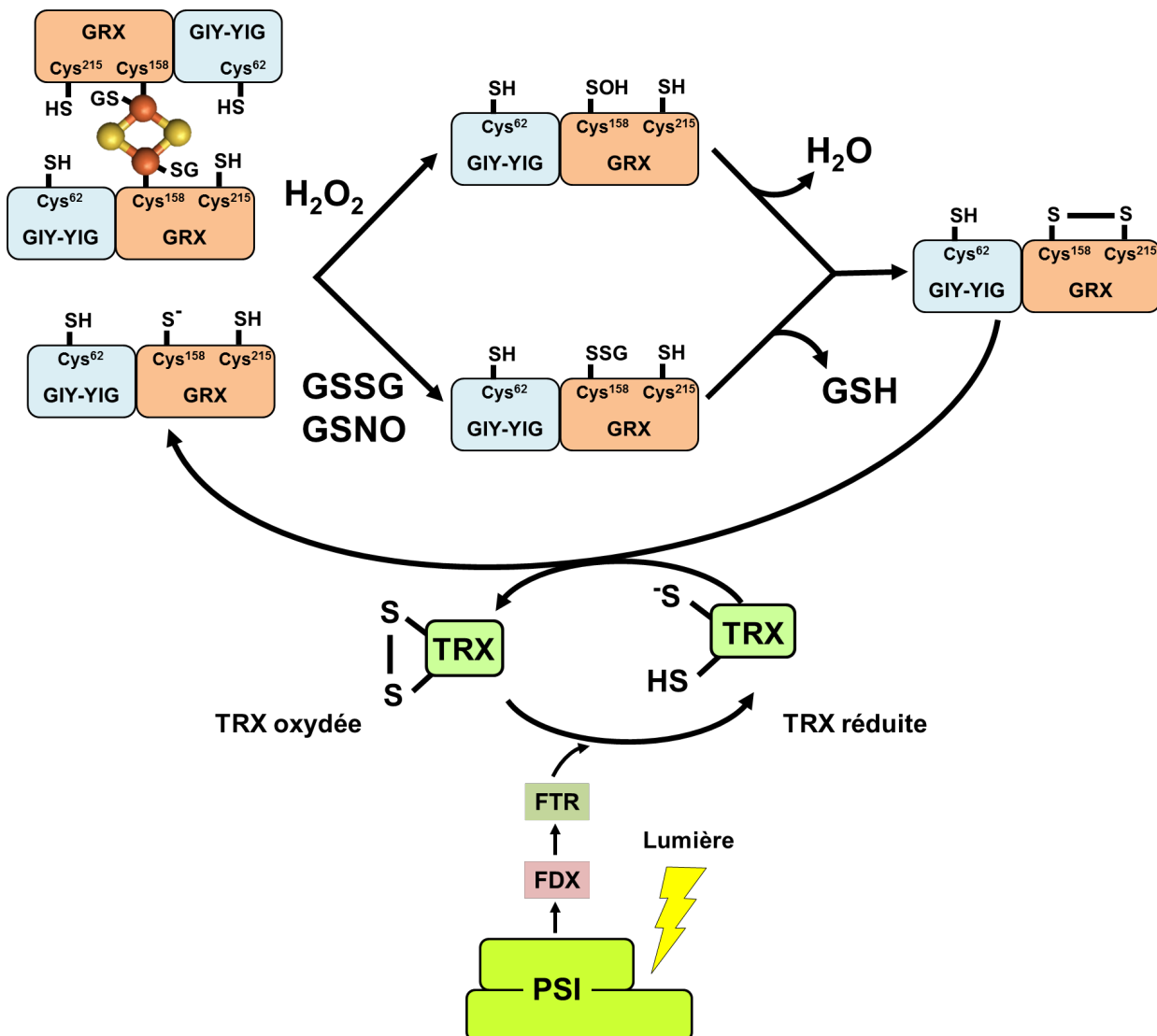


Figure 23: Régulation de l'activité de la GRXS16 d'*A. thaliana*.

La formation d'un pont disulfure intramoléculaire au sein de la GRXS16 en présence d'espèces oxydantes (H_2O_2 , GSSG et/ou GSNO, voire des substrats glutathionylés) devrait empêcher la protéine de lier un centre Fe-S et donc de participer à la maturation des protéines Fe-S. La réduction du pont disulfure par l'intermédiaire du système TRX/FTR/FDX chloroplastique suggère un contrôle du rôle de GRXS16 (et par extension de GRXS14 qui possède la même cystéine additionnelle) par la lumière.

GSNO), donc y compris des substrats glutathionylés (Figure 23). Par contre, aucune régulation redox de l'activité endonucléase de la protéine n'a été observé contrairement à ce qui avait été rapporté précédemment (Liu et al., 2013). Contrairement aux GRXs de classe I, ce pont disulfure intramoléculaire n'est pas réduit par le GSH mais par le système FTR/TRX. Cette forme d'oxydation pourrait donc représenter une forme de régulation redox des GRXs de classe II possédant ces deux cystéines conservées. Une dépendance unique vis-à-vis du système TRX/FTR ferait donc que la capacité de la GRXS16 à fixer un centre Fe-S et donc son rôle au sein de la machinerie d'assemblage des centres Fe-S chloroplastique puissent être directement liés au cycle jour/nuit et contrôlés au niveau post-traductionnel. Ces résultats font écho à l'absence de régulation transcriptionnelle observée pour la plupart des facteurs de maturation des protéines Fe-S, mais à l'observation que certains transcrits seraient traduits de manière différentielle au cours de la journée, faisant donc un autre lien potentiel avec la photosynthèse (Zhang and Krämer, 2018). Corroborent cette hypothèse, l'abondance de certaines protéines de la machinerie SUF diminue dans des feuilles soumises à une obscurité prolongée (Rey et al., 2017). Des études plus approfondies de protéomique quantitative permettraient de répondre plus clairement à cette question.

Enfin, il n'est toujours pas clair si les GRXs de classe II possèdent une activité oxydoréductase (qui serait significative au moins dans certaines conditions). Le problème des études passées concernant GRXS16 est qu'il existe deux GRXs de classe II dans le chloroplaste ainsi que deux GRX de classe I (GRX C5 et S12). La croissance végétative de simples mutants d'Arabidopsis pour GRXS14 et GRXS16 ou d'un double mutant (KO pour GRXS14 et KD pour GRXS16) étant peu ou pas affectée dans des conditions standards de croissance, il est possible que certaines fonctions soient redondantes avec celles des GRXs de classe I. Des phénotypes seraient par exemple à chercher en réponse à des contraintes environnementales spécifiques. Ainsi, chez la tomate un mutant silencieux pour la *grxs16* présente une sensibilité accrue au stress osmotique (Guo et al., 2010). Afin d'étudier la capacité de GRXS16 à (dé)glutathionyler des protéines cibles, l'étude du glutathionylome d'un mutant *grxs16* qui aurait poussé dans des conditions standard et de stress pourrait être envisageable. Des expériences complémentaires de biochimie *in vitro*, notamment des mesures d'activités enzymatiques, utilisant des protéines préalablement identifiées comme régulées par glutathionylation pourraient aussi permettre de répondre à cette question. Enfin, dans le but d'identifier des partenaires potentiels, il pourrait être pertinent d'effectuer des

expériences de pull down à l'aide de variants mutés pour les cystéines impliquées dans la formation du pont disulfure.

II. Y'a-t-il un lien entre les TRX o1 et o2 et la maturation des centres Fe-S mitochondriaux chez *A. thaliana* ?

Les plantes possèdent généralement une à deux TRXs mitochondrielles appartenant aux classes h et o. Toutefois, *A. thaliana* présente la particularité de posséder trois TRXs mitochondrielles, TRXo1, TRXo2 et TRXh2 (Gelhaye et al., 2004a; Laloi et al., 2001). En outre, ces TRXs o pourraient aussi être présentes dans le noyau et le cytosol (Delorme-Hinoux et al., 2016; Geigenberger et al., 2017) et TRX h2 dans le cytosol (Fonseca-Pereira et al., 2019a). Il a été montré que l'isoforme TRXh2 est capable de réduire l'homodimère covalent AOX permettant son activation par le pyruvate (Gelhaye et al., 2004b) alors que la TRXo1 ne serait pas impliquée dans le contrôle redox de l'AOX (Florez-Sarasa et al., 2019) et qu'un mutant *trсх2* chez *A. thaliana* présente de multiples déficiences, notamment une germination retardée des graines et des défauts photorespiratoires (Fonseca-Pereira et al., 2019a).

En ce qui concerne les TRXs o, le mutant de l'isoforme majoritaire *trxo1* et le double mutant *trxo1/trxo2* ne présentent pas de phénotypes visibles. Cependant dans des conditions de stress salin, un niveau plus important de lipides peroxydés et d'H₂O₂ est détecté. Ceci est accompagné d'activités catalase et SOD plus élevées de même qu'un niveau de fermeture des stomates plus important (Calderón et al., 2018). En accord avec cette précédente étude, d'autres données décrites la même année ont mis en avant que le mutant *trxo1* présentait une accumulation de métabolites secondaires ainsi qu'une forte conductance stomatique permettant une meilleure récupération après deux épisodes de sécheresse (Fonseca-Pereira et al., 2019b). Globalement, les études sur TRXo1 suggèrent un rôle dans la régulation (activation ou désactivation selon les cas) de diverses enzymes du cycle de Krebs (Daloso et al., 2015; Florez-Sarasa et al., 2019; Reinholdt et al., 2019; Schwarzländer and Fuchs, 2019). Dans le but d'identifier l'importance respective de ces TRX mitochondrielles chez *A. thaliana*, et la redondance entre les TRX o et la TRX h2, il serait informatif de comparer le protéome redox des mutants correspondants mais aussi de doubles mutants *trсх2 x trxo1* ou *trсх2 x trxo2* voire d'un triple mutant *trсх2/trxo1/trxo2*. De manière intéressante, les études précédentes ont permis de mettre en évidence une centaine de partenaires des TRXs o chez *A. thaliana*, dont un certain nombre évoluant dans le cycle TCA, la photorespiration, le métabolisme des acides aminés, la détoxication des ROS ou l'assemblage des centres Fe-S (Daloso et al., 2015; da Fonseca-Pereira et al., 2019; Yoshida and Hisabori, 2016; Yoshida et

al., 2013). Il serait donc pertinent de réaliser une approche comparable avec la TRX h2 puis de comparer *in vitro* les capacités respectives de ces protéines pour la réduction des cibles. C'est notamment dans ce but que les protéines recombinantes correspondant aux formes matures de TRXo1 et TRXo2 ont été produites. D'une manière surprenante, il a été observé que les TRXo1 et TRXo2 fixent un centre [4Fe-4S] au sein d'un homodimère à l'aide des deux cystéines du site actif WCGPC. Des analyses plus poussées sont nécessaires afin de caractériser davantage la nature du centre Fe-S via des expérimentations EPR ou de spectrométrie Mössbauer ou de déterminer si ce centre possède des propriétés redox. Bien que cela puisse paraître surprenant, d'autres études ont démontré la capacité de certaines TRXs ou TRXs-like à coordonner un centre Fe-S. Nous pouvons citer le cas de la PDI non conventionnelle de peuplier (*PtPDIA*) (Selles et al., 2017) et d'un variant de la Trx A d'*E. coli* (signature CACA) (Collet et al., 2005), toutes deux capables de fixer un centre [2Fe-2S] au sein d'homodimères. Une TRX atypique (*IsTRP*) présente chez un parasite de l'homme a été également décrite pour coordonner un centre de type [2Fe-2S] (Bisio et al., 2016). Enfin, une dernière étude parue cette année a démontré la capacité de la Trx A de *Bacillus subtilis* à coordonner un centre Fe-S (Zheng et al., 2019). La spécificité à coordonner un cofacteur Fe-S était jusqu'à présent attribuée principalement aux GRXs, mais il se pourrait que cela constitue une caractéristique commune à plusieurs membres de la super-famille des TRXs. Au contraire des GRXs, aucune fonction biologique n'a pour l'instant été avancée concernant la capacité de la PDIA et des TRXs à fixer un centre Fe-S. Des analyses plus poussées seraient nécessaire afin de comprendre leurs rôles. La présence de ce centre Fe-S pourrait ainsi induire une inactivation transitoire de ces enzymes permettant la régulation de leur activité, comme suggéré pour les GRXs (Lillig et al., 2005). Néanmoins, bien que la capacité de certaines TRXs à fixer un centre Fe-S *in vitro* ou lors de leur surexpression en système hétérologue ne fasse aucun doute, la présence de ces formes *in vivo* n'a pour l'instant pas été confirmée. Pour vérifier la présence de ces formes holo *in cellulo*, une possibilité serait d'exprimer ces TRXs ou dans des levures cultivées en présence de fer marqué (Fe^{57}) comme cela est couramment pratiqué chez le Pr Roland Lill (Marburg) pour l'étude des systèmes de maturation des protéines Fe-S. Après immunoprecipitation en condition anaérobie, la présence de fer radioactif (et donc potentiellement de centre Fe-S) associé à la protéine peut être détectée par scintillation.

De manière importante, l'inactivation de la TrxA ou de la thiorédoxine réductase (TrxR) diminue l'activité des enzymes Fe-S chez *B. subtilis* (Zheng et al., 2019). Ces résultats fournissent donc un lien potentiel entre régulation redox et métabolisme de centres Fe-S. Il a

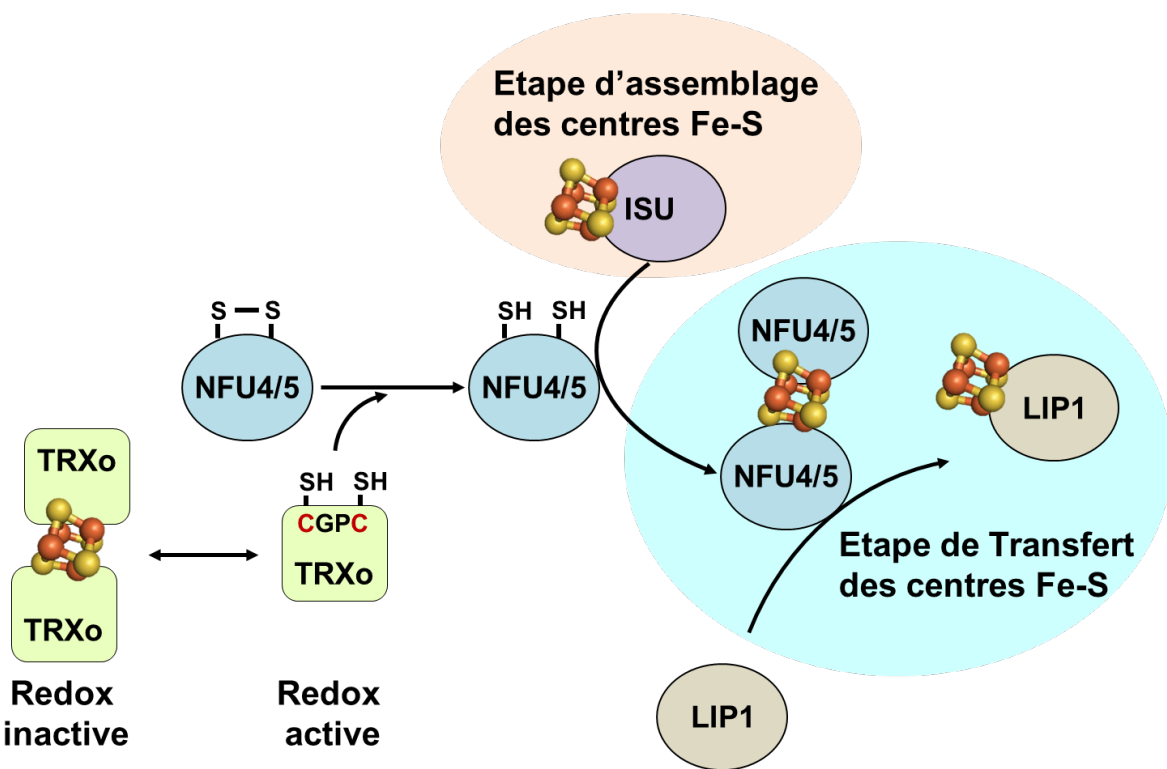


Figure 24: Modèle proposé concernant la connexion entre les TRXs o mitochondriales chez *A. thaliana* et la biogénèse des centres Fe-S.

Les TRXs o1 et o2 peuvent réduire les protéines de transfert NFU4/5 afin que ces dernières puissent fixer leur centre [4Fe-4S] et le transférer vers leur cible, telle que la lipoate synthase (LIP1). La liaison d'un centre Fe-S au sein de ces TRXs o pourrait donc moduler cette activité réductase dans certaines conditions.

été proposé que cette TRX ait une réactivité sélective vis-à-vis d'intermédiaires persulfures liés aux protéines et notamment de la cystéine désulfurase (SUFS) et de son partenaire (SUFU) suggérant un rôle comme réducteur physiologique dans les voies de transfert du soufre. Ces résultats font écho à la capacité de la TRX o1 à interagir avec des facteurs de maturation ISC (NFU5, ISCA et cystéine désulfurase NFS1) (Yoshida et al., 2013) ainsi qu'à l'interaction décrite avec des sulfurtransférases, protéines qui forment des intermédiaires persulfure sur une cystéine réactive et participent à la biosynthèse d'H₂S (Henne et al., 2015). La figure 24 décrit donc la possibilité que ces deux TRXs o servent à la réduction des protéines NFU4 et 5, comme démontré *in vitro*, mais aussi potentiellement des autre facteurs ISC ou des protéines Fe-S cibles. En condition optimale de maturation des protéines Fe-S, ces TRX o pourraient incorporer un centre Fe-S par une voie qui reste à déterminer (implication des protéines NFU et ou ISCA ?) ce qui aurait pour conséquence d'inactiver leur activité réductase.

III. La singularité de la voie MIA40 chez *A. thaliana* : le rôle central d'ERV1

Une des particularités de l'IMS est la présence d'un système d'import des protéines qui s'effectue de façon concomitante à leur repliement structural et qui implique les protéines MIA40 et ERV1. Contrairement aux Opistochontes, les études menées chez *A. thaliana* mettaient en évidence le caractère accessoire de l'oxydoréductase MIA40 et l'incapacité des deux protéines à complémer les mutants de levure correspondants (Carrie et al., 2010; Levitan et al., 2004). J'ai donc essayé de comprendre quelles caractéristiques biochimiques de MIA40 ou d'ERV1 pouvaient expliquer cette observation. Nos premiers résultats obtenus avec l'isoforme ERV1 d'*A. thaliana*, adressée de manière certaine dans l'IMS, montraient en réalité une complémentation partielle du mutant *erv1* de levure. Ceci est lié au fait qu'ERV1 d'Arabidopsis est incapable de régénérer Mia40 de levure efficacement aussi bien *in vitro* que *in vivo*, et ceci bien que l'interaction entre les 2 protéines se fasse. Il est vraisemblable que la divergence structurale des protéines ERV1 présentes chez la levure et chez les organismes photosynthétiques soit à l'origine de cette inefficacité. De manière surprenante, nous avons également mis en évidence la capacité d'*At*ERV1 à oxyder des substrats de Mia40 de levure et donc à complémer un mutant *mia40* co-exprimant une version de Mia40 inactive d'un point de vue redox mais capable de piéger ses substrats. Ceci nous a conduit à tester la capacité d'ERV1 à oxyder *in vitro* la protéine COX19. Les résultats indiquent qu'ERV1 peut oxyder COX19 en absence de MIA40 si du glutathion est présent à des concentrations (entre 5

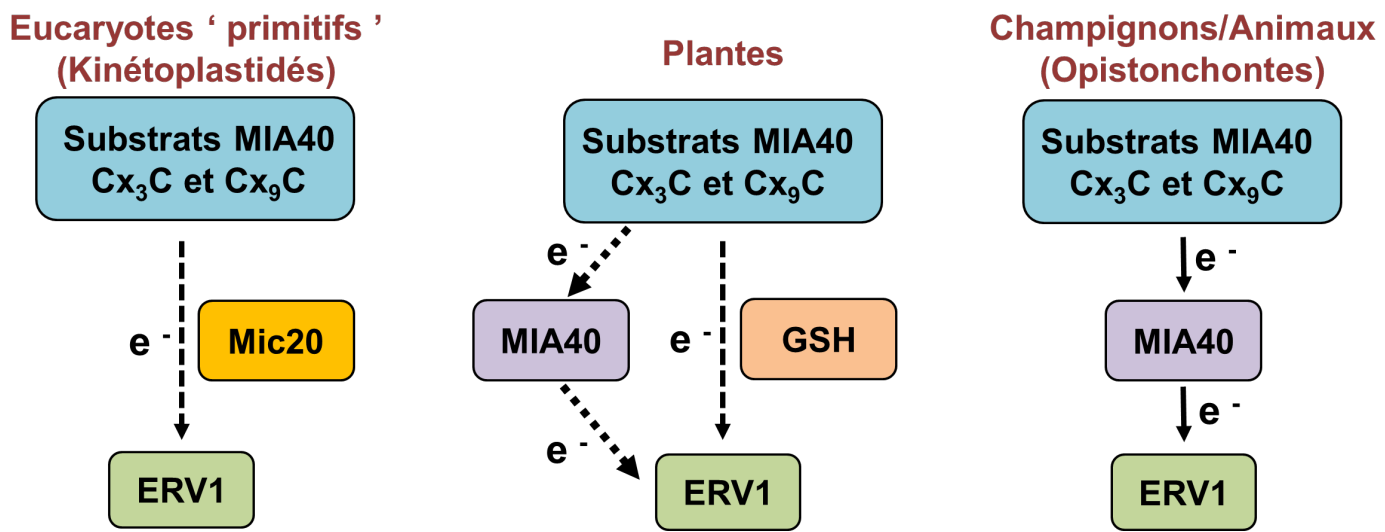


Figure 25: Modèle de l'oxydation des protéines au sein de l'IMS. Chez les Kinétochondriés qui ne possèdent pas MIA40, la fonction oxydoréductase pourrait être assurée par Mic20. Chez les Opistonchontes, l'oxydation des substrats dépend complètement de MIA40. Chez les organismes photosynthétiques, nous envisageons que selon les cibles, ERV1 pourrait agir avec MIA40 ou avec le glutathion.

et 13 mM) et potentiels redox (-255 mV à -300 mV) physiologiques (Calabrese et al., 2017; Herrmann and Riemer, 2012; Riemer et al., 2011). Ces résultats confortent une étude effectuée *in vivo* chez la levure qui concluait sur l'importance du GSH au cours de ce processus d'import et de repliement oxydatif (Bien et al., 2010). Ces résultats indiquent donc que la protéine ERV1 présente chez les organismes photosynthétiques peut oxyder directement certains substrats de MIA40 au dépend du GSH et pourrait expliquer que MIA40 n'est pas indispensable chez les plantes. La compilation de ces données permet de proposer un nouveau modèle évolutif concernant cette voie d'import des protéines au sein de l'IMS chez les plantes (Figure 25). Il est possible que ce modèle s'applique à certains organismes qui ne possèdent pas MIA40 (appartenant en particulier à l'embranchement des Kinétoplastidés) mais qui possèdent une isoforme d'ERV1 à l'architecture comparable à celle des isoformes de plantes. Cependant, des études récentes ont mis en évidence l'incapacité d'ERV1 de *Leishmania tarentolae* à oxyder les substrats de MIA40 chez la levure et l'existence d'une nouvelle oxydoréductase potentielle appelée Mic20 qui pourrait éventuellement pallier à l'absence de Mia40 (Kaurov et al., 2018; Specht et al., 2018). De nouvelles études de complémentation fonctionnelle du mutant *mia40* de levure utilisant Mic20 de Leishmania, mais aussi des approches biochimiques *in vitro* sont nécessaires afin de confirmer ces données et de continuer plus globalement à décrypter l'évolution de ce système au sein des organismes eucaryotes. Il avait été suggéré précédemment que le GSH pouvait servir pour la correction/isomérisation de ponts disulfure aberrants formés dans certaines protéines de l'IMS car l'oxydoréductase MIA40 ne présente *a priori* aucune activité isomérase (Bien et al., 2010; Hudson and Thorpe, 2015). Le rôle du GSH dans le mécanisme d'oxydation par ERV1 reste à être exploré. A l'heure actuelle, on ne sait pas si les concentrations et potentiel redox du couple GSH/GSSG dans l'IMS des mitochondries de plantes sont comparables à ceux déterminés pour *S. cerevisiae*, ni si les variations de structure au niveau d'ERV1 lui confère la capacité à être oxydé par le GSSG et donc à catalyser des réactions de glutathionylation ou à reconnaître des substrats glutathionylés. De manière analogue aux PDI intervenant dans le repliement structural et l'isomérisation des protéines sécrétées ou résidant dans le RE et qui peuvent pour certaines aussi dépendre de la présence de GSH, ERV1 pourrait aussi posséder cette activité isomérase. Il serait possible d'utiliser les substrats habituels des PDIs, notamment la RNase A, pour tester à la fois les activités d'oxydation et d'isomérisation d'ERV1. Pour confirmer un rôle du GSH dans l'import de protéines au sein de l'IMS chez les plantes, il est possible d'utiliser les mutants possédant des niveaux variables en GSH (*cad2*,

zir1, *rml1* etc) mais aussi mutés pour les glutathion réductases qui possèderont des niveaux plus importants en GSSG, peut être en les croisant avec le mutant *mia40*.

Concernant MIA40, il subsiste donc de nombreuses zones d'ombre sur sa fonction au sein de l'IMS mais aussi du peroxysome (Carrie et al., 2010). L'identification des substrats de MIA40 dans les peroxysomes est une perspective intéressante. Il est possible de réaliser des expériences de pull down par exemple par utilisation d'un mutant cystéinique du site catalytique avec des fractions enrichies en peroxysomes, voire effectuer de la co-immunoprecipitation à partir de plantes complémentées par une version peroxysomale uniquement. Il est possible que MIA40 n'ait qu'un rôle dans les peroxysomes où ERV1 est *a priori* absent mais où les concentrations et le potentiel redox du GSH sont aussi différents. Ainsi, il apparaît donc nécessaire d'effectuer une étude biochimique fine des propriétés de MIA40 mais aussi d'ERV1 de plantes vis-à-vis du GSH en déterminant par exemple les potentiels redox des ponts disulfures catalytiques et l'efficacité de leur réduction par le GSH. En somme, il est possible que MIA40 ne serve que pour le repliement de protéines non essentielles chez les plantes et potentiellement pour l'import de substrats présentant une signature atypique. Il serait donc intéressant de déterminer aussi *in vitro* la capacité de ces molécules (MIA40, ERV1 et GSH) à oxyder des protéines telles que la phosphatase SLP2 ou CCS1, le chaperon à cuivre des SOD (Carrie et al., 2010; Uhrig et al., 2017). Il est par contre possible que le rôle de certaines protéines substrats de MIA40 devienne prédominant dans certaines conditions. Il est ainsi envisageable de tester les réponses du mutant *mia40* à des conditions de stress oxydants ou réducteurs. Mes observations préliminaires indiquent que la germination du mutant *mia40* est plus sensible à la présence de DTT que des plantes sauvages. Il devient donc pertinent d'effectuer une approche de protéomique quantitative du mutant *mia40* dans cette condition de stress réducteur.

Références bibliographiques

Ahuja, U., Rozhkova, A., Glockshuber, R., Thöny-Meyer, L., and Einsle, O. (2008). Helix swapping leads to dimerization of the N-terminal domain of the *c*-type cytochrome maturation protein CcmH from *Escherichia coli*. *FEBS Letters* 582.

Alejandro, S., Rodríguez, P.L., Bellés, J.M., Yenush, L., García-Sánchez, M.J., Fernández, J.A., and Serrano, R. (2007). An *Arabidopsis* quiescin-sulfhydryl oxidase regulates cation homeostasis at the root symplast–xylem interface. *The EMBO Journal* 26.

Aller, I., and Meyer, A.J. (2013). The oxidative protein folding machinery in plant cells. *Protoplasma* 250.

d'Aloisio, E., Paolacci, A.R., Dhanapal, A.P., Tanzarella, O.A., Porceddu, E., and Ciaffi, M. (2010). The Protein Disulfide Isomerase gene family in bread wheat (*T. aestivum* L.). *BMC Plant Biology* 10.

Alves, R., Vilaprinyo, E., Sorribas, A., and Herrero, E. (2009). Evolution based on domain combinations: the case of glutaredoxins. *BMC Evolutionary Biology* 9.

Apostolou, A., Shen, Y., Liang, Y., Luo, J., and Fang, S. (2008). Armet, a UPR-upregulated protein, inhibits cell proliferation and ER stress-induced cell death. *Experimental Cell Research* 314.

Appenzeller-Herzog, C. (2006). The ER-Golgi intermediate compartment (ERGIC): in search of its identity and function. *Journal of Cell Science* 119.

Appenzeller-Herzog, C., and Ellgaard, L. (2008). The human PDI family: versatility packed into a single fold. *Biochimica et Biophysica Acta* 1783.

Aroca, A., Benito, J.M., Gotor, C., and Romero, L.C. (2017). Persulfidation proteome reveals the regulation of protein function by hydrogen sulfide in diverse biological processes in *Arabidopsis*. *Journal of Experimental Botany* 68.

Asada, K. (2006). Production and Scavenging of Reactive Oxygen Species in Chloroplasts and Their Functions. *Plant Physiology* 141.

Astier, J., Gross, I., and Durner, J. (2018). Nitric oxide production in plants: an update. *Journal of Experimental Botany* 69.

Attacha, S., Solbach, D., Bela, K., Moseler, A., Wagner, S., Schwarzländer, M., Aller, I., Müller, S.J., and Meyer, A.J. (2017). Glutathione peroxidase-like enzymes cover five distinct cell compartments and membrane surfaces in *Arabidopsis thaliana*. *Plant Cell & Environment* 40.

Bader, M., Muse, W., Ballou, D.P., Gassner, C., and Bardwell, J.C.A. (1999). Oxidative Protein Folding Is Driven by the Electron Transport System. *Cell* 98.

Bader, M.W., Hiniker, A., Regeimbal, J., Goldstone, D., Haebel, P.W., Riemer, J., Metcalf, P., and Bardwell, J.C.A. (2001). Turning a disulfide isomerase into an oxidase: DsbC mutants that imitate DsbA. *The EMBO Journal* 20.

Baker, K.M., Chakravarthi, S., Langton, K.P., Sheppard, A.M., Lu, H., and Bulleid, N.J. (2008). Low reduction potential of Ero1 α regulatory disulphides ensures tight control of substrate oxidation. *The EMBO Journal* 27.

Ball, L., Accotto, G.-P., Bechtold, U., Creissen, G., Funck, D., Jimenez, A., Kular, B., Leyland, N., Mejia-Carranza, J., Reynolds, H., et al. (2004). Evidence for a Direct Link between Glutathione Biosynthesis and Stress Defense Gene Expression in Arabidopsis. *The Plant Cell* 16.

Banci, L., Bertini, I., Cefaro, C., Ciofi-Baffoni, S., Gallo, A., Martinelli, M., Sideris, D.P., Katrakili, N., and Tokatlidis, K. (2009). MIA40 is an oxidoreductase that catalyzes oxidative protein folding in mitochondria. *Nature Structural & Molecular Biology* 16.

Banci, L., Bertini, I., Ciofi-Baffoni, S., Jaiswal, D., Neri, S., Peruzzini, R., and Winkelmann, J. (2012). Structural characterization of CHCHD5 and CHCHD7: Two atypical human twin CX9C proteins. *Journal of Structural Biology* 180.

Bandyopadhyay, S., Chandramouli, K., and Johnson, M.K. (2008). Iron–sulfur cluster biosynthesis. *Biochemical Society Transactions* 36.

Baniulis, D., Hasan, S.S., Stofleth, J.T., and Cramer, W.A. (2013). Mechanism of Enhanced Superoxide Production in the Cytochrome $b_{6}f$ Complex of Oxygenic Photosynthesis. *Biochemistry* 52.

Bedhomme, M., Zaffagnini, M., Marchand, C.H., Gao, X.-H., Moslonka-Lefebvre, M., Michelet, L., Decottignies, P., and Lemaire, S.D. (2009). Regulation by Glutathionylation of Isocitrate Lyase from *Chlamydomonas reinhardtii*. *Journal of Biological Chemistry* 284.

Bernard, D.G., Gabilly, S.T., Dujardin, G., Merchant, S., and Hamel, P.P. (2003). Overlapping Specificities of the Mitochondrial Cytochrome c and c_1 Heme Lyases. *Journal of Biological Chemistry* 278.

Bien, M., Longen, S., Wagener, N., Chwalla, I., Herrmann, J.M., and Riemer, J. (2010). Mitochondrial Disulfide Bond Formation Is Driven by Intersubunit Electron Transfer in Erv1 and Proofread by Glutathione. *Molecular Cell* 37.

Bihlmaier, K., Mesecke, N., Terziyska, N., Bien, M., Hell, K., and Herrmann, J.M. (2007). The disulfide relay system of mitochondria is connected to the respiratory chain. *The Journal of Cell Biology* 179.

Bisio, H., Bonilla, M., Manta, B., Graña, M., Salzman, V., Aguilar, P.S., Gladyshev, V.N., Comini, M.A., and Salinas, G. (2016). A New Class of Thioredoxin-Related Protein Able to Bind Iron–Sulfur Clusters. *Antioxidants & Redox Signaling* 24.

Biteau, B., Labarre, J., and Toledano, M.B. (2003). ATP-dependent reduction of cysteine-sulphinic acid by *S. cerevisiae* sulphiredoxin. *Nature* 425.

Breuza, L., Halbeisen, R., Jenö, P., Otte, S., Barlowe, C., Hong, W., and Hauri, H.-P. (2004). Proteomics of Endoplasmic Reticulum-Golgi Intermediate Compartment (ERGIC) Membranes

from Brefeldin A-treated HepG2 Cells Identifies ERGIC-32, a New Cycling Protein That Interacts with Human Erv46. *Journal of Biological Chemistry* 279.

Buchanan, B.B., and Luan, S. (2005). Redox regulation in the chloroplast thylakoid lumen: a new frontier in photosynthesis research. *Journal of Experimental Botany* 56.

Buchner, J. (1996). Supervising the fold: functional principles of molecular chaperones. *The FASEB Journal*. 10.

Calabrese, G., Morgan, B., and Riemer, J. (2017). Mitochondrial Glutathione: Regulation and Functions. *Antioxidants & Redox Signaling* 27.

Calderón, A., Sánchez-Guerrero, A., Ortiz-Espín, A., Martínez-Alcalá, I., Camejo, D., Jiménez, A., and Sevilla, F. (2018). Lack of mitochondrial thioredoxin *o* 1 is compensated by antioxidant components under salinity in *Arabidopsis thaliana* plants. *Physiologia Plantarum* 164.

Cao, Z., van Lith, M., Mitchell, L.J., Pringle, M.A., Inaba, K., and Bulleid, N.J. (2016). The membrane topology of vitamin K epoxide reductase is conserved between human isoforms and the bacterial enzyme. *Biochemical Journal* 473.

Carrie, C., Giraud, E., Duncan, O., Xu, L., Wang, Y., Huang, S., Clifton, R., Murcha, M., Filipovska, A., Rackham, O., et al. (2010). Conserved and Novel Functions for *Arabidopsis thaliana* MIA40 in Assembly of Proteins in Mitochondria and Peroxisomes. *Journal of Biological Chemistry* 28.

Cazalé, A.-C., and Clemens, S. (2001). *Arabidopsis thaliana* expresses a second functional phytochelatin synthase. *FEBS Letters* 507.

Chacinska, A., Pfannschmidt, S., Wiedemann, N., Kozjak, V., Sanjuán Szklarz, L.K., Schulze-Specking, A., Truscott, K.N., Guiard, B., Meisinger, C., and Pfanner, N. (2004). Essential role of Mia40 in import and assembly of mitochondrial intermembrane space proteins. *The EMBO Journal* 23.

Chakravarthi, S., Jessop, C.E., Willer, M., Stirling, C.J., and Bulleid, N.J. (2007). Intracellular catalysis of disulfide bond formation by the human sulfhydryl oxidase, QSOX1. *Biochemical Journal* 404.

Chatelle, C., Kraemer, S., Ren, G., Chmura, H., Marechal, N., Boyd, D., Roggemans, C., Ke, N., Riggs, P., Bardwell, J., et al. (2015). Converting a Sulfinic Acid Reductase into a Disulfide Bond Isomerase. *Antioxidants & Redox Signaling* 23.

Chibani, K., Wingsle, G., Jacquot, J.-P., Gelhaye, E., and Rouhier, N. (2009). Comparative genomic study of the thioredoxin family in photosynthetic organisms with emphasis on *Populus trichocarpa*. *Molecular Plant* 2.

Collet, J.-F., Peisach, D., Bardwell, J.C.A., and Xu, Z. (2005). The crystal structure of TrxA(CACA): Insights into the formation of a [2Fe-2S] iron-sulfur cluster in an *Escherichia coli* thioredoxin mutant. *Protein Science* 14.

Collin, V., Issakidis-Bourguet, E., Marchand, C., Hirasawa, M., Lancelin, J.-M., Knaff, D.B., and Miginiac-Maslow, M. (2003). The *Arabidopsis* Plastidial Thioredoxins: New Functions and new insights into specificity. *Journal of Biological Chemistry* 278.

Coppock, D.L., and Thorpe, C. (2006). Multidomain Flavin-Dependent Sulphydryl Oxidases. *Antioxidants & Redox Signaling* 8.

Couturier, J., Jacquot, J.-P., and Rouhier, N. (2009). Evolution and diversity of glutaredoxins in photosynthetic organisms. *Cellular and Molecular Life Sciences* 66.

Couturier, J., Didierjean, C., Jacquot, J.-P., and Rouhier, N. (2010). Engineered mutated glutaredoxins mimicking peculiar plant class III glutaredoxins bind iron–sulfur centers and possess reductase activity. *Biochemical and Biophysical Research Communications* 403.

Couturier, J., Jacquot, J.-P., and Rouhier, N. (2013a). Toward a refined classification of class I dithiol glutaredoxins from poplar: biochemical basis for the definition of two subclasses. *Frontiers in Plant Science* 4.

Couturier, J., Chibani, K., Jacquot, J.-P., and Rouhier, N. (2013b). Cysteine-based redox regulation and signaling in plants. *Frontiers in Plant Science* 4.

Couturier, J., Wu, H.-C., Dhalleine, T., Pégeot, H., Sudre, D., Gualberto, J.M., Jacquot, J.-P., Gaymard, F., Vignols, F., and Rouhier, N. (2014). Monothiol glutaredoxin-BolA interactions: redox control of *Arabidopsis thaliana* BolA2 and SufE1. *Molecular Plant* 7.

Couturier, J., Przybyla-Toscano, J., Roret, T., Didierjean, C., and Rouhier, N. (2015). The roles of glutaredoxins ligating Fe–S clusters: Sensing, transfer or repair functions? *Biochimica et Biophysica Acta (BBA) - Molecular Cell Research* 1853.

Cox, J.S., Chapman, R.E., and Walter, P. (1997). The unfolded protein response coordinates the production of endoplasmic reticulum protein and endoplasmic reticulum membrane. *Molecular Biology of the Cell* 8.

Cuozzo, J.W., and Kaiser, C.A. (1999). Competition between glutathione and protein thiols for disulphide-bond formation. *Nature Cell Biology* 1.

Daloso, D.M., Müller, K., Obata, T., Florian, A., Tohge, T., Bottcher, A., Riondet, C., Bariat, L., Carrari, F., Nunes-Nesi, A., et al. (2015). Thioredoxin, a master regulator of the tricarboxylic acid cycle in plant mitochondria. *Proceedings of the National Academy of Sciences* 112.

Danon, A. (2012). Environmentally-Induced Oxidative Stress and Its Signaling. Springer Book *Photosynthesis: Plastid biology, energy conversion and carbon assimilation* 34.

Delaunay-Moisson, A., Ponsero, A., and Toledano, M.B. (2017). Reexamining the Function of Glutathione in Oxidative Protein Folding and Secretion. *Antioxidants & Redox Signaling* 27.

Delorme-Hinoux, V., Bangash, S.A.K., Meyer, A.J., and Reichheld, J.-P. (2016). Nuclear thiol redox systems in plants. *Plant Science* 243.

Denoncin, K., Vertommen, D., Arts, I.S., Goemans, C.V., Rahuel-Clermont, S., Messens, J., and Collet, J.-F. (2014). A New Role for *Escherichia coli* DsbC Protein in Protection against Oxidative Stress. *Journal of Biological Chemistry* 289.

Depuydt, M., Leonard, S.E., Vertommen, D., Denoncin, K., Morsomme, P., Wahni, K., Messens, J., Carroll, K.S., and Collet, J.-F. (2009). A Periplasmic Reducing System Protects Single Cysteine Residues from Oxidation. *Science* 326.

Depuydt, M., Messens, J., and Collet, J.-F. (2011). How Proteins Form Disulfide Bonds. *Antioxidants & Redox Signaling* 15.

Dixon, D.P., and Edwards, R. (2010). Glutathione Transferases. *The Arabidopsis Book* 8.

Dixon, D.P., Davis, B.G., and Edwards, R. (2002). Functional Divergence in the Glutathione Transferase Superfamily in Plants: Identification of two classes with putative functions in redox homeostasis in *Arabidopsis thaliana*. *Journal of Biological Chemistry* 277.

Dixon, D.P., van Lith, M., Edwards, R., and Benham, A. (2003). Cloning and Initial Characterization of the *Arabidopsis thaliana* Endoplasmic Reticulum Oxidoreductins. *Antioxidants & Redox Signaling* 5.

Dixon, D.P., Hawkins, T., Hussey, P.J., and Edwards, R. (2009). Enzyme activities and subcellular localization of members of the *Arabidopsis* glutathione transferase superfamily. *Journal of Experimental Botany* 60.

Dóka, É., Pader, I., Bíró, A., Johansson, K., Cheng, Q., Ballagó, K., Prigge, J.R., Pastor-Flores, D., Dick, T.P., Schmidt, E.E., et al. (2016). A novel persulfide detection method reveals protein persulfide- and polysulfide-reducing functions of thioredoxin and glutathione systems. *Science Advances* 2.

Dreyfuss, B.W., Hamel, P.P., Nakamoto, S.S., and Merchant, S. (2003). Functional Analysis of a Divergent System II Protein, Ccs1, Involved in *c*-Type Cytochrome Biogenesis. *Journal of Biological Chemistry* 278.

Du, J.-J., Zhan, C.-Y., Lu, Y., Cui, H.-R., and Wang, X.-Y. (2015). The conservative cysteines in transmembrane domain of AtVKOR/LTO1 are critical for photosynthetic growth and photosystem II activity in *Arabidopsis*. *Frontiers in Plant Science* 6.

Dumont, M.E., Ernst, J.F., Hampsey, D.M., and Sherman, F. (1987). Identification and sequence of the gene encoding cytochrome c heme lyase in the yeast *Saccharomyces cerevisiae*. *The EMBO Journal* 6.

Eckers, E., Petrungaro, C., Gross, D., Riemer, J., Hell, K., and Deponte, M. (2013). Divergent Molecular Evolution of the Mitochondrial Sulphydryl:Cytochrome *c* Oxidoreductase Erv in Opisthokonts and Parasitic Protists. *Journal of Biological Chemistry* 288.

Edman, J.C., Ellis, L., Blacher, R.W., Roth, R.A., and Rutter, W.J. (1985). Sequence of protein disulphide isomerase and implications of its relationship to thioredoxin. *Nature* 317.

Eggert, E., Obata, T., Gerstenberger, A., Gier, K., Brandt, T., Fernie, A.R., Schulze, W., and Kühn, C. (2016). A sucrose transporter-interacting protein disulphide isomerase affects redox homeostasis and links sucrose partitioning with abiotic stress tolerance: StPDI1 involved in drought and salt stress tolerance. *Plant, Cell & Environment* 39.

Ellgaard, L., Sevier, C.S., and Bulleid, N.J. (2018). How Are Proteins Reduced in the Endoplasmic Reticulum ? *Trends in Biochemical Sciences* 43.

Fabianek, R.A., Hennecke, H., and Thöny-Meyer, L. (1998). The active-site cysteines of the periplasmic thioredoxin-like protein CcmG of *Escherichia coli* are important but not essential for cytochrome c maturation in vivo. *Journal of Bacteriology* 180.

Fabianek, R.A., Hennecke, H., and Thöny-Meyer, L. (2000). Periplasmic protein thiol:disulfide oxidoreductases of *Escherichia coli*. *FEMS Microbiology Reviews* 24.

Fan, F., Zhang, Y., Wang, S., Han, Y., Wang, L., and Lu, D. (2018). Characterization of the oxidative protein folding activity of a unique plant oxidoreductase, Arabidopsis protein disulfide isomerase-11. *Biochemical and Biophysical Research Communications* 495.

Fan, F., Zhang, Y., Huang, G., Zhang, Q., Wang, C., Wang, L., and Lu, D. (2019). AtERO1 and AtERO2 Exhibit Differences in Catalyzing Oxidative Protein Folding in the Endoplasmic Reticulum. *Plant Physiology* 180.

Feng, W.-K., Wang, L., Lu, Y., and Wang, X.-Y. (2011). A protein oxidase catalysing disulfide bond formation is localized to the chloroplast thylakoids: A protein oxidase in thylakoids. *FEBS Journal* 278.

Fernandes, A.P., Fladvad, M., Berndt, C., AndréSEN, C., Lillig, C.H., Neubauer, P., Sunnerhagen, M., Holmgren, A., and Vlamis-Gardikas, A. (2005). A Novel Monothiol Glutaredoxin (Grx4) from *Escherichia coli* Can Serve as a Substrate for Thioredoxin Reductase. *Journal of Biological Chemistry* 280.

Ferrer-Sueta, G., Manta, B., Botti, H., Radi, R., Trujillo, M., and Denicola, A. (2011). Factors Affecting Protein Thiol Reactivity and Specificity in Peroxide Reduction. *Chemical Research in Toxicology* 24.

Filonova, A., Haemsch, P., Gebauer, C., Weisheit, W., and Wagner, V. (2013). Protein Disulfide Isomerase 2 of *Chlamydomonas reinhardtii* Is Involved in Circadian Rhythm Regulation. *Molecular Plant* 6.

Fischer, M., and Riemer, J. (2013). The mitochondrial disulfide relay system: roles in oxidative protein folding and beyond. *International Journal of Cell Biology* 2013.

Fischer, B.B., Krieger-Liszskay, A., Hideg, É., Šnyrychová, I., Wiesendanger, M., and Eggen, R.I.L. (2007). Role of singlet oxygen in chloroplast to nucleus retrograde signaling in *Chlamydomonas reinhardtii*. *FEBS Letters* 581.

Fischer, B.B., Hideg, É., and Krieger-Liszkay, A. (2013). Production, Detection, and Signaling of Singlet Oxygen in Photosynthetic Organisms. *Antioxidants & Redox Signaling 18*.

Florez-Sarasa, I., Obata, T., Del-Saz, N.F., Reichheld, J.-P., Meyer, E.H., Rodriguez-Concepcion, M., Ribas-Carbo, M., and Fernie, A.R. (2019). The Lack of Mitochondrial Thioredoxin TRXo1 Affects In Vivo Alternative Oxidase Activity and Carbon Metabolism under Different Light Conditions. *Plant and Cell Physiology*.

Fonseca-Pereira, P., Souza, P.V.L., Hou, L., Schwab, S., Geigenberger, P., Nunes-Nesi, A., Timm, S., Fernie, A.R., Thormählen, I., Araújo, W.L., et al. (2019). Thioredoxin *h2* contributes to the redox regulation of mitochondrial photorespiratory metabolism. *Plant, Cell & Environment*.

Fonseca-Pereira, P., Daloso, D.M., Gago, J., de Oliveira Silva, F.M., Condori-Apfata, J.A., Florez-Sarasa, I., Tohge, T., Reichheld, J.-P., Nunes-Nesi, A., Fernie, A.R., et al. (2019). The Mitochondrial Thioredoxin System Contributes to the Metabolic Responses Under Drought Episodes in Arabidopsis. *Plant and Cell Physiology 60*.

Foyer, C.H., and Noctor, G. (2011). Ascorbate and Glutathione: The Heart of the Redox Hub. *Plant Physiology 155*.

Frandsen, A.R., and Kaiser, C.A. (1998). The ERO1 Gene of Yeast Is Required for Oxidation of Protein Dithiols in the Endoplasmic Reticulum. *Molecular Cell 1*.

Freedman, R.B., Hirst, T.R., and Tuite, M.F. (1994). Protein disulphide isomerase: building bridges in protein folding. *Trends in Biochemical Sciences 19*.

Freeman, J.L., Persans, M.W., Nieman, K., Albrecht, C., Peer, W., Pickering, I.J., and Salt, D.E. (2004). Increased Glutathione Biosynthesis Plays a Role in Nickel Tolerance in *Thlaspi* Nickel Hyperaccumulators. *The Plant Cell 16*.

Fujimori, T., Suno, R., Iemura, S., Natsume, T., Wada, I., and Hosokawa, N. (2017). Endoplasmic reticulum proteins SDF2 and SDF2L1 act as components of the BiP chaperone cycle to prevent protein aggregation. *Genes to Cells 22*.

Furt, F., Oostende, C. van, Widhalm, J.R., Dale, M.A., Wertz, J., and Basset, G.J.C. (2010). A bimodular oxidoreductase mediates the specific reduction of phylloquinone (vitamin K1) in chloroplasts: Plant phylloquinone reductase. *The Plant Journal 64*.

Gabily, S.T., and Hamel, P.P. (2017). Maturation of Plastid c-type Cytochromes. *Frontiers in Plant Science 8*.

Geigenberger, P., Thormählen, I., Daloso, D.M., and Fernie, A.R. (2017). The Unprecedented Versatility of the Plant Thioredoxin System. *Trends in Plant Science 22*.

Gelhaye, E., Rouhier, N., and Jacquot, J.-P. (2004a). The thioredoxin h system of higher plants. *Plant Physiology and Biochemistry 42*.

Gelhaye, E., Rouhier, N., Gerard, J., Jolivet, Y., Gualberto, J., Navrot, N., Ohlsson, P.-I., Wingsle, G., Hirasawa, M., Knaff, D.B., et al. (2004b). A specific form of thioredoxin h occurs in plant mitochondria and regulates the alternative oxidase. *Proceedings of the National Academy of Sciences* *101*

Gelhaye, E., Rouhier, N., Navrot, N., and Jacquot, J.P. (2005). The plant thioredoxin system. *Cellular and Molecular Life Sciences* *62*.

Gething, M.-J., and Sambrook, J. (1992). Protein folding in the cell. *Nature* *355*.

Giles, N.M., Watts, A.B., Giles, G.I., Fry, F.H., Littlechild, J.A., and Jacob, C. (2003). Metal and Redox Modulation of Cysteine Protein Function. *Chemistry & Biology* *10*.

Gill, S.S., Anjum, N.A., Gill, R., Yadav, S., Hasanuzzaman, M., Fujita, M., Mishra, P., Sabat, S.C., and Tuteja, N. (2015). Superoxide dismutase - - mentor of abiotic stress tolerance in crop plants. *Environmental Science and Pollution Research* *22*.

Gopalan, G., He, Z., Balmer, Y., Romano, P., Gupta, R., Heroux, A., Buchanan, B.B., Swaminathan, K., and Luan, S. (2004). Structural analysis uncovers a role for redox in regulating FKBP13, an immunophilin of the chloroplast thylakoid lumen. *Proceedings of the National Academy of Sciences* *101*.

Goulding, C.W., Sawaya, M.R., Parseghian, A., Lim, V., Eisenberg, D., and Missiakas, D. (2002). Thiol–Disulfide Exchange in an Immunoglobulin-like Fold: Structure of the N-Terminal Domain of DsbD. *Biochemistry* *41*.

Grauschopf, U., Winther, J.R., Korber, P., Zander, T., Dallinger, P., and Bardwell, J.C.A. (1995). Why is DsbA such an oxidizing disulfide catalyst ? *Cell* *83*.

Gross, E., Kastner, D.B., Kaiser, C.A., and Fass, D. (2004). Structure of Ero1p, Source of Disulfide Bonds for Oxidative Protein Folding in the Cell. *Cell* *117*.

Gross, E., Sevier, C.S., Heldman, N., Vitu, E., Bentzur, M., Kaiser, C.A., Thorpe, C., and Fass, D. (2006). Generating disulfides enzymatically: Reaction products and electron acceptors of the endoplasmic reticulum thiol oxidase Ero1p. *Proceedings of the National Academy of Sciences* *103*.

Grzam, A., Martin, M.N., Hell, R., and Meyer, A.J. (2007). γ -Glutamyl transpeptidase GGT4 initiates vacuolar degradation of glutathione S-conjugates in *Arabidopsis*. *FEBS Letters* *581*.

Guo, Y., Huang, C., Xie, Y., Song, F., and Zhou, X. (2010). A tomato glutaredoxin gene SlGRX1 regulates plant responses to oxidative, drought and salt stresses. *Planta* *232*.

Gupta, K.J., Fernie, A.R., Kaiser, W.M., and van Dongen, J.T. (2011). On the origins of nitric oxide. *Trends in Plant Science* *16*.

Gupta, R., Mould, R.M., He, Z., and Luan, S. (2002). Nonlinear partial differential equations and applications: A chloroplast FKBP interacts with and affects the accumulation of Rieske subunit of cytochrome bf complex. *Proceedings of the National Academy of Sciences* *99*.

Gütle, D.D., Roret, T., Müller, S.J., Couturier, J., Lemaire, S.D., Hecker, A., Dhalleine, T., Buchanan, B.B., Reski, R., Einsle, O., et al. (2016). Chloroplast FBPase and SBPase are thioredoxin-linked enzymes with similar architecture but different evolutionary histories. *Proceedings of the National Academy of Sciences* *113*.

Gütle, D.D., Roret, T., Hecker, A., Reski, R., and Jacquot, J.-P. (2017). Dithiol disulphide exchange in redox regulation of chloroplast enzymes in response to evolutionary and structural constraints. *Plant Science* *255*.

Gutsche, N., Thurow, C., Zachgo, S., and Gatz, C. (2015). Plant-specific CC-type glutaredoxins: functions in developmental processes and stress responses. *Biological Chemistry* *396*.

Haebel, P.W. (2002). The disulfide bond isomerase DsbC is activated by an immunoglobulin-fold thiol oxidoreductase: crystal structure of the DsbC-DsbDalpha complex. *The EMBO Journal* *21*.

Hall, M., Mishra, Y., and Schröder, W.P. (2011). Preparation of Stroma, Thylakoid Membrane, and Lumen Fractions from *Arabidopsis thaliana* Chloroplasts for Proteomic Analysis. In *Chloroplast Research in Arabidopsis*, R.P. Jarvis, ed. (Totowa, NJ: Humana Press).

Halliwell, B., and Gutteridge, J.M.C. (1992). Biologically relevant metal ion-dependent hydroxyl radical generation An update. *FEBS Letters* *307*.

Halliwell, B., and Gutteridge, J.M.C. (1995). The definition and measurement of antioxidants in biological systems. *Free Radical Biology and Medicine* *18*.

Harding, H.P., Zhang, Y., and Ron, D. (1999). Protein translation and folding are coupled by an endoplasmic-reticulum-resident kinase. *Nature* *397*.

Harding, H.P., Zhang, Y., Bertolotti, A., Zeng, H., and Ron, D. (2000). Perk Is Essential for Translational Regulation and Cell Survival during the Unfolded Protein Response. *Molecular Cell* *5*.

Harding, H.P., Zhang, Y., Zeng, H., Novoa, I., Lu, P.D., Calfon, M., Sadri, N., Yun, C., Popko, B., Paules, R., et al. (2003). An Integrated Stress Response Regulates Amino Acid Metabolism and Resistance to Oxidative Stress. *Molecular Cell* *11*.

Hartl, F.U., and Hayer-Hartl, M. (2002). Molecular chaperones in the cytosol: from nascent chain to folded protein. *Science* *295*.

Haruta, M., Sabat, G., Stecker, K., Minkoff, B.B., and Sussman, M.R. (2014). A Peptide Hormone and Its Receptor Protein Kinase Regulate Plant Cell Expansion. *Science* *343*.

Havaux, M. (2014). Carotenoid oxidation products as stress signals in plants. *The Plant Journal* *79*.

Henmi, K., Demura, T., Tsuboi, S., Fukuda, H., Iwabuchi, M., and Ogawa, K. (2005). Change in the Redox State of Glutathione Regulates Differentiation of Tracheary Elements in Zinnia Cells and Arabidopsis Roots. *Plant and Cell Physiology* *46*.

Henne, M., König, N., Triulzi, T., Baroni, S., Forlani, F., Scheibe, R., and Papenbrock, J. (2015). Sulfurtransferase and thioredoxin specifically interact as demonstrated by bimolecular fluorescence complementation analysis and biochemical tests. *FEBS Open Bio* *5*.

Herbette, S., Lenne, C., Leblanc, N., Julien, J.-L., Drevet, J.R., and Roeckel-Drevet, P. (2002). Two GPX-like proteins from *Lycopersicon esculentum* and *Helianthus annuus* are antioxidant enzymes with phospholipid hydroperoxide glutathione peroxidase and thioredoxin peroxidase activities: Dual activities for plant antioxidant enzymes. *European Journal of Biochemistry* *269*.

Herrmann, J.M., and Riemer, J. (2012). Mitochondrial Disulfide Relay: Redox-regulated Protein Import into the Intermembrane Space. *Journal of Biological Chemistry* *287*.

Hisabori, T., Hara, S., Fujii, T., Yamazaki, D., Hosoya-Matsuda, N., and Motohashi, K. (2005). Thioredoxin affinity chromatography: a useful method for further understanding the thioredoxin network. *Journal of Experimental Botany* *56*.

Hong, Z., Jin, H., Tzfira, T., and Li, J. (2008). Multiple Mechanism–Mediated Retention of a Defective Brassinosteroid Receptor in the Endoplasmic Reticulum of *Arabidopsis*. *The Plant Cell* *20*.

Hothorn, M., Wachter, A., Gromes, R., Stuwe, T., Rausch, T., and Scheffzek, K. (2006). Structural Basis for the Redox Control of Plant Glutamate Cysteine Ligase. *Journal of Biological Chemistry* *281*.

Hothorn, M., Belkadir, Y., Dreux, M., Dabi, T., Noel, Joseph.P., Wilson, I.A., and Chory, J. (2011). Structural basis of steroid hormone perception by the receptor kinase BRII. *Nature* *474*.

Howden, R., and Cobbett, C.S. (1992). Cadmium-Sensitive Mutants of *Arabidopsis thaliana*. *Plant Physiology* *100*.

Hu, J., Dong, L., and Outten, C.E. (2008). The Redox Environment in the Mitochondrial Intermembrane Space Is Maintained Separately from the Cytosol and Matrix. *Journal of Biological Chemistry* *283*.

Hu, J., Huang, X., Chen, L., Sun, X., Lu, C., Zhang, L., Wang, Y., and Zuo, J. (2015). Site-Specific Nitrosoproteomic Identification of Endogenously S -Nitrosylated Proteins in Arabidopsis. *Plant Physiology* *167*.

Huang, C.-H., Kuo, W.-Y., Weiss, C., and Jinn, T.-L. (2012). Copper Chaperone-Dependent and Independent Activation of Three Copper-Zinc Superoxide Dismutase Homologs Localized in Different Cellular Compartments in Arabidopsis. *Plant Physiology* *158*.

Huang, S., Van Aken, O., Schwarzländer, M., Belt, K., and Millar, A.H. (2016). The Roles of Mitochondrial Reactive Oxygen Species in Cellular Signaling and Stress Response in Plants. *Plant Physiology* 171.

Hudson, D.A., and Thorpe, C. (2015). Mia40 is a facile oxidant of unfolded reduced proteins but shows minimal isomerase activity. *Archives of Biochemistry and Biophysics* 579.

Hudson, D.A., Gannon, S.A., and Thorpe, C. (2015). Oxidative protein folding: From thiol? Disulfide exchange reactions to the redox poise of the endoplasmic reticulum. *Free Radical Biology and Medicine* 80.

Hurd, T.R., and Murphy, M.P. (2009). Biological Systems Relevant for Redox Signaling and Control. In *Redox Signaling and Regulation in Biology and Medicine* Wiley-VCH Verlag GmbH & Co. KGaA.

Huynen, M.A., Duarte, I., and Szklarczyk, R. (2013). Loss, replacement and gain of proteins at the origin of the mitochondria. *Biochimica et Biophysica Acta (BBA) - Bioenergetics* 1827.

Inaba, K., Murakami, S., Suzuki, M., Nakagawa, A., Yamashita, E., Okada, K., and Ito, K. (2006a). Crystal Structure of the DsbB-DsbA Complex Reveals a Mechanism of Disulfide Bond Generation. *Cell* 127.

Inaba, K., Takahashi, Y., Ito, K., and Hayashi, S. (2006b). Critical role of a thiolate-quinone charge transfer complex and its adduct form in de novo disulfide bond generation by DsbB. *Proceedings of the National Academy of Sciences*. 103.

Ito, K., and Inaba, K. (2008). The disulfide bond formation (Dsb) system. *Current Opinion in Structural Biology* 18.

Itzhak, D.N., Tyanova, S., Cox, J., and Borner, G.H. (2016). Global, quantitative and dynamic mapping of protein subcellular localization. *ELife* 5.

Ivanov, B., and Khorobrykh, S. (2003). Participation of Photosynthetic Electron Transport in Production and Scavenging of Reactive Oxygen Species. *Antioxidants & Redox Signaling* 5.

Iwasaki, K., Kamauchi, S., Wadahama, H., Ishimoto, M., Kawada, T., and Urade, R. (2009). Molecular cloning and characterization of soybean protein disulfide isomerase family proteins with nonclassic active center motifs. *FEBS Journal* 276.

Jacquot, J.-P., Rouhier, N., and Gelhaye, E. (2002a). Redox Control by Dithiol-Disulfide Exchange in Plants. *Annals of the New York Academy of Sciences* 973.

Jacquot, J.-P., Gelhaye, E., Rouhier, N., Corbier, C., Didierjean, C., and Aubry, A. (2002b). Thioredoxins and related proteins in photosynthetic organisms: molecular basis for thiol dependent regulation. *Biochemical Pharmacology* 64.

Jespersen, H.M., Kjærsgård, I.V.H., Østergaard, L., and Welinder, K.G. (1997). From sequence analysis of three novel ascorbate peroxidases from *Arabidopsis thaliana* to structure, function and evolution of seven types of ascorbate peroxidase. *Biochemical Journal* 326.

Jin, Y., Zhuang, M., and Hendershot, L.M. (2009). ERdj3, a Luminal ER DnaJ Homologue, Binds Directly to Unfolded Proteins in the Mammalian ER: Identification of Critical Residues. *Biochemistry* 48.

Johansson, C., Lillig, C.H., and Holmgren, A. (2004). Human mitochondrial glutaredoxin reduces S-glutathionylated proteins with high affinity accepting electrons from either glutathione or thioredoxin reductase. *Journal of Biological Chemistry* 279.

Joly, J.C., and Swartz, J.R. (1997). *In Vitro* and *in Vivo* Redox States of the *Escherichia coli* Periplasmic Oxidoreductases DsbA and DsbC. *Biochemistry* 36.

Kakihana, T., Nagata, K., and Sitia, R. (2012). Peroxides and peroxidases in the endoplasmic reticulum: integrating redox homeostasis and oxidative folding. *Antioxidants & Redox Signaling* 16.

Kang, Z.-H., and Wang, G.-X. (2016). Redox regulation in the thylakoid lumen. *Journal of Plant Physiology* 192.

Karamoko, M., Cline, S., Redding, K., Ruiz, N., and Hamel, P.P. (2011). Lumen Thiol Oxidoreductase1, a Disulfide Bond-Forming Catalyst, Is Required for the Assembly of Photosystem II in *Arabidopsis*. *The Plant Cell* 23.

Katzen, F., and Beckwith, J. (2000). Transmembrane Electron Transfer by the Membrane Protein DsbD Occurs via a Disulfide Bond Cascade. *Cell* 103.

Kaufman, R. (2004). Regulation of mRNA translation by protein folding in the endoplasmic reticulum. *Trends in Biochemical Sciences* 29.

Kaufman, R.J. (2002). Orchestrating the unfolded protein response in health and disease. *Journal of Clinical Investigation* 110.

Kaurov, I., Vancová, M., Schimanski, B., Cadena, L.R., Heller, J., Bílý, T., Potěšil, D., Eichenberger, C., Bruce, H., Oeljeklaus, S., et al. (2018). The Diverged Trypanosome MICOS Complex as a Hub for Mitochondrial Cristae Shaping and Protein Import. *Current Biology* 28.

Kayum, Md.A., Park, J.-I., Nath, U.K., Saha, G., Biswas, M.K., Kim, H.-T., and Nou, I.-S. (2017). Genome-wide characterization and expression profiling of PDI family gene reveals function as abiotic and biotic stress tolerance in Chinese cabbage (*Brassica rapa* ssp. *pekinensis*). *BMC Genomics* 18.

Kim, J.H., Kim, S.J., Jeong, D.G., Son, J.H., and Ryu, S.E. (2003). Crystal structure of DsbDγ reveals the mechanism of redox potential shift and substrate specificity . *FEBS Letters* 543.

Kimura, S., Higashino, Y., Kitao, Y., Masuda, T., and Urade, R. (2015). Expression and characterization of protein disulfide isomerase family proteins in bread wheat. *BMC Plant Biology* 15.

Kliebenstein, D.J., Monde, R.-A., and Last, R.L. (1998). Superoxide Dismutase in *Arabidopsis*: An Eclectic Enzyme Family with Disparate Regulation and Protein Localization. *Plant Physiology* 118.

Knuesting, J., Riondet, C., Maria, C., Kruse, I., Bécuwe, N., König, N., Berndt, C., Tourrette, S., Guilleminot-Montoya, J., Herrero, E., et al. (2015). *Arabidopsis* Glutaredoxin S17 and Its Partner, the Nuclear Factor Y Subunit C11/Negative Cofactor 2 α , Contribute to Maintenance of the Shoot Apical Meristem under Long-Day Photoperiod. *Plant Physiology* 167.

Kodali, V.K., and Thorpe, C. (2010). Oxidative Protein Folding and the Quiescin–Sulphydryl Oxidase Family of Flavoproteins. *Antioxidants & Redox Signaling* 13.

Kojer, K., and Riemer, J. (2014). Balancing oxidative protein folding: The influences of reducing pathways on disulfide bond formation. *Biochimica et Biophysica Acta (BBA) - Proteins and Proteomics* 1844.

Kojer, K., Bien, M., Gangel, H., Morgan, B., Dick, T.P., and Riemer, J. (2012). Glutathione redox potential in the mitochondrial intermembrane space is linked to the cytosol and impacts the Mia40 redox state: E_{GSH} of the IMS is maintained by the cytosol. *The EMBO Journal* 31.

Kojer, K., Peleh, V., Calabrese, G., Herrmann, J.M., and Riemer, J. (2015). Kinetic control by limiting glutaredoxin amounts enables thiol oxidation in the reducing mitochondrial intermembrane space. *Molecular Biology of the Cell* 26.

Kozlov, G., Määttänen, P., Thomas, D.Y., and Gehring, K. (2010). A structural overview of the PDI family of proteins. *FEBS Journal* 277.

Kranz, R.G., Richard-Fogal, C., Taylor, J.-S., and Frawley, E.R. (2009). Cytochrome c Biogenesis: Mechanisms for Covalent Modifications and Trafficking of Heme and for Heme-Iron Redox Control. *Microbiology and Molecular Biology Reviews* 73.

Krupp, R., Chan, C., and Missiakas, D. (2001). DsbD-catalyzed Transport of Electrons across the Membrane of *Escherichia coli*. *Journal of Biological Chemistry* 276.

Kumar, M.N., Hsieh, Y.-F., and Verslues, P.E. (2015). At14a-Like1 participates in membrane-associated mechanisms promoting growth during drought in *Arabidopsis thaliana*. *Proceedings of the National Academy of Sciences* 112.

Laloi, C., Rayapuram, N., Chartier, Y., Grienberger, J.M., Bonnard, G., and Meyer, Y. (2001). Identification and characterization of a mitochondrial thioredoxin system in plants. *Proceedings of the National Academy of Sciences* 98.

Lange, H., Lisowsky, T., Gerber, J., Mühlenhoff, U., Kispal, G., and Lill, R. (2001). An essential function of the mitochondrial sulfhydryl oxidase Erv1p/ALR in the maturation of cytosolic Fe/S proteins. *EMBO Reports*. 2.

Lee, K.O., Lee, J.R., Yoo, J.Y., Jang, H.H., Moon, J.C., Jung, B.G., Chi, Y.H., Park, S.K., Lee, S.S., Lim, C.O., et al. (2002). GSH-dependent peroxidase activity of the rice (*Oryza sativa*) glutaredoxin, a thioltransferase. *Biochemical and Biophysical Research Communications* 296.

Lemaire, S.D., Michelet, L., Zaffagnini, M., Massot, V., and Issakidis-Bourguet, E. (2007). Thioredoxins in chloroplasts. *Current Genetics* 51.

Lennartz, K., Plücken, H., Seidler, A., Westhoff, P., Bechtold, N., and Meierhoff, K. (2001). *HCF164* Encodes a Thioredoxin-Like Protein Involved in the Biogenesis of the Cytochrome *b* ₆*f* Complex in Arabidopsis. *The Plant Cell* 13.

Levitán, A., Danon, A., and Lisowsky, T. (2004). Unique Features of Plant Mitochondrial Sulphydryl Oxidase. *Journal of Biological Chemistry* 279.

Lillig, C.H., Berndt, C., Vergnolle, O., Lonn, M.E., Hudemann, C., Bill, E., and Holmgren, A. (2005). Characterization of human glutaredoxin 2 as iron-sulfur protein: A possible role as redox sensor. *Proceedings of the National Academy of Sciences* 102.

Lisenbee, C.S., Heinze, M., and Trelease, R.N. (2003). Peroxisomal Ascorbate Peroxidase Resides within a Subdomain of Rough Endoplasmic Reticulum in Wild-Type Arabidopsis Cells. *Plant Physiology* 132.

Liu, J.-X., Srivastava, R., Che, P., and Howell, S.H. (2007a). An Endoplasmic Reticulum Stress Response in *Arabidopsis* Is Mediated by Proteolytic Processing and Nuclear Relocation of a Membrane-Associated Transcription Factor, bZIP28. *The Plant Cell* 19.

Liu, J.-X., Srivastava, R., Che, P., and Howell, S.H. (2007b). Salt stress responses in Arabidopsis utilize a signal transduction pathway related to endoplasmic reticulum stress signaling: Salt stress elicits ER stress response. *The Plant Journal* 51.

Liu, X., Liu, S., Feng, Y., Liu, J.-Z., Chen, Y., Pham, K., Deng, H., Hirschi, K.D., Wang, X., and Cheng, N. (2013). Structural insights into the N-terminal GIY–YIG endonuclease activity of *Arabidopsis* glutaredoxin AtGRXS16 in chloroplasts. *Proceedings of the National Academy of Sciences* 110.

Longen, S., Bien, M., Bihlmaier, K., Kloepfel, C., Kauff, F., Hammermeister, M., Westermann, B., Herrmann, J.M., and Riemer, J. (2009). Systematic Analysis of the Twin Cx9C Protein Family. *Journal of Molecular Biology* 393.

Lu, Y., Wang, H.-R., Li, H., Cui, H.-R., Feng, Y.-G., and Wang, X.-Y. (2013). A chloroplast membrane protein LTO1/AtVKOR involving in redox regulation and ROS homeostasis. *Plant Cell Reports* 32.

Lu, Y., Du, J.-J., Yu, Z.-B., Peng, J.-J., Xu, J.-N., and Wang, X.-Y. (2015). Identification of Potential Targets for Thylakoid Oxidoreductase AtVKOR/LTO1 in Chloroplasts. *Protein & Peptide Letters* 22.

Luong, T.T., Reardon-Robinson, M.E., Siegel, S.D., and Ton-That, H. (2017). Reoxidation of the Thiol-Disulfide Oxidoreductase MdbA by a Bacterial Vitamin K Epoxide Reductase in the Biofilm-Forming Actinobacterium *Actinomyces oris*. *Journal of Bacteriology* 199.

Lüthje, S., Möller, B., Perrineau, F.C., and Wöltje, K. (2013). Plasma Membrane Electron Pathways and Oxidative Stress. *Antioxidants & Redox Signaling* 18.

Ma, Y., Brewer, J.W., Alan Diehl, J., and Hendershot, L.M. (2002). Two Distinct Stress Signaling Pathways Converge Upon the CHOP Promoter During the Mammalian Unfolded Protein Response. *Journal of Molecular Biology* 318.

Malhotra, J.D., and Kaufman, R.J. (2007). The endoplasmic reticulum and the unfolded protein response. *Seminars in Cell & Developmental Biology* 18.

Marri, L., Zaffagnini, M., Collin, V., Issakidis-Bourguet, E., Lemaire, S.D., Pupillo, P., Sparla, F., Miginiac-Maslow, M., and Trost, P. (2009). Prompt and Easy Activation by Specific Thioredoxins of Calvin Cycle Enzymes of *Arabidopsis thaliana* Associated in the GAPDH/CP12/PRK Supramolecular Complex. *Molecular Plant* 2.

Matusaki, M., Okuda, A., Masuda, T., Koishihara, K., Mita, R., Iwasaki, K., Hara, K., Naruo, Y., Hirose, A., Tsuchi, Y., et al. (2016). Cooperative Protein Folding by Two Protein Thiol Disulfide Oxidoreductases and ERO1 in Soybean. *Plant Physiology* 170.

Maughan, S.C., Pasternak, M., Cairns, N., Kiddle, G., Brach, T., Jarvis, R., Haas, F., Nieuwland, J., Lim, B., Muller, C., et al. (2010). Plant homologs of the *Plasmodium falciparum* chloroquine-resistance transporter, PfCRT, are required for glutathione homeostasis and stress responses. *Proceedings of the National Academy of Sciences* 107.

May, M.J., Hammond-Kosack, K.E., and Jones, Jdg. (1996). Involvement of Reactive Oxygen Species, Glutathione Metabolism, and Lipid Peroxidation in the Cf-Gene-Dependent Defense Response of Tomato Cotyledons Induced by Race-Specific Elicitors of *Cladosporium fulvum*. *Plant Physiology* 110.

Mesecke, N., Terziyska, N., Kozany, C., Baumann, F., Neupert, W., Hell, K., and Herrmann, J.M. (2005). A disulfide relay system in the intermembrane space of mitochondria that mediates protein import. *Cell* 121.

Mesecke, N., Bihlmaier, K., Grumblt, B., Longen, S., Terziyska, N., Hell, K., and Herrmann, J.M. (2008). The zinc-binding protein Hot13 promotes oxidation of the mitochondrial import receptor Mia40. *EMBO Reports* 9.

Meunier, L., Usherwood, Y.-K., Chung, K.T., and Hendershot, L.M. (2002). A Subset of Chaperones and Folding Enzymes Form Multiprotein Complexes in Endoplasmic Reticulum to Bind Nascent Proteins. *Molecular Biology of the Cell* 13.

Meyer, A.J., Riemer, J., and Rouhier, N. (2019). Oxidative protein folding: state-of-the-art and current avenues of research in plants. *New Phytologist* 221.

Meyer, E.H., Giege, P., Gelhaye, E., Rayapuram, N., Ahuja, U., Thony-Meyer, L., Grienberger, J.-M., and Bonnard, G. (2005). AtCCMH, an essential component of the c-type cytochrome maturation pathway in *Arabidopsis* mitochondria, interacts with apocytochrome c. *Proceedings of the National Academy of Sciences* 102.

Mhamdi, A., Queval, G., Chaouch, S., Vanderauwera, S., Van Breusegem, F., and Noctor, G. (2010). Catalase function in plants: a focus on *Arabidopsis* mutants as stress-mimic models. *Journal of Experimental Botany* 61.

Michelet, L., Zaffagnini, M., Vanacker, H., Le Maréchal, P., Marchand, C., Schroda, M., Lemaire, S.D., and Decottignies, P. (2008). In vivo targets of S-thiolation in *Chlamydomonas reinhardtii*. *Journal of Biological Chemistry* 283.

Michelet, L., Zaffagnini, M., Morisse, S., Sparla, F., Pérez-Pérez, M.E., Francia, F., Danon, A., Marchand, C.H., Fermani, S., Trost, P., et al. (2013). Redox regulation of the Calvin–Benson cycle: something old, something new. *Frontiers in Plant Science* 4.

Milenkovic, D., Ramming, T., Müller, J.M., Wenz, L.-S., Gebert, N., Schulze-Specking, A., Stojanovski, D., Rospert, S., and Chacinska, A. (2009). Identification of the Signal Directing Tim9 and Tim10 into the Intermembrane Space of Mitochondria. *Molecular Biology of the Cell* 20.

Mishanina, T.V., Libiad, M., and Banerjee, R. (2015). Biogenesis of reactive sulfur species for signaling by hydrogen sulfide oxidation pathways. *Nature Chemical Biology* 11.

Mittler, R., Vanderauwera, S., Gollery, M., and Van Breusegem, F. (2004). Reactive oxygen gene network of plants. *Trends in Plant Science* 9.

Morgenstern, M., Stiller, S.B., Lübbert, P., Peikert, C.D., Dannenmaier, S., Drepper, F., Weill, U., Höß, P., Feuerstein, R., Gebert, M., et al. (2017). Definition of a High-Confidence Mitochondrial Proteome at Quantitative Scale. *Cell Reports* 19.

Morisse, S., Zaffagnini, M., Gao, X.-H., Lemaire, S.D., and Marchand, C.H. (2014). Insight into Protein S-nitrosylation in *Chlamydomonas reinhardtii*. *Antioxidants & Redox Signaling* 21.

Moseler, A., Aller, I., Wagner, S., Nietzel, T., Przybyla-Toscano, J., Mühlenhoff, U., Lill, R., Berndt, C., Rouhier, N., Schwarzsäcker, M., et al. (2015). The mitochondrial monothiol glutaredoxin S15 is essential for iron-sulfur protein maturation in *Arabidopsis thaliana*. *Proceedings of the National Academy of Sciences* 112.

Motohashi, K., and Hisabori, T. (2006). HCF164 Receives Reducing Equivalents from Stromal Thioredoxin across the Thylakoid Membrane and Mediates Reduction of Target Proteins in the Thylakoid Lumen. *Journal of Biological Chemistry* 281.

Motohashi, K., and Hisabori, T. (2010). CcdA Is a Thylakoid Membrane Protein Required for the Transfer of Reducing Equivalents from Stroma to Thylakoid Lumen in the Higher Plant Chloroplast. *Antioxidants & Redox Signaling* 13.

Motohashi, K., Romano, P.G.N., and Hisabori, T. (2009). Identification of Thioredoxin Targeted Proteins Using Thioredoxin Single-Cysteine Mutant-Immobilized Resin., *Methods in Molecular Biology: Plant Signal Transduction* 479.

Mueller, S.J., Hoernstein, S.N.W., and Reski, R. (2017). The mitochondrial proteome of the moss *Physcomitrella patens*. *Mitochondrion* 33.

Mullen, R.T., Lisenbee, C.S., Miernyk, J.A., and Trelease, R.N. (1999). Peroxisomal Membrane Ascorbate Peroxidase Is Sorted to a Membranous Network That Resembles a Subdomain of the Endoplasmic Reticulum. *The Plant Cell* 11.

Navrot, N., Gelhaye, E., Jacquot, J.-P., and Rouhier, N. (2006). Identification of a new family of plant proteins loosely related to glutaredoxins with four CxxC motives. *Photosynthesis Research* 89.

Neal, S.E., Dabir, D.V., Wijaya, J., Boon, C., and Koehler, C.M. (2017). Osm1 facilitates the transfer of electrons from Erv1 to fumarate in the redox-regulated import pathway in the mitochondrial intermembrane space. *Molecular Biology of the Cell* 28.

Neupert, W., and Herrmann, J.M. (2007). Translocation of proteins into mitochondria. *Annual Review Biochemistry*. 76.

Nicholson, D.W., Köhler, H., and Neupert, W. (1987). Import of cytochrome c into mitochondria. Cytochrome c heme lyase. *European Journal of Biochemistry* 164.

Nikolovski, N., Rubtsov, D., Segura, M.P., Miles, G.P., Stevens, T.J., Dunkley, T.P.J., Munro, S., Lilley, K.S., and Dupree, P. (2012). Putative Glycosyltransferases and Other Plant Golgi Apparatus Proteins Are Revealed by LOPIT Proteomics. *Plant Physiology* 160.

Noctor, G. (2002). Drought and Oxidative Load in the Leaves of C3 Plants: a Predominant Role for Photorespiration ? *Annals of Botany* 89.

Noctor, G., Mhamdi, A., Chaouch, S., Han, Y., Neukermans, J., Marquez-Garcia, B., Queval, G., and Foyer, C.H. (2012). Glutathione in plants: an integrated overview: Glutathione status and functions. *Plant, Cell & Environment* 35.

Noctor, G., Mhamdi, A., and Foyer, C.H. (2014). The Roles of Reactive Oxygen Metabolism in Drought: Not So Cut and Dried. *Plant Physiology* 164.

Noctor, G., Reichheld, J.-P., and Foyer, C.H. (2018). ROS-related redox regulation and signaling in plants. *Seminars in Cell & Developmental Biology* 80.

Noguchi, T., Fujioka, S., Choe, S., Takatsuto, S., Yoshida, S., Yuan, H., Feldmann, K.A., and Tax, F.E. (1999). Brassinosteroid-Insensitive Dwarf Mutants of *Arabidopsis* Accumulate Brassinosteroids. *Plant Physiology* 121.

Okuda, A., Matsusaki, M., Higashino, Y., Masuda, T., and Urade, R. (2014). Disulfide bond formation activity of soybean quiescin sulfhydryl oxidase. *FEBS Journal* 281.

Onda, Y., Kumamaru, T., and Kawagoe, Y. (2009). ER membrane-localized oxidoreductase Ero1 is required for disulfide bond formation in the rice endosperm. *Proceedings of the National Academy of Sciences* 106.

Onda, Y., Nagamine, A., Sakurai, M., Kumamaru, T., Ogawa, M., and Kawagoe, Y. (2011). Distinct roles of protein disulfide isomerase and P5 sulfhydryl oxidoreductases in multiple pathways for oxidation of structurally diverse storage proteins in rice. *Plant Cell* 23.

Orman-Ligeza, B., Parizot, B., de Rycke, R., Fernandez, A., Himschoot, E., Van Breusegem, F., Bennett, M.J., Périlleux, C., Beeckman, T., and Draye, X. (2016). RBOH-mediated ROS production facilitates lateral root emergence in *Arabidopsis*. *Development* 143.

Østergaard, H., Tachibana, C., and Winther, J.R. (2004). Monitoring disulfide bond formation in the eukaryotic cytosol. *The Journal of Cell Biology* 166.

Ozer, H.K., Dlouhy, A.C., Thornton, J.D., Hu, J., Liu, Y., Barycki, J.J., Balk, J., and Outten, C.E. (2015). Cytosolic Fe-S Cluster Protein Maturation and Iron Regulation Are Independent of the Mitochondrial Erv1/Mia40 Import System. *Journal of Biological Chemistry* 290.

Page, M.L.D., Hamel, P.P., Gabilly, S.T., Zegzouti, H., Pereira, J.V., Alonso, J.M., Ecker, J.R., Theg, S.M., Christensen, S.K., and Merchant, S. (2004). A Homolog of Prokaryotic Thiol Disulfide Transporter CcdA Is Required for the Assembly of the Cytochrome *b*₆*f* Complex in *Arabidopsis* Chloroplasts. *Journal of Biological Chemistry* 279.

Pandey, S., Fartyal, D., Agarwal, A., Shukla, T., James, D., Kaul, T., Negi, Y.K., Arora, S., and Reddy, M.K. (2017). Abiotic Stress Tolerance in Plants: Myriad Roles of Ascorbate Peroxidase. *Frontiers in Plant Science* 8.

Pattison, D.I., Rahmanto, A.S., and Davies, M.J. (2012). Photo-oxidation of proteins. *Photochemical & Photobiological Sciences*. 11.

Paulsen, C.E., and Carroll, K.S. (2013). Cysteine-Mediated Redox Signaling: Chemistry, Biology, and Tools for Discovery. *Chemical Reviews* 113.

Peleh, V., Cordat, E., and Herrmann, J.M. (2016). Mia40 is a trans-site receptor that drives protein import into the mitochondrial intermembrane space by hydrophobic substrate binding. *Elife* 5.

Peleh, V., Zannini, F., Backes, S., Rouhier, N., and Herrmann, J.M. (2017). Erv1 of *Arabidopsis thaliana* can directly oxidize mitochondrial intermembrane space proteins in the absence of redox-active Mia40. *BMC Biology* 15.

Peng, R.-H., Qiu, J., Tian, Y.-S., Gao, J., Han, H., Fu, X.-Y., Zhu, B., Xu, J., Wang, B., Li, Z., et al. (2017). Disulfide isomerase-like protein AtPDIL1–2 is a good candidate for trichlorophenol phytodetoxification. *Scientific Reports* 7.

Peralta, F., and Huidobro-Toro, J. (2016). Zinc as Allosteric Ion Channel Modulator: Ionotropic Receptors as Metalloproteins. *International Journal of Molecular Sciences* 17.

Pinnola, A., and Bassi, R. (2018). Molecular mechanisms involved in plant photoprotection. *Biochemical Society Transactions* 46.

Pollard, M.G., Travers, K.J., and Weissman, J.S. (1998). Ero1p: A Novel and Ubiquitous Protein with an Essential Role in Oxidative Protein Folding in the Endoplasmic Reticulum. *Molecular Cell* 1.

Pucciariello, C., and Perata, P. (2017). New insights into reactive oxygen species and nitric oxide signalling under low oxygen in plants. *Plant, Cell & Environment* 40.

Qiu, X.-B., Shao, Y.-M., Miao, S., and Wang, L. (2006). The diversity of the DnaJ/Hsp40 family, the crucial partners for Hsp70 chaperones. *Cellular and Molecular Life Sciences* 63.

Queval, G., Jaillard, D., Zechmann, B., and Noctor, G. (2011). Increased intracellular H₂O₂ availability preferentially drives glutathione accumulation in vacuoles and chloroplasts: Oxidative stress and glutathione compartmentation. *Plant, Cell & Environment* 34.

Ramming, T., and Appenzeller-Herzog, C. (2013). Destroy and exploit: catalyzed removal of hydroperoxides from the endoplasmic reticulum. *International Journal of Cell Biology* 2013.

Ramming, T., Hansen, H.G., Nagata, K., Ellgaard, L., and Appenzeller-Herzog, C. (2014). GPx8 peroxidase prevents leakage of H₂O₂ from the endoplasmic reticulum. *Free Radical Biology and Medicine* 70.

Rayapuram, N., Hagenmuller, J., Grienberger, J.M., Bonnard, G., and Giegé, P. (2008). The Three Mitochondrial Encoded CcmF Proteins Form a Complex That Interacts with CCMH and *c*-Type Apocytochromes in *Arabidopsis*. *Journal of Biological Chemistry* 283.

Reardon-Robinson, M.E., and Ton-That, H. (2016). Disulfide-Bond-Forming Pathways in Gram-Positive Bacteria. *Journal of Bacteriology* 198.

Reinholdt, O., Schwab, S., Zhang, Y., Reichheld, J.-P., Fernie, A.R., Hagemann, M., and Timm, S. (2019). Redox-Regulation of Photorespiration through Mitochondrial Thioredoxin o1. *Plant Physiology* 181.

Remelli, W., Santabarbara, S., Carbonera, D., Bonomi, F., Ceriotti, A., and Casazza, A.P. (2017). Iron Binding Properties of Recombinant Class A Protein Disulfide Isomerase from *Arabidopsis thaliana*. *Biochemistry* 56.

Rey, P., and Tarrago, L. (2018). Physiological Roles of Plant Methionine Sulfoxide Reductases in Redox Homeostasis and Signaling. *Antioxidants* 7.

Rey, P., Becuwe, N., Tourrette, S., and Rouhier, N. (2017). Involvement of *Arabidopsis* glutaredoxin S14 in the maintenance of chlorophyll content. *Plant, Cell & Environment* 40.

Richard-Fogal, C.L., Frawley, E.R., Bonner, E.R., Zhu, H., San Francisco, B., and Kranz, R.G. (2009). A conserved haem redox and trafficking pathway for cofactor attachment. *The EMBO Journal* 28.

Riemer, J., Bulleid, N., and Herrmann, J.M. (2009). Disulfide formation in the ER and mitochondria: two solutions to a common process. *Science* 324.

Riemer, J., Fischer, M., and Herrmann, J.M. (2011). Oxidation-driven protein import into mitochondria: Insights and blind spots. *Biochimica et Biophysica Acta (BBA) - Biomembranes* 1808.

Riemer, J., Schwarzländer, M., Conrad, M., and Herrmann, J.M. (2015). Thiol switches in mitochondria: operation and physiological relevance. *Biological Chemistry* 396.

Rouhier, N. (2010). Plant glutaredoxins: pivotal players in redox biology and iron-sulphur centre assembly. *New Phytologist*. 186.

Rouhier, N., and Jacquot, J.-P. (2005). The plant multigenic family of thiol peroxidases☆. *Free Radical Biology and Medicine* 38.

Rouhier, N., Gelhaye, E., Sautiere, P.E., Brun, A., Laurent, P., Tagu, D., Gerard, J., de Faÿ, E., Meyer, Y., and Jacquot, J.P. (2001). Isolation and characterization of a new peroxiredoxin from poplar sieve tubes that uses either glutaredoxin or thioredoxin as a proton donor. *Plant Physiology*. 127.

Rouhier, N., Gelhaye, E., and Jacquot, J.-P. (2002). Redox Control by Dithiol-Disulfide Exchange in Plants. *Annals of the New York Academy of Sciences* 973.

Rouhier, N., Unno, H., Bandyopadhyay, S., Masip, L., Kim, S.-K., Hirasawa, M., Gualberto, J.M., Lattard, V., Kusunoki, M., Knaff, D.B., et al. (2007). Functional, structural, and spectroscopic characterization of a glutathione-ligated [2Fe-2S] cluster in poplar glutaredoxin C1. *Proceedings of the National Academy of Sciences*. 104.

Rouhier, N., Lemaire, S.D., and Jacquot, J.-P. (2008). The Role of Glutathione in Photosynthetic Organisms: Emerging Functions for Glutaredoxins and Glutathionylation. *Annual Review of Plant Biology* 59.

Rouhier, N., Cerveau, D., Couturier, J., Reichheld, J.-P., and Rey, P. (2015). Involvement of thiol-based mechanisms in plant development. *Biochimica et Biophysica Acta (BBA) - General Subjects* 1850.

Ruban, A.V. (2016). Nonphotochemical Chlorophyll Fluorescence Quenching: Mechanism and Effectiveness in Protecting Plants from Photodamage. *Plant Physiology* 170.

Salmeen, A., Andersen, J.N., Myers, M.P., Meng, T.-C., Hinks, J.A., Tonks, N.K., and Barford, D. (2003). Redox regulation of protein tyrosine phosphatase 1B involves a sulphenyl-amide intermediate. *Nature* 423.

Schafer, F.Q., and Buettner, G.R. (2001). Redox environment of the cell as viewed through the redox state of the glutathione disulfide/glutathione couple. *Free Radical Biology and Medicine* 30.

Schnaubelt, D., Queval, G., Dong, Y., Diaz-Vivancos, P., Makgopa, M.E., Howell, G., De Simone, A., Bai, J., Hannah, M.A., and Foyer, C.H. (2015). Low glutathione regulates gene expression and the redox potentials of the nucleus and cytosol in *Arabidopsis thaliana*: Glutathione-dependent gene expression. *Plant, Cell & Environment* 38.

Schulman, S., Wang, B., Li, W., and Rapoport, T.A. (2010). Vitamin K epoxide reductase prefers ER membrane-anchored thioredoxin-like redox partners. *Proceedings of the National Academy of Sciences*. 107.

Schürmann, P., and Buchanan, B.B. (2008). The Ferredoxin/Thioredoxin System of Oxygenic Photosynthesis. *Antioxidants & Redox Signaling* 10.

Schwarzländer, M., and Fuchs, P. (2019). Keeping Mitochondrial Alternative Oxidase Reduced and Active In Vivo Does Not Require Thioredoxin o1. *Plant and Cell Physiology*.

Schwarzländer, M., Fricker, M.D., Müller, C., Marty, L., Brach, T., Novak, J., Sweetlove, L.J., Hell, R., and Meyer, A.J. (2008). Confocal imaging of glutathione redox potential in living plant cells. *Journal of Microscopy* 231.

Segatori, L., Murphy, L., Arredondo, S., Kadokura, H., Gilbert, H., Beckwith, J., and Georgiou, G. (2006). Conserved Role of the Linker α -Helix of the Bacterial Disulfide Isomerase DsbC in the Avoidance of Misoxidation by DsbB. *Journal of Biological Chemistry* 281.

Selles, B., Jacquot, J.-P., and Rouhier, N. (2011). Comparative genomic study of protein disulfide isomerases from photosynthetic organisms. *Genomics* 97.

Selles, B., Zannini, F., Couturier, J., Jacquot, J.-P., and Rouhier, N. (2017). Atypical protein disulfide isomerases (PDI): Comparison of the molecular and catalytic properties of poplar PDI-A and PDI-M with PDI-L1A. *PLoS ONE* 12.

Sevier, C.S., Qu, H., Heldman, N., Gross, E., Fass, D., and Kaiser, C.A. (2007). Modulation of Cellular Disulfide-Bond Formation and the ER Redox Environment by Feedback Regulation of Ero1. *Cell* 129.

Shigeoka, S., Ishikawa, T., Tamoi, M., Miyagawa, Y., Takeda, T., Yabuta, Y., and Yoshimura, K. (2002). Regulation and function of ascorbate peroxidase isoenzymes. *Journal of Experimental Botany*. 53.

Shimizu, Y., and Hendershot, L.M. (2007). Organization of the Functions and Components of the Endoplasmic Reticulum. Advances in Experimental Medicine and Biology: In Molecular Aspects of the Stress Response: Chaperones, Membranes and Networks 594.

Sideris, D.P., Petrakis, N., Katrakili, N., Mikropoulou, D., Gallo, A., Ciofi-Baffoni, S., Banci, L., Bertini, I., and Tokatlidis, K. (2009). A novel intermembrane space–targeting signal docks cysteines onto Mia40 during mitochondrial oxidative folding. *The Journal of Cell Biology* 187.

Sidrauski, C., and Walter, P. (1997). The Transmembrane Kinase Ire1p Is a Site-Specific Endonuclease That Initiates mRNA Splicing in the Unfolded Protein Response. *Cell* 90.

Smirnoff, N., and Arnaud, D. (2019). Hydrogen peroxide metabolism and functions in plants. *New Phytologist* 221.

Sparla, F., Zaffagnini, M., Wedel, N., Scheibe, R., Pupillo, P., and Trost, P. (2005). Regulation of Photosynthetic GAPDH Dissected by Mutants. *Plant Physiology* 138.

Specht, S., Liedgens, L., Duarte, M., Stiegler, A., Wirth, U., Eberhardt, M., Tomás, A., Hell, K., and Deponte, M. (2018). A single-cysteine mutant and chimeras of essential Leishmania Erv can complement the loss of Erv1 but not of Mia40 in yeast. *Redox Biology* 15.

Spiller, M.P., Ang, S.K., Ceh-Pavia, E., Fisher, K., Wang, Q., Rigby, S.E.J., and Lu, H. (2013). Identification and characterization of mitochondrial Mia40 as an iron-sulfur protein. *Biochem. J.* 455.

Stewart, E.J. (1999). Six conserved cysteines of the membrane protein DsbD are required for the transfer of electrons from the cytoplasm to the periplasm of *Escherichia coli*. *The EMBO Journal* 18.

Strasser, R. (2018). Protein Quality Control in the Endoplasmic Reticulum of Plants. *Annual Review of Plant Biology* 69.

Ströher, E., Grassl, J., Carrie, C., Fenske, R., Whelan, J., and Millar, A.H. (2016). Glutaredoxin S15 Is Involved in Fe-S Cluster Transfer in Mitochondria Influencing Lipoic Acid-Dependent Enzymes, Plant Growth, and Arsenic Tolerance in *Arabidopsis*. *Plant Physiology* 170.

Sylvestre-Gonon, E., Law, S.R., Schwartz, M., Robe, K., Keech, O., Didierjean, C., Dubos, C., Rouhier, N., and Hecker, A. (2019). Functional, Structural and Biochemical Features of Plant Serinyl-Glutathione Transferases. *Frontiers in Plant Science* 10.

Tavender, T.J., Sheppard, A.M., and Bulleid, N.J. (2008). Peroxiredoxin IV is an endoplasmic reticulum-localized enzyme forming oligomeric complexes in human cells. *Biochemical Journal*. 411.

Terziyska, N., Lutz, T., Kozany, C., Mokranjac, D., Mesecke, N., Neupert, W., Herrmann, J.M., and Hell, K. (2005). Mia40, a novel factor for protein import into the intermembrane space of mitochondria is able to bind metal ions. *FEBS Letters* 579.

Tien, A.-C., Rajan, A., Schulze, K.L., Ryoo, H.D., Acar, M., Steller, H., and Bellen, H.J. (2008). Ero1L, a thiol oxidase, is required for Notch signaling through cysteine bridge formation of the Lin12-Notch repeats in *Drosophila melanogaster*. *The Journal of Cell Biology* 182.

Travaglini-Alcocatelli, C. (2013). Protein Machineries Involved in the Attachment of Heme to Cytochrome c: Protein Structures and Molecular Mechanisms. *Scientifica* 2013.

Travers, K.J., Patil, C.K., Wodicka, L., Lockhart, D.J., Weissman, J.S., and Walter, P. (2000). Functional and Genomic Analyses Reveal an Essential Coordination between the Unfolded Protein Response and ER-Associated Degradation. *Cell* 101.

Trost, P., Fermani, S., Calvaresi, M., and Zaffagnini, M. (2017). Biochemical basis of sulphenomics: how protein sulphenic acids may be stabilized by the protein microenvironment. *Plant, Cell & Environment* 40.

Tsukagoshi, H., Busch, W., and Benfey, P.N. (2010). Transcriptional Regulation of ROS Controls Transition from Proliferation to Differentiation in the Root. *Cell* 143.

Uhrig, R.G., Labandera, A.-M., Tang, L.-Y., Sieben, N.A., Goudreault, M., Yeung, E., Gingras, A.-C., Samuel, M.A., and Moorhead, G.B.G. (2017). Activation of Mitochondrial Protein Phosphatase SLP2 by MIA40 Regulates Seed Germination. *Plant Physiology* 173.

Urade, R. (2019). Oxidative protein folding in the plant endoplasmic reticulum. *Bioscience, Biotechnology, and Biochemistry* 83.

Verissimo, A.F., Khalfaoui-Hassani, B., Hwang, J., Steimle, S., Selamoglu, N., Sanders, C., Khatchikian, C.E., and Daldal, F. (2017). The thio reduction component CcmG confers efficiency and the heme ligation component CcmH ensures stereo-specificity during cytochrome *c* maturation. *Journal of Biological Chemistry* 292.

Vernoux, T., Wilson, R.C., Seeley, K.A., Reichheld, J.-P., Muroy, S., Brown, S., Maughan, S.C., Cobbett, C.S., Van Montagu, M., Inzé, D., et al. (2000). *The root meristemlesse 1/cadmium sensitive 2* Gene Defines a Glutathione-Dependent Pathway Involved in Initiation and Maintenance of Cell Division during Postembryonic Root Development. *The Plant Cell* 12.

Vitu, E., Bentzur, M., Lisowsky, T., Kaiser, C.A., and Fass, D. (2006). Gain of Function in an ERV/ALR Sulphydryl Oxidase by Molecular Engineering of the Shuttle Disulfide. *Journal of Molecular Biology* 362.

Vögtle, F.-N., Burkhardt, J.M., Rao, S., Gerbeth, C., Hinrichs, J., Martinou, J.-C., Chacinska, A., Sickmann, A., Zahedi, R.P., and Meisinger, C. (2012). Intermembrane Space Proteome of Yeast Mitochondria. *Molecular & Cellular Proteomics* 11.

Wadahama, H., Kamauchi, S., Ishimoto, M., Kawada, T., and Urade, R. (2007). Protein disulfide isomerase family proteins involved in soybean protein biogenesis. *FEBS Journal*. 274.

Wan, S., and Jiang, L. (2016). Endoplasmic reticulum (ER) stress and the unfolded protein response (UPR) in plants. *Protoplasma* 253.

Wang, H., Boavida, L.C., Ron, M., and McCormick, S. (2008). Truncation of a Protein Disulfide Isomerase, PDIL2-1, Delays Embryo Sac Maturation and Disrupts Pollen Tube Guidance in *Arabidopsis thaliana*. *The Plant Cell* 20.

Winterbourn, C.C., and Hampton, M.B. (2008). Thiol chemistry and specificity in redox signaling. *Free Radical Biology and Medicine* 45.

Wu, J., and Kaufman, R.J. (2006). From acute ER stress to physiological roles of the Unfolded Protein Response. *Cell Death & Differentiation* 13.

Xia, K., Zeng, X., Jiao, Z., Li, M., Xu, W., Nong, Q., Mo, H., Cheng, T., and Zhang, M. (2018). Formation of Protein Disulfide Bonds Catalyzed by OsPDIL1;1 is Mediated by MicroRNA5144-3p in Rice. *Plant and Cell Physiology* 59.

Xiang, C., Werner, B.L., Christensen, E.M., and Oliver, D.J. (2001). The Biological Functions of Glutathione Revisited in *Arabidopsis* Transgenic Plants with Altered Glutathione Levels. *Plant Physiology* 126.

Yagi-Utsumi, M., Satoh, T., and Kato, K. (2015). Structural basis of redox-dependent substrate binding of protein disulfide isomerase. *Scientific Reports* 5.

Yoshida, K., and Hisabori, T. (2016). Two distinct redox cascades cooperatively regulate chloroplast functions and sustain plant viability. *Proceedings of the National Academy of Sciences* 113.

Yoshida, H., Matsui, T., Yamamoto, A., Okada, T., and Mori, K. (2001). XBP1 mRNA Is Induced by ATF6 and Spliced by IRE1 in Response to ER Stress to Produce a Highly Active Transcription Factor. *Cell* 107.

Yoshida, K., Noguchi, K., Motohashi, K., and Hisabori, T. (2013). Systematic exploration of thioredoxin target proteins in plant mitochondria. *Plant Cell Physiol.* 54.

Yu, Z.-B., Lu, Y., Du, J.-J., Peng, J.-J., and Wang, X.-Y. (2014). The chloroplast protein LTO1/AtVKOR is involved in the xanthophyll cycle and the acceleration of D1 protein degradation. *Journal of Photochemistry and Photobiology : Biology* 130.

Zaffagnini, M., Michelet, L., Marchand, C., Sparla, F., Decottignies, P., Le Maréchal, P., Miginiac-Maslow, M., Noctor, G., Trost, P., and Lemaire, S.D. (2007). The thioredoxin-independent isoform of chloroplastic glyceraldehyde-3-phosphate dehydrogenase is selectively regulated by glutathionylation: Glutathionylation of chloroplastic GAPDH. *FEBS Journal* 274.

Zaffagnini, M., Michelet, L., Massot, V., Trost, P., and Lemaire, S.D. (2008). Biochemical Characterization of Glutaredoxins from *Chlamydomonas reinhardtii* Reveals the Unique Properties of a Chloroplastic CGFS-type Glutaredoxin. *Journal of Biological Chemistry* 283.

Zaffagnini, M., Bedhomme, M., Marchand, C.H., Couturier, J., Gao, X.-H., Rouhier, N., Trost, P., and Lemaire, S.D. (2012). Glutaredoxin S12: Unique Properties for Redox Signaling. *Antioxidants & Redox Signaling* 16.

Zaffagnini, M., De Mia, M., Morisse, S., Di Giacinto, N., Marchand, C.H., Maes, A., Lemaire, S.D., and Trost, P. (2016). Protein S-nitrosylation in photosynthetic organisms: A comprehensive overview with future perspectives. *Biochimica et Biophysica Acta (BBA) - Proteins and Proteomics* *1864*.

Zaffagnini, M., Fermani, S., Marchand, C.H., Costa, A., Sparla, F., Rouhier, N., Geigenberger, P., Lemaire, S.D., and Trost, P. (2019). Redox Homeostasis in Photosynthetic Organisms: Novel and Established Thiol-Based Molecular Mechanisms. *Antioxidants & Redox Signaling* *31*.

Zanetti, G., Pahuja, K.B., Studer, S., Shim, S., and Schekman, R. (2012). COPII and the regulation of protein sorting in mammals. *Nature Cell Biology* *14*.

Zhang, H., and Krämer, U. (2018). Differential Diel Translation of Transcripts With Roles in the Transfer and Utilization of Iron-Sulfur Clusters in *Arabidopsis*. *Frontiers in Plant Science* *9*.

Zhang, L., Niu, Y., Zhu, L., Fang, J., Wang, X., Wang, L., and Wang, C. (2014). Different Interaction Modes for Protein-disulfide Isomerase (PDI) as an Efficient Regulator and a Specific Substrate of Endoplasmic Reticulum Oxidoreductin-1 α (Ero1 α). *Journal of Biological Chemistry* *289*.

Zheng, C., Guo, S., Tennant, W.G., Pradhan, P.K., Black, K.A., and Dos Santos, P.C. (2019). The Thioredoxin System Reduces Protein Persulfide Intermediates Formed during the Synthesis of Thio-Cofactors in *Bacillus subtilis*. *Biochemistry* *58*.

Zito, E. (2013). PRDX4, an endoplasmic reticulum-localized peroxiredoxin at the crossroads between enzymatic oxidative protein folding and nonenzymatic protein oxidation. *Antioxidants & Redox Signaling* *18*.

Zito, E., Melo, E.P., Yang, Y., Wahlander, Å., Neubert, T.A., and Ron, D. (2010). Oxidative Protein Folding by an Endoplasmic Reticulum-Localized Peroxiredoxin. *Molecular Cell* *40*.

Résumé : La présence de cystéines réactives confère à de nombreuses protéines des propriétés redox et/ou la capacité à lier des ions métalliques. Ce projet, organisé en plusieurs axes, visait à caractériser des protéines possédant un motif CxxC conservé et éventuellement un repliement de type thiorédoxine (TRX) chez les plantes. Il s'avère que les TRX o1 et o2 mitochondrielles, la protéine disulfure isomérase atypique PDI-A et la glutarédoxine (GRX) S16 chloroplastique d'*A. thaliana* exprimées sous formes recombinantes dans *Escherichia coli* incorporent toutes un centre Fe-S au sein d'homodimères dont la fonction reste à déterminer. L'analyse des propriétés redox des apo-protéines indiquent que la PDI-A et la GRXS16 ne possèdent pas ou peu d'activité oxydoréductase respectivement bien que des ponts disulfure intramoléculaires soient formés entre cystéines conservées. Dans le cas de la GRXS16, la régulation de son état redox se ferait *via* la lumière puisque le pont disulfure est réductible par des TRX mais pas par le glutathion. Le dernier axe de recherche concernait l'étude des propriétés de l'oxydoréductase MIA40 et de la flavine oxydase ERV1, impliquées dans l'import et le repliement oxydatif de protéines au sein de l'espace intermembranaire des mitochondries. Les résultats suggèrent que la singularité de ce système chez les plantes repose sur la structure atypique d'ERV1 et sa capacité à oxyder des protéines en présence de glutathion mais en absence de MIA40, qui est en revanche indispensable chez la levure ou l'homme.

Mots clés : *Arabidopsis thaliana*, régulation redox, centre Fe-S, thiorédoxine, glutarédoxine, repliement oxydatif, MIA40/ERV1

Abstract : The presence of reactive cysteines confers redox properties and/or the ability to bind metal ions to numerous proteins. This project, organized in several axes, aimed at characterizing proteins with a conserved CxxC motif and possibly a thioredoxin (TRX) fold in plants. It appears that the mitochondrial TRX o1 and o2, the atypical protein disulfide isomerase PDI-A and the chloroplastic glutaredoxin (GRX) S16 from *A. thaliana* expressed as recombinant proteins in *Escherichia coli* all incorporated an Fe-S center within homodimers whose function remains to be determined. Analysis of the redox properties of apo-proteins indicates that PDI-A and GRXS16 have little or no oxidoreductase activity respectively although intramolecular disulfide bridges are formed between conserved cysteines. In the case of GRXS16, its redox state would be regulated by light as the disulfide bridge is reducible by TRX but not by glutathione. The last research axis concerned the study of the properties of the MIA40 oxidoreductase and the ERV1 flavine oxidase, involved in the import and oxidative folding of proteins within the inter-membrane space of mitochondria. The results suggest that the singularity of this system in plants is based on the atypical structure of ERV1 and its ability to oxidize proteins in the presence of glutathione but in the absence of MIA40, which is essential in yeast or humans.

Keywords: *Arabidopsis thaliana*, redox regulation, Fe-S cluster, thioredoxin, glutaredoxin, oxidative folding, MIA40/ERV1